

**Investigating lamin A mutations in  
progeroid syndromes and partial  
lipodystrophy**

Thesis submitted for the degree of  
Doctor of Philosophy  
at the University of Leicester

by

Dawn Teresca Smallwood B.Sc. (Leicester)  
Department of Genetics  
University of Leicester

November 2010

# Abstract

## **Investigating lamin A mutations in progeroid syndromes and partial lipodystrophy**

**Dawn Teresca Smallwood**

Lamin A/C is a component of the nuclear lamina that contributes to nuclear integrity, chromatin organisation, gene transcription and DNA replication. Mutation of the *LMNA* gene, encoding lamin A/C, causes a number of diseases affecting different tissues, but the mechanism(s) by which this widely expressed protein causes tissue-specific disease remains unclear.

Hutchinson-Gilford progeria syndrome (HGPS) is an early-onset premature aging disorder. The most common *LMNA* mutation (G608G) prevents complete post-translational processing of lamin A, resulting in aberrant retention of a farnesyl group. In this study, a cohort of children with progeroid phenotypes were screened for genetic defects. The G608G mutation was identified in one patient with a classical phenotype. A second patient with mild progeria carried a rare T623S mutation, which also results in aberrant farnesylation of lamin A. In contrast, a severe progeroid phenotype resulted from homozygous mutation of *ZMPSTE24*, the key enzyme in lamin A processing.

Studies of skin fibroblasts showed a correlation between farnesylated lamin A level and disease severity. FRAP studies revealed that retention of the farnesyl group causes a 50% decrease in mobility of lamin A, irrespective of the exact mutation. Interestingly, one non-farnesylated mutant also had a 50% reduction in mobility, whilst other non-farnesylated mutants had normal mobility. The results of these studies indicate that incomplete processing of lamin A is an important contributor to severity of progeroid disorders but, in agreement with other reports, is not the only disease mechanism involved.

Familial partial lipodystrophy (FPLD) is a fat wasting disorder also resulting from *LMNA* mutations. Preliminary analysis of the adipogenic potential of mesenchymal stem cells isolated from FPLD patients do not produce detectable levels of adipogenesis. Preliminary immunofluorescence and binding studies in FPLD and progeria tend to support existing evidence that mislocalisation of the adipogenic factor SREBP1 may underlie the lipodystrophy phenotype.

## Acknowledgments

I would like to thank Sue Shackleton for supervision and support. I thank the University of Leicester for the opportunity to study for a PhD and the Medical Research Council for funding my research.

I would also like to thank all colleagues in the Departments of Biochemistry and Genetics, especially Zoe Redshaw, Kayoko Tanaka, Farhana Haque, Carolyn Dent, Daniela Mazzeo, Carolyn Dent, Kees Straatman, Nicolas Sylvius and Jennifer Patel for their friendliness and advice, and Dr Chris Talbot and Dr Mark Plumb for being on my PhD committee.

I would like to say a huge thanks to my parents for their support and to my children Daniel, Elizabeth and Edward for putting up with my long hours away from home.

## Contents

Title Page:	i
Abstract:	ii
Acknowledgments:	iii
Contents:	iv
Figures and Tables	x
Cddtgxkvwpu.....	zx

### **Chapter 1: Introduction**

1.1	The nuclear envelope and nuclear lamina	1
1.2	Nuclear lamins	3
1.3	Post translational processing of lamin A	6
1.4	Lamin A/C interactions and functions	8
	<i>1.4.1 Lamins interact with chromatin</i>	8
	<i>1.4.2 Lamins in DNA replication</i>	10
	<i>1.4.3 Lamins in DNA repair</i>	10
	<i>1.4.4 Lamins in transcription and translation</i>	11
	<i>1.4.5 Lamins in cell proliferation and differentiation</i>	12
	<i>1.4.6 Lamin A and the nucleoskeleton - cytoskeleton connection</i>	13
1.5	The <i>LMNA</i> gene is mutated in a range of diseases	13
1.6	Premature aging syndromes (progeroid syndromes)	17
	<i>1.6.1 Classical Hutchinson-Gilford progeria syndrome (HGPS)</i>	17
	<i>1.6.2 Restrictive dermopathy (RD)</i>	22
	<i>1.6.3 Mandibulacral dysplasia (MAD)</i>	22
	<i>1.6.4 Progeria can result from point mutations in the LMNA gene</i>	25
	<i>1.6.5 Multiple cellular defects in classical progeria</i>	26
	<i>1.6.6 Aberrant lamin A farnesylation and farnesyltransferase inhibitors (FTIs)</i>	28
	<i>1.6.7 Treatment for progeria</i>	30
1.7	Familial partial lipodystrophy, Dunnigan variety (FPLD)	33
	<i>1.7.1 Sterol response element binding protein 1 (SREBP1): interaction with lamin A and potential role in FPLD</i>	37
1.8	Adipogenesis	38
1.9	Mesenchymal stem cells	44
1.10	Aims of this project	45

### **Chapter 2: Materials and Methods**

2.1	General reagents	46
2.2	Polymerase chain reaction (PCR)	47
	2.2.1 Agarose gel electrophoresis	48
2.3	DNA sequencing	48

2.4	Digestion of patient genomic DNA to detect LMNA R527H mutations	51
2.5	DNA cloning	51
	2.5.1 Digestion of plasmid DNA for cloning	51
	2.5.2 Gel purification of DNA fragments	51
	2.5.3 Ligation of DNA fragment inserts into plasmid vectors	52
	2.5.4 Preparation of competent cells (Inoue et al 1990)	52
	2.5.5 Transformation of DNA into DH5 $\alpha$ competent cells	53
	2.5.6 Purification of plasmid DNA by mini or midi prep	53
	2.5.7 Glycerol stocks	53
	2.5.8 Site directed mutagenesis PCR	53
	2.5.9 Production of T623S and G608G constructs from RNA	54
2.6	Glutathione-S-transferase pulldown assay	54
	2.6.1 In-vitro translation (IVT)	54
	2.6.2 Pulldown assay	54
2.7	Cell culture	56
	2.7.1 Growth media and cell culture conditions	57
	2.7.2 Subculturing of cells	57
	2.7.2.1 Cell passage number	58
	2.7.3 Thawing and freezing cells	58
	2.7.4 Seeding cells	58
	2.7.5 Transient transfection	59
	2.7.6 Amaxa Nucleofection of dermal fibroblasts and MEFs	59
	2.7.7 LentiViral transduction	59
	2.7.8 Production of cell extracts	60
	2.7.8.1 Whole cell extracts	60
	2.7.8.2 Nuclear and cytoplasmic cell extracts	61
	2.7.9 Extraction of MSCs from bone marrow	61
	2.7.10 Adipocyte fixation and staining	62
	2.7.10.1 Semi-quantitative analysis of oil-red-o staining	62
2.8	Microscopy	62
	2.8.1 Indirect Immunofluorescence microscopy	62
	2.8.2 Coverslip preparation	64
	2.8.3 Fluorescence recovery after photobleaching (FRAP) SREBP1 mobility study	64
	2.8.4 Fluorescence recovery after photobleaching (FRAP) lamin A mutant mobility study	65
2.9	Protein methods	65
	2.9.1 Sodium dodecyl sulphate-polyacrylamide gel electrophoresis (SDS-PAGE)	65
	2.9.2 Western blotting	67

### **Chapter 3: Detection of mutation in LMNA and ZMPSTE24 genes**

3.1	Introduction	70
3.2	Aim of the study	73
3.3	Methods of mutation detection	73
	3.3.1 <i>Design of PCR primers</i>	74
	3.3.2 <i>Direct sequencing of coding exons</i>	74
	3.3.3 <i>Disruption of a RsaI restriction enzyme site in MAD</i>	74
3.4	Patient population	75
	3.4.1 <i>Patient clinical information</i>	76
	3.4.1.1 <i>Patient 002</i>	76
	3.4.1.2 <i>Patient 004</i>	76
	3.4.1.3 <i>Patient 005</i>	76
	3.4.1.4 <i>Patient 006</i>	79
	3.4.1.5 <i>Patient 009</i>	79
	3.4.1.6 <i>Patient 011</i>	79
	3.4.1.7 <i>Patient 012</i>	80
3.5	Results of mutation analysis	82
	3.5.1 <i>Identification of mutations in the LMNA gene</i>	82
	3.5.1.1 <i>Identification of the classical progeria mutation, in patients 005 and 013</i>	82
	3.5.1.2 <i>Identification of an atypical progeria mutation in patient 004</i>	82
	3.5.2 <i>Identification of mutations in the ZMPSTE24 gene</i>	83
	3.5.2.1 <i>Identification of compound heterozygous ZMPSTE24 mutations in patient 012</i>	83
	3.5.3 <i>Single nucleotide polymorphisms (SNPs) detected during patient screening</i>	85
3.6	Discussion	85
	3.6.1 <i>Classical HGPS: phenotype-genotype correlation in patients carrying the LMNA G608G mutation</i>	85
	3.6.2 <i>Mild HGPS: phenotype-genotype correlation in patients carrying the LMNA T623S mutation</i>	88
	3.6.3 <i>Patient 012: A phenotype overlapping MAD, HGPS and RD</i>	89
	3.6.4 <i>Lipodystrophy patients in whom no mutation was detected</i>	92
	3.6.5 <i>Progeroid patients in whom no mutation was detected</i>	93
	3.6.6 <i>Association between LMNA SNPs and disease</i>	95

### **Chapter 4: Analysis of the expression, localisation and mobility of lamin A and associated nuclear proteins in progeria and FPLD**

4.1	Introduction	97
4.2	Aim of these studies	99

4.3	Nuclear morphology abnormalities	99
	4.3.1 <i>Results of nuclear morphology study</i>	101
4.4	Changes in protein expression and localisation	105
	4.4.1 <i>Lamin A/C and prelamin A expression</i>	105
	4.4.2 <i>Prelamin accumulation at the nuclear rim</i>	107
	4.4.3 <i>SREBP1 accumulation at the nuclear rim</i>	108
	4.4.4 <i>SUN1 expression at the nuclear envelope is increased in classical HGPS cells expressing prelamin A</i>	111
	4.4.5 <i>Emerin does not completely co-localise with either lamin A/C or prelamin A in a subpopulation of progeria cells which show thickening of the nuclear lamina</i>	112
	4.4.6 <i>Emerin mislocalisation does not result in <math>\beta</math>-catenin accumulation in progeria cell lines</i>	114
	4.4.7 <i>Lamin B1 is down regulated in progeria and old age</i>	117
	4.4.8 <i>LAP2<math>\alpha</math> and Rb are down regulated in progeria and old age</i>	119
	4.4.8.1 <i>LAP2<math>\alpha</math> down regulation in progeria and old age</i>	119
	4.4.8.2 <i>Rb down regulation in progeria and old age</i>	121
	4.4.8.3 <i>LAP2<math>\alpha</math> and Rb down regulation are linked</i>	121
	4.4.9 <i>The marker of proliferation, Ki67, is reduced in all progeria cell lines</i>	123
	4.4.10 <i>No reduction in heterochromatin protein 1<math>\gamma</math> was found in the progeria cell lines studied</i>	123
4.5	Altered mobility of lamin A mutants	126
	4.5.1 <i>FRAP constructs</i>	126
	4.5.2 <i>FRAP analysis</i>	129
	4.5.3 <i>Results of mobility study</i>	129
4.6	Discussion	132
	4.6.1 <i>Findings in FPLD fibroblasts</i>	132
	4.6.2 <i>Findings in progeria fibroblasts</i>	136
	4.6.2.1 <i>The severity of patient disease phenotype correlates with the expression level of unprocessed lamin A</i>	136
	4.6.2.2 <i>Down regulation of Rb and LAP2<math>\alpha</math> result in reduced proliferation</i>	138
	4.6.2.3 <i>Mislocalisation of SREBP1 may underlie the lipodystrophy phenotype</i>	140
	4.6.3 <i>Altered mobility of lamin A mutants</i>	141

## **Chapter 5: An investigation into the interaction between lamin A and sterol response element binding protein 1 (SREBP1)**

5.1	Introduction	144
5.2	Aim of these studies	147
5.3	SREBP1 localisation and mobility studies	148
	5.3.1 <i>Subcellular localisation of transiently transfected SREBP1 in dermal fibroblasts</i>	148

5.3.2	<i>Localisation of transiently transfected SREBP1 in <math>Lmna^{-/-}</math> MEFs</i>	150
5.3.3	<i>Detection of endogenous SREBP1</i>	150
5.3.3.1	<i>Testing of commercial ATCC and H160 anti-SREBP1 antibodies</i>	152
5.3.3.2	<i>Testing of custom made antibodies 4056 and 4057</i>	154
5.3.4	<i>Detection of transduced SREBP1</i>	156
5.3.5	<i>Mobility of SREBP1 in FPLD, progeria and old age</i>	157
5.3.6	<i>Quantification of SREBP1 binding to lamin A disease mutants by GST pull-down</i>	160
5.3.6.1	<i>Optimisation of GST pull-down assays and mapping of the lamin A binding site on SREBP1</i>	160
5.3.6.2	<i>Quantification of the SREBP1a interaction with a range of disease associated lamin A mutants</i>	165
5.4	Discussion	168
5.4.1	<i>Subcellular localisation of SREBP1 in FPLD and progeria fibroblasts</i>	168
5.4.2	<i>Detection of endogenous SREBP1</i>	169
5.4.3	<i>The use of Lentiviral GFP SREBP1</i>	170
5.4.4	<i>Localisation of SREBP1 in <math>Lmna^{-/-}</math> MEFs</i>	171
5.4.5	<i>Mobility of SREBP1 in FPLD, progeria and old age</i>	172
5.4.6	<i>Quantification of SREBP1 binding to lamin A disease mutants by GST pull-down</i>	173
5.5	Summary of findings	174

## **Chapter 6: Investigating the effect of the familial partial lipodystrophy mutation R482W on adipogenic potential**

6.1	Introduction	175
6.2	Aim of the study	177
6.3	Testing adipogenic differentiation of 3T3L1 preadipocytes	177
6.4	Mesenchymal stem cell adipogenesis studies	179
6.4.1	<i>MSCs cultured for this study</i>	179
6.4.2	<i>Growth of FPLD MSC cultures</i>	180
6.4.3	<i>FPLD patient cell lines 1 and 3 stained positively for MSC markers</i>	182
6.4.4	<i>FPLD patient MSC nuclear morphology</i>	182
6.4.5	<i>Development of a protocol allowing adipogenic conversion of control MSC using only non-specific enhancers of adipogenesis DEX, IBMX and insulin</i>	184
6.4.5.1	<i>Optimal differentiation conditions</i>	184
6.4.5.2	<i>Efficacy of basic fibroblast growth factor (bFGF)</i>	186
6.4.5.3	<i>MSCs acquired a senescent phenotype at approximately passage 6</i>	189

6.4.5.4	<i>Adipogenic conversion protocol using only the non-specific enhancers of adipogenesis DEX, IBMX and insulin</i>	189
6.4.5.5	<i>Adipogenic differentiation of FPLD MSC cell line 3</i>	191
6.5	<i>Lmna R482W mouse embryonic fibroblast (MEF) studies</i>	191
6.5.1	<i>Lmna R482W MEF nuclear morphology</i>	193
6.5.2	<i>Lmna R482W MEF adipogenic differentiation</i>	195
6.6	Discussion	196
<b>Chapter 7: Conclusions and future work</b>		
7.1	Detection of mutations in <i>LMNA</i> and <i>ZMPSTE24</i> genes	202
7.2	Analysis of the expression, localisation and mobility of lamin A and associated nuclear proteins in progeria and FPLD	204
7.3	An investigation into the interaction between lamin A and SREBP1	206
7.4	The effect of the FPLD mutation R482W on adipogenic potential	207
	<b>Bibliography</b>	209

## Figures and tables

### **Chapter 1: Introduction:**

Figure 1.1	Schematic model of interactions at the nuclear envelope	2
Figure 1.2	Nuclear lamina assembly	4
Figure 1.3	Schematic representation of human lamin genes and the major lamin proteins	5
Figure 1.4	Schematic representation of the prelamin A processing pathway in normal (A) and HGPS (B) cells	7
Figure 1.5	Mutations in the lamin A gene ( <i>LMNA</i> ) are associated with many different diseases, collectively called laminopathies	15
Figure 1.6	Hutchinson-Gilford progeria syndrome (HGPS) phenotype	19
Figure 1.7	Activation of the cryptic splice site in classical HGPS	20
Figure 1.8	Restrictive dermopathy (RD) phenotype	23
Figure 1.9	Mandibuloacral dysplasia (MAD) phenotype	24
Figure 1.10	The isoprenoid and cholesterol biosynthetic pathway	31
Figure 1.11	Familial partial lipodystrophy (FPLD) Phenotype	34
Figure 1.12	Structure of the globular tail of lamin A showing disease related substitutions	35
Figure 1.13	Key transcription factors of the adipogenic pathway and their positive and negative regulators	40
Table 1.1	Laminopathies resulting from mutation of the <i>LMNA</i> gene	14
Table 1.2	Progeria-associated mutations reported in the <i>LMNA</i> <i>ZMPSTE24</i> genes	18
Table 1.3	Familial partial lipodystrophy (FPLD) mutations reported in the <i>LMNA</i> gene	36

### **Chapter 2: Materials and Methods**

Table 2.1	General chemicals and reagents	46
Table 2.2	Basic PCR reaction mix	47
Table 2.3	Agarose gel electrophoresis reagents	48
Table 2.4	Fluorescent labelling PCR reaction	49
Table 2.5	Acrylamide sequencing gel reagents	49
Table 2.6	PCR primers and conditions for amplification of <i>LMNA</i> exons from genomic DNA.	50
Table 2.7	PCR primers and conditions for amplification of <i>ZMPSTE24</i> exons from genomic DNA	50
Table 2.8	DNA cloning solutions	51
Table 2.9	DNA ligation mix	52
Table 2.10	GST pulldown assay reagents	55
Table 2.11	General cell culture reagents	56-57
Table 2.12	General cell culture solutions	57
Table 2.13	LentiViral transduction solutions	60

Table 2.14	Nuclear and cytoplasmic cell extracts buffer	61
Table 2.15	Primary antibodies for indirect immunofluorescence microscopy (IF)	63
Table 2.16	Secondary antibodies for indirect immunofluorescence microscopy (IF)	64
Table 2.17	DNA stain for indirect immunofluorescence microscopy (IF)	64
Table 2.18	Immunofluorescence microscopy solutions	64
Table 2.19	SDS-PAGE gel reagents *Protogel: 30% acrylamide/0.8% bis-acrylamide	66
Table 2.20	SDS-PAGE solutions	66
Table 2.21	Western blotting solutions	68
Table 2.22	Primary antibodies for western blotting (WB)	68
Table 2.23	Secondary antibodies for western blotting (WB)	69

### **Chapter 3: Detection of mutations in LMNA and ZMPSTE24 genes**

Figure 3.1	Overlapping features of the progeroid laminopathies	73
Figure 3.2	<i>RsaI</i> restriction digest allows detection of the MAD mutation R527H in the <i>LMNA</i> gene	75
Figure 3.3	Clinical features observed in patient 004	78
Figure 3.4	Clinical features observed in patient 005	78
Figure 3.5	Clinical features observed in patient 012	81
Figure 3.6	Sequence chromatograms of <i>LMNA</i> and <i>ZMPSTE24</i> mutations found in the patient cohort	84
Figure 3.7	Sequence chromatograms of <i>LMNA</i> and <i>ZMPSTE24</i> SNPs identified in the patient cohort	86
Table 3.1	Most common causative mutations of FPLD and progeroid laminopathies	73
Table 3.2	Results of mutation screening showing pathogenic mutations identified and SNPs detected, - indicates no mutation or no SNP found	77
Table 3.3	A comparison of the clinical features of patient 004 with two patients previously reported to carry the <i>LMNA</i> T623S mutation. + indicates presence, - absence of the condition	89
Table 3.4	Clinical features of lamin A-related progeroid syndromes	90
Table 3.5	Overview of non <i>LMNA</i> associated genetic lipodystrophies	92
Table 3.6	Overview of non <i>LMNA</i> associated progeroid syndromes	94

### **Chapter 4: Analysis of the expression, localisation and mobility of lamin A and associated nuclear proteins in progeria and FPLD**

Figure 4.1	Nuclear envelope morphology of human dermal fibroblast cell lines	102
------------	---	-----

Figure 4.2	Percentage of cells displaying abnormal nuclear morphology	103
Figure 4.3	Western blot analysis of expression of lamin A and associated proteins	106
Figure 4.4	Analysis of localisation and expression of prelamin A and SREBP1	109
Figure 4.5	Percentage of cells displaying abnormal localisation or intensity of staining	110
Figure 4.6	Localisation and expression of SUN1/2 in classical progeria cells	113
Figure 4.7	Emerin does not completely co-localise with lamin A/C in a subpopulation of progeria cells	115
Figure 4.8	Emerin does not completely co-localise with prelamin A in classical and late onset progeria cells	116
Figure 4.9	Analysis of lamin B1 staining in cultured fibroblasts	118
Figure 4.10	Analysis of staining of LAP2 $\alpha$ in cultured fibroblasts	120
Figure 4.11	Analysis of staining of Rb in cultured fibroblasts	122
Figure 4.12	Analysis of Lap2 $\alpha$ and Rb staining in cultured fibroblasts	124
Figure 4.13	Staining of the marker of proliferation, Ki67 in cultured Fibroblasts	125
Figure 4.14	Staining of a marker of heterochromatin, HP1 $\gamma$ in cultured fibroblasts by indirect immunofluorescence microscopy	127
Figure 4.15	Bleaching and recovery during FRAP analysis of wild type and mutant lamin A	130
Figure 4.16	Recovery during FRAP analysis of wild type lamin A and various mutants as indicated	131
Figure 4.17	FRAP analysis of wild type and mutant lamin A	133
Figure 4.18	Western blot analysis of lamin A/C expression in whole cell extracts to corroborate FRAP data	133
Table 4.1	Dermal fibroblast cell lines used for localisation and expression studies	100
Table 4.2	Nuclear abnormalities observed in human dermal fibroblast cell lines	101
Table 4.3	Constructs used in mobility study FRAP experiments	128

## **Chapter 5: An investigation into the interaction between lamin A and sterol response element binding protein 1 (SREBP1)**

Figure 5.1	Domain structures of SREBP1 and SREBP2	145
Figure 5.2	Schematic representation of SREBP cleavage and translocation of the transcription factor domain to the nucleus	146
Figure 5.3	Nuclear localisation of the GFP-tagged transcription factor domain of SREBP1a (GFP-SREBP1)	149

Figure 5.4	Localisation of GFP-SREBP1 in transiently transfected fibroblasts from laminopathy patients with a lipodystrophic phenotype	149
Figure 5.5	Western blot analysis and indirect immunofluorescence shows the absence of lamin A/C proteins in <i>Lmna</i> <sup>-/-</sup> MEFs.	151
Figure 5.6	Localisation of transiently transfected pCDNA3 SREBP1a in <i>Lmna</i> null and WT MEFs	151
Figure 5.7	Testing of SREBP1 antibodies H160 and ATCC IgG-2A4	153
Figure 5.8	Characterisation of SREBP1 antibodies 4056 and 4057	155
Figure 5.9	The Lentiviral GFP-tagged transcription factor domain of SREBP1 localises to the nucleus of transfected U2OS cells	158
Figure 5.10	Human foreskin fibroblasts (hFF) are transduced by Lentiviral GFP-SREBP1a	158
Figure 5.11	Single plane confocal images of dermal fibroblasts transiently transfected with GFP-SREBP1a	159
Figure 5.12	FRAP analysis of SREBP1 in WT and laminopathy fibroblasts	159
Figure 5.13	Quantification of prelamin A expression in laminopathy fibroblasts by densitometry	161
Figure 5.14	Single plane confocal images of WT and FPLD fibroblasts transiently transfected with GFP-SREBP1a	162
Figure 5.15	FRAP analysis of GFP-SREBP1a in WT and FPLD fibroblasts where FPLD fibroblasts contain cytoplasmic SREBP1	162
Figure 5.16	Binding of GST-SREBP1c to WT lamin A alongside binding of GST-SUN1 to emerin	164
Figure 5.17	GST fused fragments of SREBP1a transcription factor domain	166
Figure 5.18	Binding of <sup>35</sup> S labelled <i>in vitro</i> translated WT lamin A to GST tagged SREBP1a fragments	166
Figure 5.19	Binding GST-lamin A disease mutants to SREBP1a	167
Table 5.1	GST-tagged constructs used for GST pulldown assays	163
Table 5.2	IVT plasmid templates used for GST pulldown assays	163

## **Chapter 6: Investigating the effect of the familial partial lipodystrophy mutation R482W on adipogenic potential**

Figure 6.1	The principle regulators in the adipogenic pathway	175
Figure 6.2	Adipogenic differentiation of 3T3L1 preadipocytes	178
Figure 6.3	Growth of FPLD patient MSCs after isolation from bone marrow	181
Figure 6.4	Isolated MSCs stained positive for markers	183
Figure 6.5	Adipogenic differentiation of MSCs with DEX, IBMX, insulin	185
Figure 6.6	Adipogenic conversion of WT control MSCs	187

Figure 6.7	The effect of basic fibroblast growth factor (bFGF) on lipid accumulation in WT control MSCs	188
Figure 6.8A	MSC senescent phenotype	190
Figure 6.8B	Adipogenic conversion of MSCs at passages 4 ad 6 the absence of Troglitazone	190
Figure 6.9	Adipogenic conversion of FPLD MSC	192
Figure 6.10	Lamin A/C staining of <i>lmna</i> R482W MEFs	194
Figure 6.11	Percentage of MEFs with abnormal nuclear morphology	194
Figure 6.12	Adipogenic differentiation of <i>lmna</i> R482W MEFs	198
Table 6.1	MSC cell lines cultured	180
Table 6.2	Percentage of abnormal nuclei in MEF cell lines	195
Table 6.3	MEF cell lines used in the adipogenic conversion study	196

## Abbreviations

A	Adenine
AD	Autosomal dominant
AD-EDMD	Autosomal-dominant Emery-Dreifuss muscular dystrophy
AR	Autosomal recessive
ATCC	American Type Culture Collection
BAF	Barrier of autointegration factor
bp	Base pair
BHLH	Basic helix-loop-helix
C	Cytosine
CAAX	Cys-aliphatic-aliphatic-any residue
CEBP	CCAAT – enhancer-binding proteins
°C	Degrees centigrade
cm	Centimeter
DAPI	4',6-Diamidino-2-phenylindole
DCM	Dilated cardiomyopathy
Dex	Dexamethasone
dH <sub>2</sub> O	Distilled water
DMSO	Dimethyl sulfoxide
DMEM	Dulbecco's Modified Eagle Medium
DNA	Deoxyribonucleic acid
dNTP	Deoxy-nucleoside triphosphate
<i>E. coli</i>	Escherichia coli
ECL	Enhanced chemiluminescence
EDTA	Ethylenediamine tetra-acetic acid
EDMD	Emery-Dreifuss muscular dystrophy
ER	Endoplasmic reticulum
FACE1	Farnesylated proteins-converting enzyme 1
FCS	Fetal calf serum
FPLD	Familial partial lipodystrophy
FRAP	Fluorescence recovery after photobleaching
FTI	Farnesyltransferase inhibitors
g	Gram
g	Gravitational force
G	Guanine
GFP	Green fluorescent protein
GST	Glutathione-S-transferase
HCl	Hydrochloric acid
HeLa	Henrietta Lack cell line
HGPS	Hutchinson-Gilford progeria syndrome
HP1	Heterochromatin binding protein 1
HEPES	4-(2-hydroxyethyl)-1-piperazineethanesulfonic acid
hFF	Human foreskin fibroblasts
hr	Hour
HRP	Horse radish peroxidase
IBMX	Methylisobutyl xanthine
INM	Inner nuclear membrane

IPTG	Isopropyl- $\beta$ -D-thiogalactosidase
IVT	In vitro translation
Kb	Kilobase
kDa	KiloDalton
KASH	Klarsicht ANC-1 Syne-1 homology
LA	Lamin A
LAP2	Lamina-associated protein 2
LBR	Lamin B receptor
LB	Luria Bertani
LEM	<u>L</u> amina-associated protein 2/ <u>e</u> merin/ <u>M</u> AN1
LINC	Linker of nucleoskeleton and cytoskeleton
LGMD	Limb girdle muscular dystrophy
<i>LMNA</i>	Human lamin A/C gene
<i>Lmna</i>	Mouse lamin A.C gene
<i>LMNB1</i>	Human lamin B1 gene
<i>LMNB2</i>	Human lamin B2 gene
M	Molar
MAD	Mandibuloacral dysplasia
MEF	Mouse embryonic fibroblast
mA	Milli amplitude
mg	Milligram
min	Minutes
ml	Milliliter
mm	Millimeter
mM	Milli Molar
MSC	Mesenchymal stem cell
NE	Nuclear envelope
NETN	Nonidet P-40/EDTA/Tris-HCL/NaCl
NETs	Nuclear envelope transmembrane proteins
ng	Nanogram
NLS	Nuclear localization signal
NPC	Nuclear pore complex
OD	Optical density
ONM	Outer nuclear membrane
PBS	Phosphate buffered saline
PCR	Polymerase chain reaction
pH	Potential of Hydrogen
PPAR $\gamma$	Peroxisome proliferator activated receptor gamma
PMSF	Phenylmethylsulphonyl fluoride
Rb	Retinoblastoma protein
RCE1	Ras-converting enzyme 1
RD	Restrictive dermatopathy
RTPCR	Reverse transcription polymerase chain reaction
rpm	Revolutions per minute
RNA	Ribonucleic acid
SCAP	SREBP cleavage activating protein
SDS-PAGE	Sodium dodecyl sulphate polyacrylamide gel electrophoresis
SREBP1	Sterol regulatory element binding protein 1
SUN	Sad1-UNC84 homologue
T	Thymine

TBE	Tris borate EDTA buffer
TB	Transformation buffer
TE	Tris EDTA
TF	Transcription factor
TEMED	Tetramethyl-ethylenediamine
μl	Microlitre
U	Unit
U2OS	Human osteosarcoma cells
USA	United States of America
UK	United Kingdom
UV	Ultra-violet
v/v	Volume to volume
WAT	White adipose tissue
Wnt	Wingless and integration-1
WS	Werner's syndrome
WT	Wild type
w/v	Weight to volume
V	Voltage
ZMPSTE24	Zinc metalloprotease (yeast) Ste24

# CHAPTER 1

## Introduction

### 1.1 The nuclear envelope and nuclear lamina

The nuclear envelope (NE) is a double membrane structure that separates chromatin from the cytoplasm in eukaryotic cells, allowing regulation of DNA replication and gene expression (reviewed in Prokocimer *et al* 2009, Hetzer 2010) (Figure 1.1). Nuclear pore complexes (NPCs) span the inner and outer nuclear membranes allowing transport across the NE. Proteins that are imported into the nucleus generally contain a nuclear localisation signal (NLS), which is recognised by carrier proteins called importins and then translocated through nuclear pores (reviewed in Kiseleva *et al* 2000, Lange *et al* 2007). The outer nuclear membrane (ONM) is continuous with the endoplasmic reticulum, whereas the inner nuclear membrane (INM) contains a unique set of integral membrane proteins (Section 1.4) which are anchored in the INM by their association with the nuclear lamina (reviewed Chi *et al* 2009). Proteomic analysis of rat liver nuclei revealed that there are more than 60 nuclear envelope transmembrane proteins (NETs) (Schirmer *et al* 2005) illustrating the complexity of interactions at the INM (reviewed in Wilson and Berk 2010). The nuclear lamina is a network of lamin intermediate filaments that underlies the INM (Aebi *et al* 1986) and consists of lamins and lamin binding proteins. The lamina provides structural support to the nucleus and nuclei of cells containing mutant lamins show morphological abnormalities (Goldman *et al* 2004, Capanni *et al* 2005, Figure 4.1). The lamina binds heterochromatin and is thought to be involved in transcriptional repression (Reddy *et al* 2008) and chromosome positioning (Meaburn *et al* 2007).

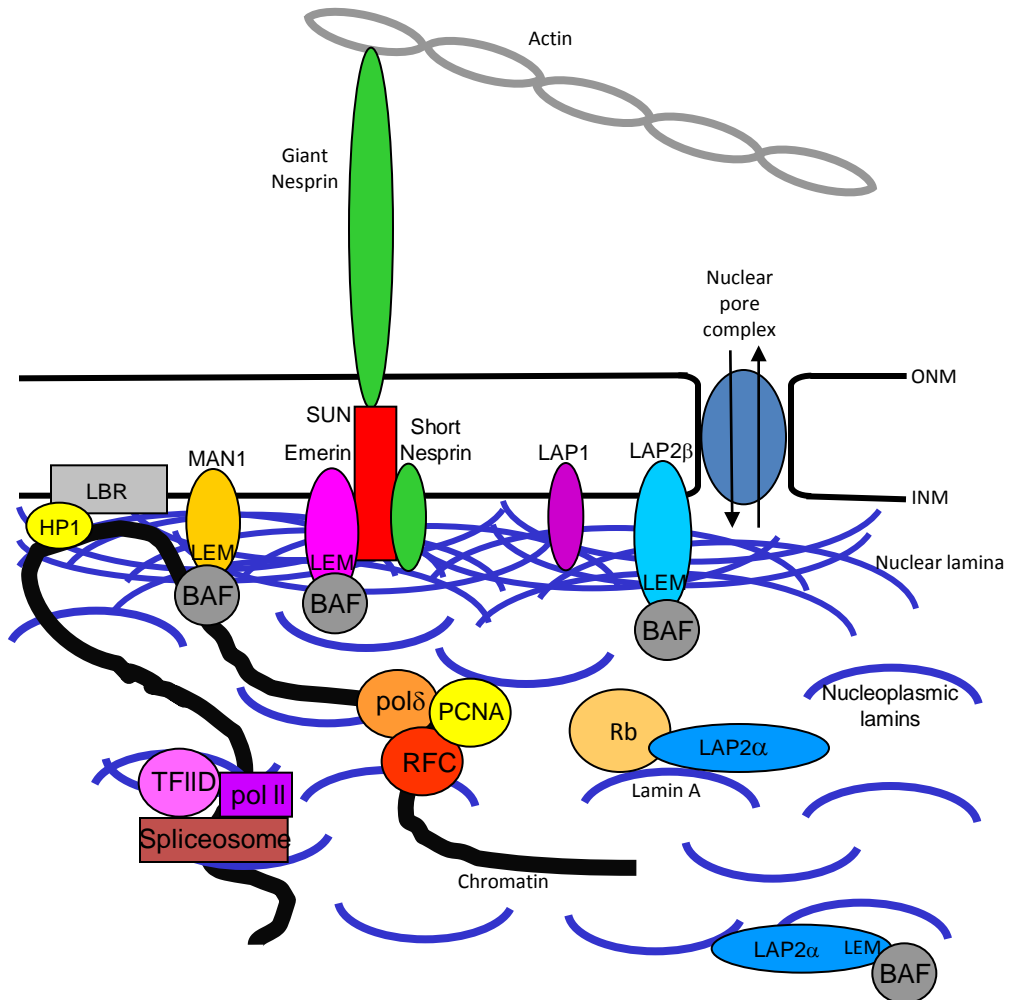


**Figure 1.1** Schematic model of interactions at the nuclear envelope. At the inner nuclear membrane (INM), a complex is formed with SUN1/2, emerin, nesprins and the nuclear lamina connecting the nucleus with the actin cytoskeleton. LAP emerin MAN1 (LEM) domain proteins interact with barrier to autointegration factor (BAF) which allows their interaction with chromatin. The lamin B receptor (LBR) interacts with heterochromatin protein 1 (HP1). Nuclear pores allow the transport of proteins across the nuclear envelope. In the nucleoplasm, a complex of lamin A, retinoblastoma protein (Rb) and LAP2 $\alpha$  is formed. Lamin A co-localises with the DNA replication complex containing DNA polymerase (pol $\delta$ ), replication factor C (RFC) and proliferating cell nuclear antigen (PCNA) and with a transcriptional complex containing RNA polymerase II (polII), transcription factor TFIID and the spliceosome. Outer nuclear membrane (ONM).

## 1.2 Nuclear lamins

Lamins were discovered by Aaronson and Blobel (1975) and Gerace *et al* (1978). To form the lamina, lamin polypeptides form coiled-coil dimers which polymerise from head-to-tail, these polymers then assemble into the paracrystalline lattice of the lamina (Aebi *et al* 1986, Heitlinger *et al* 1992, Goldberg *et al* 2008) (Figure 1.2A and 1.2B). In addition to their integration into the lamina, A and B-type lamins also form networks in the nucleoplasm (Shimi *et al* 2008). These networks consist of internal structures of foci and fibres and are present throughout the nucleus (Moir *et al* 1994, Bridger *et al* 1993). The internal structures were found to be interconnected networks of A- and B-type lamins where A-type lamins are mobile and B-type are static (Shimi *et al* 2008).

Lamins are grouped as A- or B- type based upon their primary sequence and tissue expression patterns. A-type lamins are encoded by alternative splicing of the *LMNA* gene and are expressed only in differentiated cells (Rober *et al* 1989). The major A-type isoforms are lamin A and lamin C (McKeon *et al* 1986). Lamin A/C structure consists of a short N-terminal head region, a central region of coiled coils and a nuclear localisation signal (NLS). In lamin A this is followed by a C-terminal immunoglobulin fold ending with a CAAX motif (Figure 1.3), which is not present in lamin C (Fisher *et al* 1986, McKeon *et al* 1986, Stuurman *et al* 1998). Lamins A and C are identical for the first 10 exons then lamin C has a further 6 additional unique residues, whereas lamin A has 90 additional unique residues encoded by exons 11 and 12. Also encoded by the *LMNA* gene are lamin A  $\Delta$ 10, which is a minor isoform (Machiels *et al* 1996), and lamin C2, which is germ cell specific (Furukawa *et al* 1994). The main B-type lamins, lamin B1 and B2, are encoded by the genes *LMNB1* and *LMNB2* respectively (Hoger *et al* 1988, 1990) (Figure 1.4B) and are ubiquitously expressed (Pollard *et al* 1990). A

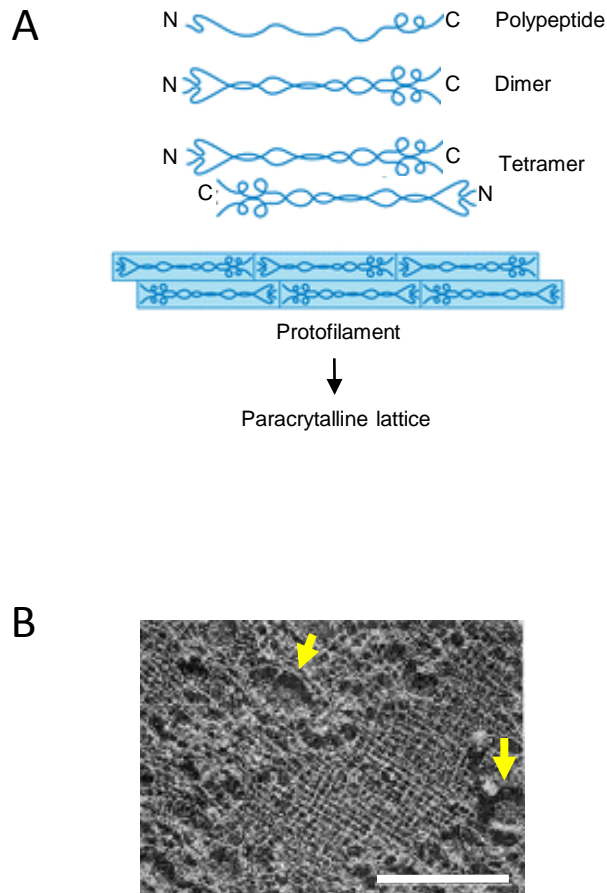


**Figure 1.2** Nuclear lamina assembly. **(A)** Construction of the intermediate filaments of the nuclear lamina. Lamin polypeptides dimerise, then assemble head to tail to form polymers, which associate to form the paracrystalline structure of the nuclear lamina. N-terminus (N) indicates start of protein, C-terminus (C) indicates end. Adapted from Monfrad 2009. **(B)** Scanning electron micrograph of the nuclear lamina in *Xenopus* oocytes. The meshwork of the lamina can be seen and rounded holes are nuclear pores (yellow arrows). Scale bar 1 $\mu$ m. Taken from Aebi *et al* 1986.

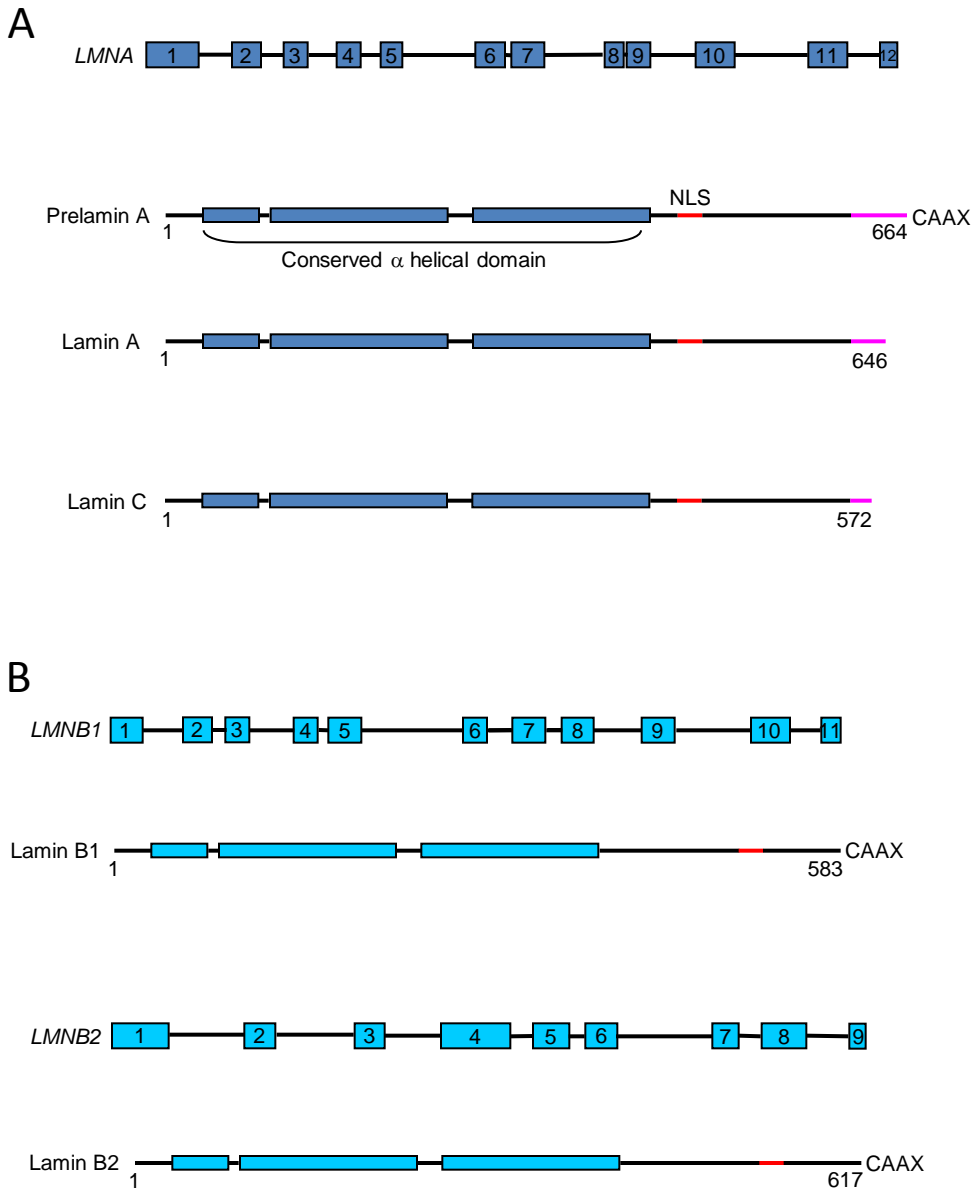


**Figure 1.3** Schematic representation of human lamin genes and the major lamin proteins. Numbers at the beginning and end of proteins indicate amino acids. The nuclear localisation signal (NLS) is shown in red. The CAAX motif is the signal for farnesylation which targets proteins to the NE. **(A)** The *LMNA* gene encodes lamins A and C which are produced by alternative splicing. Lamin A is produced as the precursor protein prelamins A which is post translationally modified to form lamin A. Pink lines indicate sequences unique to each protein. Mature lamin A and lamin C lack the CAAX motif and are not farnesylated. **(B)** Lamin B1 is encoded by the *LMNB1* gene and Lamin B2 is encoded by the *LMNB2* gene. B-type lamins are permanently farnesylated. Based on Hutchison *et al* 2001, Worman *et al* 2009.

germ cell specific lamin B isoform, lamin B3, is also encoded by *LMNB2* (Furukawa and Hotta 1993). Like lamins A/C, B-type lamins also consist of a short N-terminal head region, a central region of coiled coils, a nuclear localisation signal (NLS) and a C-terminal immunoglobulin fold and CAAX motif.

### 1.3 Post translational processing of lamin A

Lamin A is produced as the precursor protein prelamin A, which undergoes extensive post-translational modification (reviewed in Kieran et al 2007). This modification involves the addition of a 15 carbon lipid farnesyl group to the C-terminus. Small lipid groups are a general mechanism used to target proteins to membranes (reviewed in Goodsell 2003). The CAAX motif at the extreme C-terminus of lamin A is the four amino acid recognition site for farnesylation, where C stands for cysteine, A for an aliphatic amino acid and X for any amino acid. In lamin A this motif is comprised of the amino acid sequence CSIM (Figure 1.4A).

Processing of prelamin A is a four-step process mediated in part by the protease zinc metalloproteinase yeast STE24 homologue (*ZMPSTE24*), also known as farnesylated-proteins converting enzyme 1 (*FACE1*). Firstly, the cysteine residue of the CAAX motif is farnesylated by farnesyltransferase, then the C-terminal AAX tripeptide is cleaved and released either by *ZMPSTE24* or by Ras converting enzyme 1 (*RCE1*) (*FACE2* in humans). Next, the exposed farnesylated cysteine is carboxymethylated by isoprenylcysteine methyltransferase (*ICMT*). Finally cleavage by *ZMPSTE24* releases a further C-terminal 15 amino acids including the methylated farnesylcysteine residue (Beck *et al* 1990, Lutz *et al* 1992, Sinensky *et al* 1994). B-type lamins also have a C-terminal CAAX motif but remain permanently farnesylated (Farnsworth *et al* 1989)

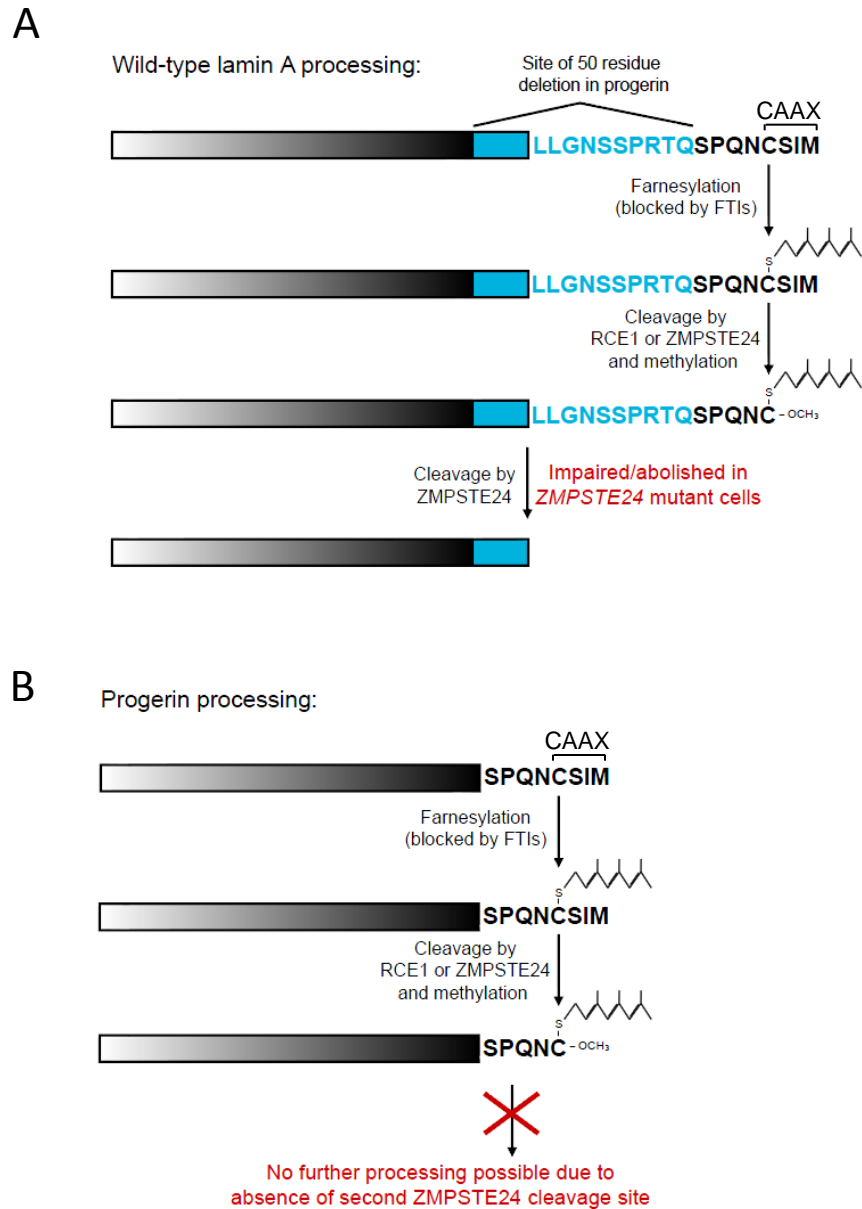


**Figure 1.4** Schematic representation of the prelamin A processing pathway in normal (A) and HGPS (B) cells. The amino acid sequence involved in processing is shown at the C-terminus. Amino acids CSIM make up the CAAX motif. (A) Processing of wild-type lamin A. The region highlighted in blue is deleted in progerin. Mutations in *ZMPSTE24* impair or abolish the final cleavage step. (B) Processing of progerin. Progerin is produced by activation of a cryptic splice site within exon 11 of the *LMNA* gene that deletes residues 607-656, including the second ZMPSTE24 cleavage site. Defects in the gene encoding ZMPSTE24 or lamin A can result in persistence of the farnesylated lamin A intermediate. Taken from Smallwood and Shackleton 2010.

whereas lamin C, which lacks the CAAX motif (Fisher *et al* 1986), cannot be farnesylated at all.

#### **1.4 Lamin A/C interactions and functions**

Lamin A/C localises to both the NE and the nucleoplasm and has many binding partners (reviewed in Prokocimer *et al* 2009) reflecting the important roles of these proteins in most nuclear processes. A number of well characterised binding partners are shown in Figure 1.1. Lamin A/C is involved in many nuclear functions including chromatin organisation, gene transcription, DNA replication and repair, nuclear envelope assembly and structural support of the nucleus (reviewed in Dechat *et al* 2008).

##### ***1.4.1 Lamins interact with chromatin***

Chromosomes are organised into territories which are thought to be linked to gene expression (Fraser and Bickmore 2007). Gene rich chromosomes tend to be positioned in the centre of the nucleus whilst gene poor chromosomes are found at the nuclear periphery (Croft *et al* 1999). Lamins are thought to anchor heterochromatin at the nuclear periphery and provide an environment of transcriptional repression. In *LMNA* null mouse fibroblasts (Sullivan *et al* 1999) and in fibroblasts from patients with *LMNA* mutations (Capanni *et al* 2003, Goldman *et al* 2004) heterochromatin is dissociated or lost from the nuclear periphery (reviewed in Dechat *et al* 2008) suggesting that intact lamin A/C is needed for heterochromatin anchorage.

A number of lamin-binding proteins interact with chromatin and DNA (Figure 1.1), and lamins also associate with chromatin through these binding partners (reviewed in Mattout-Drubezki and Gruenbaum 2003, Schirmer and Foisner 2007).

LEM domain proteins, lamina associated protein 2 (LAP2), emerin and MAN1, are lamin binding partners which all contain an N-terminal conserved motif called the LEM domain. The LEM domain binds the chromatin binding protein, barrier to autointegration factor (BAF) (reviewed in Prokocimer *et al* 2009, Wilson and Berk 2010). Through BAF, LEM domain proteins can interact with lamins and DNA and are involved in tethering chromatin at the NE (Wagner and Krohne 2007).

LAP2 $\beta$  is the INM isoform of LAP2 that binds to B-type lamins (Foisner and Gerace 1993) and to chromatin via BAF (Furukawa *et al* 1999). LAP2 $\beta$  also binds the chromatin-associated protein HA95 to play an essential role in the initiation of DNA replication (Martins *et al* 2003).

Emerin is an IMN LEM domain protein that binds lamin A and a great many other proteins although its exact function is unknown (reviewed in Bengtsson and Wilson 2004). X-linked Emery-Dreifuss muscular dystrophy results from mutation of the *EMD* gene that encodes emerin (Bione *et al* 1994). Emerin depends on lamin A for its localisation at the nuclear envelope (Vaughan *et al* 2001) and is recruited to chromatin by BAF where it is involved in the regulation of higher-order chromatin structure during nuclear assembly (Wilson *et al* 2005).

The INM LEM domain protein MAN1 binds lamin A/C, lamin B1 and a number of INM proteins (Lin *et al* 2000, Mansharamani and Wilson 2005). Like emerin, MAN1 binds BAF and depends on lamin A for NE localisation. MAN1 depletion in the absence (but not presence) of emerin is 100% embryonic lethal in *C.elegans* suggesting that MAN1 and emerin have overlapping functions (Liu *et al* 2003) which are as yet unknown. A known function of MAN1 is its inhibition of SMAD mediated transcriptional activation of transforming growth factor  $\beta$  (TGF $\beta$ ) by the sequestration

of SMADS to the nuclear periphery (Lin *et al* 2004). Loss of function mutations in MAN1 cause osteopoikilosis and Buschke–Ollendorff syndrome which are associated with enhanced TGF- $\beta$  activity (Hellemans *et al* 2004)

The lamin B receptor (LBR) was identified by Worman *et al* (1988) and binds to lamin B, DNA and the chromatin associated heterochromatin protein 1 (HP1) (Worman *et al* 1990). LBR function is not fully understood, but it is thought to contribute to the compartmentalisation of heterochromatin and to NE growth during interphase and reformation of the nucleus after mitosis. In addition, LBR has enzymatic activity and is thought to be involved in sterol biosynthesis and lamin isoprenylation in some cellular conditions (reviewed in Olins *et al* 2010).

#### ***1.4.2 Lamins in DNA replication***

Lamins are thought to be involved in DNA replication where they may act as a scaffold in the nucleoplasm on which replication can occur (reviewed in Shumaker *et al* 2003). Both lamin B (Moir *et al* 1994) and lamin A (Spann *et al* 1997) co-localise with DNA replication complexes containing DNA polymerase  $\delta$  (pol $\delta$ ), replication factor C (RFC) and proliferating cell nuclear antigen (PCNA). It has been reported that in *Xenopus* nuclei, dominant negative mutant lamins disrupted the lamina and formed aggregates in the nucleoplasm, PCNA and RFC localised to lamin aggregates and DNA replication was inhibited (Spann *et al* 1997, Moir *et al* 2000) suggesting that the lamin A-DNA replication complex interaction is necessary for DNA replication.

### ***1.4.3 Lamins in DNA repair***

The implication that lamins are involved in DNA repair comes mainly from studies of premature aging diseases (reviewed in Dechat et al 2008). The premature aging disorder Hutchinson-Gilford progeria syndrome (HGPS) is caused by mutation of lamin A. This disorder involves many cellular abnormalities including defects in DNA repair. HGPS patient fibroblasts exhibit increased phosphorylated histone H2AX indicating double strand breaks (DSBs) (Liu *et al* 2005) and decreased recruitment of DSB repair factors (Liu *et al* 2006). In addition, progeroid mouse embryonic fibroblasts (MEFs) show increased DNA damage and are more sensitive to DNA damaging agents (Liu *et al* 2005). Although evidence suggests that lamins are involved in DNA repair, their role is not yet known.

### ***1.4.4 Lamins in transcription and translation***

Lamins were first thought to be involved in transcription because of changes in lamin expression with the onset of cell differentiation (reviewed Shumaker *et al* 2003). B-type lamins are expressed throughout development, but A-type lamins are not expressed until cell differentiation begins (Rober *et al* 1989). The association of lamins with transcription factors suggests that they play a role in transcription. Lamin A binds to Rb (Ozaki *et al* 1994), Sterol response element binding protein 1 (SREBP1) (Lloyd *et al* 2002) and MOK2 (Dreuillet *et al* 2002) and lamin B binds to LAP2 $\beta$  which binds to the germ cell less transcription factor (GCL) (Nili *et al* 2001). Further evidence of a role for lamins in transcription comes from *Xenopus* nuclei where dominant negative mutant lamins have been shown to disrupt the lamina, leading to the impairment of transcription (Spann *et al* 2002).

Lamins also co-localise with splicing factors in intra-nuclear foci or speckles (Muralikrishna *et al* 2001) linking lamins to spliceosome activity.

#### ***1.4.5 Lamins in cell proliferation and differentiation***

LAP2 $\alpha$  is a nucleoplasmic isoform of LAP2 and binds specifically to A-type lamins. LAP2 $\alpha$  and lamin A tether Retinoblastoma protein (Rb) in the nucleoplasm. Rb is best known as a tumour suppressor which is frequently mutated in cancer (Friend *et al* 1986, Huang *et al* 1988) and regulates both cell proliferation (Chellappan *et al* 1991, reviewed in Dyson 1998) and differentiation (Markiewicz *et al* 2002) via the Rb-E2F pathway. Disruption of the complex between lamin A, LAP2 $\alpha$  and Rb results in loss of proliferation in human fibroblasts due to the mislocalisation of Rb (Pekovic *et al* 2007), indicating that lamin A plays a role in cell proliferation.

In addition to the control of cell cycle progression, Rb functions in the adipocyte and myoblast differentiation pathways. Rb has been found to activate the adipogenic transcription factor C/EBP $\alpha$  and over expression of Rb results in increased adipogenesis. In addition, Rb<sup>+/+</sup> mouse embryonic lung fibroblasts (ELFs) can be differentiated into adipocytes but in Rb<sup>-/-</sup> ELFs, the absence of Rb prevents adipogenesis (Chen *et al* 1996) suggesting that Rb is an essential component of the adipogenic pathway. Rb is also required for myoblast differentiation which is inhibited by the inactivation of Rb (Zacksenhaus *et al* 1996). Specifically, Rb has been shown to play a crucial role in the switch from proliferation to differentiation. Rb deletion in differentiated fibres has no effect on the normal muscle phenotype, but when Rb was deleted in proliferating myoblasts they were unable to form muscle fibres (Huh *et al* 2004).

#### ***1.4.6 Lamin A and the nucleoskeleton - cytoskeleton connection***

Lamin A interactions with IMN proteins SUN1/2, emerin and nesprins form a direct connection between the nucleoskeleton and cytoskeleton by forming the nucleoplasmic region of the LINC (linker of nucleoskeleton and cytoskeleton) complex (Crisp *et al* 2006, Haque *et al* 2010). SUN proteins bind to lamins, emerin and nesprins at the nucleoplasmic face of the NE and bridge the gap across the lumen of the nuclear envelope by binding to the luminal domain of nesprins, thus connecting the nucleus with the actin cytoskeleton (reviewed Razafsky and Hodzic 2009).

#### **1.5 The *LMNA* gene is mutated in a range of diseases**

Lamin A/C is mutated in a range of mainly tissue specific diseases in which adipose tissue, skin, bone, skeletal and cardiac muscle or neurons can be affected (Table 1.1). Pathogenic mutations have been reported in almost every exon of the *LMNA* gene resulting in more than 10 different disorders (reviewed Capell and Collins 2006, Dechat *et al* 2008, Worman and Bonne 2009) (Figure 1.5). Diseases associated with lamin A/C are referred to as laminopathies and include muscular dystrophies, lipodystrophy, premature aging syndromes and a neuropathy. The disease mechanism in most laminopathies is not well understood but appears to relate to the position of the *LMNA* mutation and its subsequent effect on lamin A/C structure or interactions. Two non-exclusive hypotheses for how different mutations in the same gene result in a range of diseases have been described by Worman and Courvalin (2004). The mechanical stress hypothesis proposes that lamin A/C mutations cause structural weakness in the nucleus resulting in increased susceptibility to damage by mechanical stress. This theory is relevant to Emery-Dreifuss muscular dystrophy (EDMD) and limb girdle muscular dystrophy type 1B (LGMD1B) which affect striated muscle, where mutations are

Disease	Inheritance	LMNA defects	Effect on protein	Clinical phenotype
Hutchinson Gilford progeria syndrome (HGPS)	<i>De novo</i>	Cryptic splice site activation	Permanently farnesylated lamin A with internal deletion	Onset of aged appearance at 1 year Lipodystrophy atherosclerosis
Atypical progeria	AD or AR	Point mutations	Unknown	Late onset aged appearance
Mandibuloacral dysplasia	AD	Point mutations	Unknown	Late onset premature aging Mild phenotype
Restrictive dermopathy	Usually <i>de novo</i>	Point mutation or splicing defect	Prelamin A accumulation which is toxic to cells	Thin tight skin Neonatal lethal
Atypical Werner syndrome	AD	Point mutations	Unknown	Late onset aged appearance
Emery-Dreifuss muscular dystrophy (EDMD) type 2	AD	Point mutations	Loss of function	Contractures Muscle wasting Cardiomyopathy
EDMD type 3	AR	One reported point mutation	Unknown	Contractures Muscle wasting Cardiomyopathy
Limb girdle muscular dystrophy (LGMD)	AD	Point mutations	Unknown	Contractures Muscle weakness Cardiomyopathy
Dilated cardiomyopathy type 1A	AD	Point mutations	Unknown	Cardiomyopathy
Charcot-Marie-Tooth disease type 2B1	AD	Point mutations	Unknown	Neuropathy Limb motor deficits Absent tendon reflexes
Familial partial lipodystrophy (FPLD)	AD	Point mutations	Unknown	Partial lipodystrophy
Generalised lipodystrophy /lipoatrophy	AD	Point mutation	Unknown	Lipodystrophy /lipoatrophy
Heart-Hand syndrome	AD	Point mutation	Unknown	Cardiac and limb deformities

**Table 1.1** Laminopathies resulting from mutation of the *LMNA* gene. Inheritance is autosomal dominant (AD) or autosomal recessive (AR). Based on Capell and Collins (2006)

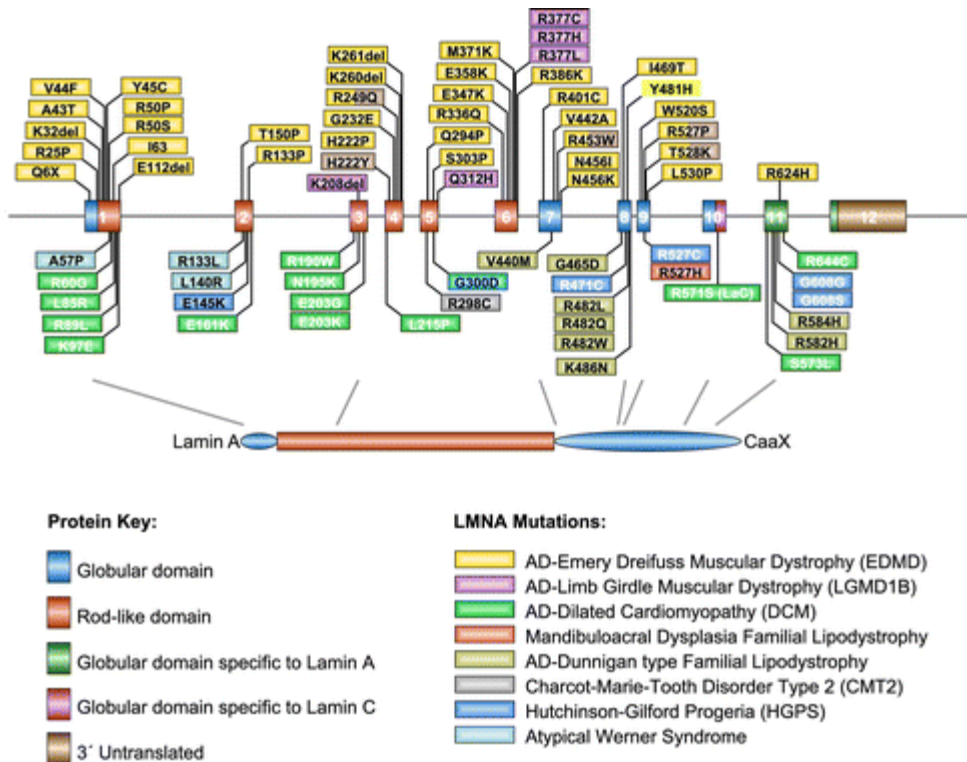


**Figure 1.5** Mutations in the lamin A gene (*LMNA*) are associated with many different diseases, collectively called laminopathies. Mutations causing certain diseases are spread throughout the gene, such as those resulting in EDMD and DCM which are thought to disrupt protein structure. Other mutations tend to be clustered in a specific domain, such as those resulting in FPLD which are thought to disrupt protein-protein interactions. Taken from Burke and Stewart (2006).

thought to weaken the lamina leading to nuclear fragility and the inability to withstand contractile stress. EDMD nuclei are reported to be so fragile that they tear, leaking chromatin into the cytoplasm (Fidzianska and Hausmanowa-Petrusewicz 2003). The second hypothesis proposes that since the NE plays a role in tissue-specific gene expression, this role could be altered by the altered interactions of mutant lamin A/C. This may be the case in familial partial lipodystrophy (FPLD), a disorder of adipose tissue, which is thought to result from the disruption of protein-protein interactions. Solution of the crystal structure of the C-terminus of lamin A (Dhe-Paganon *et al* 2002, Krimm *et al* 2002) revealed that FPLD disease mutations are clustered on the outer face of the protein where interactions are affected (Lloyd *et al* 2002) but gross protein structure is not altered. Worman and Courvalin (2004) conclude that evidence suggests both theories are correct since mechanically stressed cells have been found to suffer damage to chromatin and the NE, followed by changes in gene expression (Lammerding *et al* (2004). Another mechanism underlies changes in gene expression in the premature aging disorder Hutchison-Gilford progeria syndrome (HGPS). HGPS is caused by defective post translational processing of lamin A. This results in the aberrant retention of a farnesyl group which alters lamin A mobility and localisation causing a range of cellular defects (Goldman *et al* 2004, Scaffidi and Misteli 2006) which are discussed in detail in Section 1.6.1. Prelamin A accumulation has been reported in a number of laminopathies where it has been associated with nuclear abnormalities and a thickened rigid lamina (Goldman *et al* 2004, Navarro *et al* 2004, Shackleton *et al* 2005) along with sequestration and subsequent mislocalisation of the nuclear proteins emerin and sterol response element binding protein 1 (SREBP1). Emerin has been found to localise to intranuclear aggregates of prelamin A (Capanni *et al* 2009) and SREBP1 was reported to be sequestered to the nuclear rim by prelamin A (Capanni *et al* 2005).

## 1.6 Premature aging syndromes (progeroid syndromes)

Progeroid syndromes (Table 1.2) can result from autosomal dominant (AD) and autosomal recessive (AR) mutation of the *LMNA* gene and also result from mutation of *ZMPSTE24*. Inheritance of atypical progeria is often AR and patients generally exhibit a milder, later onset form of the disorder where some or all of the features of classical progeria develop more slowly.

### 1.6.1 Classical Hutchinson-Gilford progeria syndrome (HGPS)

Classical HGPS patients appear normal at birth, but begin to show symptoms before they are 1 year old. Early symptoms are failure to thrive, sclerodermatous skin and loss of subcutaneous fat. They go on to progressively develop the typical progeroid phenotype of impaired growth, hair loss, thin translucent skin, lipodystrophy, joint stiffness, osteolysis and distinctive facial features including prominent forehead and eyes, glyptic nose and micrognathia, giving the overall appearance of an aged person (Figure 1.6). Premature atherosclerosis leads to death from cardiovascular or cerebrovascular disease, usually in the teens. A detailed description of the phenotype is made by Hennekam *et al* 2006, Mazereeuw-Hautier *et al* 2007 and Merideth *et al* 2008.

Classical HGPS is usually caused by a *de novo*, heterozygous, silent 1824C>T mutation of the *LMNA* gene (De Sandre-Giovannoli *et al* 2003, Eriksson *et al* 2003). A single base substitution, (GGC>GGT) at codon 608 (G608G), produces a cryptic splice donor site (Figure 1.7). When the site is activated splicing occurs within exon 11 and 150 nucleotides are removed from the end of exon 11. The reading frame is not changed so that the mutant lamin A protein has an internal deletion of amino acids 607-656. The

Gene	cDNA	Protein	Inheritance	Phenotype	Reference
<i>LMNA</i>	29C>T	T101	AD	Atypical combined with Berardinelli-Seip syndrome	Csoka <i>et al</i> 2004
	428C>T	S143F	AD	Atypical with myopathy	Kirschner <i>et al</i> 2005
	433G>A	E145K	AD	Atypical	Eriksson <i>et al</i> 2003
	1411C>T	R471C	AR	Atypical with MAD/muscular dystrophy	Zirn <i>et al</i> 2008
	1579C>T	R527C	AR	Atypical/severe skeletal	Liang <i>et al</i> 2009
	1583C>T	T528M	AR	Classical	Verstraeten <i>et al</i> 2006
	1619T>C	M540T	AR	Classical	Verstraeten <i>et al</i> 2006
	1626G>C	K542N	AR	Classical	Plasilova <i>et al</i> 2004
	1733A>T	E578V	AD	Mild	Csoka <i>et al</i> 2004
	1821G>A	Δ607-656 (V607V)	AD	Severe	Moulson <i>et al</i> 2007
	1822G>A	Δ607-656 (G608S)	AD	Classical	Eriksson <i>et al</i> 2003, Cao and Hegele 2003
	1824C>T	Δ607-656 (G608G)	AD	Classical	Eriksson <i>et al</i> 2003, De Sandre-Giovannoli <i>et al</i> 2003
	1868C>G	D622-656 (T623S)	AD	Mild	Fukuchi <i>et al</i> 2004, Shalev <i>et al</i> 2007
	1930C>T	R644C	AD	Mild	Csoka <i>et al</i> 2004
	1968+1G>A	Δ567-656	AD	RD	Navarro <i>et al</i> 2004
<i>ZMPSTE24</i>	794A>G	N265S	AR	Severe	Shackleton <i>et al</i> 2005
	1085_1086insT	L362FfsX379	AR	Severe	Shackleton <i>et al</i> 2005
	1204_1225del22	V402SfsX403	AR	Classical*	Denecke <i>et al</i> 2006

**Table 1.2** Progeria-associated mutations reported in the *LMNA* and *ZMPSTE24* genes, showing cDNA sequence change, the consequent effect at the protein level and the associated disease severity. Inheritance is autosomal dominant (AD) or autosomal recessive (AR). \*Phenotype moderated by co-segregating null mutation in *LMNA* (R654X) that reduces the level of farnesylated prelamin A. Taken from Smallwood and Shackleton 2010.

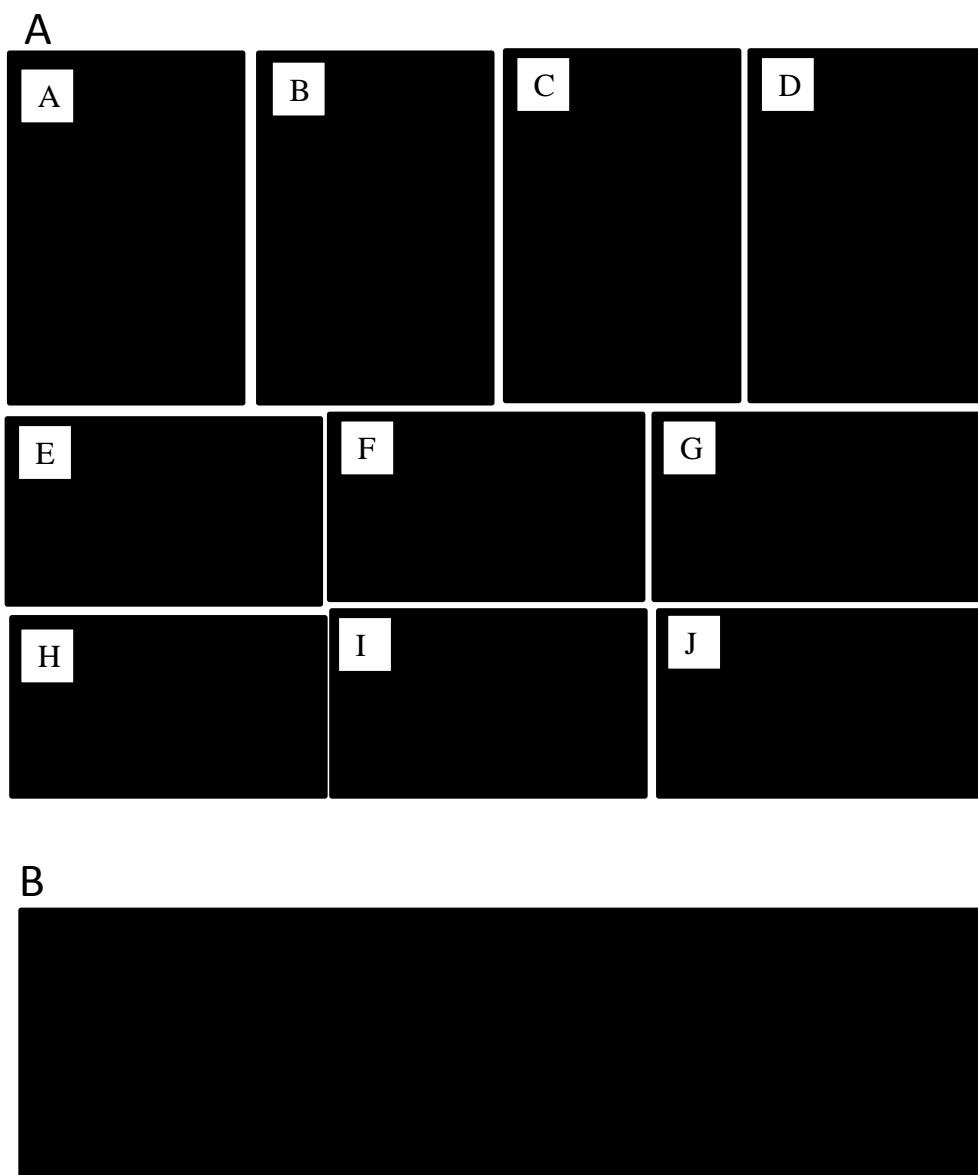


**Figure 1.6** Hutchinson-Gilford progeria syndrome (HGPS) phenotype. (A) Physical characteristics of HGPS. Photographs A, B, C are of patients aged 2.75, 4 and 7 years showing short stature, alopecia, and progressive aging. D shows lipodystrophy, prominent veins, knee joints and contractures under maximal passive extension. E and F show short bulbous fingers and joint contractures. G shows skin dimpling. H and I show abnormal skin pigmentation and abdominal outpouching. J shows circumoral cyanosis. Taken from Merideth *et al* 2007. (B) HGPS disease progression in a single HGPS patient aged 3 months, 1 year, 4 years, 6.5 years and 9 years of age. Taken from Kieran *et al* 2007.

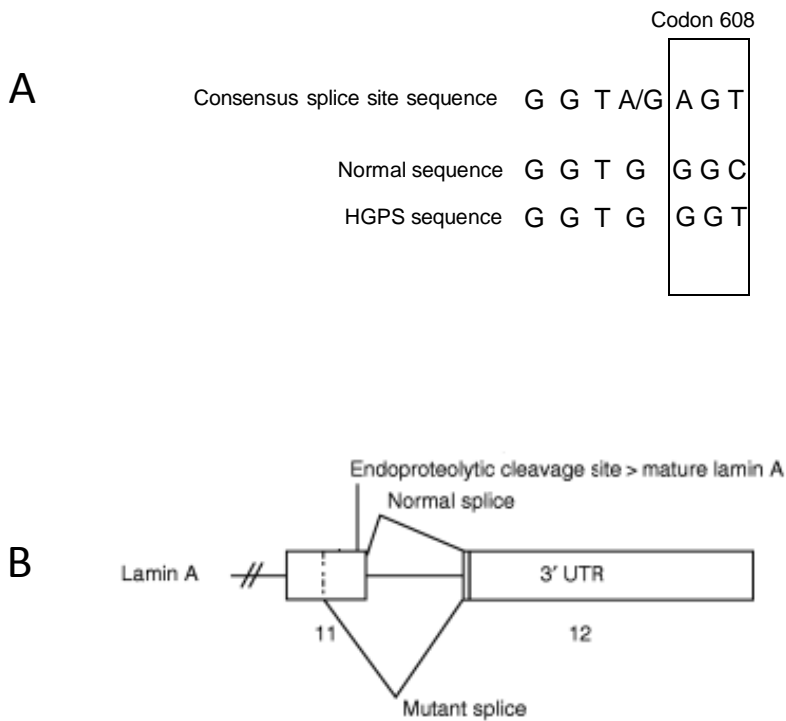


**Figure 1.7** Activation of the cryptic splice site in classical HGPS. **(A)** Nucleotide sequences for RNA splicing. The consensus splice site sequence is compared to the normal *LMNA* sequence and the G608G mutation in HGPS. **(B)** Schematic diagram of the normal splice donor and acceptor sites (normal splice) and the cryptic splice site resulting from the G608G mutation. Adapted from Pollex and Hegele 2004.

mutant protein retains the CAAX motif (corresponding to amino acids CSIM) and undergoes farnesylation, but lacks the internal site for cleavage by ZMPSTE24. This incompletely post-translationally processed, permanently farnesylated form of lamin A persists and has deleterious effects on the cell. This mutant is referred to as progerin or lamin A  $\Delta$ 50 (LAA $\Delta$ 50), (De Sandre-Giovannoli *et al* 2003, Eriksson *et al* 2003, reviewed in Davies *et al* 2009). Post-translational processing of progerin is shown in Figure 1.4. The lamin C mRNA terminates upstream of the G608G mutation site so that lamin C is unaffected.

Another progeria mutation, V607V, activates the same cryptic splice site in exon 11 as the classical HGPS G608G mutation. However, the V607V mutation results in stronger activation of the splice site, producing a much larger amount of progerin than in classical HGPS (Moulson *et al* 2007). As a result, individuals carrying the V607V mutation have a particularly severe form of the disease. Hence, disease severity appears to correlate with usage of the splice site and the amount of aberrantly farnesylated lamin A produced.

Findings in a further progeria patient support the observation that disease severity increases with the amount of farnesylated lamin A produced. Homozygous V402SfsX403 ZMPSTE24 null mutations were reported in a patient with a classical HGPS phenotype. Normally the more severe progeroid disorder restrictive dermopathy (discussed below) would be predicted to result from the complete abolition of ZMPSTE24 activity, however, in addition, this patient had a co-segregating R654X lamin A null mutation which produced a farnesylation incompetent form of lamin A (Denecke *et al* 2006). Thus, it appears that disease severity was reduced by the reduction in the amount of farnesylated prelamin A.

### ***1.6.2 Restrictive dermopathy (RD)***

The lethal neonatal laminopathy, restrictive dermopathy (RD) is the most severe *LMNA* related disorder. This disorder shares aspects of HGPS such as growth retardation, sparse eyebrows and eyelashes, osteolysis and micrognathia, but is characterised by thin, tight skin causing a restriction in joint extension and fixed facial expression with the mouth in an 'O' shape (Navarro *et al* 2004, Moulson *et al* 2005, Jagadeesh *et al* 2009) (Figure 1.8). Liveborn babies usually die from respiratory failure in the first week of life. RD inheritance is autosomal recessive, usually involving homozygous or compound heterozygous *ZMPSTE24* null mutations, of which the most frequently occurring is p.L362PhefsX19 (Navarro *et al* 2004, Navarro *et al* 2005). These mutations completely abolish *ZMPSTE24* activity, resulting in a total absence of mature lamin A and accumulation of high levels of farnesylated prelamin A (Navarro *et al* 2005, Moulson *et al* 2005, Columbaro *et al* 2010).

### ***1.6.3 Mandibulacral dysplasia (MAD)***

Mandibuloacral dysplasia (MAD) is usually caused by AR *LMNA* mutation, most commonly R527H (Novelli *et al* 2002, Shen *et al* 2003), but has also been found to result from AR mutation of *ZMPSTE24* (Agarwal *et al* 2003, 2006). In common with classical HGPS, children with MAD appear normal at birth but at around 4 years of age they progressively develop disease symptoms (Figure 1.9). Overall, disease progression is slower but skeletal damage more pronounced compared to classical HGPS. Symptoms of MAD include bone underdevelopment and dissolution, mandibular and clavicular hypoplasia, acro-osteolysis of terminal phalanges, joint contractures, mottled skin pigmentation, skin atrophy, lipodystrophy, hyperlipidaemia and insulin resistance. Life expectancy is 30 years or more (Novelli *et al* 2002, Agarwal *et al* 2003, Shen *et al*

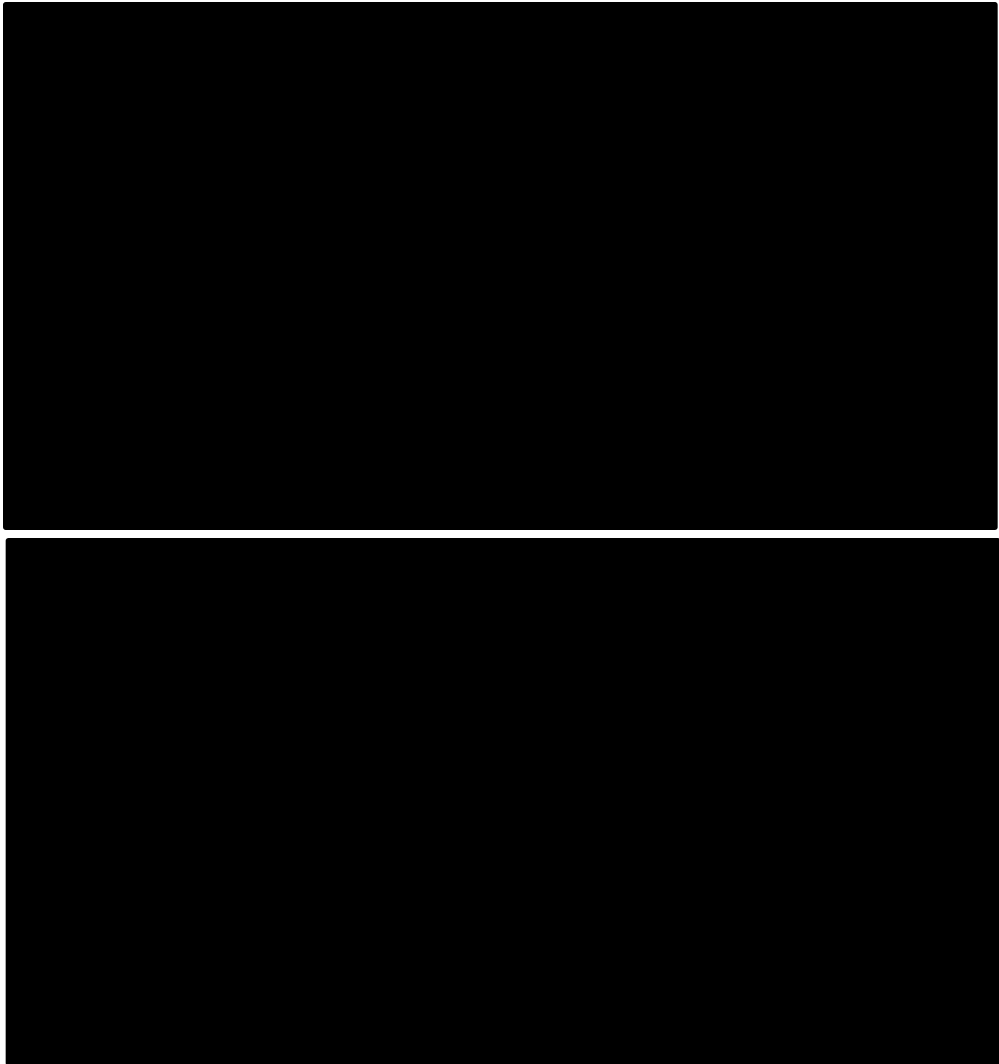


**Figure 1.8** Restrictive dermopathy (RD) phenotype. Physical characteristics of newborn patients are shown. Translucent, tight skin is visible which restricts joint extension, results in shallow respiration and causes a fixed facial expression with the mouth in an ‘o’ shape. Taken from Navarro *et al* 2004.

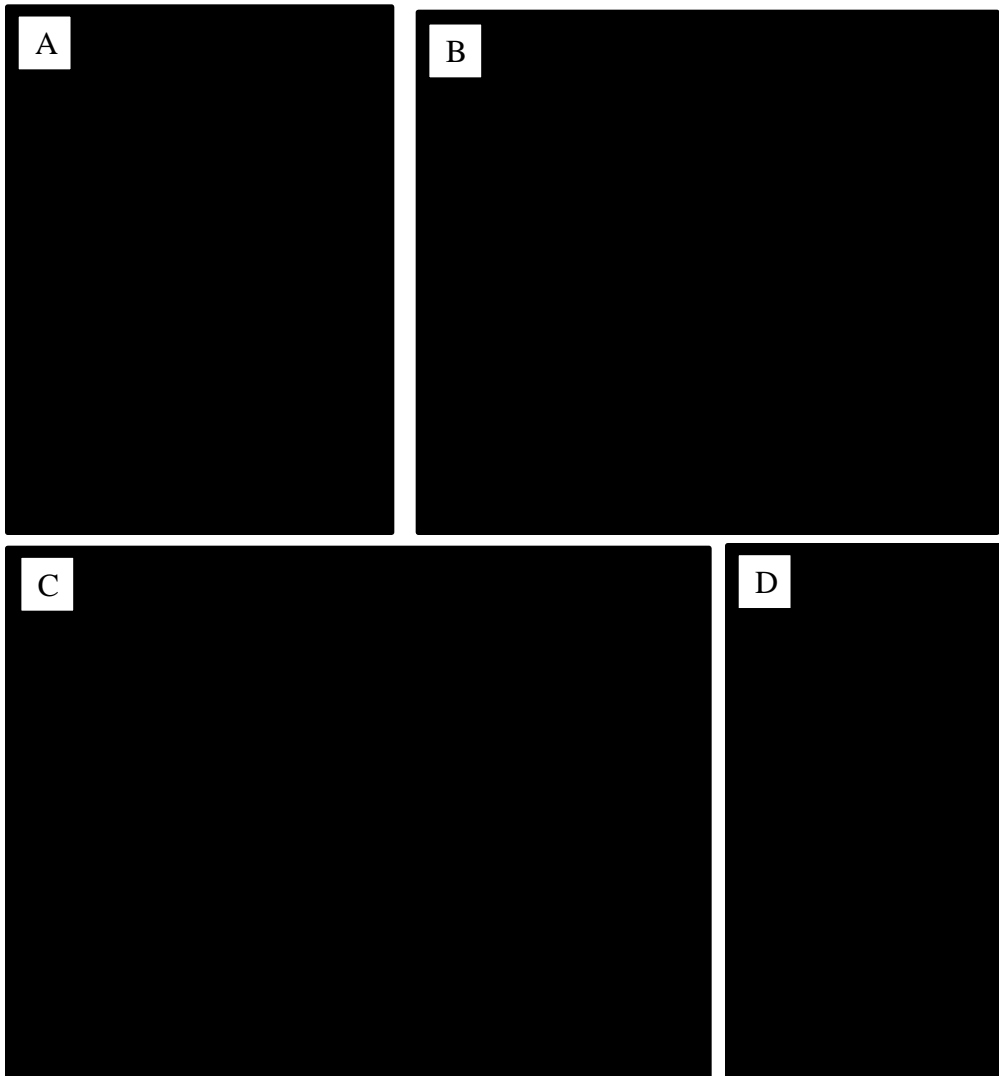


**Figure 1.9** Mandibuloacral dysplasia (MAD) phenotype. Physical characteristics of a MAD patient aged 12 years. Photograph A shows micrognathia, prominent eyes, beaked nose. B shows lipodystrophy and downward sloping shoulders. C and D show short bulbous fingertips and toes and extreme lipodystrophy in the extremities.

2003, Garg *et al* 2005, Garavelli *et al* 2009). MAD resulting from mutation of the *LMNA* gene generally causes a specific pattern of partial lipodystrophy involving loss of subcutaneous fat from the extremities with normal or a slight excess of fat in the neck and trunk, referred to as type A lipodystrophy or MAD type A. MAD resulting from mutation of the *ZMPSTE24* gene involves type B lipodystrophy where loss of subcutaneous fat is more generalised and involves the face, trunk and extremities, which is referred to as MAD type B. Patterns of lipodystrophy in MAD have been described by Simha *et al* 2003 and Agarwal *et al* 2003.

#### ***1.6.4 Progeria can result from point mutations in the LMNA gene***

Although disease severity appears generally to correlate with the presence of partially processed farnesylated prelamin A, this may not be the only mechanism underlying progeria. A number of atypical HGPS patients with recessive point mutations in *LMNA* have been reported. Most of these mutations are not predicted to directly affect lamin A processing as they lie upstream of exon 11, with some as distant as exon 1 (Table 1.2). There appear to be only two cases of amino acid substitutions in *LMNA* resulting in the classical HGPS phenotype. Homozygous K542N mutations were found in four affected siblings who showed all features of classical HGPS together with additional skeletal abnormalities usually associated with MAD (Plasilova *et al* 2004). Compound heterozygous T528M and M540T mutations were found in a 2 year old patient with a classical HGPS phenotype (Verstraeten *et al* 2006). However, there was no build up of progerin or prelamin A in cells from this individual, suggesting that permanent farnesylation of lamin A may not be the cause of disease in this patient.

Atypical HGPS patients exhibit a milder, later onset form of progeria where some or all of the features of classical HGPS develop more slowly. Atypical progeria can also be

caused by dominant point mutations and atypical progeria patients with splicing defects have been reported to carry T623S mutations (Fukuchi *et al* 2004, Shalev *et al* 2007). The T623S mutation affects splicing in a similar way to G608G and is described in Section 3.6.2. Additional disease features, not normally part of the progeria phenotype, are sometimes involved in atypical progeria. There have been reports of atypical progeria with myopathy caused by dominant S143F mutation (Kirscher *et al* 2004), with scoliosis caused by homozygous R527C mutation (Liang *et al* 2009) and with dwarfism caused by dominant R644C mutation (Csoka *et al* 2004).

### ***1.6.5 Multiple cellular defects in classical progeria***

Studies have been performed on cells expressing the lamin A mutant, progerin, either using transfected cells or dermal fibroblasts isolated from classical progeria patients. These studies point to the mutant progerin having a severe dominant-negative effect on nuclear structure and functions. The most striking visual defect is abnormal nuclear morphology, including membrane lobulations and folds and irregular lamin staining. Membrane deformation was found to increase in severity over time, correlating with increasing expression of progerin and, interestingly, increased membrane deformation also correlated with increasing expression of wild type lamin A (Goldman *et al* 2004, Bridger and Kill 2004). The nuclear lamina of HGPS cells is significantly thickened (Goldman *et al* 2004) and displays altered mechanical properties indicative of greater nuclear rigidity (Dahl *et al* 2006, Verstraeten *et al* 2008). It is thought that the permanent farnesylation of progerin results in a more stable association with the nuclear membrane and reduced lamin dynamics (Dahl *et al* 2006, Scaffidi and Misteli 2005). This in turn may alter the arrangement of the lamin network (Delbarre *et al* 2006), leading to membrane deformation.

Significant alterations in nuclear architecture have been reported in progerin-expressing HGPS cells. Initial electron microscopic observations by Goldman *et al* identified disorganisation of the peripheral heterochromatin (Goldman *et al* 2004). Subsequent studies revealed reduced expression of heterochromatin-associated proteins and aberrant histone modification (Scaffidi and Misteli 2005, Shumaker *et al* 2006) and chromosome mislocalisation (Meaburn *et al* 2007). Changes in gene expression patterns have also been reported (Meaburn *et al* 2007). A genome-wide expression study showed widespread misregulation of genes, particularly those encoding transcription factors and extracellular matrix proteins (Csoka *et al* 2004) which could explain the skeletal abnormalities in patients. In addition, abnormal clustering of nuclear pores (Goldman *et al* 2004) and impaired nuclear import (Busch *et al* 2009) have been reported in HGPS cells.

In parallel with other premature aging disorders such as Werner's syndrome and others (outlined in Table 3.6), components of the DNA maintenance machinery, genomic instability, persistent activation of DNA damage checkpoints and defective DNA repair are features HGPS (Liu *et al* 2005, Liu *et al* 2006). The cause of the genomic instability is not clear but may in part be due to increased sensitivity of HGPS cells to DNA damage (Liu *et al* 2005). Aberrant association of progerin with membranes during mitosis has also been observed, leading to mitotic defects and chromosome mis-segregation (Cao *et al* 2007, Dechat *et al* 2007). Together with increased telomere shortening, (Allsopp *et al* 1992, Huang *et al* 2008), these defects are likely to contribute to the reduced proliferation and premature cellular senescence observed in HGPS cells (Bridger and Kill 2004) which is a major feature of the HGPS phenotype.

### ***1.6.6 Aberrant lamin A farnesylation and farnesyltransferase inhibitors (FTIs)***

Although many biological abnormalities are reported in HGPS cells, little is known regarding which is the primary defect and which are subsequent downstream responses. Nuclear architecture defects are observed upon transient transfection of progerin constructs into wild type cells and nuclear envelope deformation is apparent within one hour of introducing progerin into cells, indicating that the protein has an immediate and drastic dominant-negative effect on nuclear organisation (Goldman *et al* 2004, Scaffidi and Misteli 2005). However, in HGPS fibroblasts, changes in histone methylation occur before nuclear envelope deformation becomes apparent (Shumaker *et al* 2006), suggesting that membrane disruption is not the primary event.

It has generally been thought that it is the aberrant farnesylation of lamin A that triggers all the deleterious effects of progerin, but accumulating evidence suggests that this may not be the case. Some clues come from studies on cells treated with farnesyltransferase inhibitors (FTIs) which block farnesylation of lamin A. Several groups have shown that FTI treatment reverses nuclear envelope deformation in progeria patient cells (Toth *et al* 2005, Capell *et al* 2005, Glynn and Glover 2005). Chromosome segregation defects are also ameliorated by FTI treatment (Cao *et al* 2007). These findings indicate that permanent farnesylation of lamin A is the primary cause of these abnormalities presumably by causing tight and sometimes inappropriate membrane association. In contrast, other defects are not improved by FTIs, including mechanosensitivity (Verstraeten *et al* 2008) and DNA damage defects (Liu *et al* 2006). A farnesylation incompetent progerin mutant has the same ability as farnesylated progerin to induce DNA damage (Liu *et al* 2006). These data highlight the need to carefully examine all

progerin-induced cellular phenotypes when determining the efficacy of potential treatments.

The effect of FTIs has been examined in two mouse models of progeria which closely mimic human disease. A *Zmpste24* deficient mouse (*Zmpste24*<sup>-/-</sup>) was generated by targeted disruption of the *Zmpste24* gene (Leung *et al* 2001) and an HGPS knock-in mouse (*Lmna*<sup>HG/HG</sup>) was generated by the targeted deletion of the last 150 nucleotides of *Lmna* exon 11 plus all of introns 10 and 11. Intron 10 was deleted to ensure that no lamin C was produced to compensate for mutated lamin A (Yang *et al* 2005). Both mouse models exhibited a progeroid phenotype (Bergo *et al* 2002, Yang *et al* 2005). In both mouse models, FTIs were found to improve several disease characteristics, including body weight, fat deposition and bone density, and also increased life expectancy (Fong *et al* 2006, Yang *et al* 2006). However, FTIs did not completely reverse the phenotype but rather delayed its onset, with mice eventually succumbing to the same severe disease. In a recent study, mice expressing a non-farnesylated version of progerin were found to exhibit a similar but milder phenotype to those expressing farnesylated progerin (Yang *et al* 2008), further indicating that aberrant farnesylation is not solely responsible for the HGPS phenotype.

Thus, if aberrant farnesylation is not the only factor leading to the development of HGPS, it is possible that either the internal deletion of 50 amino acids or the failure to remove the extreme C-terminal residues of prelamin A is involved. The large internal deletion may cause such a dramatic and severe phenotype compared to other laminopathies by fundamentally altering the properties of lamin A and the whole lamin network (Delbarre *et al* 2006). Alternatively, the continued presence of the C-terminal residues of prelamin A may be toxic to the cell. In support of this model, Lattanzi *et al*

found that expression of a farnesylation-incompetent prelamin A mutant induced the same changes in chromatin organisation and histone methylation seen in progeria cells (Lattanzi *et al* 2007). It would be interesting to confirm these findings in mice expressing the equivalent non-farnesylated version of wildtype lamin A.

The use of FTIs leads to a significant increase in prelamin A levels (presumably a non-farnesylated form) in both human and mouse cells expressing progerin (Toth *et al* 2005, Glyn and Glover 2005, Yang *et al* 2006) suggesting that this form of treatment will not eradicate the disease phenotype.

### ***1.6.7 Treatment for progeria***

Research findings surrounding the molecular basis of classical HGPS have led to the instigation of trials of drugs to ameliorate or reverse the disease process in HGPS children. The first drug trial in HGPS children began in the USA in 2007 (ClinicalTrials.gov identifier NCT00425607). The trial used the FTI Lonafarnib for a period of 2 years in an attempt to prevent farnesylation of lamin A (Kieran *et al* 2007, Gordon *et al* 2008, Merideth *et al* 2008) (Figure 1.10). FTIs do appear to improve some aspects of disease and increase life expectancy in mice, but evidence from mouse models suggests the disease process may not be reversed or halted (Yang *et al* 2008). Results of this drug trial have not yet been published, but it is hoped that Lonafarnib will have some therapeutic effect. Interestingly, FTI treatment also improves cellular phenotypes in cells with *LMNA* mutations that do not affect lamin A processing (Verstraeten *et al* 2006, Toth *et al* 2005) suggesting that any therapeutic effects may be applicable to progeria patients with a wide range of *LMNA* and *ZMPSTE24* mutations.

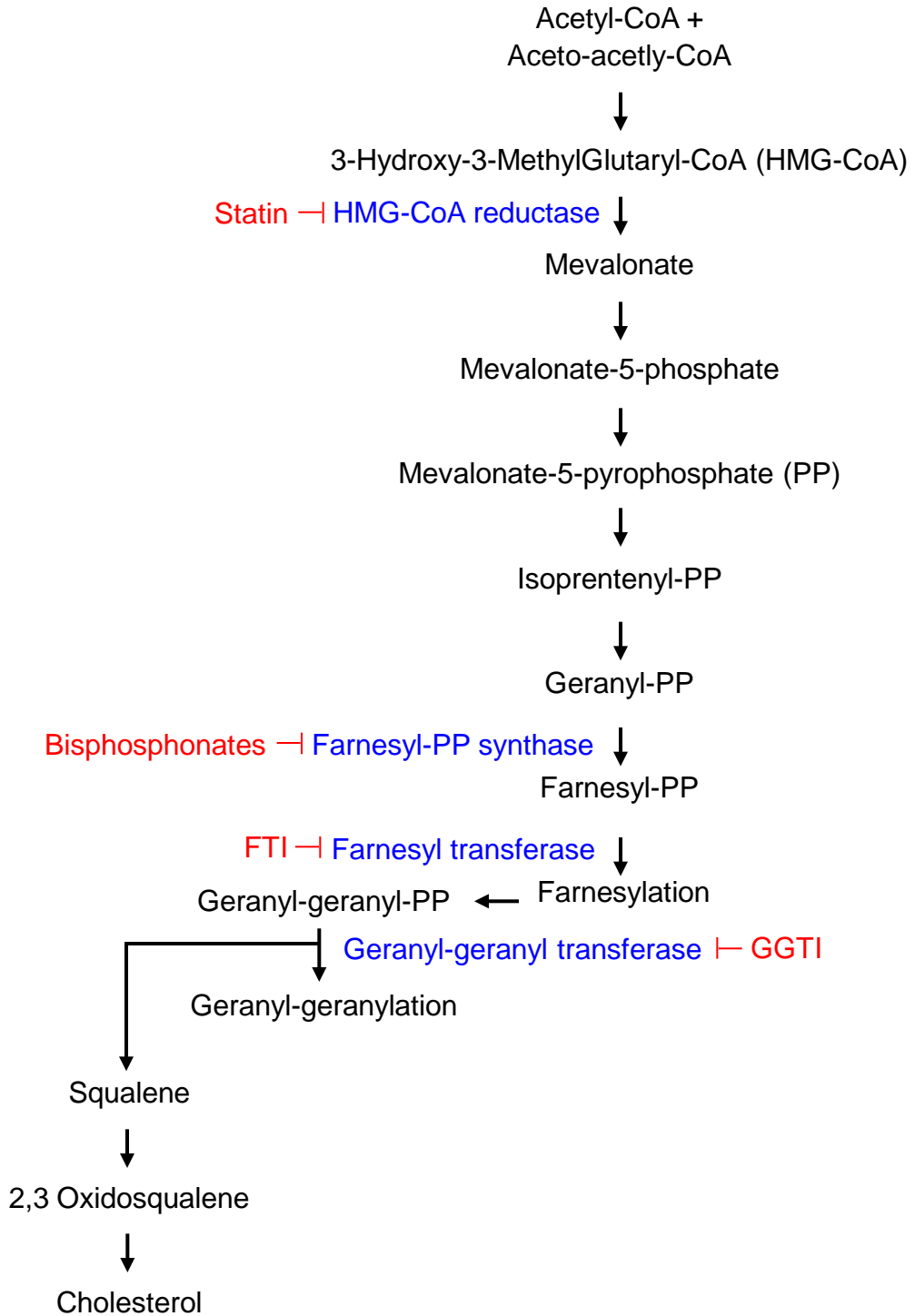


**Figure 1.10** The isoprenoid and cholesterol biosynthetic pathway. The pathway can be arrested at different stages by inhibitors (red) of essential enzymes in the pathway (blue). FTI farnesyl transferase inhibitor, GGTI geranyl-geranyl transferase inhibitor.

A European drug trial in HGPS children began in 2008 and is ongoing (ClinicalTrials.gov identifier NCT00731016). A combination of statins and bisphosphonates are being used in this trial to inhibit the isoprenoid biosynthetic pathway upstream of farnesyl transferase inhibition. In 2009, the US trial was restarted using the same statin and bisphosphonate combination. Statins and bisphosphonates are approved drugs which are well tolerated and do not show negative effects after prolonged treatment (Konstantinopoulos and Papavassiliou 2007) or overlapping toxicity (Schmidmaier *et al* 2006). The statin pravastatin acts to inhibit the enzyme 3-Hydroxy-3-MethylGlutaryl-CoA (HMG-CoA) reductase and the bisphosphonate zoledronic acid inhibits farnesyl pyrophosphate (farnesyl-PP) synthase (Figure 1.10). It has been reported that both prelamin A and progerin undergo alternative prenylation by geranylgeranyl transferase when farnesyltransferase is inhibited and that alternative prenylation could explain the low effect of FTIs in ameliorating the phenotypes of mouse models of progeria (Varela *et al* 2008). The combined use of statins and bisphosphonates to inhibit both farnesylation and geranylgeranylation resulted in a marked improvement in the phenotype of ZMPSTE24 deficient mice and extended their life expectancy (Varela *et al* 2008). It is hoped that the same dramatic improvement will be seen in progeria children.

In addition, an alternative approach to inhibition of prenylation has been tested (Scaffidi and Misteli 2005). The cryptic splice site that generates progerin was targeted using morpholino oligonucleotides to prevent its use. In HGPS fibroblasts, progerin expression was eliminated and several cellular phenotypes were reversed, including nuclear morphology, histone modification and gene expression defects. Another group, (Sagelius *et al* 2008) found that epidermis-related progeria phenotypes were reversed when progerin expression was switched off in mice with inducible keratinocyte-specific

progerin expression, suggesting that elimination of progerin may reverse the disease process rather than simply halt it. It remains to be seen, however, whether oligonucleotides can be effectively administered to patients.

### **1.7 Familial partial lipodystrophy, Dunnigan variety (FPLD)**

The FPLD phenotype involves post-pubertal wasting of subcutaneous fat in the trunk and limbs, accumulation of fat in the face and neck, muscle hypertrophy and acanthosis nigricans (Garg *et al* 2001, Schmidt *et al* 2001) (Figure 1.11). The pattern of adipose tissue distribution may be related to tissue origin; osteocytes, myocytes and adipocytes in the body are derived from mesoderm, whereas the head is of ectodermal origin. It has been suggested that laminopathies only affect tissues of mesodermal origin. In FPLD, lack of subcutaneous fat means that excess calories cannot be stored in adipose tissue, instead they are stored as triglyceride in liver, skeletal and cardiac muscle and pancreatic  $\beta$  cells, leading to hyperlipidaemia and insulin resistance, resulting in diabetes and atherosclerosis (Savage and O’Rahilly 2002).

FPLD is caused by AD *LMNA* point mutations (Shackleton *et al* 2000, Speckman *et al* 2000, Cao and Hegele 2000). When the crystal structure of the globular domain of lamin A was solved, it revealed that reported FPLD mutations were clustered in a small area on the surface of the protein, suggesting protein-protein interactions may be disrupted (Dhe-Paganon *et al* 2002) (Figure 1.12). Lamin A-related FPLD mutations reported to date are shown in Table 1.3. The most frequently occurring FPLD mutation is R482W which affects both lamin A and C (Shackleton *et al* 2000). An AD point mutation, R582H in exon 11, has been reported to result in a milder FPLD phenotype (Speckman *et al* 2000, Garg *et al* 2001), possibly because lamin C is unaffected. There is a great deal of phenotypic heterogeneity in patients with FPLD (Garg *et al* 2001).



**Figure 1.11** Familial partial lipodystrophy (FPLD) Phenotype. Physical characteristics of an FPLD patient aged 36 years. Photograph shows loss of subcutaneous fat from the trunk and limbs with excess fat deposition in the face. Prominent veins, muscle hypertrophy and acanthosis nigricans (dark, thickened underarm skin) are visible. Taken from Schmidt *et al* 2001.

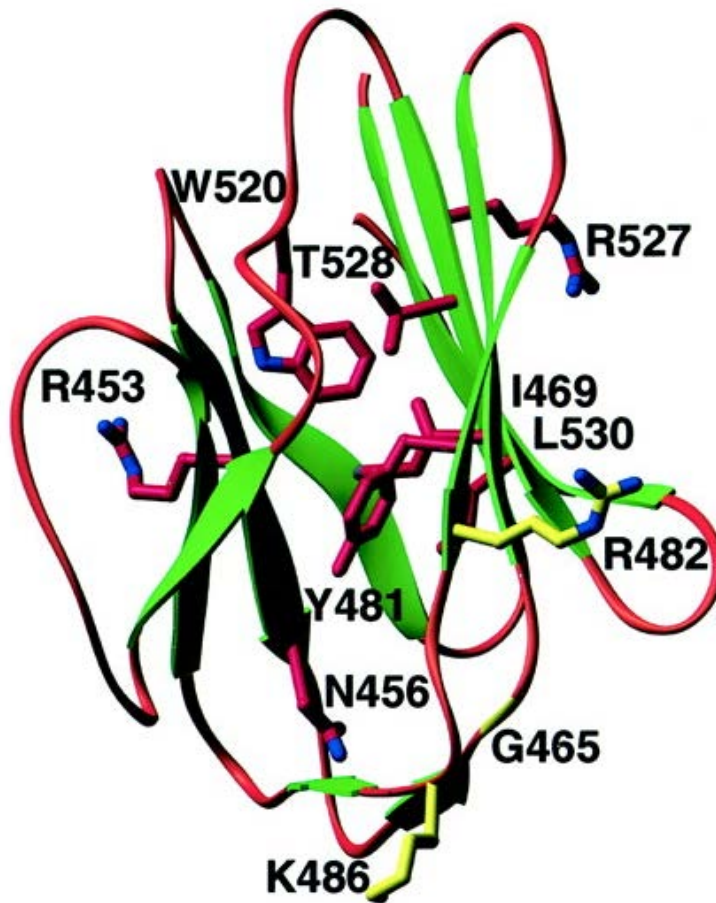


**Figure 1.12** Structure of the globular tail of lamin A showing disease related substitutions. FPLD associated residues R482, G465 and K486 (yellow) map to the surface of a distinct corner of the lamin A protein. Also shown are Emery-Dreifuss and limb girdle muscular dystrophies (red), which are mainly located in the core of the globular region. Taken from Dhe-Paganon *et al* 2002.

Gene	cDNA	Protein	Inheritance	Phenotype additional to partial lipodystrophy	Reference
<i>LMNA</i>	82C>T	R28W	AD		Garg <i>et al</i> 2002
	178C>G	R60G	AD	Cardiomyopathy	Van der Kooi <i>et al</i> 2002
	184C>G	R62G	AD	Cardiomyopathy	Garg <i>et al</i> 2002
	574A>T	D192V	AD	Cardiomyopathy	Subramanyam <i>et al</i> 2010
	668G>A	D230N	AD		Lanktree <i>et al</i> 2007
	895A>G	I299V	AD	Cardiomyopathy	Aravjo-Vilar <i>et al</i> 2008
	1195C>T	R399C	AD	Steatosis	Lanktree <i>et al</i> 2007
	1318G>A	V440M	AD	Severe phenotype	Hegele <i>et al</i> 2000
	1394G>A	G465D	AD		Speckman <i>et al</i> 2000
	1411C>G	R471G	AD		Muschke <i>et al</i> 2008
	1444C>T	R482W	AD		Hegele <i>et al</i> 2000, Vigouroux <i>et al</i> 2000, Shackleton <i>et al</i> 2000
	1445G>A	R482Q	AD		Cao <i>et al</i> 2000, Speckman <i>et al</i> 2000, Hegele <i>et al</i> 2000
	1445G>T	R482L	AD		Shackleton <i>et al</i> 2000
	1458G>C	K486N	AD		Shackleton <i>et al</i> 2000
	1488+5G>C	I497VfsX21	AD	Severe phenotype	Morel <i>et al</i> 2006
	1745G>A	R582H	AD		Speckman <i>et al</i> 2000, Hegele <i>et al</i> 2000
	1583C>T 1748C>T	T528M S583L	AR		Savage <i>et al</i> 2004
	17772G>T	C591F	AD	Cardiomyopathy Muscle weakness	Aravjo-Villar 2008

**Table 1.3** Familial partial lipodystrophy (FPLD) mutations reported in the *LMNA* gene, showing cDNA sequence change, the consequent effect at the protein level and associated disease phenotype. Inheritance is autosomal dominant (AD) or autosomal recessive (AR). Taken from Leiden Open Source Variation Database (LOVD).

Disease is generally more severe in women than men, however, the typical FPLD phenotype is not always evident, especially in lean individuals and hypertriglyceridaemia and insulin resistance vary and are not always present (Vigouroux *et al* 2000).

Nuclear envelope disorganisation has been reported in FPLD fibroblasts carrying R482W/Q mutation in the lamin A/C gene (Vigouroux *et al* 2001). FPLD dermal fibroblasts were found to have abnormal nuclear morphology involving irregular shape and budding of nuclei, where a subpopulation of buds contained a honeycomb pattern of lamin A/C staining and lamin B was lost. Structural disorganisation of the lamina was reported. Heat shocking of FPLD fibroblasts resulted in a two-fold reduction in survival rate compared to the control and FPLD cells showed reduced resistance to salt extraction suggesting that mechanical properties of the nuclear envelope were impaired (Vigouroux *et al* 2001).

### ***1.7.1 Sterol response element binding protein 1 (SREBP1): interaction with lamin A and potential role in FPLD***

A yeast two-hybrid screen using a cDNA encoding the C-terminal domain of lamin A as bait to probe a mouse adipocyte library, identified SREBP1 as a lamin A binding protein (Lloyd *et al* 2002).

SREBP1 is a transcription factor and regulator of lipid homeostasis. The two isoforms of SREBP1, SREBP1a and SREBP1c, are produced from alternative transcription start sites in the *SREBF-1* gene (Hua *et al* 1994). They differ only in the first exon, where the N-terminal activation domain sequence of SREBP1a is longer making SREBP1a the

stronger transcriptional activator (Shimano *et al* 1997). SREBP1a is the predominantly expressed isoform in cultured cells including NIH3T3, mouse embryonic fibroblasts and human fibroblasts whereas SREBP1c is predominantly expressed in liver (Shimomura *et al* 1997). SREBP1 proteins are produced as inactive precursors which reside in the endoplasmic reticulum until activation results in release of the N-terminal transcription factor domain which subsequently enters the nucleus (Wang *et al* 1994, Brown and Goldstein 1997).

SREBP1 is part of the adipogenic pathway (see Section 1.8) and is therefore of great interest as a possible link between lamin A and adipogenesis. Binding of lamin A to SREBP1 was found to be reduced by familial partial lipodystrophy (FPLD) mutations (Lloyd *et al* 2002) suggesting that impaired binding disrupts adipogenesis, perhaps due to loss of SREBP1 from the nucleus. On the other hand, SREBP1 has been found to bind prelamin A at the nuclear rim of FPLD and progeroid fibroblasts and it has been suggested that this binding sequesters SREBP1 away from its site of normal transcriptional activity, impairing adipogenesis and resulting in the lipodystrophy phenotype (Capanni *et al* 2005).

## **1.8 Adipogenesis**

Adipogenesis is the process by which multipotent mesenchymal stem cells differentiate into mature adipocytes (reviewed in Rosen 2000). The molecular mechanism of adipogenesis has been studied extensively in the mouse 3T3L1 and 3T3F442A preadipocyte model cell lines which were established from NIH3T3 cells and are committed to the adipogenic lineage (Green and Kehinde 1975, 1976). These cells differentiate into mature adipocytes when grown to confluence and exposed to a cocktail of adipogenic reagents (Green and Kehinde 1975).

There are two types of adipose tissue, white and brown. Brown adipocyte differentiation takes place before birth and humans are born with large brown fat deposits for thermogenesis. In adulthood, however, there are very few brown fat deposits and they are dispersed in white adipose tissue (WAT) (described in Rosen and MacDougald 2006). WAT is the main energy store in mammals, excess energy is stored as lipid and released when energy levels are low. WAT is also a complex secretory organ which secretes proteins to regulate metabolic activity (reviewed in Avram *et al* 2007, Ferris and Crowther 2011). A recent proteomic study identified 80 different adipose secretory proteins (Rosenow *et al* 2010).

Adipogenesis is controlled by the interactions of transcriptional activators, repressors and cofactors, hormones and cell cycle regulators. Preadipocyte cell lines 3T3L1 and 3T3F442A have been used to identify and characterise key transcription factors in the adipogenic pathway (reviewed in Rosen 2005, Farmer 2006). The key transcription factors are well established (reviewed in Rosen 2005, Farmer 2006) (Figure 1.13), but new factors influencing the pathway are still being reported (reviewed in Lowe *et al* 2011).

The nuclear transcription factor peroxisome proliferator-activated receptor gamma (PPAR $\gamma$ ) is known as the master regulator of adipogenesis (Farmer 2006, Rosen and MacDougald 2006). The two isoforms of PPAR $\gamma$ , PPAR $\gamma$ 1 and PPAR $\gamma$ 2 are produced by alternative splicing and promoter use of the same gene (Fajas *et al* 1997). PPAR $\gamma$ 1 is expressed in many tissues but PPAR $\gamma$ 2 is almost exclusively expressed in adipose tissue (Mueller *et al* 2002). Knock down of PPAR $\gamma$ 2 in mouse white adipose tissue results in severe lipodystrophy (Koutnikova *et al* 2003) and ectopic expression of PPAR $\gamma$ 2 alone

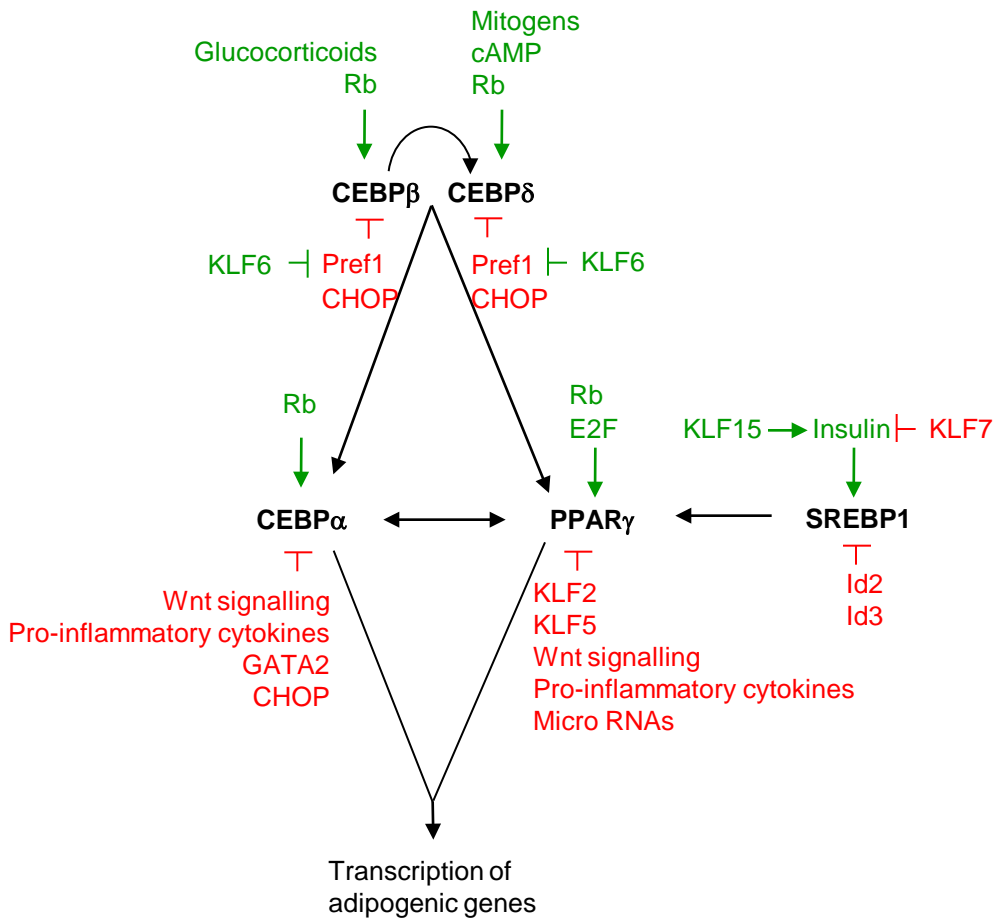


**Figure 1.13** Key transcription factors of the adipogenic pathway and their positive and negative regulators. Key transcription factors (black) are positively (green) and negatively (red) regulated by a range of molecules and pathways. Only examples of the most well documented regulators are shown, a great many more additional factors influence adipogenesis than could be shown here.

can induce adipogenesis in mouse fibroblasts (Tontonoz *et al* 1994). In the presence of ligand, PPAR $\gamma$  heterodimerises with cofactor retinoid X receptor (RXR) to activate gene transcription (Ijpenberg *et al* 1997). A number of possible endogenous ligands of PPAR $\gamma$  have been reported. These include fatty acids (Xu *et al* 1999), prostaglandin J, which is synthesised from fatty acids, (Forman *et al* 1995), and recently farnesyl pyrophosphate, a metabolite of the cholesterol and isoprenoid pathway, (Goto *et al* 2011), which all induce or enhance adipogenesis. Synthetic PPAR $\gamma$  ligands include the antidiabetic drug thiazolidinedione (Lehmann *et al* 1995) (discussed in Section 4.1).

The CEBP family of transcription factors, CEBP $\alpha$ , CEBP $\beta$ , CEBP $\delta$ , and CEBP $\gamma$  are also essential for adipogenesis. CEBP $\alpha$  is sometimes referred to as a master regulator of adipogenesis alongside PPAR $\gamma$  (Farmer 2006). CEBP $\alpha$  is required for white adipose tissue formation (Wang *et al* 1995) and the ectopic expression of CEBP $\alpha$  can induce adipogenesis in mouse fibroblasts (Freytag *et al* 1994).

The key adipogenic pathway begins with expression of CEBP $\beta$  and CEBP $\delta$  (Cao *et al* 1991) which stimulate PPAR $\gamma$  expression (Christy *et al* 1991). In turn, CEBP $\beta$ , CEBP $\delta$  and PPAR $\gamma$  go on to stimulate expression of CEBP $\alpha$  (Figure 1.13). It has been shown that CEBP $\beta$  and  $\delta$  cannot stimulate CEBP $\alpha$  expression in the absence of PPAR $\gamma$  (Zuo *et al* 2006). CEBP $\beta$  is activated by cyclic adenosine monophosphate (cAMP) signalling through cAMP regulatory element-binding protein (CREB) (Cao *et al* 1991) and also by the transcription factor Krox20 which is induced by cell mitogens (Chen *et al* 2005). CEBP $\delta$  is activated by the glucocorticoid class of steroid hormones and by CEBP $\beta$  (Cao *et al* 1991).

SREBP1 is a transcription factor and regulator of lipid homeostasis and is produced in response to insulin production (Kim *et al* 1998). SREBP1 function in adipogenesis was discovered when very high levels of SREBP1 mRNA were found in differentiating 3T3L1 cells (Kim and Spiegelman 1996). SREBP1 was found to be an essential component of the adipogenic pathway when differentiation was repressed in 3T3L1 cells expressing a dominant negative form of SREBP1 (Kim and Spiegelman 1996). Subsequently, SREBP1 was found to be an activator of PPAR $\gamma$  when ectopic expression of SREBP1 induced the production of endogenous PPAR $\gamma$  mRNA (Fajas *et al* 1999). SREBP1 is thought to activate PPAR $\gamma$  by contributing to the production of endogenous PPAR $\gamma$  ligand (Kim *et al* 1998).

Adipogenesis is positively and negatively regulated by many external signals (reviewed in Avram *et al* 2007), some of which are described below. The transcription factor CREBP homologous protein (CHOP) binds to CEBP $\alpha$  and CEBP $\beta$  (Ron and Habener 1992) and inhibits their activity by directing them away from their classic binding sites (Batchvarova *et al* 1995). Preadipocyte factor 1 (Pref1) inhibits adipogenesis by induction of the transcription factor Sex determining region Y – box9 (Sox9) which represses CEBP $\delta$  and CEBP $\beta$  (Wang and Sul 2009). The GATA2 transcription factor, which binds the DNA sequence GATA, is an inhibitor of CEBP $\alpha$  (Tong *et al* 2005). SREBP1 activity is inhibited by inhibitor of DNA binding (Id) 2 and Id3 proteins which act as functional antagonists to inhibit the formation of SREBP1 complexes with DNA (Moldes *et al* 1999). Growth factors are pro-proliferative and therefore work against differentiation. Pro-inflammatory cytokines inhibit adipogenesis, for example, the cytokine tumour necrosis factor  $\alpha$  (TNF $\alpha$ ) prevents the induction of PPAR $\gamma$  and

CEBP $\alpha$  (Petruschke *et al* 1993). Recently, microRNAs have been found to target the PPAR family (McGregor and Choi 2011).

Adipogenesis is both positively and negatively regulated by the Kuppel like factor (KLF) family of transcription factors. Positive regulators are KLF5 which is induced by CEBP  $\beta$  and  $\delta$ , then goes on to induce PPAR $\gamma$  (Oishi *et al* 2005), KLF6 which inhibits Pref1 (Li *et al* 2005) and KLF15 which promotes adipogenesis by inducing expression of the insulin sensitive glucose transporter GLUT4 (Gray *et al* 2002). Negative regulators are KLF2 which represses the PPAR $\gamma$ 2 promotor (Banerjee *et al* 2003) and KLF7 which impairs insulin biosynthesis (Kawamura *et al* 2006).

Differentiation is influenced by the response of upstream signalling pathways to intracellular and extracellular conditions (reviewed in Rosen and MacDougald 2006). These pathways include the Wingless and integration-1 (Wnt) pathway, which inhibits adipogenesis and the Retinoblastoma protein (Rb) signalling pathway which promotes adipogenesis.

Wnt signalling controls cell proliferation and differentiation (reviewed in Komiya and Habas 2008) including the maintenance and activation of stem cells (Reya *et al* 2003, Reya and Clevers 2005). The canonical Wnt pathway activates target genes via the transcriptional coactivator  $\beta$ -catenin. Activation of canonical Wnt signalling inhibits adipogenesis (Ross *et al* 2000), whereas inhibition of Wnt signalling stimulates adipogenesis (Ross *et al* 2000, Bennett *et al* 2002). Wnt signalling has been found to prevent adipogenesis by inhibition of the transcription factors PPAR $\gamma$  and CEBP $\alpha$  (Bennett *et al* 2005, Kang *et al* 2007).

Rb functions as a regulator of transcription and controls cell proliferation by repression of the E2F family of transcription factors which regulate cell cycle progression. Rb binds E2F, preventing transcription of cell cycle genes and arresting cells in G1 (Chellappan *et al* 1991). In addition to the control of cell cycle progression, Rb has an essential role in adipocyte terminal differentiation where it activates differentiation transcription factors. Rb has been shown to bind and activate transcription by all four CEBP proteins (Chen *et al* 1996) and Rb null mouse fibroblasts are unable to differentiate into adipocytes (Chen *et al* 1996). Interestingly, E2F1 has been found to induce PPAR $\gamma$  expression and the absence of E2F also impairs adipogenesis (Fajas *et al* 2002).

### **1.9 Mesenchymal stem cells**

Stem cells are undifferentiated cells from an embryo, foetus or adult that are able to generate differentiated cells when stimulated *in vivo* and *in vitro*. Embryonic and foetal stem cells are pluripotent (able to generate any mesoderm, endoderm or ectoderm cell type) whereas adult stem cells are multipotent (able to generate cells of a limited number of lineages) (described in Csaki *et al* 2007). Adult stem cells have been isolated from peripheral blood (Till and McCulloch 1980), bone marrow (Caplan 1991) and a number of tissues including adipose tissue (Zuk *et al* 2001). Mesenchymal stem cells (MSCs) are cells of the mesenchyme which is derived from mesoderm. The most accessible source of MSCs is bone marrow. MSCs are multipotent cells which can replicate as undifferentiated cells and can differentiate into bone, cartilage, fat, tendon, muscle and bone marrow stroma (described in Pittenger *et al* 1999, reviewed in Kemp *et al* 2005). In a bone marrow culture, MSCs can be identified by adherence to cell culture plates plus the expression of specific markers plus their ability to differentiate

into adipocytes, chondrocytes and osteoblasts in culture (Dominici et al 2006). MSCs can be induced to differentiate specifically into adipocytes, chondrocytes and osteoblasts in culture by the addition of specific pro differentiation factors (Pittenger *et al* 1999). MSCs are of great interest as cell based therapeutic approaches such as tissue engineering to repair damaged tissue (reviewed in Baksh *et al* 2004).

### **1.10 Aims of this project**

The aims of this project were to:

1. Screen genomic DNA samples from patients with a lipodystrophic phenotype for mutation of the *LMNA* gene, and patients with a progeroid phenotype for mutation of both *LMNA* and *ZMPSTE24* genes.
2. Make novel comparisons of nuclear morphology and nuclear protein properties in progeroid syndromes and FPLD by investigation of the localisation and expression and mobility of nuclear proteins in cultured fibroblasts.
3. Gain information about the subcellular localisation of the SREBP1 transcription factor domain and its interaction with lamin A in lipodystrophy.
4. Investigate the effect of the most common FPLD lamin A mutation (R482W) on adipogenic differentiation.

## CHAPTER 2

### Materials and Methods

#### 2.1 General reagents

General chemicals and reagents were supplied by Sigma Aldrich (UK), VWR/BDH (UK) or Fisher Scientific (UK) except those listed in Table 2.1

Reagent	Supplier
Agarose	Bio Gene (UK)
Ampicillin	Melford Laboratories (UK)
Bovine serum albumin	Amersham Pharmacia (UK)
dNTPs	GE Healthcare (UK)
Precision Plus Dual Colour Protein Marker	Bio-Rad (UK)
Glutathione sepharose beads	Amersham Pharmacia (UK)
Hyperladder I DNA Marker	Bioline (UK)
IPTG	Melford Laboratories (UK)
LE agarose	BioWhittaker Molecular Applications (UK)
Long Ranger acrylamide	FMC Bioproducts (USA)
L-[ <sup>35</sup> S] Methionine	GE Healthcare (UK)
Nitrocellulose membrane	Schleicher and Schuell (Germany)
Nonidet P-40	ICL Biomedical Ltd (UK)
Protogel	National Diagnostics (UK)

**Table 2.1** General chemicals and reagents

## 2.2 Polymerase chain reaction (PCR)

The PCR reaction below (and Table 2.2) was used for most applications including amplification of genomic DNA for sequencing. Patient genomic DNA samples were provided by their clinicians for mutation screening (detailed in Section 3.4). For specific PCR, the manufacturer's protocol was followed.

Reagent	Volume
10X PCR Buffer*	1 $\mu$ l
dNTPs (2mM)	1 $\mu$ l
MgCl <sub>2</sub> (15mM)	1 $\mu$ l
Forward primer (5 $\mu$ M)	0.5 $\mu$ l
Reverse primer (5 $\mu$ M)	0.5 $\mu$ l
Taq polymerase	0.1 $\mu$ l
Genomic DNA (50ng) or Plasmid DNA (2ng)	
dH <sub>2</sub> O to final volume of 10 $\mu$ l	

**Table 2.2** Basic PCR reaction mix. \*Composition of the 10X concentrate: 100 mM Tris-HCl (Tris(hydroxymethyl)aminomethane hydrochloride) pH 8.3 at 25 °C, 500 mM KCl, 0.01% gelatin

PCRs were carried out in a Dyad or Tetrad (MJ Research), or G-Storm GS1 Thermocycler (GRI) under the conditions below, then analysed on an agarose gel:

94 °C	1 minute	} 30 cycles
94 °C	30 seconds	
Anneal*	30 seconds	
72 °C	30 seconds	
72 °C	30 seconds	

\*Annealing temperatures varied between 45 °C and 65 °C

### 2.2.1 Agarose gel electrophoresis

Agarose was melted in 1X Tris-borate buffer (TBE) (Table 2.3) to a concentration of 1% (w/v), melted agarose was cooled until it was hand hot then ethidium bromide was added to a final concentration of 50 ng/ml. The gel was allowed to set in a gel-casting tray. Before loading, samples were mixed 1:5 with sucrose loading dye (Table 2.3), and then they were run alongside a 1 kb DNA ladder (Table 2.1). Gels were run in 1X TBE at 100V for approximately 1 hour. DNA bands were visualised under UV (ultraviolet) illumination in a Synegene transilluminator.

Solution	Recipe
6X Sucrose loading dye	35% (w/v) sucrose, 6X TBE, 0.25% (w/v) bromophenol blue, 0.25% (w/v) xylene cyanol
10X Tris-borate buffer (TBE)	0.89M Tris base, 0.89M boric acid, 20mM EDTA-NaOH pH 8

**Table 2.3** Agarose gel electrophoresis reagents

### 2.3 DNA sequencing

Individual exons were amplified by PCR using intronic primers (Tables 2.6 and 2.7). Primers were subsequently removed by digesting with 0.3% (v/v) shrimp alkaline phosphatase (SAP) and 0.1% exonuclease 1 (EXO1), then incubating at 37 °C for 45 minutes, 80 °C for 15 minutes and 4 °C for 2 minutes. DNA was fluorescently labelled using a BigDye Terminator kit (Applied Biosystems (UK)), the fluorescent labelling PCR reaction is shown in Table 2.4.

Reagent	Volume
BigDye Terminator Mix	2 $\mu$ l
Forward or reverse primer (5 $\mu$ M)	0.6 $\mu$ l
Plasmid DNA (200ng) or PCR amplified genomic DNA (1 $\mu$ g)	
dH <sub>2</sub> O to final volume of 10 $\mu$ l	

**Table 2.4** Fluorescent labelling PCR reaction

Fluorescent labelling PCR reactions were carried out under the following conditions:

96 <sup>o</sup> C	10 seconds	} 28 cycles
50 <sup>o</sup> C	5 seconds	
60 <sup>o</sup> C	4 minutes	

Fluorescently labelled DNA was purified using a DyeEx 2.0 Spin Kit (QIAGEN (UK)), according to the manufacturer's instructions. Residual ethanol was removed by evaporation at 70 °C and the dried DNA pellet resuspended in 4  $\mu$ l formamide loading dye (Table 2.5), denatured at 95 °C for 3 minutes then kept on ice. Finally, 1.6  $\mu$ l of sample was loaded onto a 5% acrylamide sequencing gel (Table 2.5) and run in 1X TBE on an ABI PRISM 377 sequencer (Applied Biosystems (UK)). Samples were analysed using SeqEd v1.0.3 software (Applied Biosystems (UK)).

Solution	Recipe
Formamide loading dye	Formamide: 25mM EDTA 5:1, 0.05% (w/v) blue dextran
5% acrylamide sequencing gel	10.8g urea, 3ml Long Ranger acrylamide (FMC Bioproducts), 3ml 10X TBE, 15.6ml dH <sub>2</sub> O, 21 $\mu$ l TEMED, 150 $\mu$ l 10% APS

**Table 2.5** Acrylamide sequencing gel reagents

Exon	Forward (5'-3')	Reverse (5'-3')	T <sub>a</sub> °C	Amplicon size (bp)
1	GCAGCGCTGCCAACCTG	AGGCACGCAGCCACCTG	66	406
2	CAGACTCCTTCTCTTAAATC	CCTAGGTAGAAGAGTGAGTG	54	270
3	GTCTCCTTCAAGTTCCTGTG	GCGAGCTCTGACACAGCTGG	64	379
4	TTGGCCTCCCAGGAACTAAT	GTAAGGGTAGGGCTGCCAAG	62	290
5	GCAGTGATGCCCAACTCAGG	CCTGCGTTCAGCCTGCATC	68	273
6	CTACACCGACCCACGTCCCTC	CCAGAGGACACTGCCAGCAC	66	343
7	GTGCTGGCAGTGTCTCTGG	CCACTCTCTCCCTGATGCAG	64	347
8/9	TCAATTGCAGGCAGGCAGAG	CCTCCGATGTTGGCCATCAG	65	473
10	GTAAGCAGCAGGCCGGACAAAG	CACAGGAATAATCCATGGCATC	64	460
11	GCACAGAACCACACCTTCT	CCTACCCCTCGATGACCAG	67	455
12	AGATGCTACCTCCCTTCTAG	TCCCATGACGTGCAGGGCAG	60	207

**Table 2.6** PCR primers and conditions for amplification of *LMNA* exons from genomic DNA. Primers were designed previously in the laboratory except for exon 1, which are taken from Wolford *et al* 2001. T<sub>a</sub>=annealing temperature, bp=base pairs.

Exon	Forward (5'-3')	Reverse (5'-3')	T <sub>a</sub> °C	Amplicon size (bp)
1	TGCGAAAGAACGGATATTGC	GGGCAAGTTACGAGACTCA	60	330
2	TGGCAAGCTATAAACCATTCG	TTGCTCCACAGCCGTTACTA	52	339
3	AGGCATGAGCCACCGTACTG	CAAATCTTAACATTGGCAGA	64	352
4	TTTTTGAAGGCAGGGATGATA	GCCCCAAGACTTTCAGCTA	52	301
5	TAGTTTCACTGCATGTTAAT	ATACTCCTGTGTCTACAATC	50	402
6	ACTATTTGGGCCTGGGAATAC	CCAAAAGGTAACTCCTAGCC	56	401
7	ATTTTCTAGGAGTCTCTCCAAAGG	GGAGCCATGGTTTTTCATCTG	59	356
8	GCAGTGGTTCAGGGAATGTT	CCTTCTATGCCTGCCATAGT	59	391
9	TTATGGATGCTACTGATCCC	CTATCCTGAAAGCTCTAGAT	56	244
10	TTCTTTTGTCTGCCATTCC	TCAAGAGCTGGAACATGCTG	59	375

**Table 2.7** PCR primers and conditions for amplification of *ZMPSTE24* exons from genomic DNA. T<sub>a</sub>=annealing temperature, bp=base pairs

## 2.4 Digestion of patient genomic DNA to detect LMNA R527H mutations

*LMNA* exon 8/9 was amplified from patient genomic DNA by PCR, alongside DNA from an unaffected control, (Table 4.1) and 2.5 U of the restriction enzyme *RsaI* was added directly to the PCR mix. Samples were incubated at 37 °C for 2 hours then run on an agarose gel and visualised under UV illumination (Section 2.2.1).

## 2.5 DNA cloning

A number of plasmids were produced for this study and are listed in Tables 4.2, 5.1 and 5.2. Restriction enzymes were purchased from New England Biolabs (UK) or Life Technologies Ltd (UK). Solutions used for cloning are given in Table 2.8.

<b>Solution</b>	<b>Recipe</b>
Luria broth (LB) medium	1% (w/v) bactotryptone, 0.5% (w/v) bacto-yeast extract, 0.85M NaCl
Luria broth (LB) agar	LB medium/1.5% (w/v)
Transformation buffer	15mM CaCl <sub>2</sub> , 250mM KCl, 10mM PIPES pH 6.7, 55mM MnCl <sub>2</sub>

**Table 2.8** DNA cloning solutions

### 2.5.1 Digestion of plasmid DNA for cloning

DNA (1.5 µg) was digested with 5U of appropriate restriction enzyme in 5 µl of the appropriate buffer (supplied with the enzyme). dH<sub>2</sub>O was added to a final volume of 50 µl. Digestions were carried out at 37 °C for 1 hour.

### 2.5.2 Gel purification of DNA fragments

For gel purification, bands were visualised and excised from the gel on a Dark Reader (Clare Chemical Research UK) or SynGene Transilluminator. DNA was purified using

a QIAquick Gel Extraction Kit (QIAGEN (UK)) according to the manufacturer's instructions and eluted from columns in 30µl dH<sub>2</sub>O.

### ***2.5.3 Ligation of DNA fragment inserts into plasmid vectors***

DNA was ligated using T4 DNA ligase (New England Biolabs (UK)) in a 10 µl reaction mix (Table 2.9). Reactions were incubated at 16 °C over night.

<b>Reagent</b>	<b>Volume</b>
T4 DNA ligase	1µl
10X ligase buffer (supplied with enzyme)	1µl
Vector and insert DNA in a molar ratio of approximately 1:10	

**Table 2.9** DNA ligation mix

### ***2.5.4 Preparation of competent cells (Inoue et al 1990)***

DH5α *E.coli* were streaked onto an LB agar plate (Table 2.8) and grown at 37 °C overnight. One colony was used to inoculate a 2 ml overnight culture, 0.75 ml of the overnight culture was added to 500 ml LB containing 2.5 ml 2M MgCl<sub>2</sub> and grown at 10 °C with slow shaking to an OD<sub>600</sub> of 0.6. The culture was then cooled on ice and spun down at 2500 g, 0 °C. The rest of the procedure took place in the cold room at 4 °C. The pellet was resuspended in 150 ml ice cold filter sterilised transformation buffer (TB) (Table 2.8), spun again as above and the pellet resuspended in 40 ml TB. Finally, 3 ml dimethyl sulphoxide (DMSO) was added and the cell suspension aliquoted into eppendorf tubes. Aliquots were snap frozen in liquid nitrogen and stored at -80 °C.

### ***2.5.5 Transformation of DNA into DH5 $\alpha$ competent cells***

An aliquot of frozen competent cells was thawed at room temperature then immediately kept on ice. Approximately 50 ng of DNA was added and mixed gently by stirring. Cells were incubated on ice for 30 minutes, at 42 °C for 90 seconds then ice for 5 minutes. Cells were then plated onto LB agar plates containing the appropriate antibiotic for selection (50  $\mu$ g/ml ampicillin or 30  $\mu$ g/ml kanamycin) and grown at 37 °C overnight.

### ***2.5.6 Purification of plasmid DNA by Mini or Midi prep***

Overnight cultures were grown in LB (Table 2.8), plus the appropriate antibiotic, from individual colonies on LB plates following transformation of DNA into competent cells. Glycerol stocks were prepared (Section 2.5.7). Plasmid DNA was purified from the remaining culture using QIAGEN Plasmid Mini or Midi kits according to the manufacturer's protocol (QIAGEN (UK)). Mini prep DNA was eluted from columns in 50  $\mu$ l dH<sub>2</sub>O, midi prep DNA in 200  $\mu$ l.

### ***2.5.7 Glycerol stocks***

Glycerol stocks were prepared by adding 750  $\mu$ l overnight culture to 250  $\mu$ l sterile 80% glycerol (v/v). Stocks were stored at – 80 °C.

### ***2.5.8 Site directed mutagenesis PCR***

*LMNA* mutations were inserted into the pCI neo mammalian expression vector (Promega (UK)) containing the wild type *LMNA* sequence (pCI lamin A WT) which had been previously produced in the laboratory. Mutations were introduced using the GeneTailor Site-Directed Mutagenesis System (Invitrogen (UK)) according to the

manufacturer's instructions. All constructs were sequenced to confirm mutations were present and no PCR errors had been introduced.

### ***2.5.9 Production of T623S and G608G constructs from RNA***

The G608G construct was produced by a student in the laboratory. RNA was extracted from cells using an RNeasy kit (QIAGEN (UK)), according to the manufacturer's protocol. Approximately  $5 \times 10^5$  fibroblast cells were used per extraction. Following extraction, RNA was aliquoted and stored at  $-80^\circ\text{C}$ . (Reverse transcription polymerase chain reaction) RTPCR was performed using SuperScript II reverse transcriptase (Invitrogen (UK)) according to the manufacturer's protocol. PCR products were cloned into TA vector pCR2.1 using an Invitrogen TOPO TA cloning kit according to the protocol and subsequently into pEGFPC1 vector (BD Biosciences Clontech (USA)).

## **2.6 Glutathione-S-transferase pulldown assay**

### ***2.6.1 In-vitro translation (IVT)***

IVTs of emerin, lamin A and SREBP1a constructs (Table 5.2) were prepared using TNT T7 Quick Coupled Transcription/Translation Systems (Promega (UK)). The TNT T7 Master Mix was incubated with L- $^{35}\text{S}$  Methionine and the plasmid DNA template according to the manufacturer's instructions to produce the radiolabeled plasmid.

### ***2.6.2 Pulldown assay***

Glycerol stocks of DH5- $\alpha$  bacteria containing pGEX (GE Healthcare (UK)) constructs were streaked onto LB (Table 2.8) agar plates containing 50  $\mu\text{g/ml}$  ampicillin. Single colonies were used for 5 ml overnight cultures. LB was then inoculated with 1:20 with the overnight culture and shaken at  $30^\circ\text{C}$  for 2 hrs . Isopropyl  $\beta$ -D-1-

thiogalactopyranoside (IPTG) was then added to a final concentration of 0.2 mM and cultures grown for a further 2 hours at 30 °C. Bacteria were pelleted by centrifugation at 3500 g for 15 minutes at 4 °C then stored at -80 °C or used directly.

Bacterial pellets were resuspended in 2 ml Nonidet P-40/EDTA/Tris-HCL/NaCl (NETN) buffer (Table 2.10), sonicated for 3X 15 second bursts of 12 microns in a Soniprep 150 (MSE) then centrifuged at 11000 rpm in a Sorvall RC-5B centrifuge for 10 minutes at 4 °C. Supernatants were added to 40 µl of 50% glutathione sepharose beads and allowed to bind for 1 hour on a Spiramix at 4 °C. Beads were washed 3X in cold NETN by centrifugation at 500 g for 5 minutes and removing supernatants. Fresh NETN (500 µl) was used to transfer beads to eppendorfs. IVT and the protease inhibitor phenylmethylsulfonyl fluoride (PMSF) (1 mM) was added to each sample. Samples were incubated on a rotating wheel for 90 minutes at 4 °C. Following incubation with the IVT, beads were washed 3X, supernatants removed and beads resuspended in Laemmli buffer then boiled. IVT (10% input) was resuspended in Laemmli buffer and boiled. Proteins were separated by SDS-PAGE, gels were then Coomassie stained, destained, dried and the IVT was visualised by autoradiography.

<b>Solution</b>	<b>Recipe</b>
NETN buffer	1mM EDTA pH 8, 20mM Tris HCl pH 8, 100mM NaCl, 1% (v/v) Nonidet P-40, 1mM PMSF
Coomassie stain	40% methanol (v/v), 10% acetic acid (v/v), 0.05% Coomassie blue stain (v/v)
Destain	40% methanol (v/v), 10% acetic acid (v/v)

**Table 2.10** GST pulldown assay reagents

## 2.7 Cell Culture

Patient dermal fibroblast cell lines were obtained from their clinicians or purchased from the Coriell Cell Repository, except human foreskin fibroblasts which were a gift from Dr Katherine Clark (Leicester, UK) (Table 4.1). Mesenchymal stem cells (MSCs) were extracted from bone marrow samples (Table 6.1). Mouse embryonic fibroblast (MEF) cell lines were produced in the laboratory (Table 6.2 and 6.3) except *Lmna* null MEFs and wild type littermate controls which were a gift from Professor Colin Stewart (Maryland, USA). HeLa cells were a gift from Professor Andrew Fry (Leicester, UK), 293T cells were a gift from Dr Emmanuel Debrand (Leicester, UK). Human osteosarcoma cells (U2OS) and 3T3-L1 cells were purchased from the American Type Culture Collection (ATCC). Cell culture reagents and solutions are listed in Tables 2.11 and 2.12.

Reagent	Supplier
Dulbecco's modified Eagle's medium 4500 mg/l glucose	GIBCO, Invitrogen (UK)
Foetal Bovine Serum	GIBCO, Invitrogen (UK)
GlutaMAX	GIBCO, Invitrogen (UK)
Lipofectamine 2000	Invitrogen (UK)
OptiMEM	GIBCO, Invitrogen (UK)
Penicillin-streptomycin	GIBCO, Invitrogen (UK)
Trypsin-EDTA	GIBCO, Invitrogen (UK)
Dimethyl sulfoxide (DMSO)	Sigma-Aldrich (UK)
Basic fibroblast growth factor	Sigma-Aldrich (UK)
Dexamethasone	Sigma-Aldrich (UK)
Methylisobutyl xanthine	Sigma-Aldrich (UK)

Insulin	Sigma-Aldrich (UK)
Troglitazone	Sigma-Aldrich (UK)
RosetteSep Human Mesenchymal Stem Cell Enrichment Cocktail	Stem Cell Technologies (France)
Ficoll-Paque	Stem Cell Technologies (France)

**Table 2.11** General cell culture reagents

Solution	Recipe
10X Phosphate buffered saline (PBS)  (Diluted to 1X working solution before use)	137 mM NaCl, 2.7 mM KCl, 4.3 mM, Na <sub>2</sub> HPO <sub>4</sub> , 1.4 mM KH <sub>2</sub> PO <sub>4</sub>

**Table 2.12** General cell culture solutions

### ***2.7.1 Growth Media and cell culture conditions***

Cells were cultured in 75 or 25 cm<sup>2</sup> tissue culture flasks or 10 cm plates. All cells were grown at 37 °C, 5% CO<sub>2</sub> in Dulbecco's modified Eagle's medium (DMEM) 4500 mg/l glucose with 862 mg/ml Glutamax-I (1-Alanyl-L-Glutamine), 110 mg/l sodium pyruvate, 10% fetal calf serum plus 100 µg/ml streptomycin, 100 units/ml penicillin. In addition, 3 ng/ml basic fibroblast growth factor was added to mesenchymal stem cell growth medium. Medium was changed every 3-4 days.

### ***2.7.2 Subculturing of cells***

Cells were subcultured when they reached 80-90% confluence. Medium was removed and cells washed in autoclaved 1X phosphate buffered saline (PBS), then incubated with 0.05% Trypsin-ethylenediaminetetraacetic acid (EDTA) in 1X PBS for 5 minutes at 37 °C. Detached cells were then washed down the flask in 5 ml fresh medium and centrifuged at 135 g for 5 minutes. The supernatant was aspirated and the cell pellet resuspended in 5-10 ml fresh medium and a proportion transferred to a new flask.

### *2.7.2.1 Cell passage number*

During subculturing, primary human dermal fibroblasts and primary MEF cell lines were always split 1:4 and this split denoted a single passage number. Immortalised cell lines were split 1:10.

### *2.7.3 Thawing and freezing cells*

Cell aliquots recovered from liquid nitrogen were thawed by addition to a vial of warm growth medium then pelleted by centrifugation at 135 g for 5 minutes. The cell pellet was resuspended in 5ml medium and transferred to a 25 cm<sup>2</sup> flask.

Cells were frozen down in 1 ml aliquots. Cells were trypsinised and pelleted (Section 2.7.2). Pellets were resuspended in growth medium containing 5% DMSO and aliquoted into 1 ml tubes. Aliquots were placed in insulated boxes to avoid rapid freezing, then frozen overnight at -80 °C before transferring to liquid nitrogen for long term storage.

### *2.7.4 Seeding cells*

Cells were seeded for a number of experiments. First, cells were counted using a haemocytometer (BS 748 Hawksley UK). The number of cells per ml was calculated using the equation below and seeded in the amounts of  $2 \times 10^5$  U2OS, HeLa, 3T3L1 or MEF cells,  $3 \times 10^4$  dermal fibroblasts or M SC per 3 c m plate with fresh growth medium.

$$\text{Cells/ml} = \frac{\text{Total number of cells counted}}{\text{Number of 4X4 grids}} \times 10^4$$

### ***2.7.5 Transient transfection***

Cells were transfected at 80-90% confluence using Lipofectamine 2000 transfection reagent according to the manufacturer's instructions. For 3cm dishes containing 2 ml growth medium, 3  $\mu$ l of Lipofectamine 2000 was incubated in 100  $\mu$ l Optimem for 5 minutes, the solution was then added to 1  $\mu$ g plasmid DNA and incubated for a further 20 minutes before adding to cells. Transfection reagent volumes were adjusted according to the volume of growth medium.

### ***2.7.6 Amaxa Nucleofection of dermal fibroblasts and MEFs***

Lipofectamine transfection of dermal fibroblasts and MEFs resulted in very low transfection rates, these cells were nucleofected to try to improve the uptake of plasmid DNA. A total of  $5 \times 10^5$  sub-confluent cells were used per nucleofection. Cells were trypsinised and pelleted (Section 2.7.2), then resuspended in nucleofection solution and nucleofected with 2  $\mu$ g plasmid DNA in an Amaxa nucleofector device (Lonza) using program U-23 according to the manufacturer's instructions. Immediately after nucleofection, warm growth medium was added to cells and the sample transferred onto a coverslip in a tissue culture dish for subsequent use.

### ***2.7.7 LentiViral transduction***

LentiViral transduction was performed following the 'Tronolab' protocol, published on Lentiweb.com.

Day 1:  $2.5 \times 10^6$  293T cells were seeded onto a 10 cm plate, 6 ml growth medium was added.

Day 2: A calcium phosphate transfection precipitate was prepared and added to cells: 20 µg expression vector, 15 µg packaging plasmid and 6 µg envelope plasmid were added to an eppendorf tube, 0.5 ml dH<sub>2</sub>O was added and 0.5 ml 2X 4-(2-hydroxyethyl)-1-piperazineethanesulfonic acid (HEPES) buffered saline (HBS), the solution was mixed, 50 µl 2.5M CaCl<sub>2</sub> was added and the tube shaken then incubated at room temperature for 20 minutes before adding drop wise to the plate and mixing gently. Growth medium was changed after 6 hours.

Day 4: Growth medium was harvested, filtered and used directly to transduce cells. Each batch of virus should be tested to obtain optimal transduction, in this study, virus was diluted 1:256 in growth medium.

Solution	Recipe
2X 4-(2-hydroxyethyl)-1-piperazineethanesulfonic acid (HEPES) buffered saline (HBS) buffer	8 g NaCl, 0.38 g KCl, 0.1 g Na <sub>2</sub> HPO <sub>4</sub> , 5 g HEPES, 1 g glucose, pH to 7.05, make up to 500 ml with dH <sub>2</sub> O

**Table 2.13** LentiViral transduction solutions

## 2.7.8 Production of cell extracts

### 2.7.8.1 Whole cell extracts

Cells were trypsinised, pelleted and resuspended in 1 ml cold PBS containing 1 mM PMSF and transferred to eppendorf tubes. Cells were pelleted again and pellets resuspended in an appropriate volume of PBS. An equal volume of Laemmli buffer was added to samples before boiling and running on an SDS-polyacrylamide gel (Section 2.9.1).

### 2.7.8.2 Nuclear and cytoplasmic cell extracts

Cells were kept on ice throughout this procedure. Cells were pelleted (as described in Section 2.7.2) then resuspended in 200  $\mu$ l ice cold HEPES, MgCl<sub>2</sub>, NaCl (HMN) buffer for 30 minutes, cells were homogenised using a tight Dounce homogeniser 100 X then spun at 2000 g, 4 °C for 20 minutes. Following centrifugation, the top 100  $\mu$ l was removed, this is the cytoplasmic fraction. The remaining supernatant was discarded and the pellet resuspended in 200  $\mu$ l cold 1X phosphate buffered saline (PBS) containing 1 mM phenylmethylsulphonyl fluoride (PMSF) and spun as before. The supernatant was then removed and the pellet resuspended in 200  $\mu$ l HMN buffer, this is the nuclear fraction. Both fractions were resuspended in an equal volume of Laemmli buffer and boiled for 5 minutes before use.

Solution	Recipe
HEPES, MgCl <sub>2</sub> , NaCl (HMN) buffer	10 $\mu$ l 1M HEPES pH 7.4, 2 $\mu$ l 1M MgCl <sub>2</sub> , 2 $\mu$ l 5M NaCl, 10 $\mu$ l 100 mM PMSF, 50 $\mu$ l 10% NP40, 200 $\mu$ l 40% sucrose, make up to 1 ml with dH <sub>2</sub> O

**Table 2.14** Nuclear and cytoplasmic cell extracts buffer

### 2.7.9 Extraction of MSCs from bone marrow

Bone marrow samples volumes were between 2 and 5 ml. RosetteSep Human Mesenchymal Stem Cell Enrichment Cocktail was used according to the protocol to select away unwanted cells. The sample was then spun through Ficoll-Paque and the MSC enriched cell layer removed for culture. Cells were added to 10 ml growth medium in a small tissue culture flask and left untouched for 7 days to allow adherence to the flask. Subsequently, cells were cultured as described (Section 2.7.1 and 2.7.2).

### ***2.7.10 Adipocyte fixation and staining***

Following adipogenic conversion (Section 6.3 for 3T3L1, 6.4.5.1 for MSCs) cells were fixed in 10% formalin at room temperature for 20 minutes, then washed twice for 2 minutes in 1X phosphate buffered saline (PBS) (Table 2.12). Lipid droplets were stained by incubation in a solution of 0.5% oil-red-o (v/v) in isopropanol for 15 minutes, and then washed twice for 2 minutes in dH<sub>2</sub>O. For cell imaging on a light microscope, cells were overlaid with 1X PBS.

#### ***2.7.10.1 Semi-quantitative analysis of oil-red-o staining***

To compare adipogenic conversion of cell lines, following incubation in 0.5% oil-red-o in isopropanol, cells were washed in dH<sub>2</sub>O, then stain was eluted in 100% isopropanol (250 µl for a 6 cm dish) for 15 minutes. The OD<sub>520</sub> of eluted stain was measured.

## **2.8 Microscopy**

### ***2.8.1 Indirect Immunofluorescence microscopy***

Growth medium was removed and cells on coverslips washed twice in 1X phosphate buffered saline (PBS) (Table 2.12). Cells were then fixed in methanol for at least 10 minutes at -20 °C and washed 3 X in 1X PBS. Cells were blocked in 1% Bovine Serum Albumen (BSA) (v/v) in 1X PBS for half an hour to block non-specific antibody binding before incubating for 1 hour with a primary antibody (Table 2.15) diluted in 3% BSA (v/v) in 1X PBS. Cells were incubated for 1 hour with the appropriate secondary antibody (table 2.16) and in most cases Hoechst or 4',6-diamidino-2-phenylindole dihydrochloride (DAPI) were added to stain DNA according to the manufacturer's protocol. Cells were washed for 4 X 5 minutes in 1X PBS after each antibody

incubation. Coverslips were mounted upside down onto microscope slides with one drop of mounting medium, edges were sealed with clear nail varnish to prevent drying and slides were stored in the dark at 4 °C. Cells were viewed and photographed with a Nikon TE300 inverted microscope using an ORCA ER charge couple device camera (Hamamatsu) and Openlab 7 software (Improvision).

<b>Antibody</b>	<b>Dilution</b>	<b>Supplier</b>
β-actin (mouse)	1:5000	Sigma-Aldrich
Emerin AP8 (rabbit)	1:500	Gift from Dr Juliette Ellis, London, UK
GFP (mouse)	1:1000	Abcam
HP1γ (mouse)	1:1000	Neomarkers
Ki67 (rabbit)	1:200	Neomarkers
Lamin A/C (mouse)	1:100	Chemicon
Lamin A/C 6215 (goat)	1:500	SantaCruz biotechnology
Lamin B1 6217 (goat)	1:500	SantaCruz biotechnology
LAP2α (rabbit)	1:1000	ImmuQuest
Myc (mouse)	1:500	Zymed
Prelamin A (goat)	1:100	SantaCruz biotechnology
Retinoblastoma protein (mouse)	1:100	SantaCruz biotechnology
SREBP1 H160 (rabbit)	1:100	SantaCruz biotechnology
α-tubulin (mouse)	1:2000	Sigma-Aldrich

**Table 2.15** Primary antibodies for indirect immunofluorescence microscopy (IF)

<b>Antibody</b>	<b>Dilution</b>	<b>Supplier</b>
Alexa Fluor 488 rabbit anti-mouse	1:200	Molecular Probes (UK)
Alexa Fluor 594 donkey anti-rabbit	1:500	Molecular Probes (UK)
Alexa Fluor 594 donkey anti-goat	1:500	Molecular Probes (UK)

**Table 2.16** Secondary antibodies for indirect immunofluorescence microscopy (IF)

<b>DNA stain</b>	<b>Supplier</b>
Hoechst	Sigma-Aldrich (UK)
4',6-diamidino-2-phenylindole dihydrochloride (DAPI)	Sigma-Aldrich (UK)

**Table 2.17** DNA stain for indirect immunofluorescence microscopy (IF)

<b>Solution</b>	<b>Recipe</b>
Mounting Medium	3% (v/v) n-propyl gallate, 80% (v/v) glycerol

**Table 2.18** Immunofluorescence microscopy solutions

### ***2.8.2 Coverslip preparation***

Coverslips were acid treated to enhance cell adherence by incubating in 1M HCl for 30 minutes and rinsing with distilled water. They were then washed in 100% ethanol for 30 minutes, dried on 3MM Whatman paper and baked at 160 °C.

### ***2.8.3 Fluorescence recovery after photobleaching (FRAP) SREBP1 mobility study***

Dermal fibroblasts were seeded onto La Con 42 mm coverslips and transfected with the GFP-tagged SREBP1a1-487 construct using a dermal fibroblast nucleofector kit and an Amaxa nucleofector device (Lonza). FRAP was performed on a n Axiovert 100M inverted microscope using an LSM 510 laser scanning confocal unit (Zeiss) and analysed using LSM 510 software . Cells were maintained in culture medium at 37 °C and supplied with CO<sub>2</sub>. Regions of interest of 5 µm by 5 µm were bleached with an

argon 488 laser; after bleaching images were taken at one second intervals for 30 seconds.

#### ***2.8.4 Fluorescence recovery after photobleaching (FRAP) lamin A mutant mobility study***

HeLa cells were seeded onto LaCon 42 mm coverslips and transfected with GFP-tagged lamin A constructs 24 hours later using Lipofectamine 2000. For live imaging, cells were maintained in culture medium at 37 °C and supplied with CO<sub>2</sub>. Photobleaching was performed using a Leica TCS SP5 confocal microscope and analysed with Leica LAS AF software. Regions of interest of 5 µm by 2 µm were bleached with an argon laser and 6 images were obtained after bleaching at 5 minute intervals for 30 minutes.

### **2.9 Protein methods**

#### ***2.9.1 Sodium dodecyl sulphate-polyacrylamide gel electrophoresis (SDS-PAGE)***

SDS-PAGE gels were poured using Protean III casting apparatus (BioRad (UK)) according to the manufacturer's instructions. Solutions and gels were prepared as listed in Tables 2.19 and 2.20. A 3% stacking gel was used on top of the separating gel. Samples in Laemmli buffer (20 µl) were boiled for 3 minutes then loaded onto the gel alongside the Precision Plus Dual Colour Protein Marker (BioRad (UK)). Gels were run in 400 ml 1X gel running buffer at 150V for approximately 1 hour.

<b>Stacking gel</b>	<b>3% (v/v) Acrylamide</b>		
Protogel* (Flowgen)	325 $\mu$ l		
Upper buffer	625 $\mu$ l		
Water	1.5ml		
10% APS	75 $\mu$ l		
TEMED	5 $\mu$ l		
<b>Separating gel</b>	<b>7.5% (v/v) Acrylamide</b>	<b>10% (v/v) Acrylamide</b>	<b>12% (v/v) Acrylamide</b>
Protogel* (Flowgen)	1.5 ml	2 ml	2.4 ml
Lower buffer	1.5 ml	1.5 ml	1.5 ml
Water	3 ml	2.5 ml	2.1 ml
10% APS	75 $\mu$ l	75 $\mu$ l	75 $\mu$ l
TEMED	5 $\mu$ l	5 $\mu$ l	5 $\mu$ l

**Table 2.19** SDS-PAGE gel reagents \*Protogel: 30% acrylamide/0.8% bis-acrylamide

<b>Solution</b>	<b>Recipe</b>
Leammi buffer	62.5mM Tris-HCl pH 6.8, 5% (v/v) B-mercaptoethanol, 2% (w/v) SDS, 10% (v/v) glycerol, 0.2% (w/v) bromophenol blue
10 X SDS-PAGE running buffer	250mM Tris, 1.92M glycine, 1 % SDS, to 1 litre with dH <sub>2</sub> O
Upper SDS-PAGE buffer	1.5 M Tris-HCl pH 8.8, 0.4% (w/v) SDS
Lower SDS-PAGE buffer	1.5 M Tris-HCl pH 6.8, 0.4% (w/v) SDS
Transfer buffer	25mM Tris, 192mM glycine, 20% (v/v) methanol fresh before use

**Table 2.20** SDS-PAGE solutions

### ***2.9.2 Western blotting***

Proteins separated by SDS-PAGE (Section 2.9.1) were transferred onto nitrocellulose transfer membranes. Membranes cut to 6 X 9 cm in size were soaked in transfer buffer for 10 minutes. Gels were placed onto membranes and sandwiched between 6 layers of 3 MM Whatman paper soaked in transfer buffer. Proteins were transferred to membranes using a Hoefer SemiPhor semi-dry transfer unit according to the manufacturer's instructions and run at 1mA per cm<sup>2</sup> for 1 hour. The membrane was then washed briefly in water, stained using Ponceau S (Table 2.21) to visualise proteins, washed again briefly in water to remove excess stain and allowed to dry.

Membranes were blocked in 5% dried skimmed milk (v/v) in 1X phosphate buffered saline 0.1% (v/v) Tween 20 (PBST) (Table 2.21) for 30 minutes then probed by incubating (with agitation) for 1 hour with primary antibodies (Table 2.22) diluted in 2 ml 5% dried skimmed milk (v/v) in 1X PBST. Membranes were given 4 washes in 1X PBST for 5 minutes each, then membranes were incubated for 1 hour with a secondary antibody (Table 2.23) diluted in 2 ml 1X PBST plus 5% milk and then washed 4X.

Proteins were detected using the ECL Plus Western Blotting Detection System (Amersham Biosciences UK) or EZ-ECL (Geneflow) according to the manufacturer's instructions. Following exposure to ECL reagents, membranes were wrapped in cling film and exposed to photographic film for between 10 seconds and 10 minutes as required. Films were developed using a Xograph Compact X4 imaging system.

<b>Solution</b>	<b>Recipe</b>
Ponceau S stain	0.1 % (w/v) Ponceau S, 5 % (v/v) acetic acid in dH <sub>2</sub> O
Phosphate buffered saline/Tween 20 (PBST)	1X phosphate buffered saline (Table 2.12) 0.1% (v/v) Tween 20

**Table 2.21** Western blotting solutions

<b>Antibody</b>	<b>Dilution</b>	<b>Supplier</b>
$\alpha$ -tubulin	1:5000	Sigma-Aldrich (UK)
$\beta$ -actin	1:5000	Sigma-Aldrich (UK)
$\beta$ -catenin (mouse)	1:2000	BD Pharmingen (Europe)
Active $\beta$ -catenin (mouse)	1:500	Millipore (UK)
Emerin AP8 (rabbit)	1:3000	Gift from Dr Juliette Ellis, London, UK
GAPDH (mouse)	1:5000	Sigma-Aldrich (UK)
GFP (mouse)	1:8000	Abcam (UK)
Lamin A/C (mouse)	1:100	Chemicon (UK)
Lamin A/C 6215 (goat)	1:1000	SantaCruz biotechnology (Europe)
Lamin B1 6217 (goat)	1:500	SantaCruz biotechnology (Europe)
LAP2 $\alpha$ (rabbit)	1:2500	ImmuQuest (UK)
Myc (mouse)	1:500	Zymed (UK)
Prelamin A (goat)	1:100	SantaCruz biotechnology (Europe)
Retinoblastoma protein (mouse)	1:400	BD Pharmingen (Europe)
SREBP1 H160 (rabbit)	1:400	SantaCruz biotechnology (Europe)

**Table 2.22** Primary antibodies for western blotting (WB)

<b>Antibody</b>	<b>Dilution</b>	<b>Supplier</b>
Anti-rabbit HRP	1:3000	Sigma-Aldrich (UK)
Anti-mouse HRP	1:6000	Sigma-Aldrich (UK)
Anti-goat HRP	1:5000	Sigma-Aldrich (UK)

**Table 2.23** Secondary antibodies for western blotting (WB)

## CHAPTER 3

### Detection of mutations in *LMNA* and *ZMPSTE24* genes

#### 3.1 Introduction

Laminopathies are rare tissue specific diseases caused by the mutation of nuclear A- or B-type lamins or their binding partners. Laminopathies include cardiomyopathies, muscular dystrophies, a neuropathy, lipodystrophy and progeroid syndromes and are described in Section 1.5. Patients investigated in this study had either lipodystrophic or progeroid phenotypes.

Familial partial lipodystrophy, Dunnigan variety (FPLD) (described in Section 1.7) results from mutation of the *LMNA* gene (Shackleton *et al* 2000, Speckman *et al* 2000, Cao and Hegele 2000). Abnormal adipose tissue distribution in this disorder involves loss of fat from the extremities and trunk, with excess accumulation in the face and neck, leading to metabolic disorders such as diabetes mellitus, hypertriglyceridemia and atherosclerosis (reviewed in Garg 2000). The pattern of adipose tissue distribution is consistent among FPLD patients, although disease severity varies significantly between individuals (Garg *et al* 2001, Vigouroux *et al* 2000).

Progeroid, or premature ageing, laminopathies result from mutation of the *LMNA* gene (reviewed Worman and Bonne 2007) or from mutation of the *ZMPSTE24* gene (Agarwal *et al* 2003, Novarro *et al* 2005) and are described Section 1.6. Progeroid laminopathies include the disorders, Mandibuloacral dysplasia (MAD), atypical Hutchison-Gilford progeria syndrome (HGPS), classical HGPS and restrictive dermopathy (RD). These disorders have overlapping features such that they appear to

form a spectrum of severity with MAD at the least severe end of the spectrum and RD at the most severe (Figure 3.1)

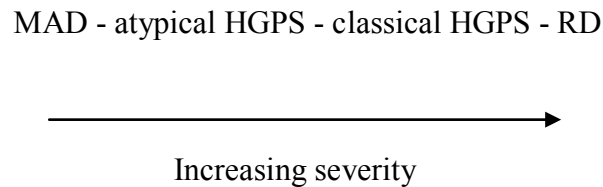


**Figure 3.1** Overlapping features of the progeroid laminopathies appear to form a spectrum of severity

The best characterised progeroid laminopathy is classical Hutchison-Gilford progeria syndrome (HGPS), which is caused by autosomal dominant (AD) mutation of the *LMNA* gene resulting in a splicing defect (De Sandre-Giovannoli *et al* 2003, Eriksson *et al* 2003). Age of disease onset is around 1 year and symptoms include impaired growth, alopecia, lipodystrophy, joint stiffness, osteolysis, micrognathia, prominent forehead and eyes and glyphic nose. Death from atherosclerosis usually occurs in the teens (described in Section 1.6.1). Atypical HGPS involves a variable phenotype which usually results from AD point mutation of the *LMNA* gene, a number of different point mutations and a splicing defect have been reported (Table 1.2). Atypical HGPS patients exhibit a milder, later onset form of progeria where some or all of the features of classical HGPS develop more slowly (described in Section 1.6.4). Mandibuloacral dysplasia (MAD) involves a phenotype which overlaps with classical HGPS but disease onset is later and disease progression slower with more pronounced skeletal damage (described in Section 1.6.3). MAD is usually caused by autosomal recessive (AR) *LMNA* mutation, most commonly R527H (Novelli *et al* 2002), but has also been found

to result from AR *ZMPSTE24* mutation (Agarwal *et al* 2003, Agarwal *et al* 2006). Restrictive dermopathy (RD) is the most severe reported form of lamin A-related progeria. This lethal neonatal disorder is characterised by thin, tight skin and shares aspects of classical HGPS such as, growth retardation and micrognathia. Liveborn babies usually die from respiratory failure in the first week of life (described in Section 1.6.2). RD results from homozygous or compound heterozygous mutation of *ZMPSTE24* (Agarwal *et al* 2003, Navarro *et al* 2005).

Patients involved in this study had been clinically diagnosed with progeroid or lipodystrophic disorders, however, the rarity of these disorders and variation in patient phenotypes can make clinical diagnosis difficult. Identification of causative mutations can be very helpful to both clinician and patient by allowing more accurate diagnosis, prognosis and perhaps appropriate treatment. Mutation detection also aids genetic counselling for families.

### 3.2 Aim of the study

The aim of this study was to screen genomic DNA samples from patients with a lipodystrophic phenotype for mutation of the *LMNA* gene, and patients with a progeroid phenotype for mutation of both *LMNA* and *ZMPSTE24* genes. Genomic DNA samples from the patients were provided by their clinicians for mutational screening. The first pathogenic *LMNA* mutation was found in 1999 and new mutations are still being reported, therefore screening also provides the possibility of finding novel mutations.

### 3.3 Methods of mutation detection

The basic mutation detection strategy involved direct sequencing of all 12 exons of the *LMNA* gene and when appropriate the *ZMPSTE24* gene was also sequenced. In progeroid patients where a clinical diagnosis or description of the phenotype was provided by the clinician, this information was compared to the literature to identify candidate mutations likely to cause the phenotype. Exons containing likely mutations were sequenced first. In patients with a lipodystrophy phenotype, for example, *LMNA* exon 8 was sequenced first because FPLD mutations are clustered in this exon (Shackleton *et al* 2000, Cao and Hegele 2000). Mutation hotspots for lipodystrophy and progeroid laminopathies are listed in Table 3.1.

Disease	Most common causative mutation					
	Inheritance	Gene	Exon	DNA	Protein	Reference
FPLD	<i>AD</i>	<i>LMNA</i>	8	c.1444C>T	p.R482W	Shackleton <i>et al</i> 2000
Classical HGPS	<i>AD</i>	<i>LMNA</i>	11	c.1824C>T	p.G608G	Eriksson <i>et al</i> 2003
MAD	<i>AR</i>	<i>LMNA</i>	9	c.1580G>A	p.R527H	Novelli <i>et al</i> 2002
RD	<i>AR</i>	<i>ZMPSTE24</i>	9	c.1085_1086insT	p.Leu362PhefsX19	Navarro <i>et al</i> 2004

**Table 3.1** Most common causative mutations of FPLD and progeroid laminopathies. (*AD* autosomal dominant, *AR* autosomal recessive.)

If the most common causative mutations were not present, the whole *LMNA* gene was sequenced. Where no *LMNA* mutation was found, sequencing of the *ZMPSTE24* gene was undertaken in patients with a progeroid phenotype.

### ***3.3.1 Design of PCR primers***

Primers for the amplification of individual *LMNA* exons were designed previously (Shackleton *et al* 2000) except for exon 1 primers, which were taken from Wolford *et al* (2001). Primer binding sites were located in introns to allow sequencing of intron-exon boundaries as well as coding sequence. Primers were designed to amplify *LMNA* exons 8 and 9 as one amplicon since they are short in length, containing 108 and 120 base pairs respectively with an intron of 84 base pairs between them. Primers for the amplification of *ZMPSTE24* exons were designed using Custom Primers - OligoPerfect Designer (Invitrogen). Optimal annealing temperatures for primer pairs were obtained by gradient PCR using a temperature gradient from 50-65 °C set up across the block in an MJ Research Dyad PCR machine. Primer sequences, annealing temperatures and amplicon sizes are given in Tables 2.4 and 2.5.

### ***3.3.2 Direct sequencing of coding exons***

Individual exons or exon pairs were amplified by PCR, then DNA was fluorescently labelled and samples were run on acrylamide sequencing gels (Section 2.3).

### ***3.3.3 Disruption of an *RsaI* restriction enzyme site in MAD***

The most common causative mutation in MAD is *LMNA* R527H (CGT>CAT) which disrupts an *RsaI* restriction enzyme site (GTAC) in exon 9. Patients with a MAD phenotype were tested for the R527H mutation by performing an *RsaI* restriction digest

on the PCR amplicon containing exons 8 and 9 (Section 2.4). If the mutation is absent, the restriction site is intact and DNA is cut into fragments of 383 and 90 base pairs. If the mutation is present, the site is destroyed and DNA remains uncut (Figure 3.2).

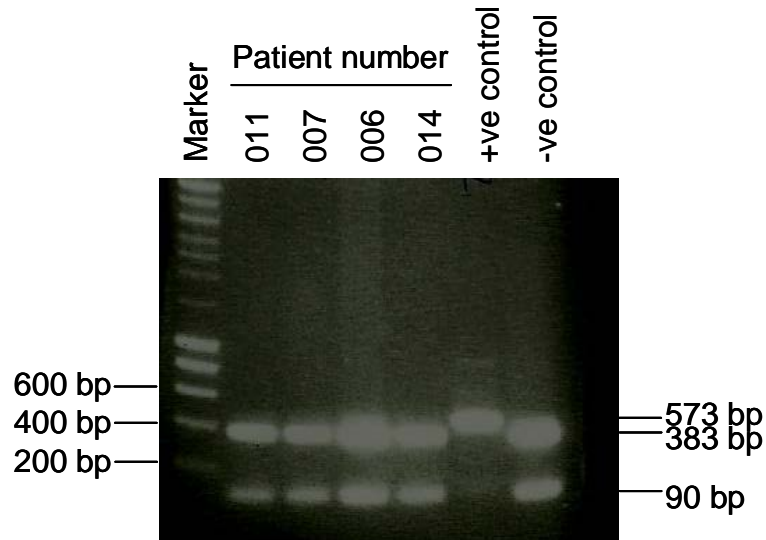


**Figure 3.2** *RsaI* restriction digest allows detection of the MAD mutation R527H in the *LMNA* gene. Positive (+ve) control (R527H mutation present) shows disrupted *RsaI* site: 573 base pair (bp) band of uncut exon 8/9 amplicon. Negative (-ve) control shows intact *RsaI* site: 573bp exon 8/9 amplicon cut into 383bp plus 90bp bands. Four patient samples shown are negative for the R527H mutation.

### 3.4 Patient population

Genomic DNA samples from 11 patients with progeroid phenotypes were obtained from clinicians Dr. L. Wilson and Prof. P. Clayton at Great Ormond Street Hospital, London. Samples from 3 patients with a lipodystrophic phenotype were obtained from clinicians Dr. S. Ball, Dr. L. Brueton and Prof. R. Trembath. Clinical diagnoses of patients screened and mutations detected are shown in Table 3.2.

### ***3.4.1 Patient clinical information***

Clinical information was available for some of the patients in this study and is detailed in this section. For some patients a description of the phenotype was included by their clinician, for others information was scant. For patients not listed below, all available information is contained in Table 3.2.

#### *3.4.1.1 Patient 002*

This patient was diagnosed with atypical partial lipodystrophy involving the face and neck, upper limbs and upper trunk; lower limbs were unaffected. She also had dyslipidaemia, hypertension, hyperandrogenism and growth acceleration.

#### *3.4.1.2 Patient 004*

Patient 004 was initially diagnosed with possible Ehlers-Damlos syndrome, a connective tissue disorder. This was later changed to atypical progeria when she developed a mild, late onset progeria phenotype. She was born to healthy unrelated parents and appeared healthy until there was a progressive change in her appearance from 4 years of age. Her lower face appeared smaller as she became older, she had fine hair, thin brittle nails, dry skin, lipodystrophy, joint stiffness, dental crowding and delayed secondary dentition. Onset of menses was normal but breast development was absent. At the time of screening the patient was 15 years of age and showed no evidence of osteolysis or cardiac defects. Clinical pictures of patient 004 are shown in Figure 3.3.

#### *3.4.1.3 Patient 005*

Patient 005 had a classical progeroid phenotype. This phenotype is described in Section 1.6.1. Clinical pictures of patient 005 are shown in Figure 3.4.

Patient	Year of birth	Age at sampling	Clinical diagnosis	Gene(s) sequenced	Result of LMNA and ZMPSTE24 mutation screening	Exonic SNPs detected
001	1965	38 years	Lipodystrophy	<i>LMNA</i>	–	–
002	1972	32 years	Atypical partial lipodystrophy	<i>LMNA</i>	–	Heterozygous LMNA p.S51S c.261C>T
003	1973	28 years	Abnormal fat distribution	<i>LMNA</i>	–	Heterozygous LMNA p.H566H c.1908C>T
004	1989	15 years	Progeria	<i>LMNA</i>	Heterozygous LMNA p.T623S c.1868 C>G	Whole LMNA gene not sequenced
005	1993	11 years	Progeria	<i>LMNA</i>	Heterozygous LMNA p.G608G c.1824 C>T	Whole LMNA gene not sequenced
006	1994	10 years	MAD	<i>LMNA</i> <i>ZMPSTE24</i>	–	Heterozygous LMNA p.H566H c.1908C>T
007	1995	11 years	Progeria	<i>LMNA</i> <i>ZMPSTE24</i>	–	Heterozygous ZMPSTE24 p.D117D c.816T>C
008	1996	8 years	Short stature, small jaw, calcinosis	<i>LMNA</i> <i>ZMPSTE24</i>	–	Homozygous LMNA p.H566H c.1908C>T
009	1997	7 years	SHORT syndrome	<i>LMNA</i> <i>ZMPSTE24</i>	–	Heterozygous LMNA p.D446D c.1549T>C
010	1999	5 years	MAD or progeria	<i>LMNA</i> <i>ZMPSTE24</i>	–	Heterozygous LMNA p.H566H c.1908C>T
011	1999	5 years	Wiedermann-Rautenstrauch syndrome	<i>LMNA</i> <i>ZMPSTE24</i>	–	Heterozygous LMNA p.H566H c.1908C>T
012	2000	2 years	Progeria	<i>LMNA</i> <i>ZMPSTE24</i>	Compound heterozygous ZMPSTE24 c.1085_1086insT p. Leu362PhefsX19 c.794 A>G pN265S	None detected in LMNA ZMPSTE24 sequenced in laboratory of A. Garg
013	2003	1 year	Progeria	<i>LMNA</i>	Heterozygous LMNA p.G608G c.1824 C>T	Whole LMNA gene not sequenced
014	2006	5 years	Laminopathy	<i>LMNA</i> <i>ZMPSTE24</i>	–	–

**Table 3.2** Results of mutation screening showing pathogenic mutations identified and SNPs detected, - indicates no mutation or no SNP found. Standard mutation nomenclature has been used (described by Ogino *et al* 2007). ‘Age at sampling’ refers to the age of the patient when a blood sample was taken for DNA extraction. Clinical diagnoses were made before mutation screening.

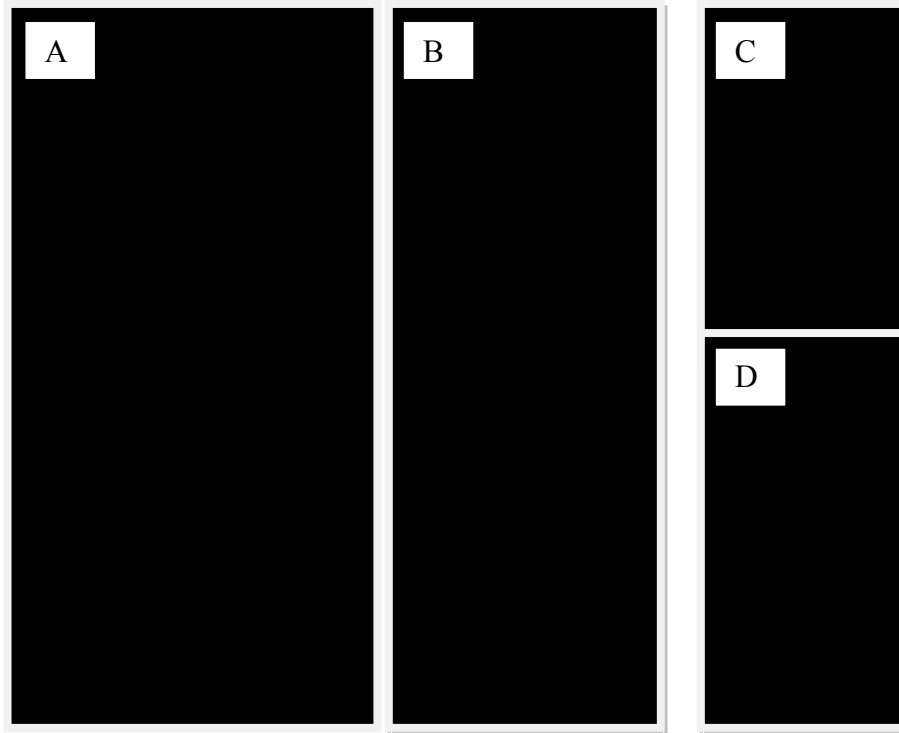


**Figure 3.3** Images removed to protect confidentiality. Clinical features observed in patient 004 aged 17 years. (A) thin, fine hair, (B) lipodystrophy of the legs, (C) and (D) dystrophic fingers and toes.

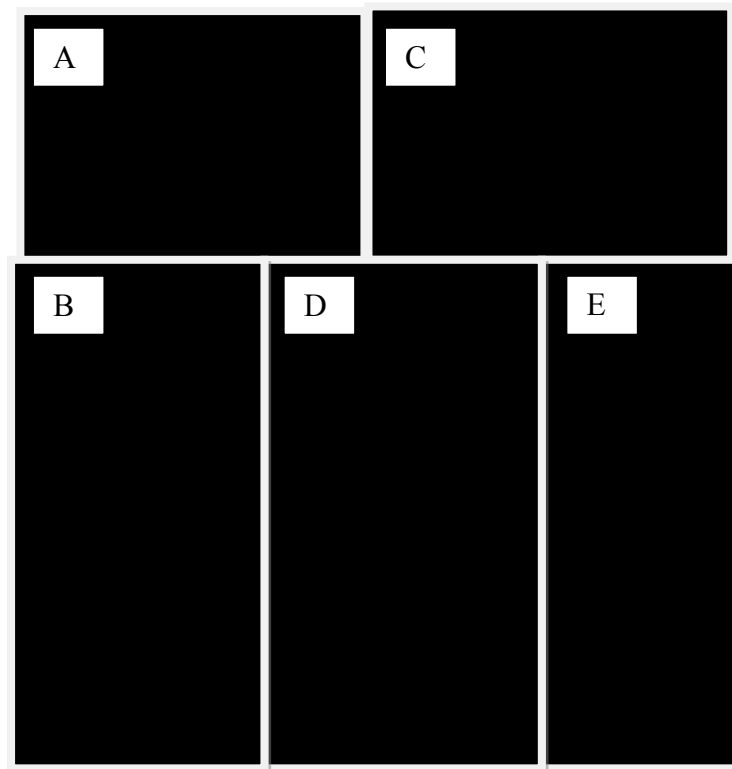


**Figure 3.4** Images removed to protect confidentiality. Clinical features observed in patient 005. Abnormal, shiny, indurated and inelastic skin at age 10 months, on (a) the abdomen, and (b) lower part of the back. (c) Irregular bumps on the buttocks at the age of 9 months. (d) Extension of sclerodermatous skin to the legs at the age of 18 months with increased visibility of the veins. (e) Appearance of a horse-riding stance. Taken from Mazereeuw-Hautier *et al* 2007.

#### 3.4.1.4 Patient 006

A diagnosis of MAD was considered for patient 006, the MAD phenotype is described in Section 1.6.3. She had abnormal toes and short distal phalanges; ventricular arrhythmia was diagnosed at age 7 years. She had no skeletal abnormalities, lipodystrophy or muscle weakness.

#### 3.4.1.5 Patient 009

Patient 009 had micrognathia, a small pinched beak nose, large sunken eyes, prominent forehead, delayed dentition, anterior segment dysgenesis and low height and weight. He was said to have a progeroid appearance and had been diagnosed with SHORT syndrome. SHORT syndrome is an acronym for short stature, joint hyperextensibility or hernia, ocular depression, Reiger anomaly (defects in the iris and anterior peripheral segment of the eye), delayed teething) (Gorlin *et al* 1975). In addition, the syndrome involves lipoatrophy or partial lipodystrophy, slow weight gain, delayed speech, wide nasal bridge and micrognathia (reviewed in Schwingshandl *et al* 1993). The genetic basis of SHORT syndrome is not yet known.

#### 3.4.1.6 Patient 011

Patient 011 was diagnosed with Wiedemann-Rautenstrauch syndrome. She was described as very small and had progressive joint contractures. Wiedemann-Rautenstrauch syndrome is a neonatal progeroid disorder. Phenotypic features are a large head, aged triangular face, wrinkled skin, natal teeth and micrognathia, generalised lipoatrophy, and lack of hair, eyebrows and eye lashes. The average age of death is 7 months, but there is much variation and children can live into their teens. The causative gene is not yet known.

death is 7 months, but there is much variation and children can live into their teens. The causative gene is not yet known.

#### *3.4.1.7 Patient 012*

Patient 012 was born to healthy unrelated parents and showed features of MAD, HGPS and RD. She was clinically diagnosed with HGPS. Clinical features included poor weight gain, lipodystrophy of the lower limbs and dry, shiny, tight skin over the abdomen, trunk and lower limbs causing stiffness of joints and restricted movement. Radiology revealed a small under developed mandible, osteolysis of fingertips and both clavicles and a thin skull with Wormian bones. Following the breakdown of large areas of sclerotic skin, she developed respiratory failure and died at 2 years 9 months. Clinical pictures of patient 012 are shown in Figure 3.5.

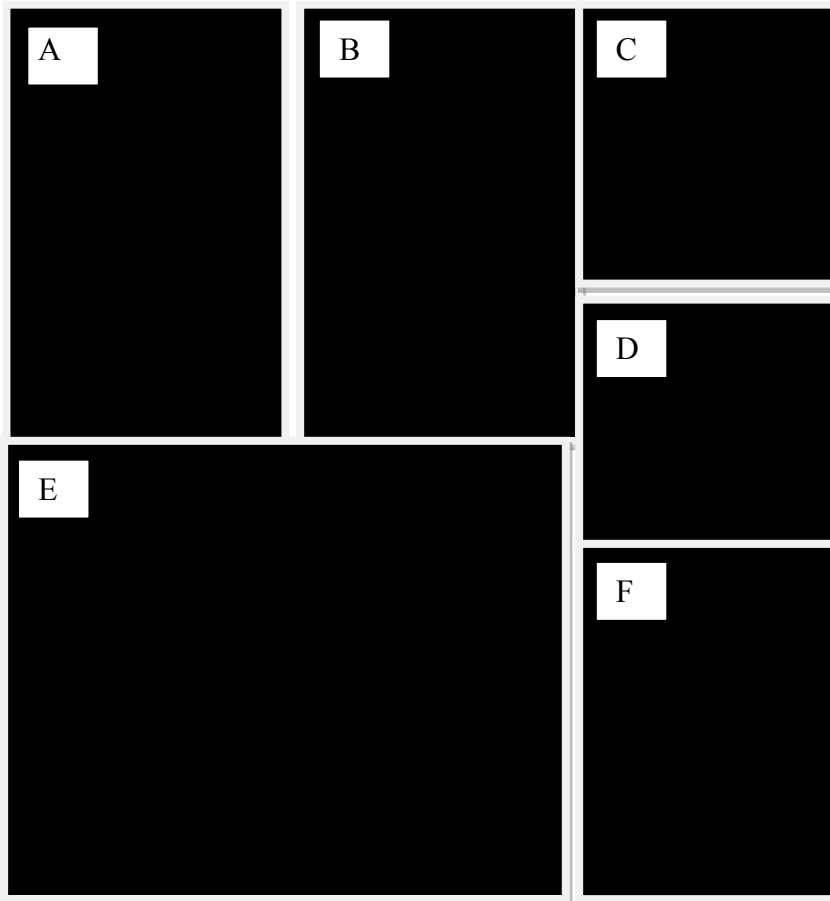


**Figure 3.5** Images removed to protect confidentiality. Clinical features observed in patient 012. (A) Age 4 months, showing her fine hair, "glyphic" nose, and micrognathia. (B) Age 2 years 4 months. (C–D) Radiology at age 4 months showing acro-osteolysis (C) and photograph at age 2 years 4 months (D) showing short, bulbous distal phalanges and nails. (E) Chest *x* ray age 2 years 4 months, showing marked osteolysis of the clavicles with an irregular mass of callus overlying the left clavicular remnant (arrow) and a fracture of the left upper humerus (arrowhead). (F) Dry, shiny and tight skin on lower leg at 4 months. Taken from Shackleton *et al* 2005.

### 3.5 Results of mutation analysis

#### 3.5.1 Identification of mutations in the *LMNA* gene

Screening of genomic DNA from patients 004, 005 and 013 revealed mutation of the *LMNA* gene. Sequencing of the whole *LMNA* gene in all other patients revealed no mutations.

##### 3.5.1.1 Identification of the classical progeria mutation, in patients 005 and 013

Patients 005 and 013 were found to have heterozygous *LMNA* c.1824 C>T mutations, shown in the sequencing chromatogram in Figure 3.6 (A). This single base substitution, (GGC>GGT) at codon 608 (G608G), produces a cryptic splice donor site and leads to production of the mutant lamin A protein, progerin (Eriksson *et al* 2003, De Sandre-Giovannoli *et al* 2003) (described in Section 1.6.1).

##### 3.5.1.2 Identification of an atypical progeria mutation in patient 004

Patient 004 was found to have a heterozygous *LMNA* c.1868 C>G mutation, shown in the sequencing chromatogram in Figure 3.6 (B). At the protein level this results in a T623S (ACT>AGT) base change and leads to the creation of a cryptic splice site and production of the mutant lamin A protein, LA $\Delta$ 35. This mutation was previously identified in a Japanese patient (Fukuchi *et al* 2004) and an Israeli patient (Shalev *et al* 2007), both with mild progeria.

### ***3.5.2 Identification of mutations in the ZMPSTE24 gene***

#### *3.5.2.1 Identification of compound heterozygous ZMPSTE24 mutations in patient 012*

No *LMNA* mutation was found in patient 012. Due to the similarities between her phenotype and the features of MAD and RD, her *ZMPSTE24* gene was screened for mutation by collaborators A. K. Agarwal and A. Garg at the University of Texas Southwestern Medical Center, Dallas, USA. This group had previously reported that *ZMPSTE24* is mutated in MAD (Agarwal *et al* 2003). The coding exons of *ZMPSTE24* were directly sequenced and compound heterozygous mutations were identified. Sequencing chromatograms are shown in Figure 3.6 (C). The first mutation, c.1085\_1086insT in exon 9, (Leu362PhefsX19 at protein level), results from the insertion of a T after position 1085 of the *ZMPSTE24* cDNA, causing a frameshift and resulting in the introduction of a premature stop codon 19 amino acids downstream of the insertion. This mutation has been previously reported in RD (Navarro *et al* 2004, 2005) and MAD (Agarwal *et al* 2003). The second mutation, c.794 A>G in exon 7 (N265S at protein level) has not previously been reported and results in a missense amino acid change. This mutation was not observed in 100 unaffected controls. The healthy parents of patient 012 were each found to be heterozygous for one mutation (data not shown).

Following the discovery of *ZMPSTE24* mutations in patient 012, primers were designed and *ZMPSTE24* sequencing was undertaken as part of this study. The *ZMPSTE24* gene was sequenced in all patients with a progeroid phenotype in which no *LMNA* mutation was found.

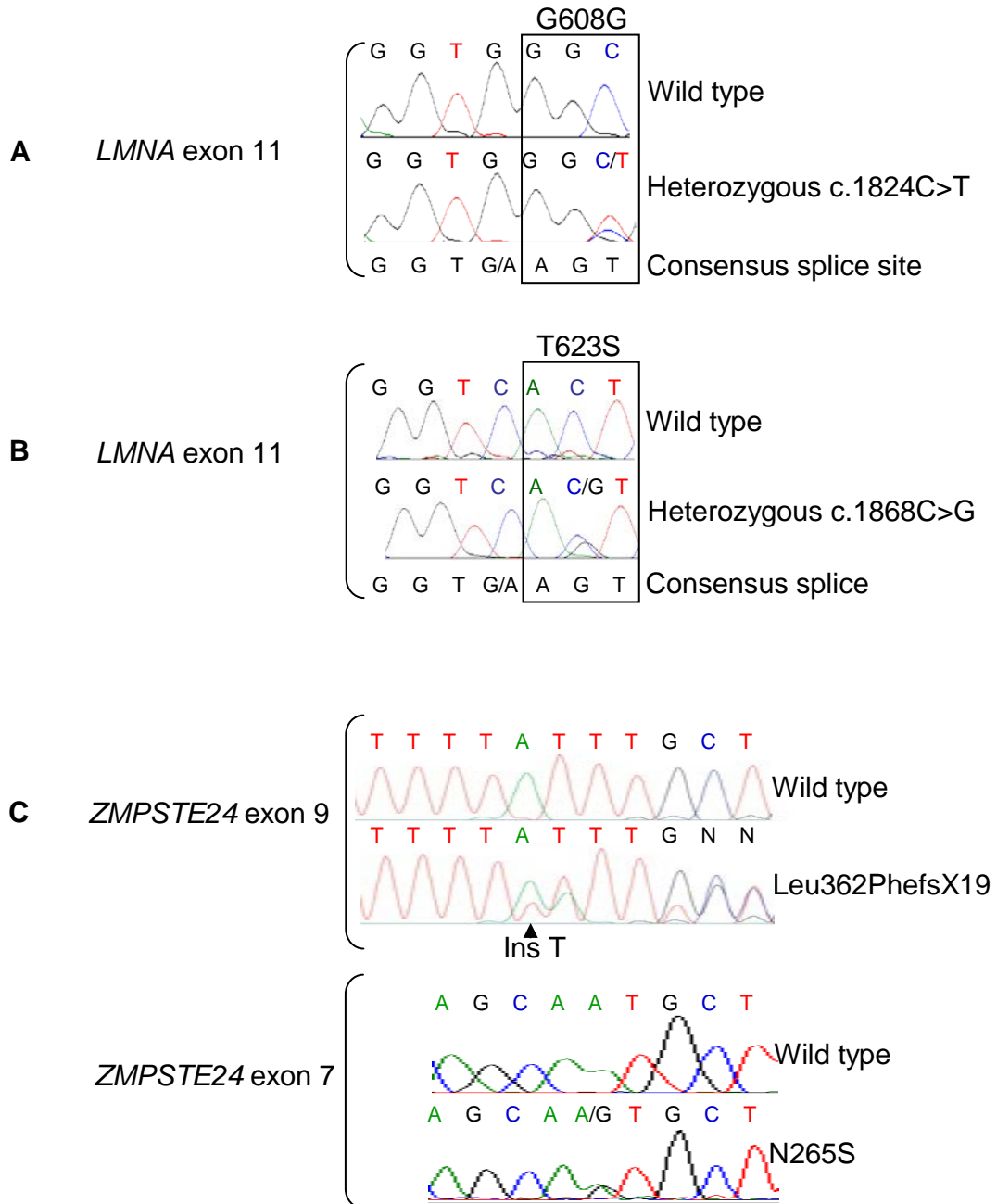


**Figure 3.6** Sequence chromatograms of *LMNA* and *ZMPSTE24* mutations found in the patient cohort. (A) Heterozygous *LMNA* G608G cryptic splice site production resulting in classical HGPS in patients 005 and 013. (B) Heterozygous *LMNA* T623S cryptic splice site production resulting in atypical progeria in patient 004. (C) Compound heterozygous *ZMPSTE24* mutations resulting in severe progeria in patient 012.

### 3.5.3 Single nucleotide polymorphisms (SNPs) detected during patient screening

Sequencing revealed a number of silent SNPs in the patients, shown in sequencing chromatograms in Figure 3.7. In patient 002, a heterozygous SNP was found in exon 1 of the *LMNA* gene at position 261C>T, (p.S51S). In patient 009 a heterozygous SNP was found in *LMNA* exon 7 detected at 1549C>T (p.D446D). Patients 003, 006, 010 and 011 were found to be heterozygous, and patient 008 homozygous, for *LMNA* SNPs in exon 10 at position 1908C>T (p.H566H). A heterozygous SNP in *ZMPSTE24* exon 6 at position 13857 T>C (p.D117D) was detected in patient 007.

## 3.6 Discussion

In this study, causative mutations were successfully identified in four patients. Two patients with a classical HGPS phenotype were found to be carrying identical *LMNA* G608G mutations. One patient with mild, late onset, atypical progeria carried a *LMNA* T623S mutation. Compound heterozygous *ZMPSTE24* mutations were identified by collaborators in a patient with a severe progeroid phenotype.

### 3.6.1 Classical HGPS: phenotype-genotype correlation in patients carrying the *LMNA* G608G mutation

Classical HGPS has been described extensively and studies of patient genotype and phenotype suggest that the G608G mutation results in a consistent phenotype (Mazereeuw-Hautier *et al* 2007, Hennekam *et al* 2006). The report by Mazereeuw-Hautier *et al* 2007 compared the clinical features of three classical HGPS children, including patient 005 from this study and the phenotype was found to be uniform.

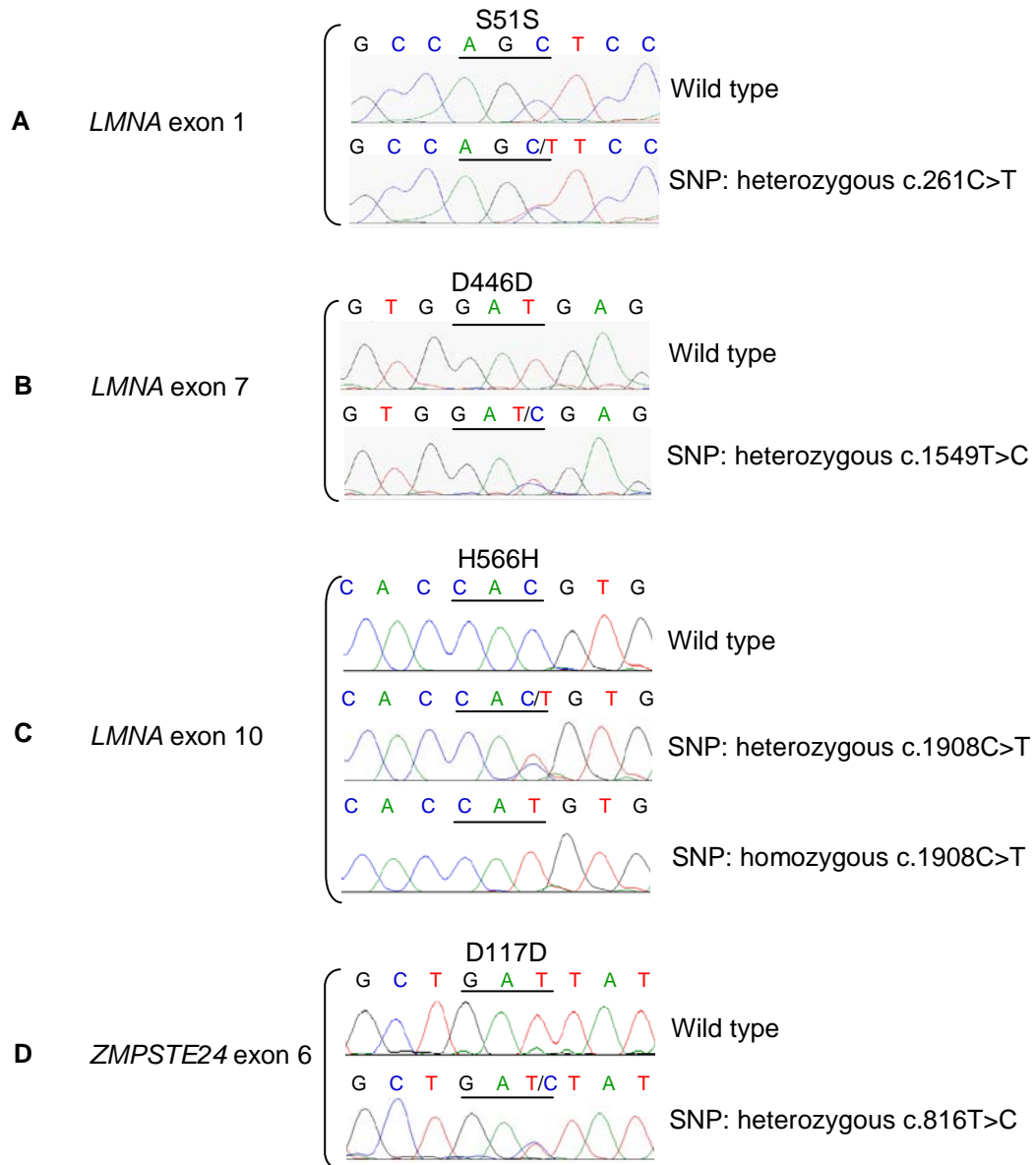


**Figure 3.7** Sequence chromatograms of *LMNA* and *ZMPSTE24* SNPs identified in the patient cohort. (A) *LMNA* S51S found in patient 002 (heterozygous), (B) *LMNA* D446D found in patient 009 (heterozygous), (C) *LMNA* 566H found in patients 003, 006, 010 and 011 (heterozygous) and in patient ZBR (homozygous) (D) *ZMPSTE24* D117D found in patient 007 (heterozygous).

The mutant lamin A protein produced as a result of the G608G mutation is referred to as progerin (described in Section 1.6.1). Studies performed on progerin expressing cells indicate that this mutant form of lamin A has a severe dominant negative effect on nuclear structure and function (Goldman *et al* 2004). It has also been suggested that the amount of progerin expressed in cells correlates with disease severity (Moulson *et al* 2007). Therefore, the consistent phenotype among patients carrying the G608G mutation may result from a similar level of cryptic splice site activity and consequently similar progerin levels among classical HGPS patients.

Evidence for this correlation comes from other heterozygous sequence variations shown to result in activation of the same cryptic splice site created by the G608G mutation. A silent V607V base change was found to result in accelerated disease progression where the patient died aged 3.5 years. A 1968+1G>A mutation in intron 11 resulted in severe HGPS where the patient died aged 26 days. Both mutations are reported to activate the same cryptic splice site used in classical HGPS but increased disease severity is reportedly due to increased use of the cryptic splice site resulting in levels of progerin expression much higher than in typical HGPS (Moulson *et al* 2007).

The consistent phenotype in classical HGPS resulting from the G608G mutation was recognised in patients 005 and 013 by their clinicians as lamin A-linked progeria. The condition was confirmed by *LMNA* sequencing as part of this study. Patients and their families then had the opportunity to take part in FTI drug trials (Kieran *et al* 2007) described in Section 1.6.7.

### ***3.6.2 Mild HGPS: phenotype-genotype correlation in patients carrying the LMNA T623S mutation***

The *LMNA* T623S mutation has previously been reported in an 11 year old Israeli female (Shalev *et al* 2007) and 45 year old Japanese male (Ogihara *et al* 1986, Fukuchi *et al* 2004). A comparison of phenotypic information available for these two patients and patient 004 is shown in Table 3.3 and reveals very similar phenotypes. By the age of 45 years, the Japanese patient had progressively developed many of the features of classical HGPS. He died of myocardial infarction aged 45 years. Patient 004, therefore, could be expected to have a significantly longer lifespan than classical HGPS patients. The Israeli patient was reported to show a rare association between HGPS and malignancy. This is the only published report of cancer in an HGPS patient.

The T623S mutation results in a later onset, milder and more slowly progressing HGPS phenotype than the G608G mutation. The phenotype appears to be consistent in the three cases of T623S progeria compared, therefore may result from a similar level of cryptic splice site activity and consequently similar LA $\Delta$ 35 levels among these patients. The milder phenotype compared to classical HGPS may be explained by lower levels of mutant protein produced by a less active splice site. Another possibility to be considered is that the LA $\Delta$ 35 mutant exerts a less detrimental effect on cells than progerin. These hypotheses are further investigated in Chapter 4.

The LA $\Delta$ 35 mutant, due to its similarity to LA $\Delta$ 50, is also predicted to be permanently farnesylated and patients found to be carrying the rare *LMNA* T623S mutation are also accepted onto FTI drug trials. Following *LMNA* sequencing, therefore, patient 004 would have the opportunity to take part in FTI drug trials.

Clinical features	Patient 004 aged 15 years	Israeli patient aged 11 years	Japanese patient aged 45 years
Lipodystrophy	+	+	+
Thin hair / alopecia	+	+	+
Dystrophic nails	+	+	+
Micrognathia	+	+	+
Dental overcrowding and delayed dentition	+	+	NR
Osteolysis	NR	+	NR
High pitched voice	NR	+	+
Pinched, glyptic nose	NR	+	+
Prominent forehead and eyes	-	-	+
Horse riding stance	-	-	+
Cardiac defect	-	-	+
Malignancy	NR	+	NR

**Table 3.3** A comparison of the clinical features of patient 004 with two patients previously reported to carry the *LMNA* T623S mutation. + indicates presence, - absence of the condition. NR indicates data not reported. Additional clinical features seen in the Japanese patient are likely to be due to his being significantly older than the other patients.

### 3.6.3 Patient 012: A phenotype overlapping MAD, HGPS and RD

Compound heterozygous mutations were found in patient 012 who had a severe progeroid phenotype. The parents were each heterozygous for one of the two mutations, but had no obvious phenotype, supporting an autosomal recessive inheritance for this individual. Patient 012 showed features of RD, HGPS and MAD and a comparison of clinical features of early onset progeroid syndromes with the phenotype of patient 012 is made in Table 3.4. This patient represents the first reported case of *ZMPSTE24* as a causative gene for a severe progeroid disorder resembling HGPS.

	RD	Classical HGFS	Atypical HGFS <sup>a</sup>	MAD type A (OMIM 248370)	MAD type B (OMIM 608612)	Patient FT
Inheritance	AD	AD, sporadic	AR	AR	AR	AR
LMNA mutation	IVS11+1G→A c.1824C→T (G608G)	G608G G608S	K542N	R527H	NR	-
ZMPSTE24 mutation	c.1085_1086insT	NR	NR	NR	c.1085_1086insT W340R	c.1085_1086insT N265S
Presentation	3rd trimester/congenital	6 m-2 y	18 m-2 y	4 y	2 y	10 weeks
Average life span	Weeks	13 y	10-16 y	3rd decade or later	3rd decade or later	2.7 years
Growth retardation	Intrauterine	6 m-1 y	+	4-5 y	2 y	Infancy
Joint contractures	Intrauterine, generalised joint, thin skin	From infancy, sclerodermoid changes, atrophic changes	Atrophic, sclerodermoid changes, mottled pigmentation	From childhood	From childhood	Neonatal
Skin abnormalities	-	Generalised	Generalised	Atrophic, hyperpigmentation	Atrophic, hyperpigmentation	Neonatal, sclerodermoid, indurated over trunk-lower limbs, oedema
Lipodystrophy	-	From childhood	Generalised	Partial (extremities)	Generalised	Lower limbs
Alopecia	+	From infancy	+	From childhood	From childhood	-
Osteolysis	-	+	-	+	+	Present at 10 weeks
Insulin resistance	-	+	-	NR	NR	-
Dyslipidaemia	-	+	NR	NR	NR	Mild
Atherosclerosis	-	+	NR	NR	NR	Possible transient ischaemic attack
Facial features	Pinched nose, small "O" shaped mouth, micrognathia	Prominent veins, "glyhic" nose, micrognathic, sparse eyebrows	Pinched nose, sparse eyebrows and lashes, prominent eyes, micrognathia	Beaked nose, micrognathia, pinched face	Beaked nose, micrognathia, pinched face	Prominent scalp veins, "glyptic nose", micrognathia
Skeletal features	Large fontanelle, thin, dysplastic clavicles, reduced bone density, oventubulated long bones	Delayed closure of cranial sutures, wormian bones, osteolysis of distal phalanges and clavicles, osteoporosis, pyriform thorax, coxa valga	Delayed closure of cranial sutures, clavicular hypoplasia,acro-osteolysis	Delayed closure of cranial sutures, clavicular hypoplasia, osteolysis of distal phalanges, mandible and clavicles	Delayed closure of cranial sutures, clavicular hypoplasia, osteolysis of distal phalanges and clavicles, Calcified nodules on digits	Thin skull, wormian bones, osteolysis of distal phalanges and clavicles, fractures, lytic areas in tibia, humerus-cervical spine
Other	Polyhydramnios, premature rupture of membranes, pulmonary hypoplasia	Horse-riding stance, absent sexual maturation, delayed dentition	Absent/impaired sexual maturation, crowded teeth	Premature loss of dentition	Premature loss of dentition, delayed sexual maturation	Focal segmental glomerulosclerosis, collapsing variant

<sup>a</sup>Two cases of lethal neonatal MAD have been reported<sup>21, 22</sup>. TAI at least one additional mutation, in the same or a second gene, is likely to be required.

m, months; HGFS, Hutchinson-Gilford progeria syndrome; MAD, mandibuloacral dysplasia; NR, not reported; RD, restrictive dermopathy; y, years.

**Table 3.4 Clinical features of lamin A-related progeroid syndromes. Taken from Shackleton et al (2005)**  
**Table 3.4 Clinical features of lamin A-related progeroid syndromes. Patient 012 is referred to as FT. Taken from Shackleton et al (2005)**

Homozygous ZMPSTE24 L362PhefsX19 mutations have been reported in a number of RD patients. The L362PhefsX19 mutant has been shown to be functionally inactive in a yeast halo assay testing its ability to complement a p processing defect in the STE24 homologue (Agarwal *et al* 2003). In patient 012, the L362PhefsX19 null mutation in combination with N265S resulted in a slightly less devastating phenotype than that of RD. Presumably, the N265S mutation allowed the retention of some proteolytic activity, therefore allowing some prelamin A processing to occur. Partial prelamin A processing resulting in a small reduction in farnesylated prelamin A may have rescued patient 012 from full blown RD. Codon 265 is upstream of the ZMPSTE24 catalytic site, which consists of amino acids HELGH at codons 335-339, indicating that the catalytic site is not disrupted directly. A reduction in activity may be due to the effect of the mutation on the ability of ZMPSTE24 to form its normal conformation or bind to its substrate, prelamin A. The gain of a hydroxyl group due to an amino acid change from asparagine (N) to serine (S) may result in additional hydrogen bonding, perhaps altering ZMPSTE24 conformation or binding abilities.

A MAD patient has also been reported to carry the L362PhefsX19 ZMPSTE24 mutation and harboured a different missense mutation (W340R) on the second allele (Agarwal *et al* 2003). This patient presented at 2 years and survived to 24 years. The earlier onset and increased severity of the disease in patient 012 may at least in part be attributable to functional differences between these alleles, although this is surprising since W340 is right next to the catalytic site and tryptophan (W) to arginine (R) is a significant change of side group.

Detection of these mutations has important implications for genetic counselling in the family of patient 012, as the autosomal recessive inheritance identified is associated

with a 25% recurrence risk, in contrast to the low recurrence risk in classical HGPS where the majority of cases arise from de novo *LMNA* mutations.

### 3.6.4 Lipodystrophy patients in whom no mutation was detected

Four lipodystrophy patients in this study were found to have no *LMNA* or *ZMPSTE24* mutation. *LMNA*-associated lipodystrophy is only one of a number of genetic disorders of adipose tissue. Other lipodystrophies include congenital generalised lipodystrophy, FPLD associated with PPAR $\gamma$  mutation, FPLD associated with AKT2 mutation, and SHORT syndrome, (reviewed Agarwal and Garg 2006). A basic overview of these disorders is contained in Table 3.5.

Disease	Age of onset	Gene	Function	Basic phenotype
Congenital generalised lipodystrophy type 1	Birth	AGPAT2	Triglyceride biosynthesis	Generalised lipodystrophy
Congenital generalised lipodystrophy type 2	Birth	BSCL2	Seipin protein unknown function	Generalised lipodystrophy
FPLD PPAR $\gamma$ associated	Puberty to early adult	PPAR $\gamma$	Key adipogenic transcription factor	Partial lipodystrophy
FPLD AKT2 associated	Adult	AKT2	Kinase involved in insulin signalling	Partial lipodystrophy
SHORT syndrome	Birth	Unknown	Unknown	Lipodystrophy affecting face upper extremities and trunk

**Table 3.5** Overview of non *LMNA* associated genetic lipodystrophies

Further genetic analysis may be useful for the lipodystrophy patients in this study, however, analyses of genes associated with non *LMNA* related lipodystrophies were beyond the scope of this study.

Patient 001 was clinically diagnosed with lipodystrophy and patient 003 with abnormal fat distribution. No other information was available for these patients. Their ages, 38 years and 28 years respectively, suggest that the involvement of progeroid disorders is unlikely. These patients may benefit from mutation analysis of the genes associated with non *LMNA* related lipodystrophies.

Patient 002 did not have the pattern of fat loss normally resulting *LMNA*- associated FPLD where the face and neck is spared. In this patient, lipodystrophy involved the face and neck, upper limbs and upper trunk, whereas lower limbs were unaffected. She also had accelerated growth and hyperandrogenism, which are features of Berardinelli-Seip congenital generalised lipodystrophy type 2. This patient may benefit from mutation analysis of the *BSCL2* gene.

A diagnosis of SHORT syndrome was made for patient 009 and may be the correct diagnosis for the patient; specific mutational analysis for this disorder is not possible since the genetic basis is as yet unknown.

### ***3.6.5 Progeroid patients in whom no mutation was detected***

Six children in this study were found to have no *LMNA* or *ZMPSTE24* mutation. For these patients, sequencing of genes from related disorders may be relevant. There are a number of premature ageing disorders involving mutation of DNA helicases leading to defects in DNA repair which may be candidates for sequencing, depending upon the patient phenotype. Non *LMNA* related progeroid disorders are listed in Table 3.6.

<b>Disease</b>	<b>Age of onset</b>	<b>Gene</b>	<b>Function</b>	<b>Basic phenotype</b>
Werner's syndrome	Puberty	<i>WRN</i> DNA helicase	DNA synthesis and repair	Progeroid
Rothmund-Thomson syndrome	11 years	<i>RECQL4</i>	DNA synthesis and repair	Facial rash Cancer Progeroid
Bloom syndrome	Usually before 1 year	<i>BLM</i> helicase	DNA synthesis and repair	Facial rash Cancer Progeroid
Cockayne Syndrome	2 years	<i>ERCC6</i> <i>ERCC8</i>	DNA repair	Progeroid Impaired vision, hearing and nervous system
Trichothiodystrophy	2 years	<i>XPD</i>	DNA repair of UV damage	Brittle hair and nails Growth retardation Possible mental retardation
Xeroderma pigmentosum	2 years	<i>XPD</i>	DNA repair of UV damage	Skin malignancy Growth retardation Possible mental retardation
Hallerman-Streiff Syndrome	Before 2 years	Unknown	Unknown	Progeroid Cataracts Narrow airway
Wiedemann-Rautenstrauch Syndrome	Birth	Unknown	Unknown	Progeroid

**Table 3.6** Overview of non *LMNA* associated progeroid syndromes

Clinical information available for patients 007, 010, 008 and 014 was sparse and detailed phenotypic information would be necessary before appropriate further genetic analysis could take place.

Patient 006 was diagnosed with MAD. She had abnormal toes and short distal phalanges which are present in this disorder but she lacks skeletal abnormalities and lipodystrophy which are typical features of MAD. Sequencing of genes from related disorders may benefit this patient.

A diagnosis of Wiedermann-Rautenstrauch syndrome was made for patient 011 and may be the correct diagnosis for this patient; mutational analysis for this disorder is not possible since the genetic basis is as yet unknown.

Further genetic analysis may be useful for progeroid patients in this study found to have no *LMNA* or *ZMPSTE24* mutation. Analyses of genes associated with non *LMNA* related progeroid syndromes were beyond the scope of this study. In all patients, further analysis would be needed to completely exclude the possibility of *LMNA* and *ZMPSTE24* mutation. Only coding exons were screened as part of this study, so that the presence of promoter mutation or intronic mutation resulting, for example, in a splicing defect cannot be discounted. Large deletions or rearrangements that prevented amplification of the mutant allele would also be undetected by the sequencing method employed in this study.

### ***3.6.6 Association between LMNA SNPs and disease***

An association has been reported between the *LMNA* C>T SNP identified at position 1908 (H566H) and type 2 diabetes in Danish subjects (Wegner *et al* 2007) and metabolic syndrome in aboriginal Canadians (Hegele *et al* 2000), Japanese subjects (Murase *et al*

2002) and the Old Order Amish (Steinle *et al* 2004). Conflictingly, in UK subjects, no association was found with type 2 diabetes (Owen *et al* 2007, Mesa *et al* 2007) or metabolic syndrome (Mesa *et al* 2007). Metabolic syndrome is characterised by elevated fasting glucose and triglyceride levels, low high-density lipoprotein levels and high blood pressure. The presence of the H566H variation may affect the development of metabolic syndrome and diabetes, perhaps increasing susceptibility. The *LMNA* C>T SNP identified at position 1549 (p.D 446D) was included in type 2 diabetes and metabolic syndrome association studies of UK subjects but no significant association was found (Owen *et al* 2007, Mesa *et al* 2007). The *LMNA* C>T SNP identified at position 261 (p.S 51S) is included on the Leiden Open Variation Database (LOVD) ([www.dmd.nl/nmdb/home](http://www.dmd.nl/nmdb/home)) and has no known pathogenicity. LOVD displays sequence variations in a large number of genes including *LMNA* and *ZMPSTE24*.

The *ZMPSTE24* T>C SNP identified at position 816 (p.D117D) has not been reported elsewhere. An online splice site prediction site ([www.fruitfly.org/seq\\_tools/splice.html](http://www.fruitfly.org/seq_tools/splice.html)) revealed that this base change is not predicted to result in a splicing defect. This prediction was supported by western blot analysis of dermal fibroblast extracts from this patient probed with a lamin A/C antibody which showed two bands corresponding to lamin A and lamin C (data not shown).

## CHAPTER 4

### Analysis of the expression, localisation and mobility of lamin

#### A and associated nuclear proteins in progeria and FPLD

##### 4.1 Introduction

There have been a number of studies examining dermal fibroblasts from laminopathy patients. Classical Hutchinson-Gilford Progeria Syndrome (HGPS) fibroblasts, in particular, have been studied extensively and defects in NE structure such as lobulation of the NE, thickening of the lamina, loss of peripheral heterochromatin and nuclear pore clustering have been reported in subpopulations of cells (Goldman *et al* 2004) (Section 1.6.5). Lobulation of the NE and thickening of the lamina have also been reported in the premature ageing disorders mandibuloacral dysplasia (MAD) (Novelli *et al* 2002), severe progeria (Shackleton *et al* 2005) and restrictive dermopathy (RD) (Navarro *et al* 2004). In addition, abnormal expression and localisation of nuclear proteins have been reported in premature ageing disorders. The unprocessed wild type lamin A precursor, prelamin A, has been found to accumulate in classical HGPS (Goldman *et al* 2004), the progeroid syndromes mandibuloacral dysplasia (MAD) and (Capanni *et al* 2005), severe progeria (Shackleton *et al* 2005) and restrictive dermopathy (RD) (Navarro *et al* 2004). The presence of prelamin A has been associated with thickening of the lamina (Goldman *et al* 2004) and mislocalisation of lamin A interacting proteins (Capanni *et al* 2005, Capanni *et al* 2009).

Although interesting observations of defects in NE structure and the properties of lamin A interacting proteins have been made in a number of premature ageing cell lines, there have been no comparative studies of classical and atypical progerias.

Interestingly, prelamin A accumulation has been detected both in fibroblasts from patients with progeroid syndromes and in FPLD fibroblasts, where it is proposed to sequester the transcriptional regulator of lipid homeostasis sterol response element binding protein 1 (SREBP1) away from its site of normal transcriptional activity resulting in impaired adipogenesis (Capanni *et al* 2005). This finding suggests a common mechanism underlies the lipodystrophy phenotype in FPLD and progeria and raises the question of whether other cellular defects reported in progeria may be present in FPLD.

Aberrant farnesylation is thought to be a major determinant of the classical progeria phenotype (Section 1.6.6). The mobility of progerin, or LA $\Delta$ 50, the mutant form of lamin A present in classical HGPS, was found to be significantly reduced compared to wild type in fluorescence recovery after photobleaching (FRAP) experiments (Goldman *et al* 2004, Dahl *et al* 2006), most likely because its farnesyl group causes it to be retarded at the nuclear membrane. In contrast, FRAP analysis of lamin A mutants by Gilchrist *et al* (2004) showed the R482W lipodystrophy associated mutant to have a similar mobility to wild type. Since progerin, which is known to be permanently farnesylated (Capell *et al* 2005), has reduced mobility whilst the R482W mutant, whose properties suggest it is not farnesylated, has similar mobility to wild type, it appears that lamin A mobility may be an indicator of farnesylation status.

## 4.2 Aim of these studies

The aim of these studies was to gain information about the disease mechanisms in FPLD and progeria and possible causes of disease variability in progeroid syndromes.

Novel comparisons of nuclear morphology and nuclear protein properties were made in progeroid syndromes and FPLD by investigation of the localisation and expression of nuclear proteins in cultured fibroblasts. Dermal fibroblasts investigated in this study were from one patient harbouring the most commonly occurring lamin A associated FPLD mutation and three patients harbouring different lamin A associated progeroid mutations resulting in different disease severities.

Mobility studies were used to investigate the hypothesis that abnormal farnesylation of lamin A mutants contributes to the disease phenotype in atypical progeroid syndromes. FRAP was used to determine the mobility of lamin A mutants. FRAP data, alongside Western blot analysis of lamin A in cell extracts from atypical progeria patients, was used to identify the farnesylation status of lamin A mutants.

## 4.3 Nuclear morphology abnormalities

Nuclear morphology was compared in three progeria patients and an FPLD patient. Dermal fibroblasts cell lines used in these studies are listed in Table 4.1. The FPLD cell line was derived from a patient involved in a previous mutation analysis study in the laboratory (Shackleton *et al* 2000). Late onset progeria and severe progeria patient cell lines were from patients 004 and 012 respectively who were involved in the mutation analysis study described in Section 3. Where possible, cells of similar passage number (passage 12-14) (Section 2.7.2.1) were compared because the proportion of cells with

abnormal nuclear morphology and the severity of abnormalities have been shown to increase with passage number (Goldman *et al* 2004). Descriptions of the phenotypes associated with late onset and severe progeria are given in Section 3.4.1.2 (patient 004) and Section 3.4.1.7 (patient 012) respectively. Classical progeria is described in Section 1.6.6. Progeroid syndromes are described in Section 1.6 and the FPLD phenotype is described in Section 1.7.

Cell line	Mutation	Age of donor	Passage number used in study
Human foreskin fibroblast (hFF) (gift from Dr Katherine Clark, Leicester, UK)	Wild type control	Infant	Passage 12-14
Normal human dermal fibroblast (NHDF). Adult donor, C-12352 (PromoCell, Germany)	Wild type control	Adult of unspecified age	Passage 12-14
Human dermal fibroblast from aged unaffected individual AG07657 (Coriell Cell Repository, USA)	Wild type aged individual	88 years	Passage 12-14
FPLD patient	Lamin A p.R482W	Unknown	Passage 12-14
Atypical progeria patient 004	Lamin A p.T623S	15 years	Passage 12-14
Classical progeria AG11513 (Coriell Cell Repository, USA)	Lamin A p.G608G	8 years	Passage 12-14
Severe progeria patient 012	Compound heterozygous ZMPSTE24 p.Leu362PhefsX19 p.N265S	2 years	Passage 17-18

**Table 4.1** Dermal fibroblast cell lines used for localisation and expression studies. Unless stated otherwise, cell lines were obtained from the patient's clinician following mutation analysis in this laboratory.

For morphology data, nuclei were visualised by lamin A/C staining, the antibody recognises wild type and mutant forms of lamin A. Micronucleation, or those nuclei that possessed more than two lobulations or buds or contained aggregates of lamin A/C were classed as abnormal.

### 4.3.1 Results of nuclear morphology study

Nuclear morphology abnormalities were observed in a subpopulation of nuclei in all fibroblast cell lines (Table 4.2, Figure 4.1). Abnormalities included blebs or lobulation, budding, folding, micronucleation and lamin A/C aggregation. Quantification of these abnormalities is shown in Figure 4.2 which represents the average of 8 separate experiments; at least 300 cells were counted per experiment. P values are shown on the graph (Figure 4.2) to represent the statistical significance of nuclear abnormalities. P values were calculated using the Student's T-test, 2 tailed, 2 sample, unequal variance. Stars denote increasing statistical significance. All disease cell lines and the control aged 88 years, displayed a statistically significant number of nuclei with abnormal morphology compared to the WT hFF control.

Cell line	Nuclear abnormalities observed	% of cells affected
Control hFF	Minor lobulation	1%
Control aged 88 years	Lobulation Micronucleation	12%
FPLD (LA/C R482W)	Buds containing honeycomb LA/C staining Nucleoplasmic aggregates	6%
Late onset progeria (LA T623S)	Lobulation Micronucleation Thickened lamina Faint LA/C staining in nucleoplasm	24%
Classical progeria (LA G608G)	Lobulation Micronucleation Thickened lamina Faint LA/C staining in nucleoplasm	54%
Severe progeria (ZMPSTE24 mutated)	Lobulation Micronucleation Thickened lamina Faint LA/C staining in nucleoplasm	57%

**Table 4.2** Nuclear abnormalities observed in human dermal fibroblast cell lines

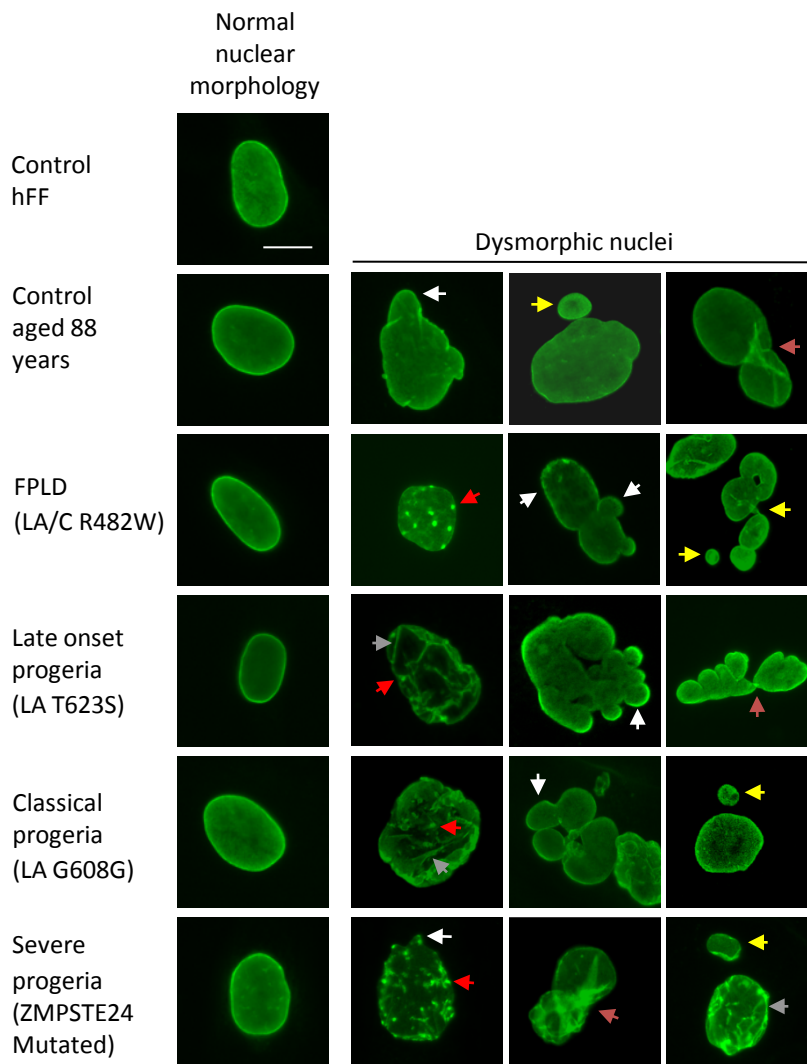


**Figure 4.1.** Nuclear envelope morphology of human dermal fibroblast cell lines. Lamin A/C staining shows examples of normal and abnormal nuclear morphology. Arrows indicate abnormalities observed; white: lobulations and buds, red: aggregates, blue: folding, yellow: microneucleation and grey: thickening of the lamina. Progeroid cell lines show faint nucleoplasmic LA/C staining. Bar, 10  $\mu$ m. LA, lamin A, LA/C lamin A and C.

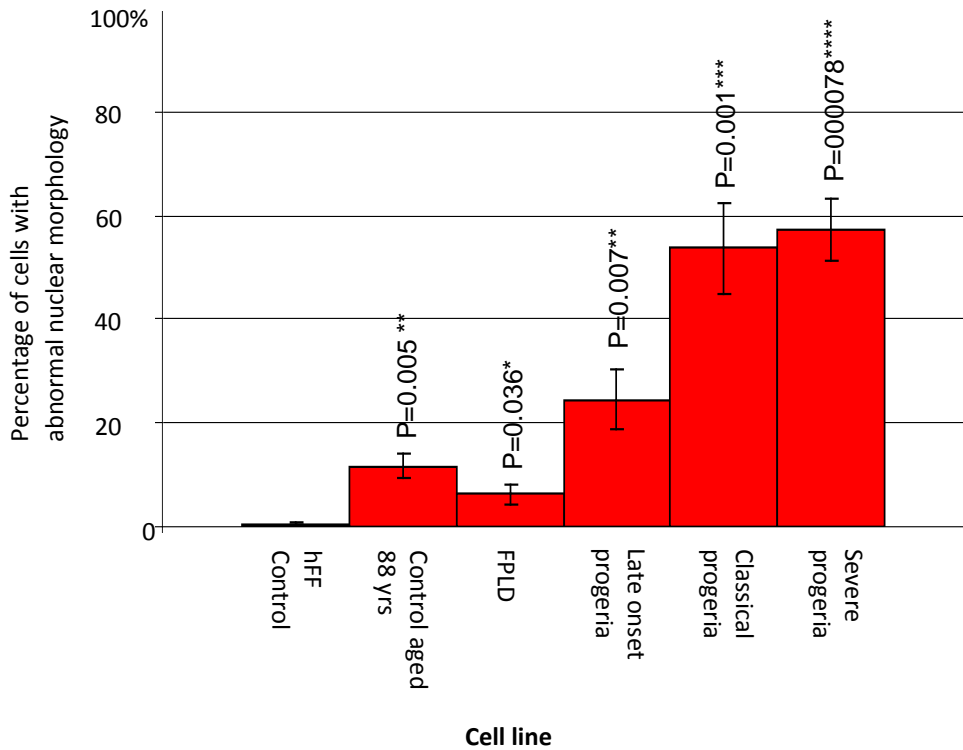


**Figure 4.2.** Percentage of cells displaying abnormal nuclear morphology classified as multinucleate cells or nuclei that possessed more than two lobulations or contained aggregates of lamin A/C. Average of 8 separate experiments, n=2500, +/- s.e.m. P indicates P value, stars indicate statistical significance.

Nuclear abnormalities were extremely rare in the hFF cell line, they consisted of minor lobulations and appeared in less than 1% of nuclei. In the aged control cell line, 12% of nuclei were abnormal suggesting that the frequency of abnormality may increase with chronological age. Abnormalities observed consisted mainly of lobulation or micronucleation.

Abnormalities observed in FPLD nuclei were low in frequency at 6%. Abnormalities included lobulations and micronucleation and two types of abnormalities specific to FPLD and not seen in control or progeria cell lines; aggregates which appear nucleoplasmic and nuclear buds containing a honeycomb meshwork of lamin A/C, suggesting that the R482W mutation disrupts polymerisation, albeit in only a low percentage of cells.

All three progeroid cell lines displayed the same type of abnormal morphology; lobulations, micronucleation, thickening of the lamina and faint lamin A/C nucleoplasmic staining. The vast majority of abnormal nuclei contained a nuclear envelope with many lobulations and a thickened lamina. In late onset progeria 24% of nuclei were abnormal, compared to 54% of classical progeria nuclei and 57% of severe progeria nuclei. The proportion of abnormal nuclei correlated with disease severity, although a direct comparison cannot be made since late onset and classical progeria fibroblasts were passage 12-14 whilst severe progeria cells were only available at higher passages of 17-18. Therefore, the higher passage number of severe progeria cells may contribute to the higher proportion of abnormalities.

Although classical progeria cell lines have been cultured to passage 26 (Goldman *et al* 2004) and passage 30 (Scaffidi and Misteli 2005), it was not possible to age the classical HGPS cell line beyond passage 14. This may be a property of the particular

cell line used in this study. It has also been reported that a wide range of growth potentials are exhibited by atypical HGPS cells, such that some do not thrive and others proliferate at almost the same rate as normal controls (Bridger and Kill 2004).

#### **4.4 Changes in protein expression and localisation**

Western blotting was used to investigate protein expression. Protein localisation was investigated by indirect immunofluorescence microscopy and in addition, intensity of protein staining was recorded. Whole cell extracts were used for Western blotting (Section 2.9.2). For indirect immunofluorescence microscopy, cells were grown on coverslips, then fixed and stained for observation (Section 2.8.1). Cell lines used are listed in Table 4.1.

##### ***4.4.1 Lamin A/C and prelamin A expression***

To determine the effect of lamin A mutations on prelamin A processing, Western blots of cell extracts were probed with lamin A/C and prelamin A antibodies (Figure 4.3). Probing with the lamin A/C antibody revealed bands corresponding to lamin A (upper band) and lamin C (lower band) in hFF and aged control cell lines. FPLD fibroblasts showed bands of the same size and intensity as control cell lines. This is expected since the R482W point mutation is not predicted to affect the farnesylation status or size of the protein. Similar findings have been previously reported in FPLD patients carrying R482W and R482Q mutations (Vigouroux *et al* 2001) and an R482L mutation (Capanni *et al* 2005). Late onset and classical progeria cell extracts contained bands corresponding to lamin A and C plus additional bands of intermediate molecular weight. Late onset progeria caused by the T623S mutation and classical progeria caused by the G608G mutation both result from activation of cryptic splice sites resulting in the

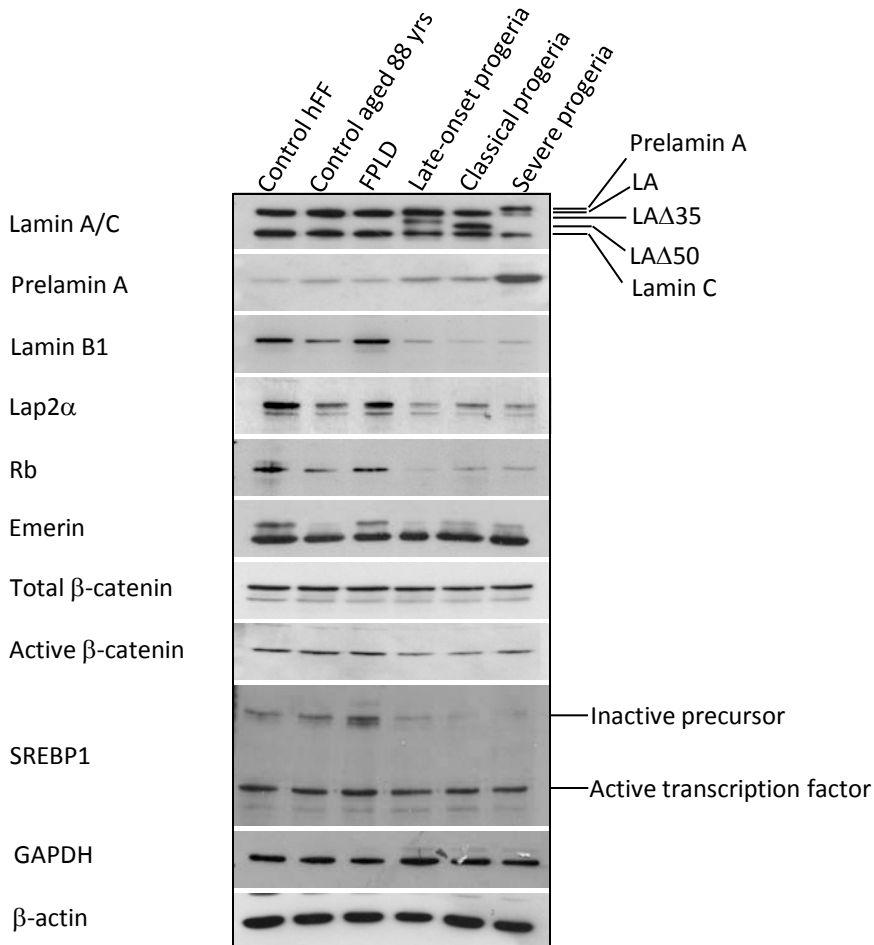


**Figure 4.3** Western blot analysis of expression of lamin A and associated proteins in fibroblast whole cell extracts. Data represents two separately prepared sets of cell extracts probed with antibodies against lamin A/C, prelamin A, lamin B1, SREBP1, LAP2 $\alpha$ , Rb, emerlin and total and active  $\beta$ -catenin. GAPDH and  $\beta$ -actin are loading controls. Rb antibody detects both phosphorylated (P) and unphosphorylated (UN-P) proteins. Active  $\beta$ -catenin antibody detects only UN-P protein. All cell lines were between passages 12 and 14, except severe progeria cells which were passage 17 or 18.

production of truncated forms of lamin A (described in Sections 3.5.1.2 and 1.6.1). The classical progeria mutant is referred to as progerin or LA $\Delta$ 50 and has a 50 amino acid internal deletion (Eriksson *et al* 2003, De Sandre-Giovannoli *et al* 2003), the late onset progeria mutant contains a 35 amino acid internal deletion (Fukuchi *et al* 2004) and in this study is referred to as LA $\Delta$ 35. The intensity of the LA $\Delta$ 50 band is much stronger than the LA $\Delta$ 35 band (Figure 4.3), suggesting that the classical progeria splice site is more active, resulting in a higher concentration of mutant lamin A in classical progeria compared with late onset progeria. The severe progeria fibroblast extracts showed a very faint mature lamin A band, plus an additional higher molecular weight band consistent with the size of prelamin A. Lamin C levels were unchanged compared with the control. Prelamin A accumulation is due to mutation of ZMPSTE24 in this patient.

The higher molecular weight band observed in severe progeria fibroblasts was confirmed as prelamin A by probing cell extracts with anti-prelamin A antibodies. Very faint prelamin A bands were found in the hFF and aged control cell extracts and in FPLD. Bands of slightly higher intensity than those in control extracts were visible in late onset and classical progeria extracts (Figure 4.3). The prelamin A antibody does not detect LA $\Delta$ 50 or LA $\Delta$ 35 proteins.

#### ***4.4.2 Prelamin accumulation at the nuclear rim***

Indirect immunofluorescence microscopy showed prelamin A in all severe progeria fibroblasts, confirming Western blotting results. Prelamin A was also detected at the nuclear rim in a subpopulation of classical progeria fibroblasts. No prelamin A was detected in the hFF, aged control, FPLD or late onset progeria fibroblasts (Figure 4.4). Cell counts revealed that prelamin A was visible in 46% of classical progeria nuclei

whilst 100% of severe progeria nuclei showed strong prelamin A staining (Figure 4.5 A).

#### ***4.4.3 SREBP1 accumulation at the nuclear rim***

Prelamin A accumulation has been associated with the mislocalisation of SREBP1 in FPLD and premature ageing fibroblasts (Capanni *et al* 2005). The effect of prelamin A accumulation on SREBP1 localisation was investigated in this study.

Indirect immunofluorescence microscopy showed SREBP1 was clearly visible at the nuclear rim in classical and severe progeria fibroblasts and was detectable, although faint, at the nuclear rim of late onset progeria and FPLD fibroblasts, therefore SREBP1 intensity at the nuclear rim does not correlate exactly with prelamin A intensity in these cell lines. Faint SREBP1 was detected in most fibroblasts from the aged individual and in a small number of wild type hFF cells.fibroblasts (Figure 4.4). Cell counts showed SREBP1 was detectable at the nuclear rim of 100% of classical, late onset progeria and FPLD nuclei, 97% of severe progeria nuclei, 74% of aged control nuclei and 12% of hFF nuclei (Figure 4.5 B).

Western blotting showed bands of equal intensity corresponding to the expected size of the transcription factor domain of SREBP1 for all cell lines and bands corresponding to the expected size of uncleaved SREBP1 in control cell lines and FPLD. Uncleaved SREBP1 bands were significantly weaker in all three progeria samples (Figure 4.3). This result does not support the indirect immunofluorescence microscopy result (Figure 4.4), where staining of SREBP1 was significantly fainter in hFF nuclei compared to the other cell lines.

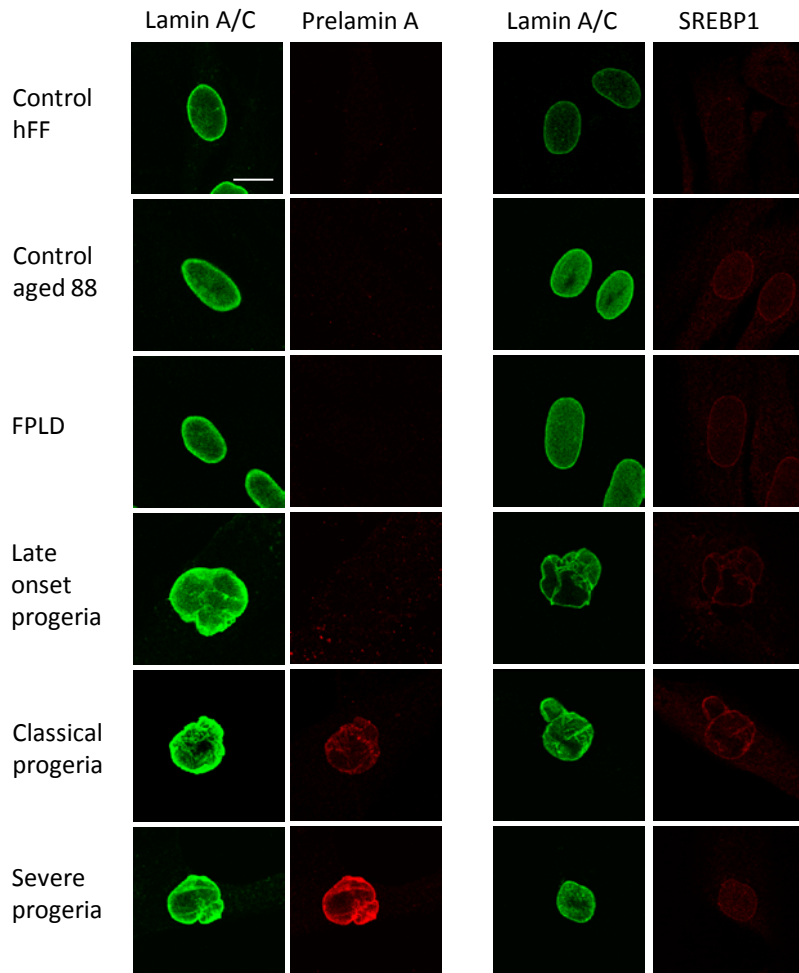


**Figure 4.4** Analysis of localisation and expression of prelamin A and SREBP1 (red) in cultured fibroblasts by indirect immunofluorescence microscopy. Cells were co-stained with lamin A/C (green) to visualise nuclei. The lamin A/C antibody also detects prelamin A, LA $\Delta$ 35 and LA $\Delta$ 50. All cell lines imaged were between passages 12 and 14, except severe progeria cells which were passage 17 or 18. Bar, 10  $\mu$ m.

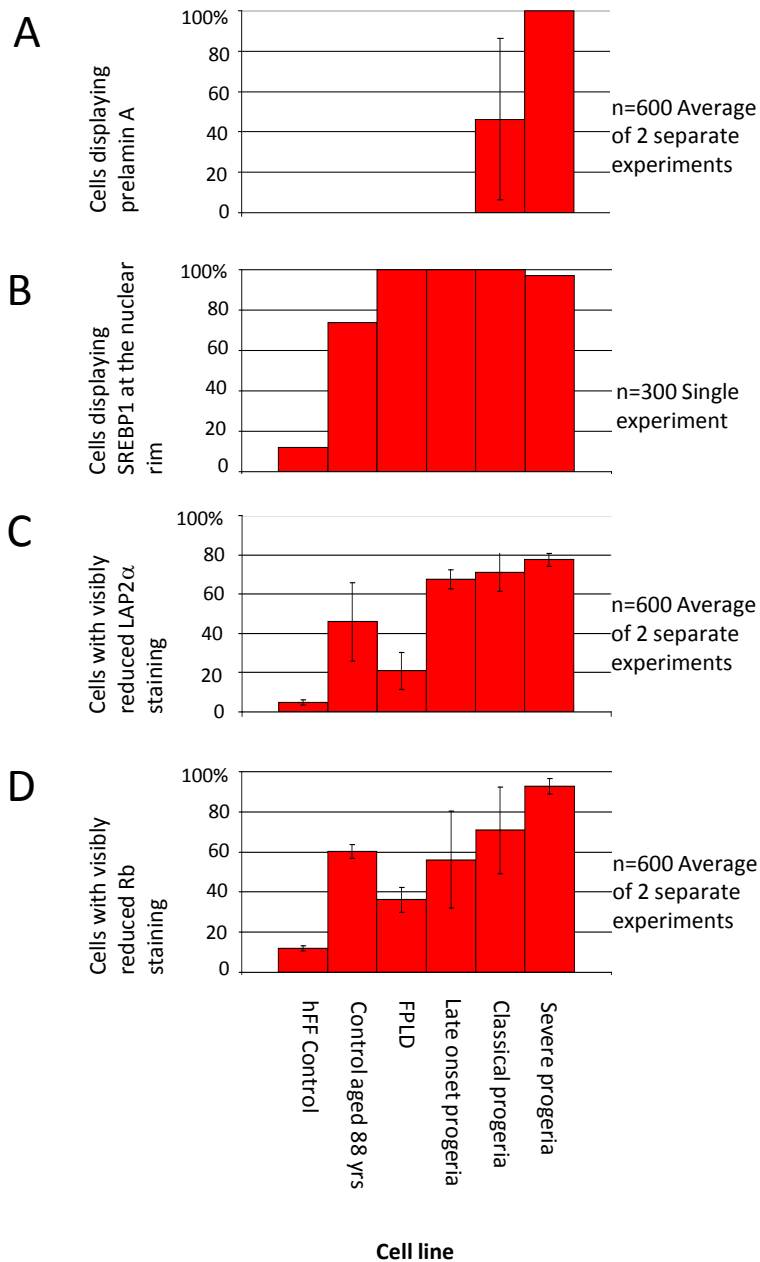


**Figure 4.5.** Percentage of cells displaying abnormal localisation or intensity of staining of lamin A associated proteins by counts of cells visualised by indirect immunofluorescence microscopy. Graphs of mean ( $\pm$  s.e.m) percentage of cells displaying abnormal prelamin A, LAP2 $\alpha$  and Rb are averaged over at least 600 cells per cell line from two separate experiments. The percentage of cells expressing abnormal SREBP1 is averaged over at least 300 cells in a single experiment.

The existing SREBP1 antibody in the laboratory (Santa Cruz sc-8984) used for the immunofluorescence shown in Figure 4.4, stopped working. A replacement batch did not detect endogenous SREBP1 by immunofluorescence so this result could not be confirmed. Western blotting was performed with the new sc-8984 antibody and detected bands of 68 kDa and 125 kDa, corresponding to the size of the SREBP1 active transcription factor and uncleaved precursor protein respectively. However, this result may not be reliable and further testing of the reliability of SREBP1 antibodies is described in Section 5.3.3.

Graphs of indirect immunofluorescence data (Figure 4.5) summarise the percentage of fibroblasts displaying abnormal localisation of lamin A associated proteins or reduced staining compared to wild type control. Data was obtained by counting at least 300 cells per cell line for each experiment. For protein localisation data, cells were categorised by the visible presence or absence of protein at the nuclear rim. For protein staining data, cells were categorised as displaying normal (denoted by bright staining) or abnormal (denoted by dim staining) levels of protein when compared to the wild type hFF control.

#### ***4.4.4 SUN1 expression at the nuclear envelope is increased in classical HGPS cells expressing prelamin A.***

The presence of prelamin A has also been found to affect levels of the NE protein SUN1. SUN proteins (SUN1 and SUN2) are lamin A binding proteins and form part of the LINC complex which stretches across the NE connecting the nucleoskeleton and the cytoskeleton. Pulldown experiments in the laboratory revealed that the presence of the G608G mutation disrupts the interaction of lamin A with SUN1 and SUN2 (Haque *et al* 2010). Indirect immunofluorescence microscopy was employed to determine whether disruption of the interaction between SUN1 and SUN2 and the lamin A mutant progerin

led to SUN1 and SUN2 mislocalisation in classical HGPS cells. Both SUN proteins localised normally in classical HGPS cells, but whilst SUN2 staining was uniform, SUN1 staining varied from cell to cell (Figure 4.6 panels A and C). It has been reported that SUN1 binds more strongly to prelamin A than mature lamin A (Crisp *et al* 2006), therefore, the possibility that prelamin A accumulation led to increased recruitment of SUN1 at the NE was tested by co-staining HGPS cells with SUN1 and prelamin A. HGPS cells stained with SUN1 and prelamin A were compared to those stained with SUN2 and prelamin A (Figure 4.6 panels A and C). Cells that expressed prelamin A also expressed high levels of SUN1, suggesting that prelamin A recruits SUN1 to the nuclear envelope. Scatter plots of prelamin A versus SUN1 or SUN2 were prepared with Dr Kees Straatman (Leicester, UK). These plots show a strong positive correlation between prelamin A and SUN1, but little correlation between prelamin A and SUN2 (Figure 4.6 B and D).

***4.4.5 Emerin does not completely co-localise with either lamin A/C or prelamin A in a subpopulation of progeria cells which show thickening of the nuclear lamina.***

Prelamin A accumulation has also been associated with the mislocalisation of the nuclear membrane protein emerin. Emerin is an inner nuclear membrane protein of unknown function which interacts with a large number of nuclear proteins (reviewed Holaska and Wilson 2007). Emerin is anchored at the NE by lamin A (Vaughan 2001), but in human fibroblasts forced to accumulate prelamin A, emerin has been found to co-localise with prelamin A in intranuclear aggregates (Capanni *et al* 2009).

Western blotting showed that emerin expression levels were unchanged in FPLD and progeria compared to wild type. In FPLD and control cell lines, however, an additional,

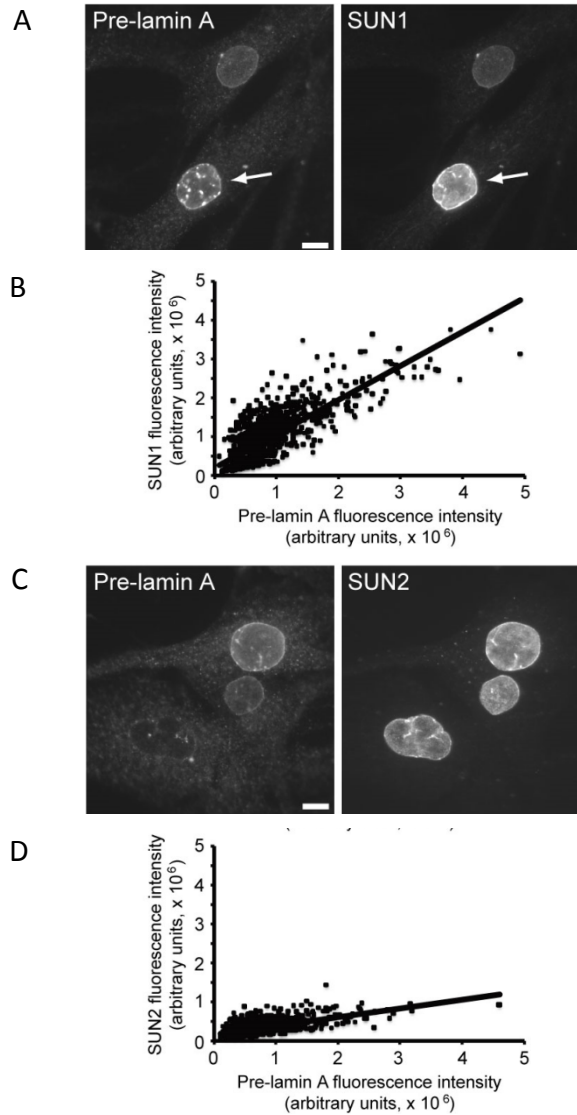


**Figure 4.6** Localisation and expression of SUN1/2 in classical progeria cells. A and C show co-staining of classical progeria cells carrying the G608G mutation with antibodies against prelamin A (left panels) and either SUN1 (A, right panel) or SUN2 (C, right panel). Arrows in A illustrate that in cells with accumulation of prelamin A, SUN1 expression is correspondingly higher. In contrast, expression levels of SUN2 are not affected by accumulation of prelamin A (C). Scatter plots of prelamin A versus SUN1 (B) or SUN2 (D) are shown. Fluorescence intensity in approximately 1000 cells reveals a strong positive correlation between prelamin A and SUN1 intensities, whereas SUN2 intensity does not vary significantly and does not correlate with prelamin A intensity as shown by the gradient of best fit lines. Bars 10  $\mu\text{m}$ .

higher molecular weight band was detected which was absent in progeroid and aged control samples (Figure 4.3). This band is likely to represent mitotically phosphorylated emerin (Ellis *et al* 1998) and its reduction in the progeroid cell lines supports the reduced proliferation observed with Ki67 staining (Figure 4.13).

Indirect immunofluorescence microscopy showed that emerin localised to the nuclear envelope in FPLD and progeroid fibroblasts in the presence of lamin A disease mutants. Immunofluorescence microscopy also showed sites of emerin accumulation which did not co-localise with lamin A/C in double stained late onset, classical and severe progeria fibroblasts. Lack of co-localisation only appeared in cells with abnormal nuclear morphology usually involving a thickened lamina (Figure 4.7).

It has also been reported that in transfected cells carboxymethylated farnesylated prelamin A co-localises with emerin in cells with normal nuclear envelope morphology, but in cells with nuclear envelope invaginations, emerin only partially co-localised with prelamin A (Capanni *et al* 2009). In agreement with this finding, in this study, double staining of fibroblasts with emerin and prelamin A revealed that progeroid cells with a thickened nuclear lamina contained sites of emerin accumulation which did not co-localise with prelamin A (Figure 4.8).

#### ***4.4.6 Emerin mislocalisation does not result in $\beta$ -catenin accumulation in progeria cell lines***

The transcription factor  $\beta$ -catenin exists either bound to a scaffolding complex in the cytoplasm, bound to cadherin at the cell membrane or free in the nucleus in its active transcription factor form. Free  $\beta$ -catenin in the cytoplasm is degraded. Active  $\beta$ -catenin can inhibit adipogenesis via the canonical Wnt signalling pathway (Ross *et al* 2000).

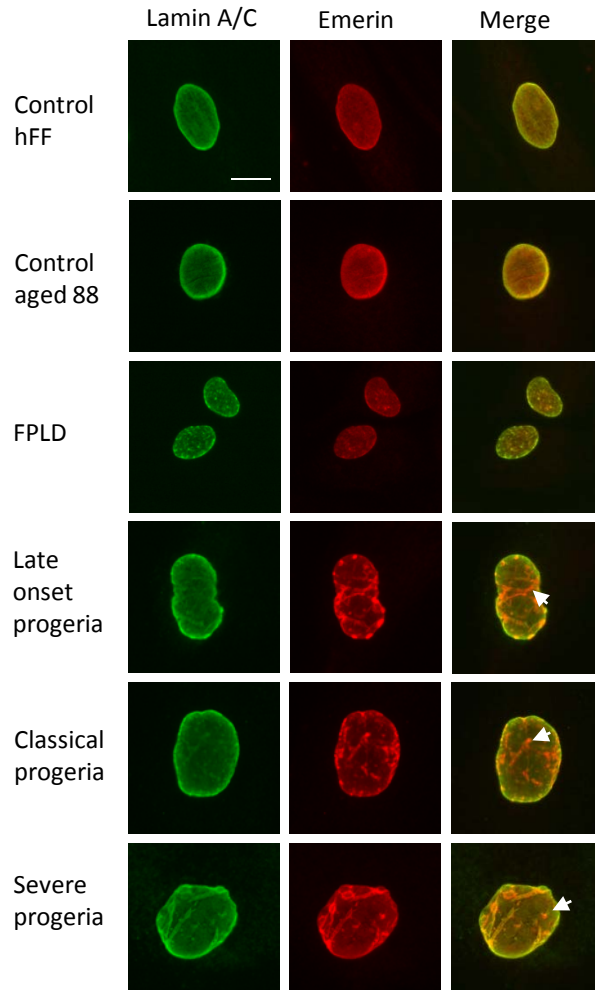


**Figure 4.7** Emerin does not completely co-localise with lamin A/C in a subpopulation of progeria cells showing thickening of the nuclear lamina. Cells were co-stained for lamin A/C (green) and emerin (red). The lamin A/C antibody also detects prelamin A. Merged images show co-localisation and areas where co-localisation does not occur are indicated by white arrows. In FPLD nuclei containing lamin A/C aggregates, emerin appears to co-localise with lamin A/C. Bar 10 $\mu$ m

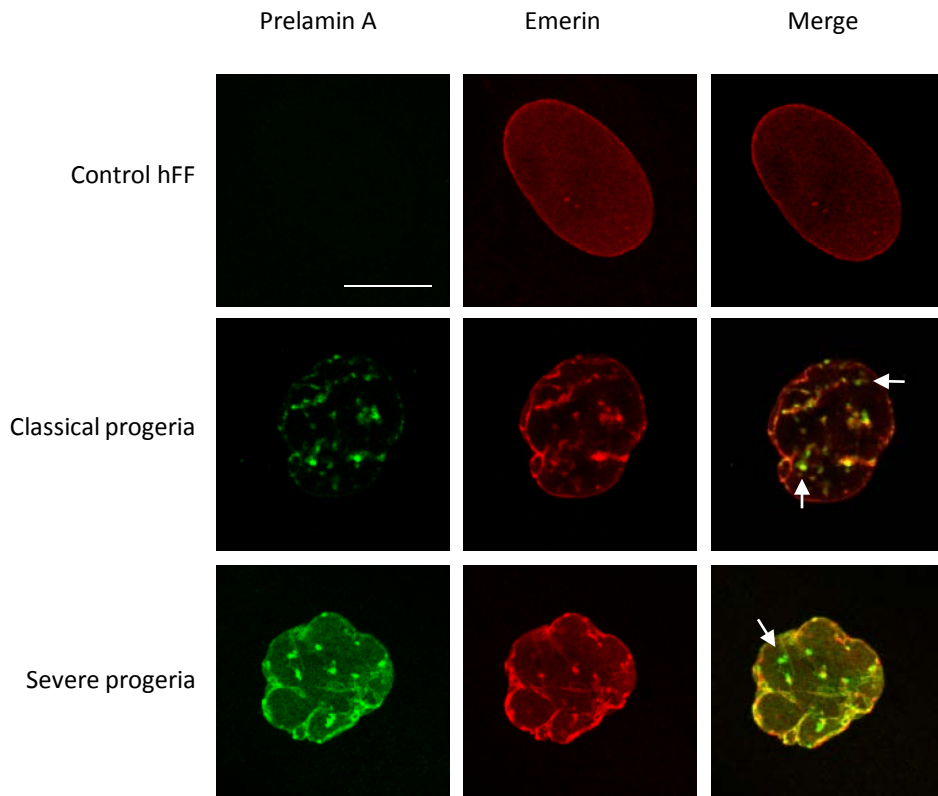


**Figure 4.8** Emerin does not completely co-localise with prelamin A in classical and late onset progeria cells showing thickening of the nuclear lamina. Cells were co-stained for prelamin A (green) and emerin (red). Merged images show areas where co-localisation does not occur, indicated by white arrows. Prelamin A was not detected in the hFF control cell line. Bar 10  $\mu\text{m}$

Emerin has been found to inhibit  $\beta$ -catenin activity by preventing its accumulation in the nucleus, leading to its degradation in the cytoplasm (Markiewicz *et al* 2006). Thus, it was hypothesised that mislocalisation of emerin in progeria allows accumulation of  $\beta$ -catenin in the nucleus resulting in increased inhibition of adipogenesis and contributing to the lipodystrophy phenotype. As a preliminary investigation of this hypothesis, levels of  $\beta$ -catenin in the progeria cell lines were compared to control and FPLD cells. Western blotting revealed equal levels of total  $\beta$ -catenin in all patient and control cell lines (Figure 4.3). However, levels of active  $\beta$ -catenin appear to be decreased in all progeria cell lines, which is the opposite of the result predicted. Nonetheless,  $\beta$ -catenin is involved in many cellular events and its down regulation may be relevant to progeria via another signalling pathway.

#### ***4.4.7 Lamin B1 is down regulated in progeria and old age***

Lamin B depletion has been reported in classical progeria fibroblasts (Scaffidi and Misteli 2005) and in buds in abnormal FPLD nuclei (Vigouroux *et al* 2001). In this study, lamin B levels were compared in classical and atypical HGPS and loss of lamin B from nuclear buds was investigated in the FPLD patient cell line. Indirect immunofluorescence microscopy revealed that lamin B1 staining was indeed reduced in atypical as well as classical progeria cell lines and to a lesser extent in the aged control cell line (Figure 4.9). In the small number of FPLD cells containing nuclear buds, lamin B1 was depleted in the buds. In the progeria cell lines, lamin B1 was completely or partially depleted from the entire cell; however, complete lamin B1 depletion from nuclear buds was visible in progeria cells in which lamin B1 was partially depleted (Figure 4.9). Lamin B1 down regulation in progeria and in the control aged 88 years was confirmed by Western blotting (Figure 4.3).

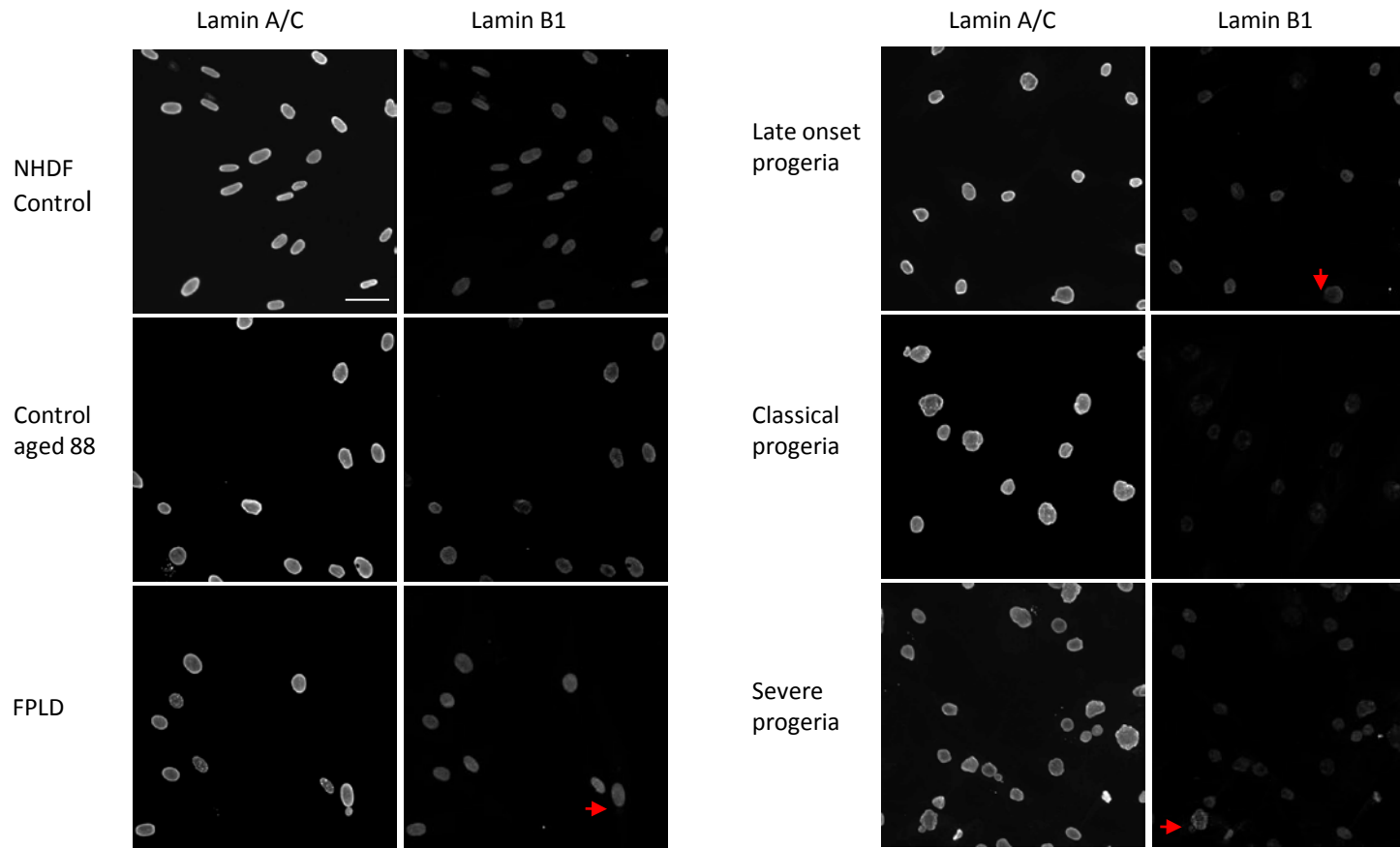


**Figure 4.9** Analysis of lamin B1 staining in cultured fibroblasts by indirect immunofluorescence microscopy. Lamin B1 depletion from nuclear buds is indicated by red arrows. Cells were co-stained with lamin A/C to visualise nuclei. The lamin A/C antibody also detects pre-lamin A. All cell lines were stained by the same antibody mix and all images taken using the same settings. Bar 50  $\mu$ m

#### ***4.4.8 LAP2 $\alpha$ and Rb are down regulated in progeria and old age***

Nucleoplasmic proteins lamina-associated polypeptide isoform 2 $\alpha$  (LAP2 $\alpha$ ) and retinoblastoma protein (Rb) are down-regulated in classical HGPS (Scaffidi and Misteli 2005, Meaburn *et al* 2007)). Normally, A-type lamins interact with the nucleoplasmic lamina-associated polypeptide isoform, LAP2 $\alpha$  (Dechat *et al* 2000) and with the transcription factor Rb p110 isoform (Ozaki *et al* 1994). LAP2 $\alpha$ , in complex with nucleoplasmic lamin A/C, anchors Rb in the nucleoplasm thus regulating cell proliferation and differentiation via the Rb-E2F pathway (Markiewicz *et al* 2002).

Loss of lamin A from the nucleoplasm was observed in all progeria cell lines in this study (Figure 4.1, Section 4.3.1, Table 1.2) and has been previously reported in classical HGPS (Goldman *et al* 2004). The effect of loss of nucleoplasmic lamin A on the nucleoplasmic proteins LAP2 $\alpha$  and Rb was investigated in progeria and compared to FPLD where nucleoplasmic lamin A is not reported to be lost.

##### *4.4.8.1 LAP2 $\alpha$ down regulation in progeria and old age*

Indirect immunofluorescence microscopy showed that LAP2 $\alpha$  staining was significantly reduced in progeria and the control aged 88 years compared to the hFF control (Figure 4.10). Cell counts show that LAP2 $\alpha$  staining was visible but faint in 68% of late onset progeria nuclei, 71% of classical progeria nuclei and 78% of severe progeria nuclei. In the control aged 88 years, 46% of nuclei had reduced LAP2 $\alpha$  and in FPLD this was 21%. In contrast, there was a reduction in LAP2 $\alpha$  staining in only 5% of nuclei in hFF control fibroblasts (Figure 4.5C). Down regulation of LAP2 $\alpha$  appears to correlate with disease severity in progeria.

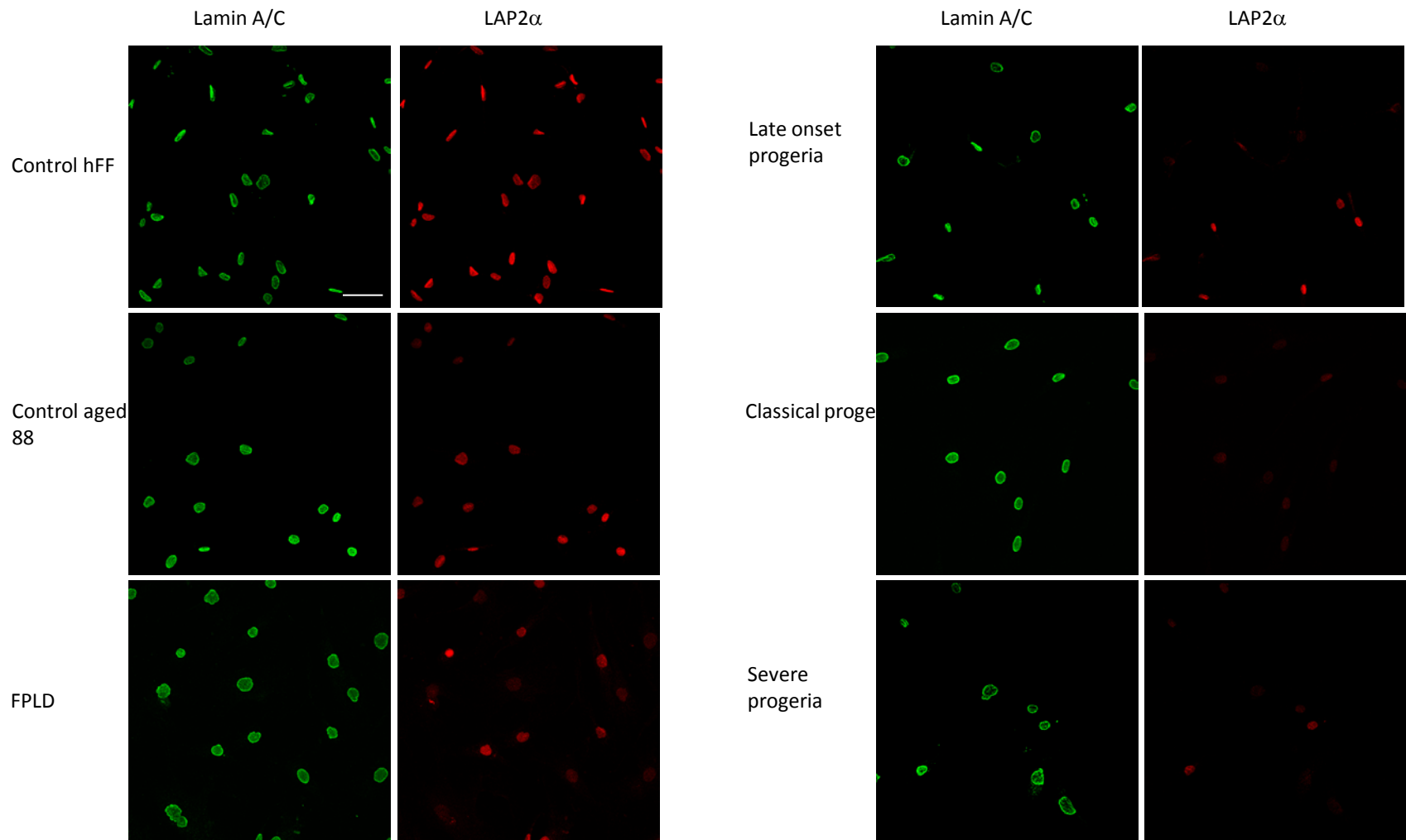


**Figure 4.10** Analysis of staining of LAP2a (red) in cultured fibroblasts by indirect immunofluorescence microscopy. Cells were co-stained for lamin A/C (green) to visualise nuclei. The lamin A/C antibody also detects pre-lamin A. Bar 50  $\mu$ m

Western blotting confirmed immunofluorescence microscopy results, with a significant reduction in band intensity in all progeria samples and old age and a slight decrease in the intensity of the FPLD band compared to the hFF control (Figure 4.3).

#### *4.4.8.2 Rb down regulation in progeria and old age*

The pattern of reduction in staining was the same for both LAP $\alpha$  and Rb. Indirect immunofluorescence microscopy revealed a significant reduction in Rb levels in progeria and the control aged 88 years and a slight reduction in FPLD (Figure 4.11). This is supported by Western blotting which shows a reduction in band intensity in all progeria samples and the control aged 88 years and a slight decrease in the intensity of the FPLD band compared to the hFF control (Figure 4.3).

Cell counts show faint Rb staining in 56% of late onset progeria nuclei, 71% of classical progeria nuclei and 93% of severe progeria nuclei. In the control aged 88 years, 60% of nuclei showed faint Rb staining and in 36% of FPLD nuclei and 12% of hFF control nuclei, Rb was faint (Figure 4.5D). In common with LAP2 $\alpha$ , Rb down regulation also appears to correlate with disease severity in progeria.

#### *4.4.8.3 LAP2 $\alpha$ and Rb down regulation are linked*

Based on the suggestion that lamin A and LAP2 $\alpha$  complexes anchor Rb in the nucleoplasm (Pekovic *et al* 2007), the possibility of a correlation between LAP2 $\alpha$  and Rb down regulation was investigated. Fibroblasts were double stained with LAP2 $\alpha$  and Rb to see if a reduction in LAP2 $\alpha$  staining coincided with a reduction in Rb staining in individual nuclei. Indirect immunofluorescence microscopy showed that, in individual nuclei, Rb and LAP2 $\alpha$  are mostly reduced concomitantly (Figure 4.12). There were a

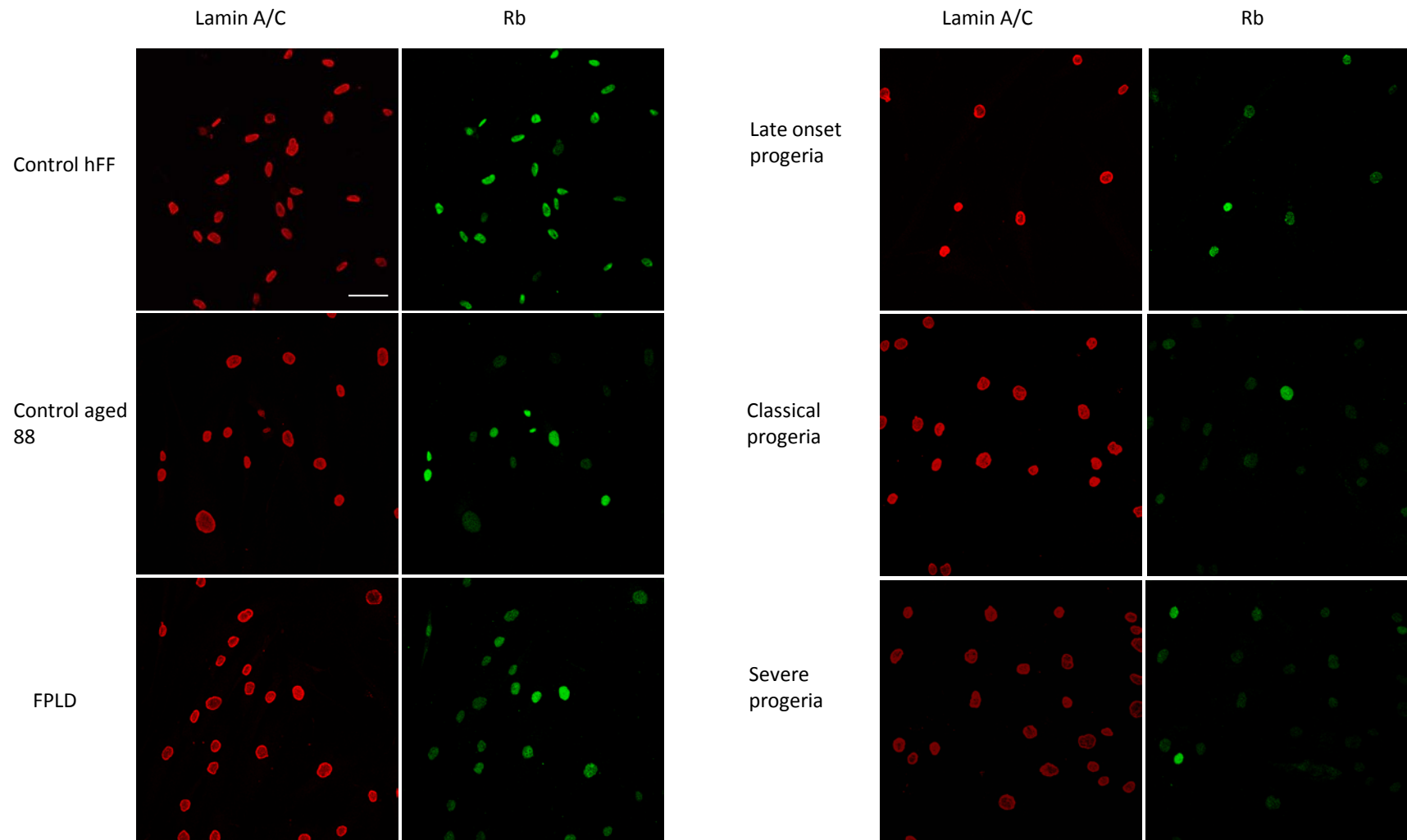


**Figure 4.11** Analysis of staining of Rb (green) in cultured fibroblasts by immunofluorescence microscopy. Cells were co-stained for lamin A/C (red) to visualise nuclei. The lamin A/C antibody also detects pre-lamin A. Bar 50  $\mu$ m

small number of nuclei, however, where either LAP2 $\alpha$  or Rb staining but not both was reduced. This occurred in 2% of hFF and aged control nuclei, 0.3% of FPLD, 6% of late onset, 3% of classical and 12% of severe progeria nuclei, and may suggest that LAP2 $\alpha$  and Rb do not depend on each other for nucleoplasmic localisation.

#### ***4.4.9 The marker of proliferation, Ki67, is reduced in all progeria cell lines***

Loss of LAP2 $\alpha$  has been linked to an increase in proliferation in HeLa cells (Dorner *et al* 2006) and in mouse primary fibroblasts (Naetar *et al* 2008). In contrast, loss of LAP2 $\alpha$  has also been found to result in cell cycle arrest in human dermal fibroblasts (Pekovic *et al* 2007). Proliferation in the fibroblast cell lines in this study was investigated by immunofluorescence microscopy using an antibody against the marker of proliferation, Ki67. In agreement with Pekovic *et al*, proliferation appeared to be significantly reduced in all progeria cell lines compared to the normal human dermal fibroblast (NHDF) cell line used as the control in this experiment (Figure 4.13). To a lesser extent, proliferation also appeared reduced in the aged control. FPLD fibroblast proliferation appeared to equal that of the NHDF cell line.

#### ***4.4.10 No reduction in heterochromatin protein 1 $\gamma$ was found in the progeria cell lines studied***

Members of the heterochromatin protein 1 (HP1) family are heterochromatin binding proteins which are involved in heterochromatin formation and gene silencing (reviewed Fanti and Pimpinelli 2008). Due to their binding properties, HP1 proteins have been used as markers of heterochromatin. HP1 $\alpha$  and HP1 $\gamma$  have been found to be down regulated in classical progeria (Scaffidi and Misteli 2005, 2008), due to loss of heterochromatin in progeria cells. Heterochromatin loss can lead to changes in gene

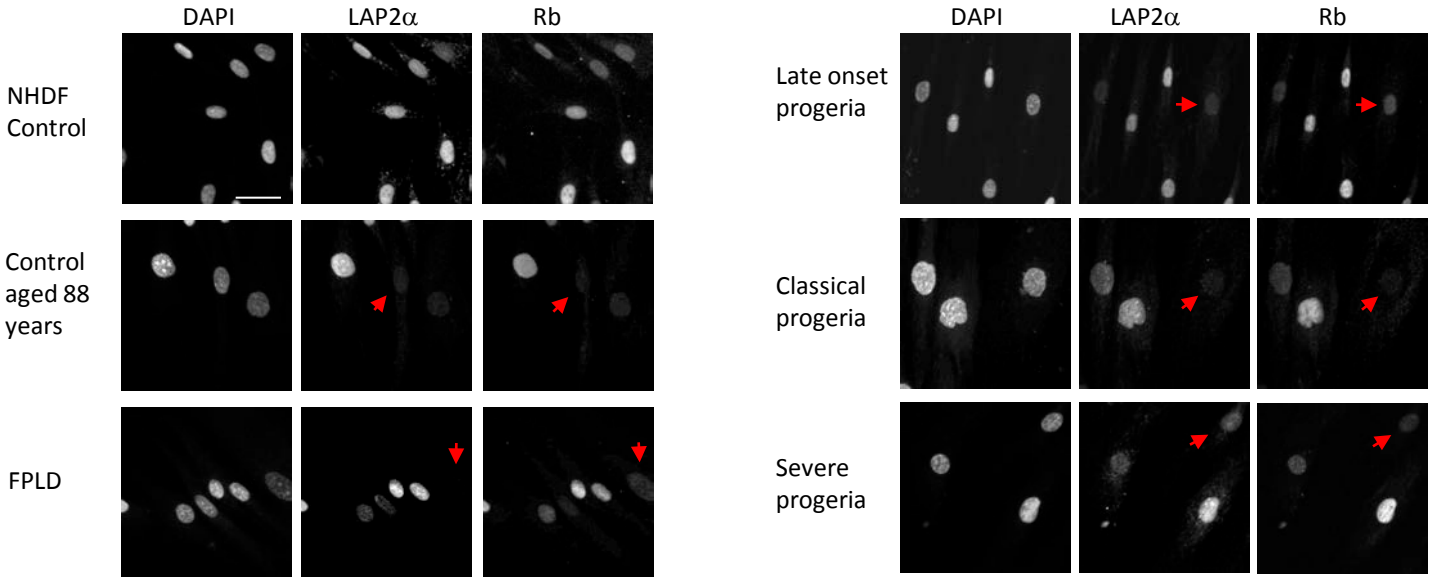


**Figure 4.12** Analysis of Lap2 $\alpha$  and Rb staining in cultured fibroblasts by indirect immunofluorescence microscopy. Cells were double stained with Rb and LAP2 $\alpha$  to show staining levels of both proteins in individual cells. Cells were stained with DAPI to visualise nuclei. Red arrows indicate examples of nuclei which show reduced staining of LAP2 $\alpha$  and Rb. Bar 50  $\mu$ m

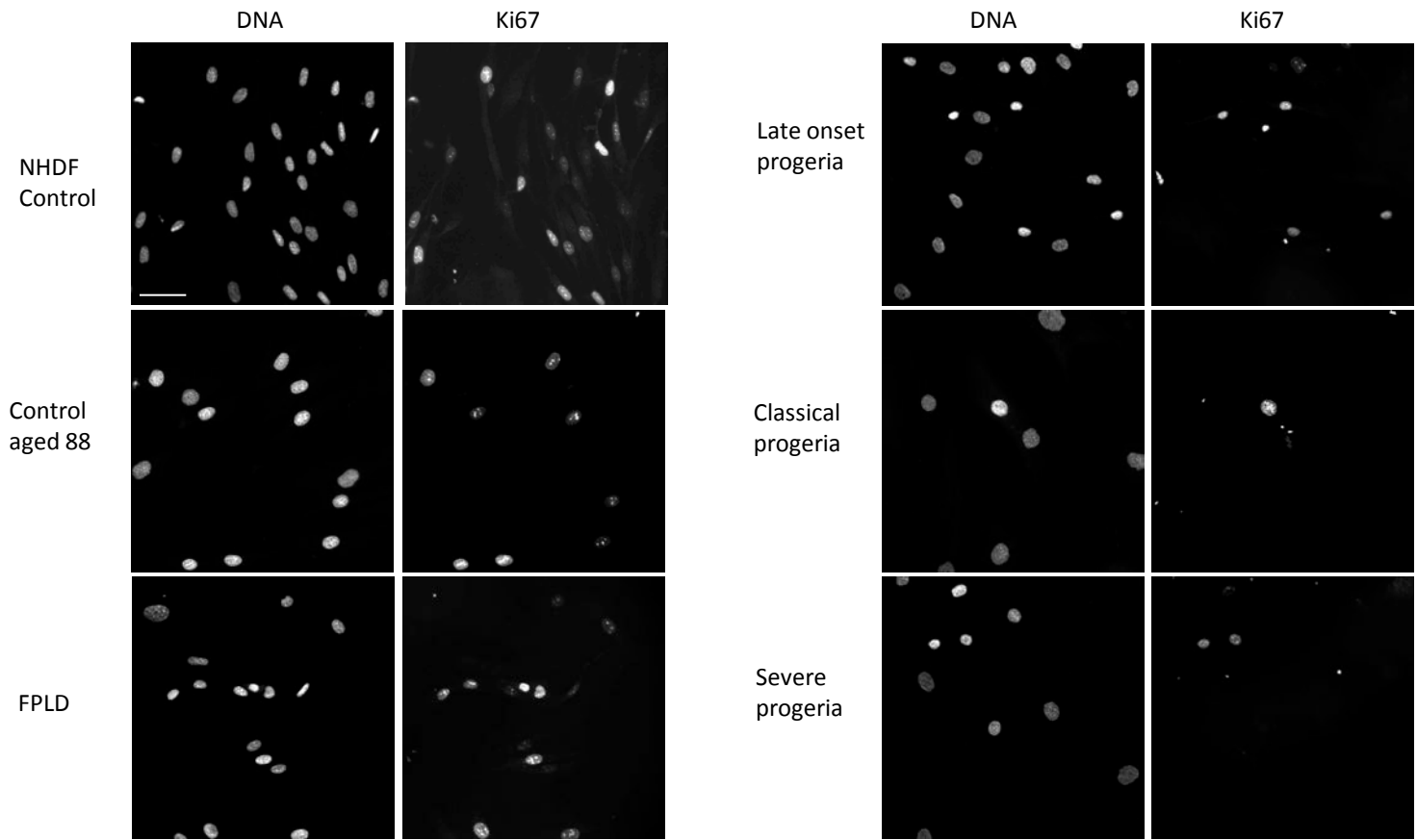


**Figure 4.13** Staining of the marker of proliferation, Ki67 in cultured fibroblasts by indirect immunofluorescence microscopy. Nuclei were DAPI stained for visualisation. Bar 50  $\mu$ m

expression and potentially DNA damage. However, there was no visible reduction in staining of HP1 $\gamma$  by immunofluorescence microscopy in any of the cell lines in this study (Figure 4.14).

#### **4.5 Altered mobility of lamin A mutants**

Mobility studies were used to investigate the hypothesis that abnormal farnesylation of lamin A mutants contributes to the disease phenotype in atypical progeroid syndromes. FRAP was used to determine the mobility of lamin A mutants. FRAP data, alongside Western blot analysis of lamin A in cell extracts from atypical progeria patients, was used to identify the farnesylation status of lamin A mutants.

##### **4.5.1 FRAP constructs**

HeLa cells were used for the mobility study because transfection efficiency of dermal fibroblasts was poor and the health of the cells was badly affected. HeLas were transfected with the GFP-tagged LA constructs listed in Table 4.3.

The GFP LA WT construct was made previously in the laboratory and GFP LA SX, GFP LA E578V and GFP LA S143F were made by student Joaquim Moreno Càceres. Other constructs were made by excision of the mutant LMNA sequence from pCIneo plasmids and ligation into the GFP LA WT construct at the same sites replacing the WT sequence with the mutated sequence or by mutation of the WT sequence using an Invitrogen GeneTailor mutagenesis kit. The GFP LA G608G and T623S constructs were produced by reverse transcription of mRNA extracted from patient fibroblasts.

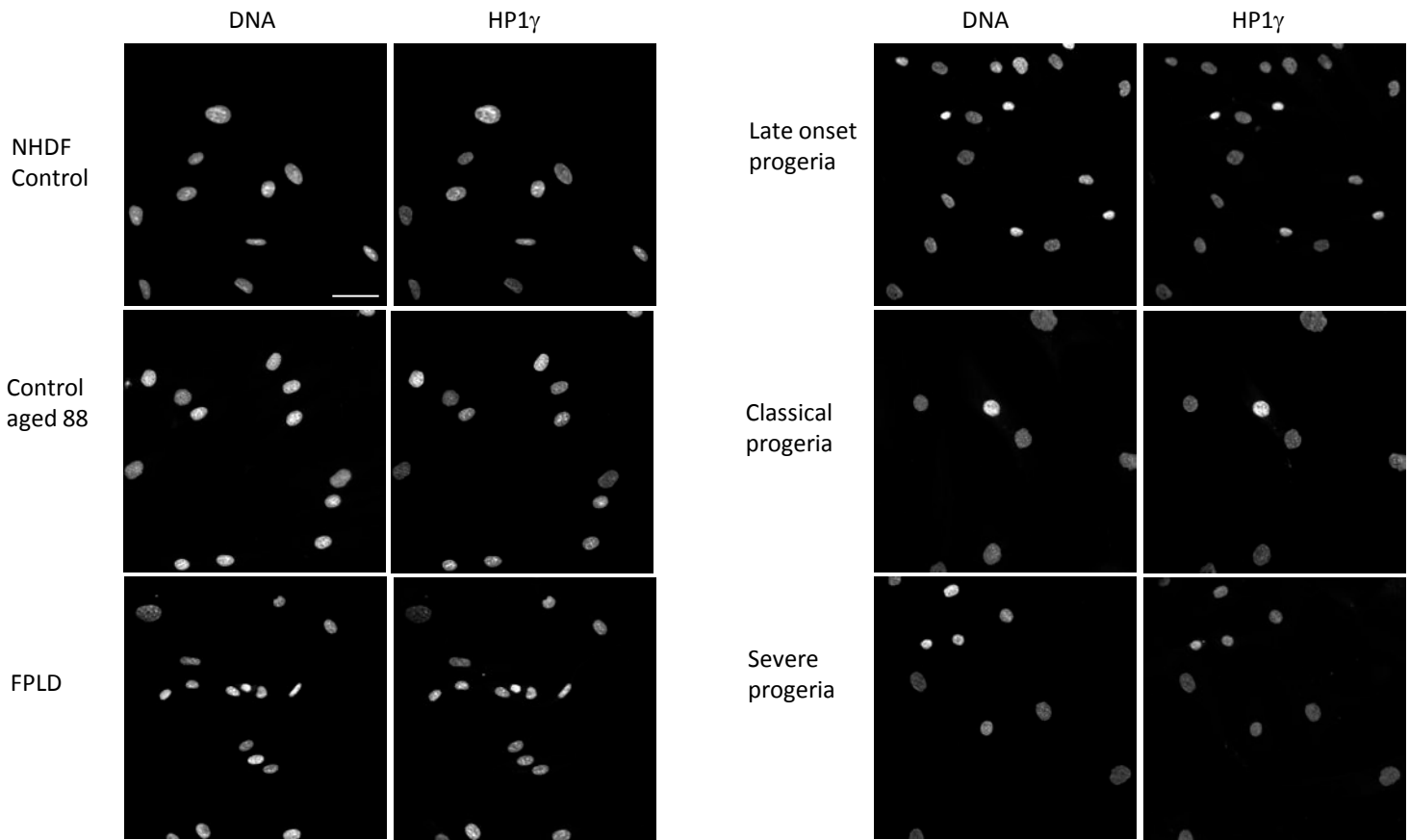


**Figure 4.14** Staining of a marker of heterochromatin, HP1 $\gamma$  in cultured fibroblasts by indirect immunofluorescence microscopy. Nuclei were DAPI stained for visualisation. Bar 50  $\mu$ m

Construct	Description
GFP LMNA WT (control)	Wild type lamin A
GFP LA SX (control)	Farnesylation incompetent prelamin A
GFP LA L647R (control)	Cleavage incompetent, permanently farnesylated prelamin A
GFP LA R482W	Most commonly occurring AD FPLD point mutation
GFP LA R527H	AR point mutation resulting in mandibuloacral dysplasia
GFP LA K542N	AR point mutation resulting in classical progeroid phenotype
GFP LA E578V	AD point mutation resulting in atypical progeria
GFP LA S143F	AD point mutation resulting in atypical progeria with myopathy
GFP LA T623S	AD cryptic splice site activation mutation resulting in atypical progeria
GFP LA G608G	AD cryptic splice site activation mutation resulting in classical progeria

**Table 4.3** Constructs used in mobility study FRAP experiments. AR: autosomal recessive. AD: autosomal dominant.

The GFP LA WT construct contains the wild type prelamin A sequence which is post translationally processed in HeLa cells to produce the mature lamin A protein. This was confirmed by western blotting (data not shown).

The GFP LA SX construct was designed to allow confirmation that the mobility of non-farnesylated prelamin A is equal to wild type mature lamin A. This will confirm that mobility is reduced by the farnesyl group and not the prelamin A sequence. LA SX contains a stop codon to replace the serine residue at position 662 so the prelamin A sequence is retained but cannot be farnesylated or cleaved.

The GFP LA L647R construct was designed to confirm the reduced mobility of farnesylated lamin A. LA L647R mimics permanently farnesylated prelamin A. The leucine residue at position 647 has been replaced with arginine so that the final post

translational cleavage by ZMPSTE24 between amino acids 646 and 647 cannot occur resulting in a permanently farnesylated form of prelamin A.

For the mobility study, all mutant constructs were transfected into HeLa cells and all localised normally to the nuclear envelope in the majority of cells (Figure 4.15). The GFP LA SX mutant construct formed aggregates in some cells and did not localise to the nuclear envelope, possibly because it is farnesylation incompetent and therefore not targeted to the nuclear envelope. Only cells in which the LA SX mutant localised to the nuclear envelope were used in this mobility study.

#### ***4.5.2 FRAP analysis***

FRAP was performed to compare mobility of mutant constructs with wild type. Photobleaching was performed using a Leica TCS SP5 confocal microscope and analysed with Leica LAS AF software. Regions of interest of 5  $\mu\text{m}$  by 2  $\mu\text{m}$  were bleached with an argon laser and 6 images were obtained after bleaching at 5 minute intervals.

#### ***4.5.3 Results of mobility study***

Relative fluorescence recovery data over time was plotted for mutant proteins alongside wild type (Figure 4.16). To compare all mutants, a single graph showing recovery over time was plotted (Figure 4.17).

The only progeria mutant to be studied previously is G608G classical progeria (Goldman *et al* 2004, Dahl *et al* 2006). Reduced mobility of this mutant was confirmed. The LA L647R and LA T623S constructs also had reduced mobility, which correlates with the presence of a farnesyl group. Interestingly, LA S143F also had reduced

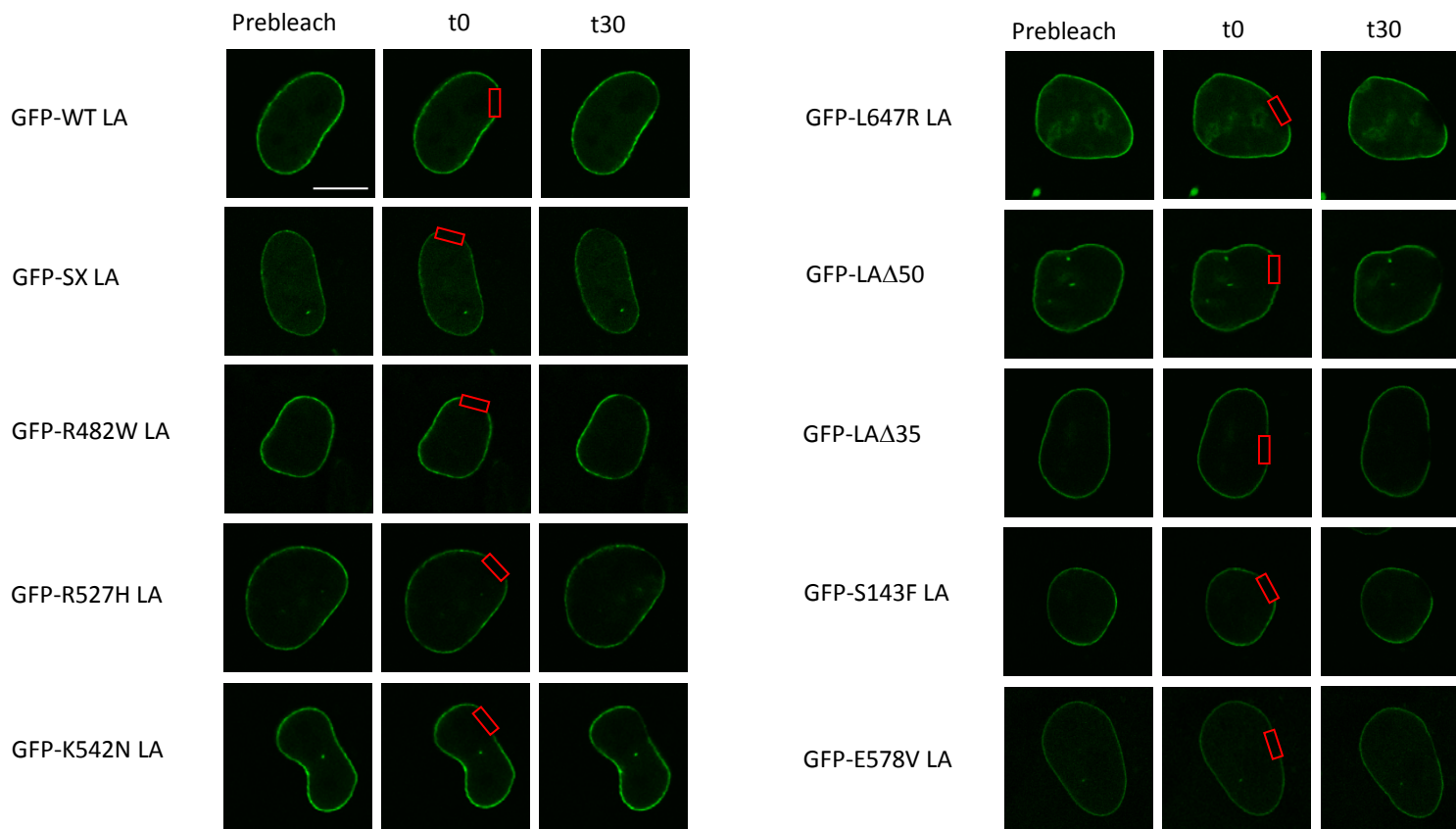


**Figure 4.15** Bleaching and recovery during FRAP analysis of wild type and mutant lamin A. Single plane confocal images of HeLa cells transiently transfected with GFP-tagged WT and mutant lamin A. The area within the red box was bleached. Images show nuclei before (prebleach), immediately after (t0) and 30 (t30) minutes after photobleaching. Bar 10  $\mu$ m

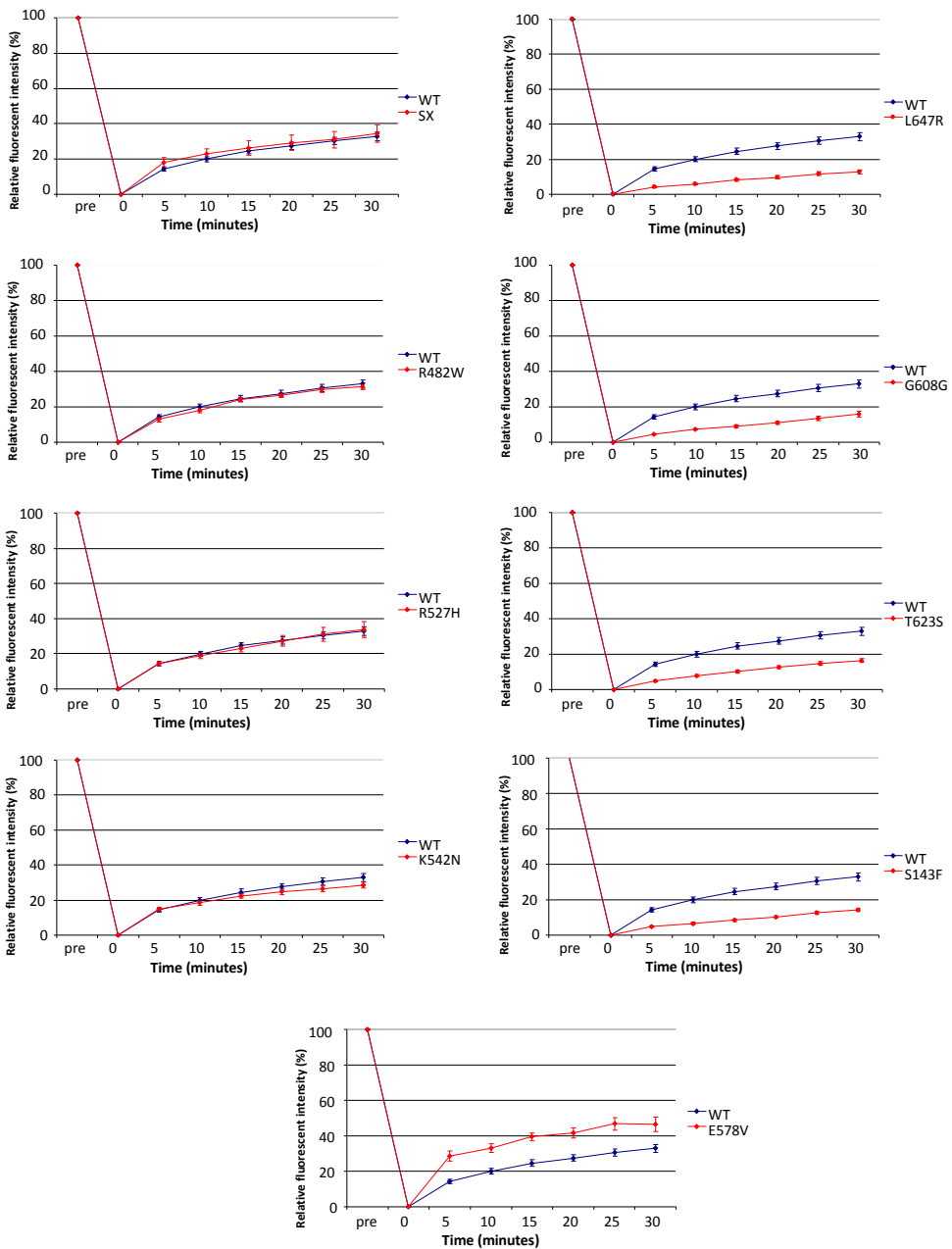


**Figure 4.16** Recovery during FRAP analysis of wild type lamin A and various mutants as indicated. In each graph, data for WT (blue) and a mutant (red) are compared. Mean relative GFP intensity in the bleached area (shown as a red box in figure 4.15) was plotted as a function of time. Each data point represents the average intensity of at least 9 cells. Error bars represent SEM

mobility even though it is not aberrantly farnesylated (as shown by Western blot in Figure 4.18).

LA R527H is an autosomal recessive point mutation which causes mandibuloacral dysplasia (MAD). LA K542N is also an autosomal recessive point mutation and results in a classical progeria phenotype. These proteins are not predicted to be permanently farnesylated (Figure 4.18) and both showed mobility similar to WT. The LA SX non-farnesylated prelamin A construct also showed a similar mobility to WT, confirming that mobility is reduced by the farnesyl group and not the prelamin A sequence.

LA E578V is an autosomal dominant point mutation which causes a mild progeria phenotype. Surprisingly, this mutant showed mobility approximately twice that of wild type lamin A.

## **4.6 Discussion**

### ***4.6.1 Findings in FPLD fibroblasts***

Nuclear abnormalities observed in the R482W FPLD patient in this study affected 6% of passage 12-14 nuclei. Abnormalities have previously been reported to affect 13% of passage 10 nuclei from two patients carrying the R482W mutation and 22% of passage 10 nuclei from a patient carrying the R482Q mutation (Vigouroux *et al* 2001). The finding of this study, taken together with the findings of Vigouroux *et al*, suggests that there is variation in the number of abnormal nuclei both between patients carrying different FPLD mutations and between different individuals carrying the same mutation. Indeed, disease expression in patients has been found to vary between both patients carrying different FPLD point mutations (Cao and Hegel 2000) and between patients

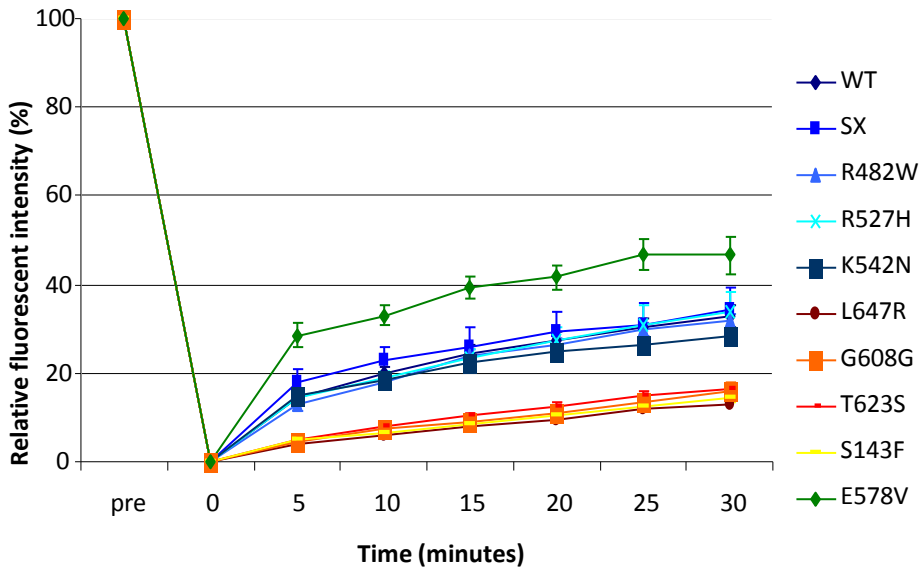


**Figure 4.17** FRAP analysis of wild type and mutant lamin A. Mean relative GFP intensity in the bleached area (shown as a red box in figure 4.14) was plotted as a function of time. Each data point represents the average intensity of at least 9 cells.

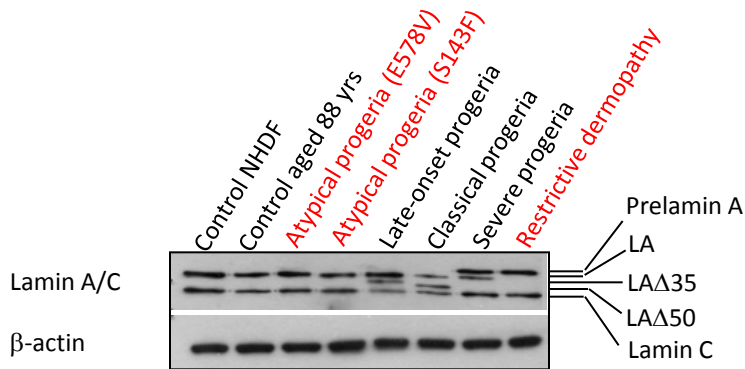


**Figure 4.18** Western blot analysis of lamin A/C expression in whole cell extracts to corroborate FRAP data. Additional cell lines which were not available for the rest of this study are shown in red with *LMNA* mutations in brackets. The restrictive dermatopathy patient carried homozygous *ZMPSTE24* mutations. Cell extracts were produced by Zaahidah Variava under my supervision, western blotting was performed by the student.

(Vigouroux *et al* 2000) and family members (Cao and Hegel 2000) carrying the same point mutation.

Nuclei containing buds were observed in 10 % of dysmorphic FPLD nuclei, and only 3 nuclei out of 2500 counted were observed to have nuclear buds containing the honeycomb meshwork of lamin A/C staining illustrated in Figure 4.1. Lamin B1 was always depleted in nuclear buds even when the lamin A/C honeycomb meshwork was absent, Figure 4.11. Depletion of lamin B in nuclear buds in FPLD has been previously reported (Vigouroux *et al* 2001); in their study of 3 FPLD patient cell lines, two carrying the R482W mutation and one the R482Q mutation, nuclei containing buds were observed in 1%, 15% and 50% of dysmorphic nuclei respectively. The findings of this study, taken together with the findings of Vigouroux *et al*, suggest that there is variation in the nature as well as extent of nuclear abnormality in FPLD.

In this study, aggregates of lamin A/C were detected in 20% of dysmorphic FPLD nuclei, illustrated in Figure 4.1. Lamin A/C aggregates have been previously reported in fibroblast nuclei from an R482L patient (Capanni *et al* 2003), however Vigouroux *et al* 2001 found no lamin A/C aggregates in R482W or R482Q patient nuclei.

In the sub population of FPLD cells found to contain nuclear buds, lamin B1 was always lost from buds, Figure 4.11. The antibody used in this study detected only lamin B1. Loss of B-type lamins from nuclear buds in FPLD has been previously been detected (Vigouroux 2001). It has been shown that A-type lamins and B-type lamins form separate homopolymers in the lamina (Delbarre *et al* 2006). In FPLD the presence of mutant R482W lamin A appears to result in a modified structure of the lamina which does not contain lamin B homopolymers in nuclear buds. An alteration in the distribution of lamin A, such as honeycomb structures is unlikely to be the mechanism

by which lamin B is lost, since lamin B loss also occurs in buds containing normal lamin A staining. Lamin A is present only in differentiated cells whereas lamin B is ubiquitously expressed, also lamins B1 and B2 have been found to localise to the nuclear rim in the adrenal cortex carcinoma cell line SW13 which expresses extremely low levels of lamin A, illustrating that lamin A is not necessary for normal lamin B localisation (Vaughan *et al* 2001). It seems likely, therefore, that in nuclear buds mutant R482W lamin A exerts a dominant negative effect at the lamina, leading to loss of lamin B.

Fibroblasts from an FPLD patient carrying the R482L mutation have been reported to accumulate prelamin A and SREBP1 at the nuclear rim (Capanni *et al* 2005). This group also found that SREBP1 binds prelamin A but not mature lamin A and suggest the mechanism underlying FPLD may be the sequestering of SREBP1 away from its site of transcriptional activity to the nuclear rim by prelamin A.

In this study, prelamin A was not detected in R482W fibroblasts by immunofluorescence microscopy, and was also undetectable in the hFF control cell line by this technique. Western blotting of total cell extracts revealed a very faint prelamin A band in R482W fibroblast extracts and a prelamin A band of similar intensity was detected in the hFF wild type control, suggesting that R482W lamin A is processed normally.

There are a number of possible reasons why the results of this study differ from those of Capanni *et al*. Prelamin A accumulation may not have occurred in our R482W patient fibroblasts for a number of reasons, although patients carrying R482W or R482L mutations display a Dunnigan-type FPLD phenotype, there is a large variation in disease severity between FPLD patients. The R482L patient may have a more severe

FPLD phenotype than the R482W patient due, for example, to environmental or genetic factors affecting disease penetrance. Fibroblasts used by Capanni *et al* were at passages 10 to 15, similar to those used in this study at passages 12 to 14. However, if the R482W fibroblast donor in this study was of a younger chronological age than the R482L donor, the disease phenotype may have been less advanced.

Western blotting and immunofluorescence microscopy revealed no differences in expression or localisation of other proteins investigated. No proliferation defects were detected by Ki67 staining, concomitantly, no down regulation of LAP2 $\alpha$  or Rb was detected. HP1 $\gamma$  was not down regulated, suggesting that there is no loss of heterochromatin.

Unfortunately, the results of this study do not offer further information on the FPLD disease mechanism. However, taken together with reports in the literature, they indicate that in FPLD, the patient disease phenotype, age and possibly other environmental factors, as well as mutation type, may be important influences on the cellular phenotype.

#### ***4.6.2 Findings in progeria fibroblasts***

##### *4.6.2.1 The severity of patient disease phenotype correlates with the expression level of unprocessed lamin A*

The severe progeria patient in this study carried compound heterozygous ZMPSTE24 mutations which resulted in defective prelamin A processing. Western blotting of cell extracts with an anti lamin A/C antibody revealed that severe progeria fibroblasts showed very high levels of prelamin A accumulation and barely detectable levels of

mature lamin A (Figure 4.3). Prelamin A accumulation appears to be responsible for the disease phenotype of this patient.

Classical (G608G) and late onset (T623S) progeria mutations are both caused by activation of cryptic splice sites resulting in the production of truncated, permanently farnesylated forms of lamin A as described above. The results of this study indicate that the disease mechanism is the same in both types of progeria and the increased severity of disease found in classical progeria appears to be due to a higher level of mutant LA $\Delta$ 50 protein present in classical HGPS compared to LA $\Delta$ 35 in late onset HGPS. Although the possibility that the 15 amino acids deleted in LA $\Delta$ 50, but present in LA $\Delta$ 35, may result in a detrimental affect contributing to the more severe classical progeria phenotype has not been ruled out. Western blotting of cell extracts with an anti lamin A/C antibody revealed at least twice as much mutant lamin A protein in classical compared to late onset progeria fibroblasts (Figure 4.3). This result was confirmed by qPCR analysis performed in the laboratory by Dr Nicolas Sylvius, where there was a 2.5 fold higher level of G608G mRNA compared to T623S mRNA when normalised to levels of WT mRNA.

The results of this study further indicate that the cellular effects of LA $\Delta$ 35 and LA $\Delta$ 50 mutant proteins in late onset and classical progeria and prelamin A accumulation in the severe progeria patient appear to be identical and disease severity increases with an increase in the level of abnormal lamin A.

Prelamin A accumulation has been previously reported in classical progeria (Goldman *et al* 2004) and slightly increased levels of prelamin A were detected by Western blotting in late onset and classical progeria in this study. By indirect immunofluorescence microscopy, prelamin A was not detectable late onset progeria

fibroblasts. This difference may be due to sensitivity of the techniques. Prelamin A visualisation in classical progeria may have been aided by its accumulation in aggregates which are stained brightly by this technique. The cause of pre lamin A accumulation in the presence of progerin or other lamin A mutants is not known. It may be possible that lamin A mutants form an abnormal association with ZMPSTE24 interfering with the processing of wild type lamin A. Alternatively, permanently farnesylated mutants may block access to ZMPSTE24 by accumulating at the nuclear membrane. Prelamin A is toxic to cells and is responsible for the disease phenotype of the severe progeria patient in this study and partly or wholly responsible for the restrictive dermopathy phenotype (Moulson *et al* 2005), thus the accumulation of prelamin A in progeria is likely to contribute to the disease phenotype.

#### *4.6.2.2 Down regulation of Rb and LAP2 $\alpha$ result in reduced proliferation*

LAP2 $\alpha$ , in complex with nucleoplasmic lamin A/C, anchors Rb in the nucleoplasm (Markiewicz *et al* 2002). LAP2 $\alpha$  and Rb were down regulated in severe, late onset and classical progeria nuclei and double-staining of nuclei for LAP2 $\alpha$  and Rb showed that in individual nuclei they are mostly reduced concomitantly. It has been reported that in *Lmna*<sup>-/-</sup> MEFs, which do not express A-type lamins, Rb levels were found to be dramatically decreased due to proteasome mediated degradation, and that the introduction of lamin A increased Rb levels (Johnson *et al* 2004). Consequently, the increase in farnesylated lamin A and reduction in nucleoplasmic lamin A found in late onset, classical and severe progeria may be responsible for downregulation of Rb and LAP2 $\alpha$  due to disruption of nucleoplasmic complexes of lamin A, LAP2 $\alpha$  and Rb.

Significantly reduced proliferation in late onset, classical and severe progeria cells was detected by Ki67 staining. In addition, western blotting with an anti-emerin antibody

revealed higher molecular weight bands in control hFF and FPLD fibroblasts which are thought to represent mitotically phosphorylated emerin (Ellis *et al* 1998). Very faint bands of phosphorylated emerin in late onset, classical and severe progeria cells and the aged control supports the reduced proliferation observed with Ki67 staining.

There have been conflicting reports on the effect of the loss of LAP2 $\alpha$  on cell proliferation. Loss of LAP2 $\alpha$  has been linked to increased proliferation in HeLa cells (Dorner *et al* 2006) and in mouse primary fibroblasts (Naetar *et al* 2008). Conversely, loss of LAP2 $\alpha$  has also been found to result in cell cycle arrest in human dermal fibroblasts (Pekovic *et al* 2007). Reduced proliferation of progeria fibroblasts in this study supports the finding of Pekovic *et al*, and suggests that disruption of the complex of lamin A, LAP2 $\alpha$  and Rb somehow disrupts proliferation. Pekovic *et al* found that human dermal fibroblasts respond to loss of LAP2 $\alpha$  by inducing cell cycle checkpoint arrest and suggest that the checkpoint is abrogated in transformed cell lines such as HeLa. The results of Naetar *et al*, compared to the results of Pekovic *et al* and of this study, appear to suggest that the response to loss of LAP2 $\alpha$  differs in mouse and human fibroblasts.

Interestingly, a reduction in Rb may have implications for the lipodystrophy phenotype in progeria. It has been reported that Rb<sup>-/-</sup> ELF cells (mouse embryonic lung fibroblasts) cannot form adipocytes whereas Rb<sup>+/+</sup> cell can be differentiated (Chen *et al* 1996). In addition, Rb over expression results in increased adipogenesis through the direct activation of Rb with the adipogenic transcription factor C/EBP $\alpha$  (Chen *et al* 1996). Decreased Rb levels, therefore, may reduce adipogenic conversion in progeria.

#### 4.6.2.3 Mislocalisation of SREBP1 may underlie the lipodystrophy phenotype

Immunofluorescence microscopy revealed SREBP1 at the nuclear rim of progeroid nuclei and in most nuclei from the aged control. This supports the finding of Capanni *et al* 2005, who detected SREBP1 accumulation at the nuclear rim of FPLD, MAD and Werner's syndrome fibroblasts. Capanni *et al* suggest that in their cell lines SREBP1 sequestration to the nuclear rim by prelamin A may result in reduced transcription of adipogenic genes, contributing to the lipodystrophic phenotype. The results of this study indicate that SREBP1 accumulation at the nuclear rim may contribute to lipodystrophy in progeria. The unreliability of subsequent SREBP1 antibodies when the original antibody stopped working meant that SREBP1 localisation could not be investigated further.

Emerin has been reported to restrict the accumulation of active  $\beta$ -catenin in the nucleus (Markiewicz *et al* 2006), since  $\beta$ -catenin acts to inhibit adipogenesis (Kennell and MacDougald 2005), it was hypothesised that mislocalisation of emerin in progeria may lead to an increase in active  $\beta$ -catenin in the nucleus, contributing to the lipodystrophy phenotype.

First, emerin localisation was investigated in progeria cells co-stained with antibodies against emerin and lamin A/C. The lamin A/C antibody also detects prelamin A and the LA $\Delta$ 35 and LA $\Delta$ 50 lamin A mutants. Emerin did not completely co-localise with lamin A/C in a subpopulation of morphologically abnormal nuclei. When emerin aggregates were in the plane of focus, aggregates of lamin A/C were not visible, suggesting that abnormal emerin distribution is not the result of sequestration by lamin A/C. Since emerin has been shown to localise to intranuclear aggregates of prelamin A in mevinolin treated fibroblasts (Capanni *et al* 2009), next, the possibility that prelamin A

sequestered emerin into aggregates was tested. The effect of prelamin A on emerin localisation in classical and severe progeria fibroblasts was investigated by co-staining with an emerin antibody and a prelamin A specific antibody. Emerin localised to prelamin A aggregates, as reported by Capanni *et al*, but not all aggregated emerin co-localised with prelamin A even in severe progeria fibroblasts which accumulate very high prelamin A levels. This suggests that sequestration by prelamin A is not the only mechanism by which emerin is localised to intranuclear aggregates in progeria.

Decreased emerin activity, was predicted to result in an increase in  $\beta$ -catenin activity and thus, increased inhibition of adipogenesis contributing to the lipodystrophic progeria phenotype. By western blotting, levels of total  $\beta$ -catenin, consisting of both hypophosphorylated nuclear and hyperphosphorylated cytoplasmic forms, were the same in progeroid and control fibroblasts. The level of active  $\beta$ -catenin, found in the nucleus, was reduced in progeroid compared to control fibroblasts. A decrease in nuclear  $\beta$ -catenin would be expected to decrease adipogenic inhibition, the opposite to the result predicted. Although preliminary, these results do not suggest emerin mislocalisation and subsequent  $\beta$ -catenin dysregulation contributes to the lipodystrophy phenotype in progeria. However,  $\beta$ -catenin is involved in many diverse functions (reviewed Nelson and Nusse 2004) and therefore may have a role in progeria which is not yet understood.

#### ***4.6.3 Altered mobility of lamin A mutants***

The LA G608G mutant has already been shown to have reduced mobility (Goldman *et al* 2004, Dahl *et al* 2006). It is generally assumed that it is likely to be the farnesyl group that causes retention of the protein at the nuclear membrane, this theory is

supported by the presence of a thickened lamina in G608G progeria patient cells. We aimed to find out whether reduced mobility was a general phenomenon for aberrantly farnesylated lamin A mutants. All mutants known to be farnesylated did indeed have reduced mobility.

The LA L647R construct, which mimics permanently farnesylated prelamin A, the LA T623S construct (late onset progeria) and the LA G608G construct (classical progeria), all had significantly reduced mobility compared to the WT LA construct. These mutants were all predicted to be permanently farnesylated. Progerin has been shown to retain its farnesyl group during post translational processing (Glynn and Glover 2005), presumably because the internal deletion of amino acids 606-656 removes the site, amino acids 646 and 647 (Weber *et al* 1989), of the final cleavage by ZMPSTE24. It is probable, therefore, that the internal deletion of amino acids 621-656 resulting from the T623S lamin A mutation also results in retention of the farnesyl group since the final ZMPSTE24 cleavage site is missing from the T623S mutant. The LA L647R construct mimics permanently farnesylated prelamin A which is predicted to accumulate in severe progeria patient 012 due to lack of the enzyme ZMPSTE24, thus confirming the altered mobility of lamin A in this patient.

Mobility of the lamin A mutant R482W, present in FPLD, has been reported to be identical to wild type lamin A in FRAP studies (Gilchrist *et al* 2004). In agreement, the LA R482W construct in this study showed the same mobility as the LA WT construct.

LA R527H and LA K542N premature aging mutants also showed mobility approximately equal to that of LA WT. Unfortunately; fibroblast cell lines from these patients were not available for western blotting. However, mutants contain point mutations upstream of the ZMPSTE24 cleavage site and therefore would not be

predicted to be permanently farnesylated. In addition, R527H and K542N are recessive mutations whereas all farnesylation mutations are dominant; therefore they are unlikely to be aberrantly farnesylated.

Surprisingly, the LA S143F construct showed reduced mobility. This was unexpected since the site of the point mutation (in exon 2) would not be expected to interfere with post translational processing making permanent farnesylation highly unlikely. Western blotting of a cell line received near the end of my studies, revealed a lamin A band of the same size the control, suggesting that post translational processing and cleavage is normal. This unexpected result could perhaps be caused by abnormal protein structure interfering with mobility. Or perhaps an unusually high transfection rate saturated ZMPSTE24 in the HeLa cell line so that transfected protein was not correctly processed, although this is unlikely since exceptionally bright staining was not observed during the experiment.

The LA E578V mutant showed mobility approximately twice that of wild type lamin A, indicating that the progeroid disease phenotype resulting from the point mutation involves a looser association with lamin A at the nuclear envelope. This is the opposite to what would be expected for the lamina of a progeria cell, which usually show thickening and increased stiffening of the lamina (Dahl *et al* 2006). Western blotting revealed lamin A of the same size as the control, indicating that, as the mobility suggests, lamin A is not abnormally farnesylated.

## CHAPTER 5

### An investigation into the interaction between lamin A and sterol response element binding protein 1 (SREBP1)

#### 5.1 Introduction

SREBP1 and SREBP2 are regulators of lipid homeostasis; they are basic helix-loop-helix (bHLH) leucine zipper transcription factors (Figure 5.1) which reside in the endoplasmic reticulum (ER). In sterol depleted cells, SREBPs are escorted from the ER to the Golgi by SREBP cleavage activating protein (SCAP) where they are cleaved by proteases, releasing the N-terminal transcription factor domain. SREBP transcription factors are translocated to the nucleus, where they bind the sterol response element (SRE) sequence of promoters of SREBP target lipogenic genes (Figure 5.2) (Wang *et al* 1994, Brown and Goldstein 1997, reviewed by Eberle *et al* 2004 and Bengoechea-Alonso *et al* 2007).

SREBP2 is encoded by the *SREBF-2* gene and is ubiquitously expressed; it is predominantly involved in cholesterol biosynthesis (Horton *et al* 1998, Pai *et al* 1998). SREBP1a and 1c are produced by alternative transcription of the *SREBF-1* gene and are identical except that SREBP1a has a slightly longer N-terminal acidic activation domain and is a stronger transcriptional activator (Brown and Goldstein 1997) (Figure 5.1). SREBP1 is predominantly involved in fatty acid synthesis (Horton *et al* 1998, Pai *et al* 1998). SREBP1a is highly expressed in cultured cell lines and SREBP1c is the predominant isoform in white adipose tissue and liver (Shimomura *et al* 1997). SREBP1 is part of the adipogenic pathway where it activates the key adipogenic transcription

factor, PPAR $\gamma$  (Kim *et al* 1998) and is a lamin A binding protein (Lloyd *et al* 2002). SREBP1 is therefore of interest as a possible link between lamin A and adipogenesis (Section 1.7.1).

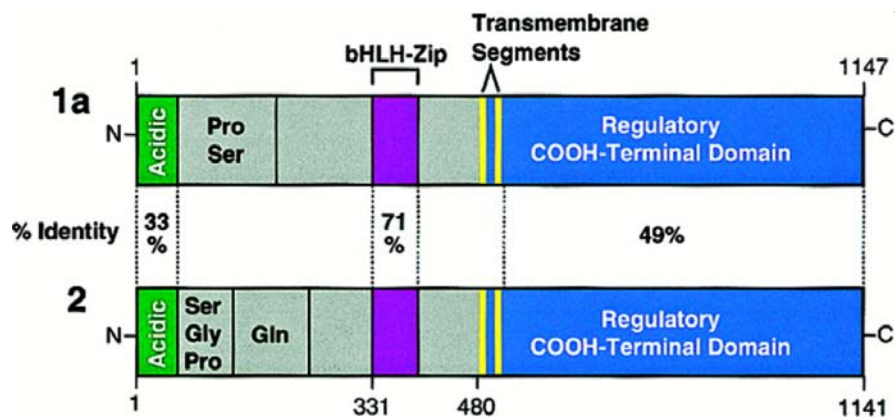


**Figure 5.1** Domain structures of SREBP1a and SREBP2. SREBP1c (not shown) is identical to SREBP1a except that SREBP1a N-terminal acidic domain consists of 42 amino acids, whereas SREBP1c consists of 24 amino acids. (Taken from Brown and Goldstein 1997.)

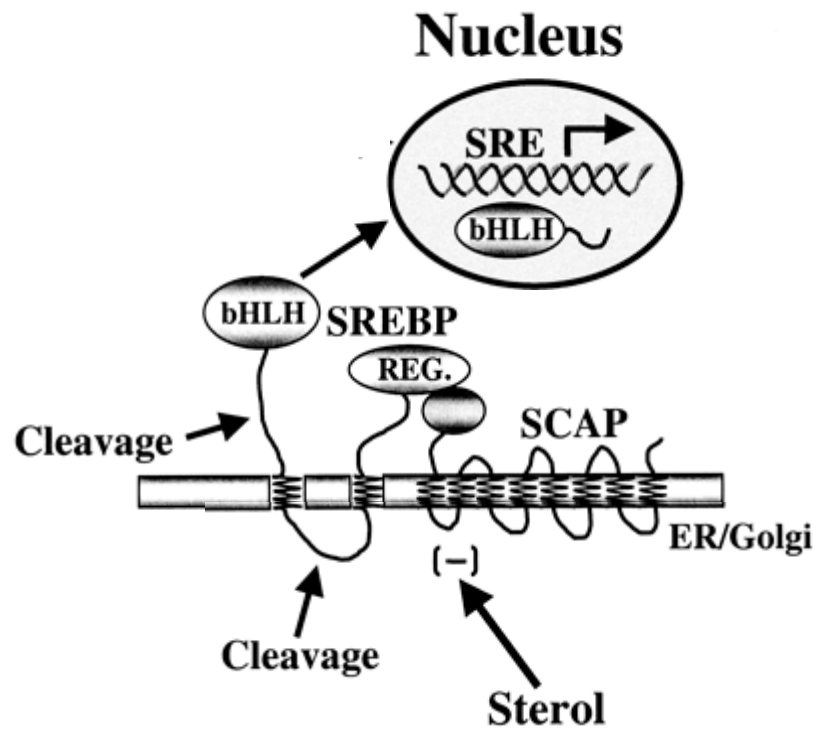


**Figure 5.2** Schematic representation of SREBP cleavage and translocation of the transcription factor domain to the nucleus. SREBP is escorted from the ER to the Golgi by SCAP (SREBP cleavage activating protein) then cleaved by proteases, releasing the bHLH (basic helix-loop-helix) transcription factor (TF) domain. The TF domain is translocated to the nucleus where it binds the sterol response element (SRE) in the promoters of SREBP target lipogenic genes (Adapted from Wang *et al* 1994).

## 5.2 Aims of these studies

The aim of these studies was to gain information about the subcellular localisation of SREBP1 transcription factor domain and its interaction with lamin A in lipodystrophy.

It is hypothesised that familial partial lipodystrophy (FPLD) (Section 1.7) specific mutations in lamin A/C, disrupt its interaction with SREBP1 and impair SREBP1 function (Lloyd *et al* 2002). The role of the SREBP1-lamin A interaction is not yet known and disruption of the interaction could have 2 opposite consequences. Retention of SREBP1 in the nucleus may be impaired so that SREBP1 is lost from its site of transcriptional activity. Alternatively Capanni *et al* (2005) suggest that SREBP1 may be sequestered to the nuclear rim away from its site of transcriptional activity.

To investigate these two opposite potential consequences, SREBP1 subcellular localisation and mobility was examined in wild type (WT) and FPLD cells and the interaction between lamin A and SREBP1 was further characterised. The subcellular localisation of transfected SREBP1a was examined by indirect immunofluorescence microscopy in fibroblasts from an FPLD patient and progeria patients (Section 1.6) with a lipodystrophic phenotype to confirm whether lipodystrophic *LMNA* mutations result in SREBP1 mislocalisation to the cytoplasm. The localisation of transfected SREBP1 was also examined in *Lmna*<sup>-/-</sup> MEFs to find out whether the presence of lamin A is necessary for the retention of SREBP1 in the nucleus. The mobility of SREBP1 was examined by FRAP in fibroblasts from FPLD and progeria patients. On one hand, SREBP1 mobility may be increased in lipodystrophy if its anchorage in the nucleus is disrupted due to reduced lamin A binding. On the other hand, the mobility of SREBP1 may be decreased in lipodystrophy if it is retained at the nuclear rim due to prelamin A

binding. Glutathione S-transferase (GST) pull-down assays were used to characterise the binding of SREBP1 to WT lamin A and disease mutants.

### **5.3 SREBP1 localisation and mobility studies**

The cell lines used for SREBP1 localisation and mobility studies and antibody tests are listed in Table 4.1. In these experiments, all dermal fibroblasts were at passage 8-11. SREBP1 constructs contain the human cDNA sequence of SREBP1a transcription factor domain (Table 5.1).

#### ***5.3.1 Subcellular localisation of transiently transfected SREBP1 in dermal fibroblasts***

The SREBP1a transcription factor domain sequence (amino acids 1-487) was excised from vector pCDNA3 (Invitrogen (UK)) and ligated into pEGFP C1 (Clontech (UK)), then construct cDNA was sequenced to ensure correct ligation. The GFP-tag allowed visualisation of transfected protein before fixation and staining and was used in FRAP mobility studies (Section 5.3.5). The GFP SREBP1 construct localised to the nucleus of transiently transfected U2OS cells, (Figure 5.3).

Localisation of GFP SREBP1 was observed in transiently transfected control fibroblasts and fibroblasts from FPLD, late onset progeria and classical progeria patients who exhibit a lipodystrophic phenotype (Figure 5.4). These cells were nucleofected as lipid-based transfection with Lipofectamine 2000 gave poor transfection efficiency. At least 80 cells per cell line were counted in two separate experiments. In both the control and late onset progeria cell lines, 98% of SREBP1 localised to the nucleus. In FPLD, 26% of fibroblasts contained cytoplasmic SREBP1 and in classical progeria 97% of fibroblasts contained cytoplasmic SREBP1. Normal localisation of SREBP1 in late onset progeria compared to the other patient cell lines is unexpected, since all 3 patients

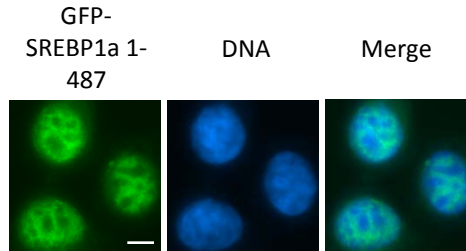


**Figure 5.3** Nuclear localisation of the GFP-tagged transcription factor domain of SREBP1a (GFP-SREBP1) (green) in transiently transfected U2OS cells. Bar 10  $\mu$ m

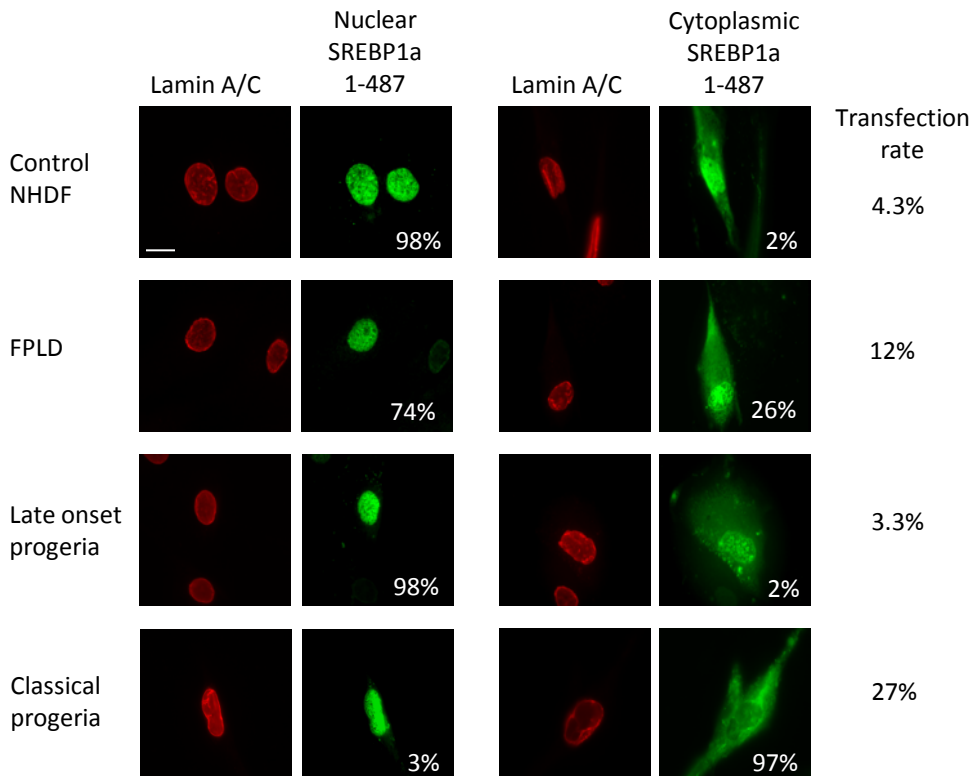


**Figure 5.4** Localisation of GFP-SREBP1 (green) detected by antibody H160 in transiently transfected fibroblasts from laminopathy patients with a lipodystrophic phenotype. Cells were co-stained with lamin A/C (red) to visualise nuclei. White figures show the percentage of cells containing nucleoplasmic or cytoplasmic GFP-SREBP1a,  $n$ =at least 80 cells per cell line in two separate experiments. Transfection rate indicates the percentage of cells expressing GFP-tagged SREBP1. Bar, 10  $\mu$ m

display a lipodystrophy phenotype. Unlike the findings of Capanni *et al*, SREBP1 was not detected at the nuclear rim; however, this effect could be masked by the overexpression obtained in transfection studies.

### **5.3.2 Localisation of transiently transfected SREBP1 in *Lmna*<sup>-/-</sup> MEFs**

Lamin A/C is not expressed in *Lmna*<sup>-/-</sup> MEFs (Figure 5.5). This cell line was used to find out whether lamin A/C was required for SREBP1 retention in the nucleus. SREBP1 was transiently transfected by nucleofection and its localisation observed in *Lmna*<sup>-/-</sup> and WT MEFs (Figure 5.6). In 58% of *Lmna*<sup>-/-</sup> cells and 64% of WT cells, SREBP1 was exclusively nuclear; indicating lamin A/C was not required for SREBP1 retention in the nucleus. A second set of cells were simultaneously co-transfected with SREBP1 and lamin A to find out whether cytoplasmic localisation of SREBP1 could be rescued by the addition of lamin A. The percentage of co-transfected cells expressing exclusively nuclear SREBP1 increased to 72% in both *Lmna*<sup>-/-</sup> and WT cell lines; this could indicate a partial rescue or may be a variation between counts.

### **5.3.3 Detection of endogenous SREBP1**

The examination of subcellular localisation of transfected SREBP1 revealed that cells are damaged by the transfection technique resulting in high cell death rates and low transfection rates, making it difficult to obtain trusted results. With the aim of investigating subcellular localisation of endogenous SREBP1, a number of antibodies were tested for their ability to detect the endogenous protein.

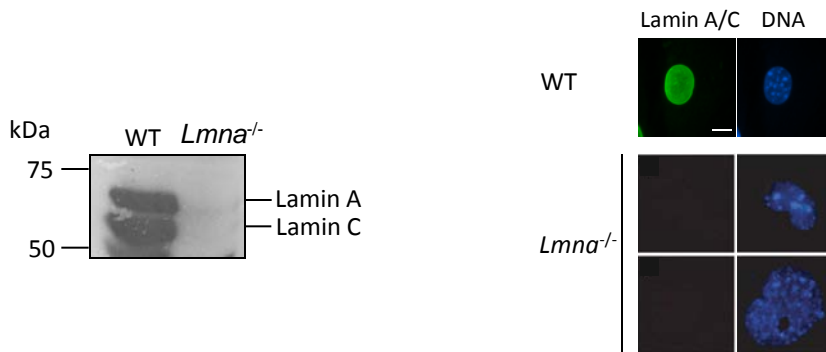


**Figure 5.5** Western blot analysis and indirect immunofluorescence shows the absence of lamin A/C proteins in *Lmna*<sup>-/-</sup> MEFs. (*Lmna*<sup>-/-</sup> indirect immunofluorescence images taken by Dr Sue shackleton.)

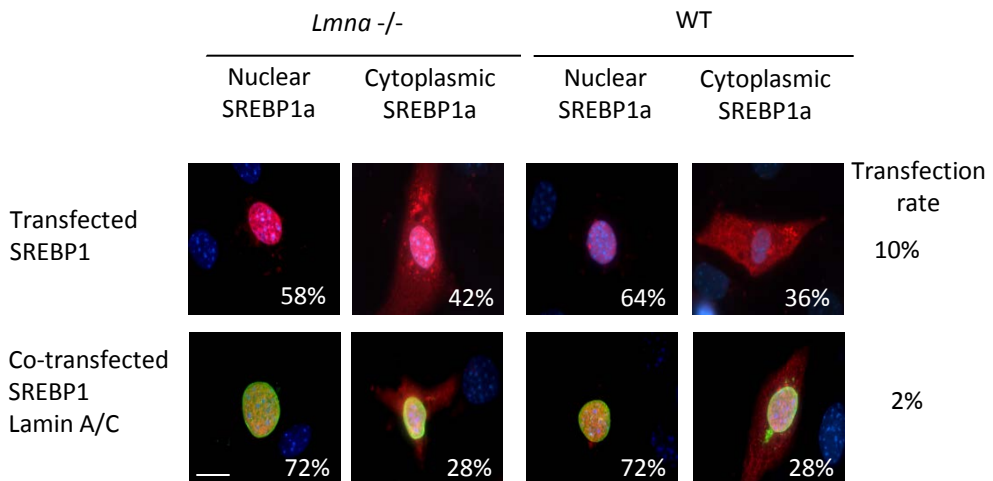


**Figure 5.6** Localisation of transiently transfected pCDNA3 SREBP1a (red) detected by antibody H160 in *Lmna* null and WT MEFs (top panel). Localisation of SREBP1a co-transfected with WT lamin A (green) (bottom panel). Nuclei were visualised by Hoechst staining (blue). White figures show the percentage of cells containing nucleoplasmic or cytoplasmic SREBP1, n=80 cells in two separate experiments. Ttransfection rate indicates the percentage of cells expressing SREBP1a (top panel) or expressing both SREBP1 and lamin A (bottom panel). Arrows indicate untransfected cells showing that only transfected SREBP1 is detected. Bar 10  $\mu$ m

### 5.3.3.1 Testing of commercial ATCC and H160 anti-SREBP1 antibodies

The efficiencies of 2 commercial antibodies were tested; mouse anti-SREBP1 ATCC IgG-2A4 (American Type Culture Collection (USA)), referred to as ATCC, with an epitope which recognises human N-terminal amino acids 301-407, and Rabbit anti-SREBP1 H160 sc-8984 (SantaCruz), referred to as H160 (epitope not published, recognises human protein). Antibodies were tested by indirect immunofluorescence microscopy on untransfected and pCDNA3 SREBP1 (1-487) transfected U2OS cells. Only transfected SREBP1 was detected by this technique (Figure 5.7A). The antibodies were then tested by Western blotting of untransfected and GFP-SREBP1 transfected U2OS cell extracts (Figure 5.7B). An anti-GFP antibody was used to show the presence of transfected protein. In untransfected cells the H160 antibody detected the endogenous SREBP1 precursor protein (top arrow) and SREBP1 transcription factor domain (bottom arrow). In transfected cells both endogenous and GFP-SREBP1 bands are visible. The ATCC antibody was able to detect only transfected GFP-SREBP1.

Following tests on transfected protein, the ATCC and H160 antibodies were tested by western blotting for detection of endogenous SREBP1 in WT and FPLD fibroblast extracts (Figure 5.7C). Total, nuclear and cytoplasmic extracts were produced to find the fraction in which SREBP1 transcription factor domain was detected, this should be nuclear in the control cell line. The H160 antibody detected what appears to be the SREBP1 precursor and transcription factor in total cell extracts, however, the transcription factor domain was detected in the cytoplasmic fraction of both cell lines, rather than the nuclear fraction as expected. The SREBP1 precursor was detected only

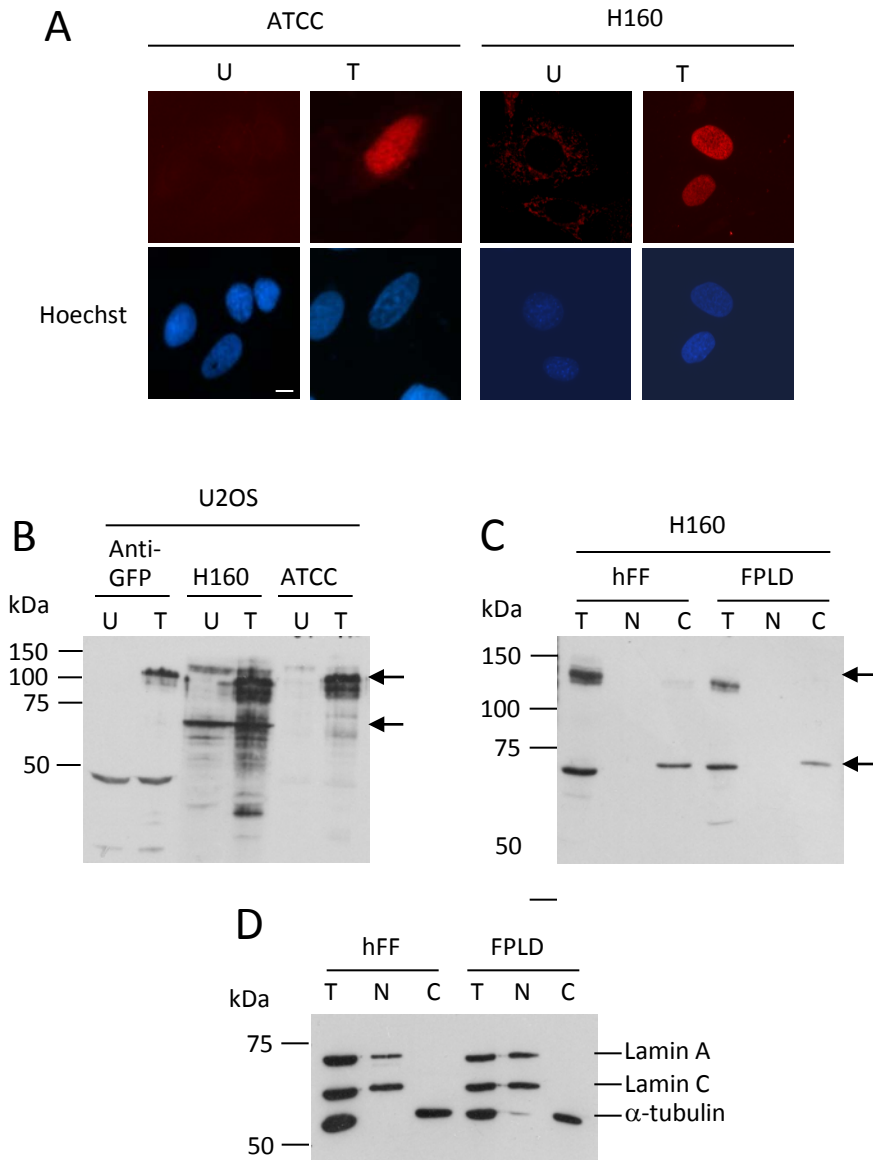


**Figure 5.7** Testing of SREBP1 antibodies H160 and ATCC IgG-2A4. **(A)** Indirect immunofluorescence microscopy showing untransfected U2OS cells and cells transfected with pCDNA3 SREBP1 (red). Nuclei were visualised by Hoechst staining (blue). **(B)** Western blot showing H160 and ATCC IgG-2A4 antibody probing of untransfected and GFP-SREBP1 1-487 transfected total U2OS cell extracts. Probing with an anti GFP antibody confirms the presence of transfected protein. **(C)** Western blot showing total (T), nuclear (N) and cytoplasmic (C) hFF and FPLD fibroblast extracts probed with H160 antibody **(D)** Western blot showing correct separation of WT (hFF) and FPLD fibroblast nuclear and cytoplasmic cell extracts. Blot was double-probed with lamin A/C and  $\alpha$ -tubulin antibodies. Nuclear extracts contain only lamin A/C, cytoplasmic extracts contain only  $\alpha$ -tubulin, total cell extracts contain both proteins. Bar 10  $\mu$ m

in total cell extracts. To ensure that nuclear and cytoplasmic fractions had been effectively separated, extracts were probed with an antibody against exclusively nuclear proteins lamins A and C and the exclusively cytoplasmic protein  $\alpha$ -tubulin. These proteins were detected in the appropriate fractions (Figure 5.7D), indicating that the fractionation had worked correctly. The conclusion of these tests was that the ATCC antibody does not detect endogenous protein and the H160 antibody cannot be trusted.

#### *5.3.3.2 Testing of custom made antibodies 4056 and 4057*

Custom made antibodies rabbit anti-SREBP1 4056 and 4057 (Cambridge Research Biochemicals) were designed previously in the laboratory. N-terminal amino acids 197-315 were chosen as the epitope for antibody 4056, amino acid 395-487 were chosen for antibody 4057. Antibodies were tested for detection of SREBP1 by indirect immunofluorescence microscopy which showed that transfected GFP-SREBP1 1-487 is detected in HeLa cells by both antibodies (Figure 5.8A). Probing with pre immune sera did not detect SREBP1, suggesting that antigen detection by post immune sera is specific to SREBP1.

Western blotting of HeLa cell extracts (Figure 5.8B) showed that both antibodies detected the transfected SREBP1 1-487 protein (upper arrow) and the endogenous SREBP1 transcription factor domain (lower arrow). Antibody 4056 appears to detect SREBP1 more strongly than antibody 4057. Pre immune sera do not detect SREBP1. The anti-GFP antibody shows the presence of transfected protein.

Antibodies were tested on WT, FPLD and classical progeria fibroblast total cell extracts to test whether endogenous SREBP1 could be detected in these cells by Western blotting (Figure 5.8C). Bands of the appropriate size were not detected in any of the

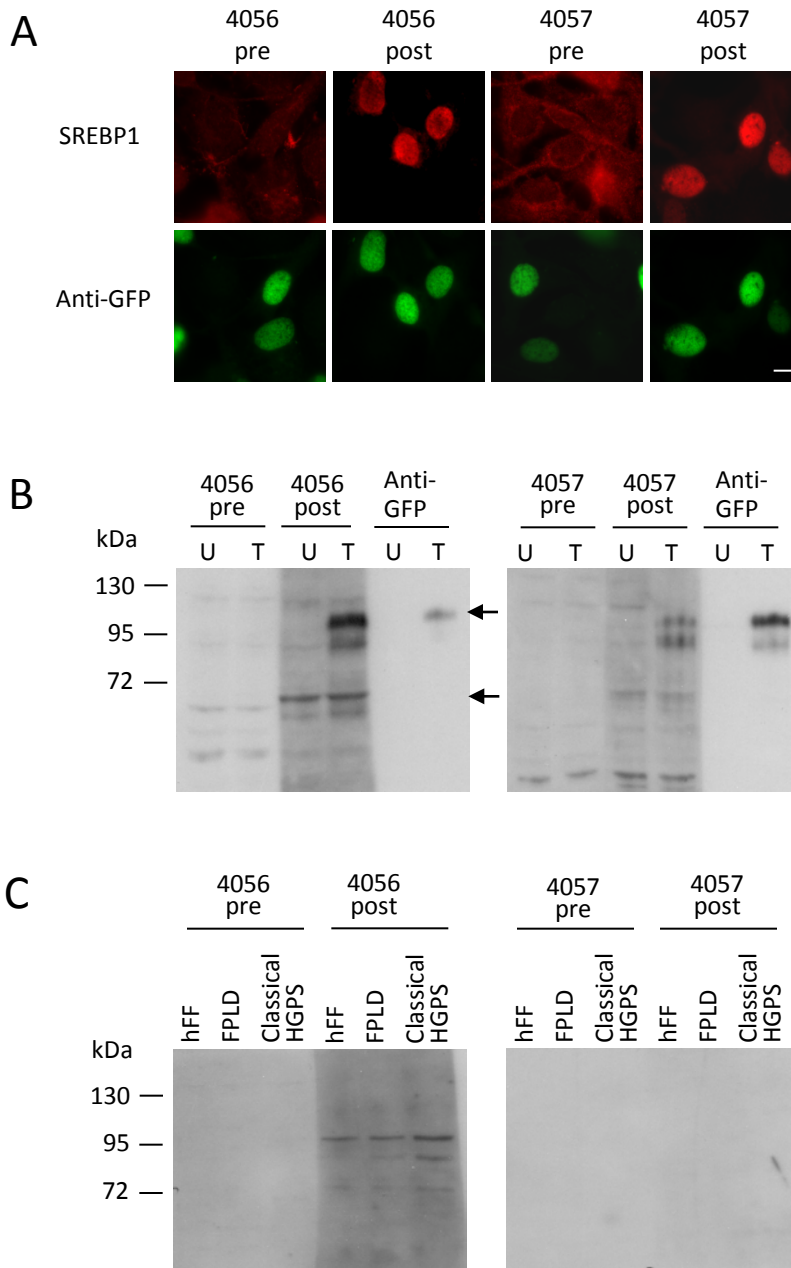


**Figure 5.8** Characterisation of SREBP1 antibodies 4056 and 4057. **(A)** Immunofluorescence microscopy showing pre and post immune serum on HeLa cells transfected with GFP-tagged SREBP1 (red). Transfected cells were visualised by GFP staining (green). **(B)** Western blots showing pre and post immune serum tested on total protein extracts from untransfected and GFP-SREBP1 transfected total HeLa cell extracts. Probing with an anti GFP antibody confirms the presence of transfected protein. **(C)** Western blots showing pre and post immune serum tested on total protein extracts from WT (hFF), FPLD and classical progeria fibroblasts.

samples suggesting that either SREBP1 is not expressed at detectable levels in these cells, or that the antibody is not good enough to detect endogenous protein. Antibody detection of endogenous SREBP1 was not pursued further. SREBP1 may have been detected by the 4056 antibody if more concentrated fibroblasts extracts were available, but time constraints prevented the production of more cell extracts.

### ***5.3.4 Detection of transduced SREBP1***

Continuing the aim of investigating subcellular localisation of SREBP1, the Lentiviral expression system was used to induce cells to express GFP SREBP 1-487. Lentivector pRRLsin.cPPT.CMV.GFP.Wpre into was a gift from Dr Daniele Bano and Prof PierLuigi Nicotera, MRC Toxicology Unit, University of Leicester. Advantages of the use of Lentivirus over Lipofectamine transfection or nucleofection are that the transduction rate is high, cells are not damaged during transduction and non dividing cells can be infected which is useful for slow growing HGPS cells. SREBP1a 1-487 transcription factor cDNA sequence and the GFP tag was cloned into Lentiviral expression vector pRRLsin.cPPT.CMV.GFP.Wpre at the multiple cloning site, replacing the vector GFP sequence. The Lenti GFP SREBP1 construct was sequenced to ensure correct ligation. Correct localisation of the Lenti GFP SREBP1 construct was confirmed by Lipofectamine transfection of U2OS cells (Figure 5.9).

Having shown that the construct was capable of producing GFP SREBP1 1-487, ViraPower packaging plasmids (Invitrogen) plus Lenti GFP SREBP1 were calcium chloride transfected into 293T cells in which virus is subsequently produced. The packaging plasmids were a gift from Dr Emmanuel Debrand. After 48 hours viral particles released into the growth medium of the infected 293T cells were harvested. Filtered 293T growth media was used at a dilution of 1:256 to achieve a transduction

rate of 100% in hFFs (Figure 5.10). Harvested medium was stored at  $-80^{\circ}\text{C}$ , but was ineffective when recovered. Several attempts were made to produce more virus but were unsuccessful and time constraints prevented further attempts.

### ***5.3.5 Mobility of SREBP1 in FPLD, progeria and old age***

FRAP studies were used to investigate the mobility of SREBP1 in fibroblasts from FPLD, late onset progeria and classical progeria patients and an 88 year old control individual, compared to an adult control (WT) 24 hours after transfection. FRAP was performed on an Axiovert 100M inverted microscope using an LSM 510 laser scanning confocal unit (Zeiss) and analysed using LSM 510 software. A  $5\mu\text{m}$  by  $5\mu\text{m}$  area of the nucleus was bleached, as illustrated in Figure 5.11. Relative fluorescence recovery of the bleached area over time was then plotted to compare SREBP1 mobility in patient and aged control fibroblasts to WT in at least 7 cells and in at least two separate experiments (Figure 5.12).

There was trend towards reduced SREBP1 mobility in late onset and classical progeria and in the control cell line from an 88 year old donor. This suggests there may be some sequestration of SREBP1 away from its normal sites of transcriptional activity, but this could be masked by the saturation of SREBP1 binding sites due to SREBP1 over expression.

Prelamin A is reported to bind SREBP1, resulting in its abnormal redistribution to the nuclear rim (Capanni *et al* 2005). To see if a decrease in SREBP1 mobility correlates with increased levels of prelamin A, SREBP1 mobility was compared to prelamin A expression (Figure 5.13). SREBP1 mobility is represented by the mean relative fluorescence intensity of at least 7 cells after 30 seconds recovery, normalised to control

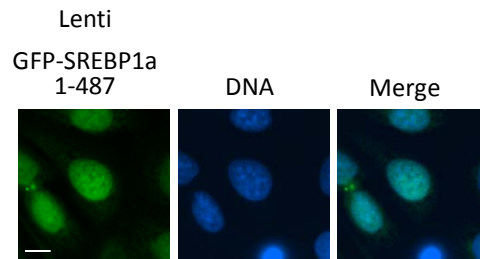


**Figure 5.9** The Lentiviral GFP-tagged transcription factor domain of SREBP1 (green) localises to the nucleus of transfected U2OS cells. Cells were stained with Hoechst to visualise nuclei.

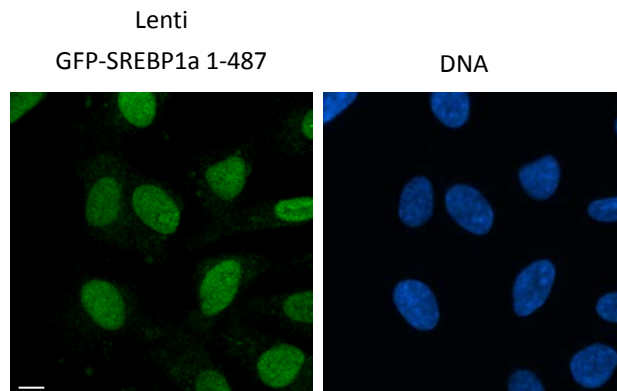


**Figure 5.10** Human foreskin fibroblasts (hFF) are transduced by Lentiviral GFP-SREBP1a (green) at a rate of 100%. Bar 10  $\mu\text{m}$

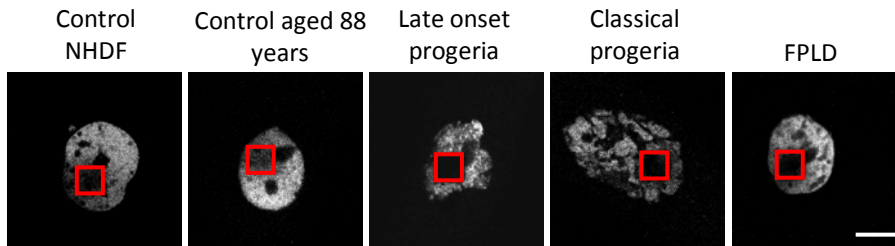


**Figure 5.11** Single plane confocal images of dermal fibroblasts transiently transfected with GFP-SREBP1a. The 5  $\mu\text{m}$  by 5  $\mu\text{m}$  area inside the red box was bleached. Images show nuclei immediately after photobleaching (time 0). Bar 10 $\mu\text{m}$

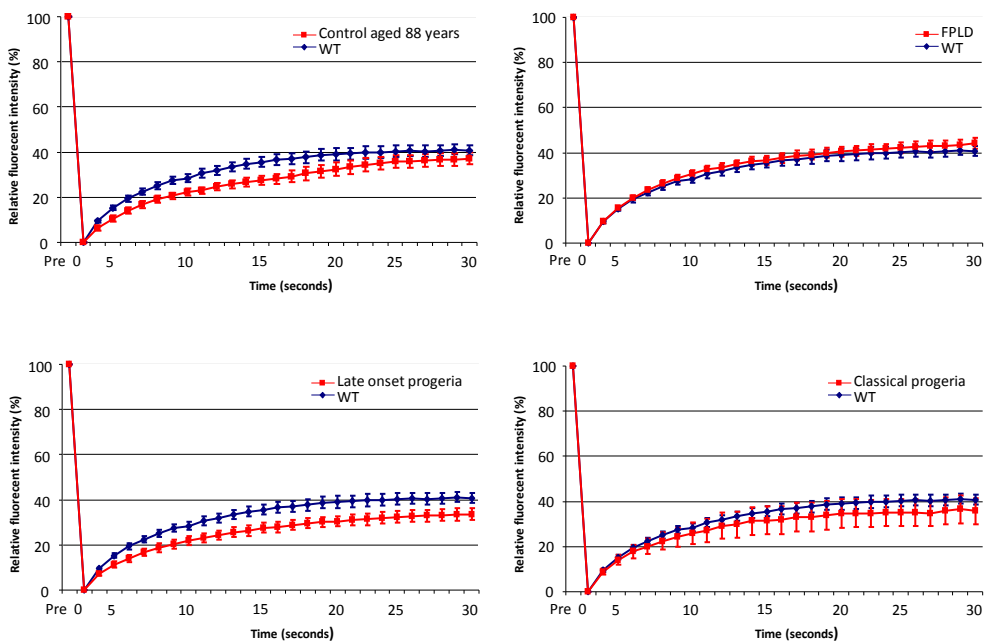


**Figure 5.12** FRAP analysis of SREBP1 in WT and laminopathy fibroblasts. In each graph data for WT (blue) and patient or aged control (red) cells are compared. Mean relative GFP intensity in the bleached area (shown as a red box in Figure 5.5) is plotted as a function of time. Each data point represents the average intensity of at least 7 cells  $\pm$  SEM.

hFF (Figure 5.13A). Prelamin A expression was detected by Western blot analysis and then quantified by densitometry, normalised to control hFF (Figure 5.13B). There appears to be general trend towards an inverse correlation between prelamin A accumulation and SREBP1 mobility.

Nuclear SREBP1 mobility was also assessed in FPLD fibroblasts expressing cytoplasmic SREBP1 (Figure 5.14) to investigate whether mobility was increased perhaps because SREBP1 shuttles between the nucleus and cytoplasm due to the loss of binding sites in the nucleus. Relative fluorescence recovery of the bleached area over time, compared to control NHDF, revealed that the mobility of nuclear SREBP1 was not altered in cells expressing cytoplasmic SREBP1 (Figure 5.15). The pattern of recovery was identical to that of FPLD cells exclusively expressing nuclear SREBP1, suggesting that SREBP1 does not shuttle between the nucleus and cytoplasm.

### ***5.3.6 Quantification of SREBP1 binding to lamin A disease mutants by GST pull-down***

To produce constructs for pulldown assays, lamin A sequences were ligated into pGEX bacterial expression vector containing the GST sequence. GST-tagged constructs are listed in Table 5.1. GST-tagged lamin A WT and disease mutant constructs were truncated and contain amino acids 389-664 to increase solubility.

#### ***5.3.6.1 Optimisation of GST pull-down assays and mapping of the lamin A binding site on SREBP1***

Previous GST pull-down assays in the laboratory have shown altered binding of lamin A mutants to SREBP1. For these assays, the interaction was quantifiable but weak

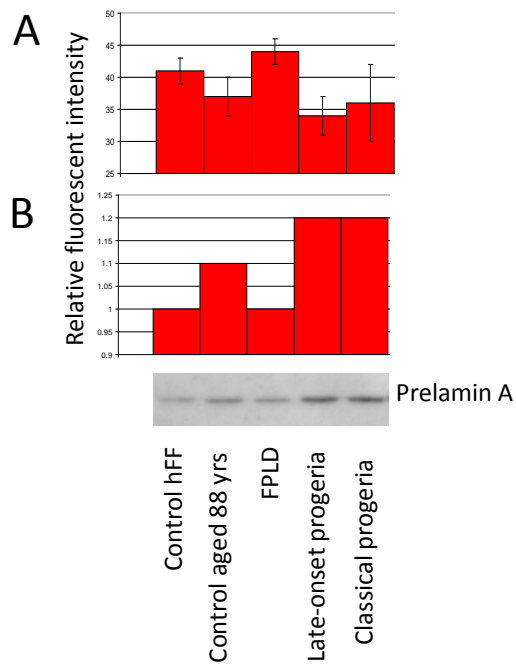


**Figure 5.13 (A)** Relative fluorescent intensity after 30 seconds recovery as an indicator of SREBP1 mobility. Results are shown as a percentage of WT recovery (mean  $\pm$  SEM of at least 7 cells). **(B)** Western blot analysis of prelamin A expression in WT and laminopathy fibroblasts taken from figure 4.3. Protein expression was quantified by densitometry and is shown as a percentage of WT expression.

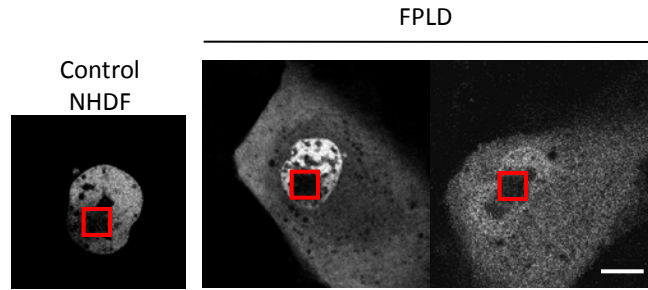


**Figure 5.14** Single plane confocal images of WT and FPLD fibroblasts transiently transfected with GFP-SREBP1a. FPLD fibroblasts expressing cytoplasmic SREBP1 were chosen for imaging. The  $5\mu\text{m}$  by  $5\mu\text{m}$  area inside the red box was bleached. Images show nuclei immediately after photobleaching (time 0). Bar  $10\mu\text{m}$

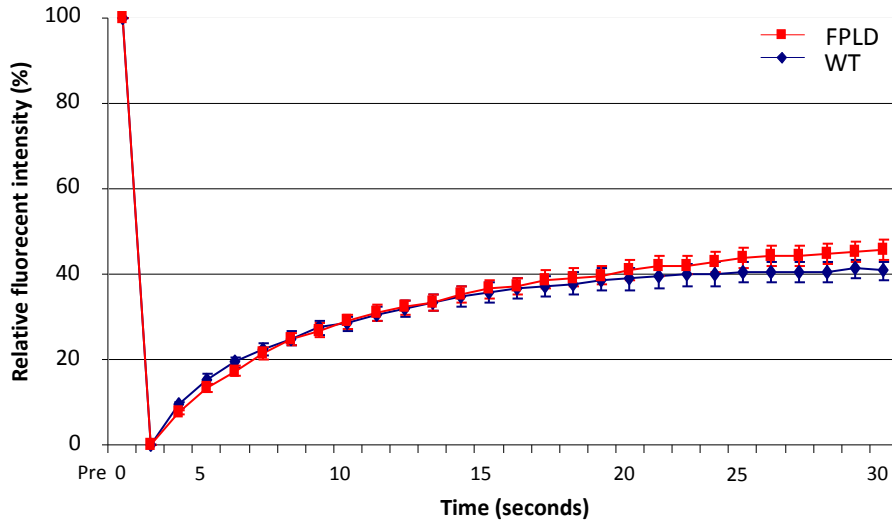


**Figure 5.15** FRAP analysis of GFP-SREBP1a in WT and FPLD fibroblasts where FPLD fibroblasts containing cytoplasmic SREBP1 were chosen for imaging and compared to WT fibroblasts containing nuclear SREBP1. Mean relative GFP intensity in the bleached area (shown as a red box in Figure 5.8) is plotted for WT (blue) and FPLD patient (red) as a function of time. Each data point represents the average intensity of at least 6 cells  $n=2 \pm$  SEM.

Construct	Description
GST SREBP1c	GST-tagged SREBP1c 1-463 transcription factor domain
GST SREBP1a 1-227* GST SREBP1a 227-323* GST SREBP1a 320-405* GST SREBP1a 400-487*	GST-tagged fragments of SREBP1a transcription factor domain
GST SUN1 1-355*	GST-tagged SUN1 control construct
GST Lamin A WT* GST Lamin A R482W* GST Lamin A G645D* GST Lamin A T623S GST Lamin A G608G* GST Lamin A R527H GST Lamin A K542N GST Lamin A R527P* GST Lamin A R453W* GST Lamin A R644C*	Wild type prelamin A sequence FPLD mutant FPLD mutant Late onset progeria mutant Classical progeria mutant Mandibuloacral dysplasia mutant Atypical progeria mutant Emery Dreifuss muscular dystrophy mutant Emery Dreifuss muscular dystrophy mutant Emery Dreifuss muscular dystrophy mutant
GST Lamin A L647R	GST-tagged cleavage incompetent, permanently farnesylated prelamin A ( amino acids 389-661)

**Table 5.1** GST-tagged constructs used for GST pulldown assays. \*Denotes constructs made previously in the laboratory.

Construct	Description
pCDNA3 Emerin*	Untagged wild type emerin
pCI Lamin A WT*	Wild type lamin A prelamin A sequence 1-664
pCI Lamin A L647R	Cleavage incompetent, permanently farnesylated prelamin A 1-661
pEGFP C1 SREBP1a	GFP-tagged SREBP1a 1-487 transcription factor domain

**Table 5.2** IVT plasmid templates used for GST pulldown assays. \* Denotes constructs made previously in the laboratory.

compared to 10% input (Lloyd *et al* 2002). In this study, when GST-tagged SREBP1c transcription factor domain was incubated with *in vitro* translated WT lamin A using the same constructs as Lloyd *et al* (2002) (Tables 5.1 and 5.2), the interaction was extremely weak, Figure 5.16A. Robust binding of *in vitro* translated emerin to GST-tagged SUN1 1-355, performed alongside GST-tagged SREBP1 and WT lamin A, showed the technique was functioning, Figure 5.16B.

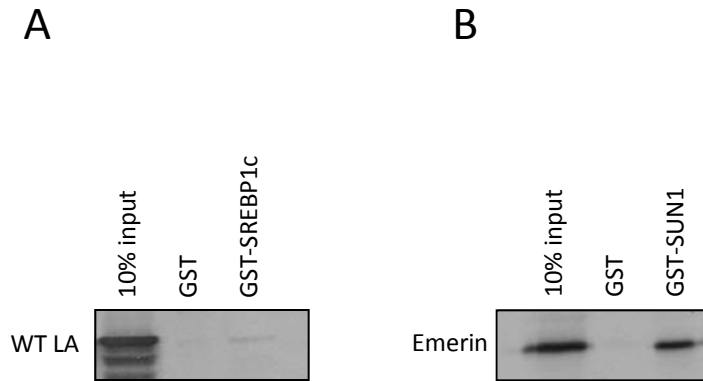


**Figure 5.16** (A) Binding of WT lamin A to GST-SREBP1c.  $^{35}\text{S}$  labelled *in vitro* translated WT lamin A was incubated with GST-SREBP1. (B) Binding of emerlin to GST-SUN1 was performed alongside (A).  $^{35}\text{S}$  labelled *in vitro* translated emerlin was bound to GST-SUN1. 10% input is 10% of input *in vitro* translation products

GST-tagged fragments of SREBP1a were produced previously in the laboratory (Figure 5.17). These fragments were used to pull-down *in vitro* translated WT lamin A to narrow down the binding site and investigate whether binding could be improved by using a smaller SREBP1 fragment. Binding of WT lamin A to SREBP1a 320-405 was still relatively weak (Figure 5.18). Very weak binding to fragment 400-487 and lack of detectable binding of fragments covering residues 1-323, suggests the lamin A binding site coincides with the DNA binding site.

Ultimately, reversing the pulldown, where *in vitro* translated SREBP1a transcription factor domain was pulled-down by GST-tagged lamin A (residues 389-664) resulted in a quantifiable interaction (Figure 5.19).

#### *5.3.6.2 Quantification of the SREBP1a interaction with a range of disease associated lamin A mutants*

The pulldown assay was used to test the effect of laminopathy associated lamin A mutants on the interaction between lamin A and SREBP1. GST-tagged WT and lamin A disease mutants (Table 5.1) were used to pull-down *in vitro* translated SREBP1 (Figure 5.19A). GST-tagged lamin A disease mutants are listed in Table 5.1, alongside the disease they represent. Quantification of binding by densitometry shows SREBP1 binding to disease mutants as a percentage of WT binding averaged over two experiments. Error bars show standard error of the mean (SEM) (Figure 5.19B). Unfortunately, the sample number (n=2) was not large enough for statistical analysis. Results show that all disease mutants are able to bind SREBP1. Contrary to earlier GST-pulldown findings in the laboratory for FPLD mutants, (Lloyd *et al* 2002), FPLD mutants bound more strongly to SREBP1 than WT. All lamin A disease mutants in this study bound equally or more strongly to SREBP1 than WT.

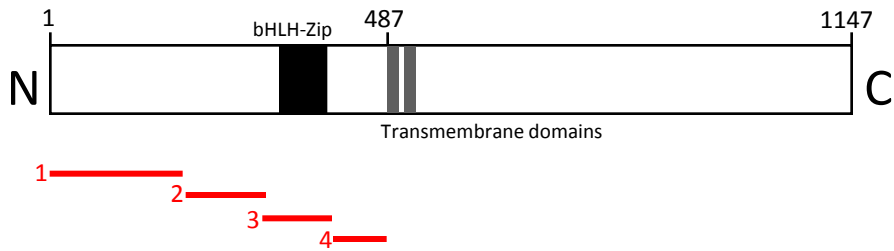


**Figure 5.17** GST fused fragments of SREBP1a transcription factor domain. N- amino terminus, C- carboxy terminus, bHLH-zip- basic helix-loop-helix leucine zipper motif. Fragments were designed previously in the laboratory as follows: Fragment 1=amino acids 1-227, 2=227-323, 3=320-405, 4=400-487.

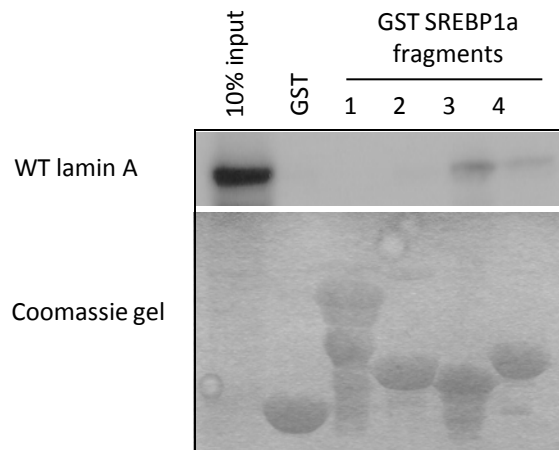


**Figure 5.18** Top panel; Binding of  $^{35}\text{S}$  labelled *in vitro* translated WT lamin A to GST tagged SREBP1a fragments 1 to 4. 10% input is 10% of input *in vitro* translation products. Bottom panel: Coomassie gel shows equal expression of GST-SREBP1a fragments.

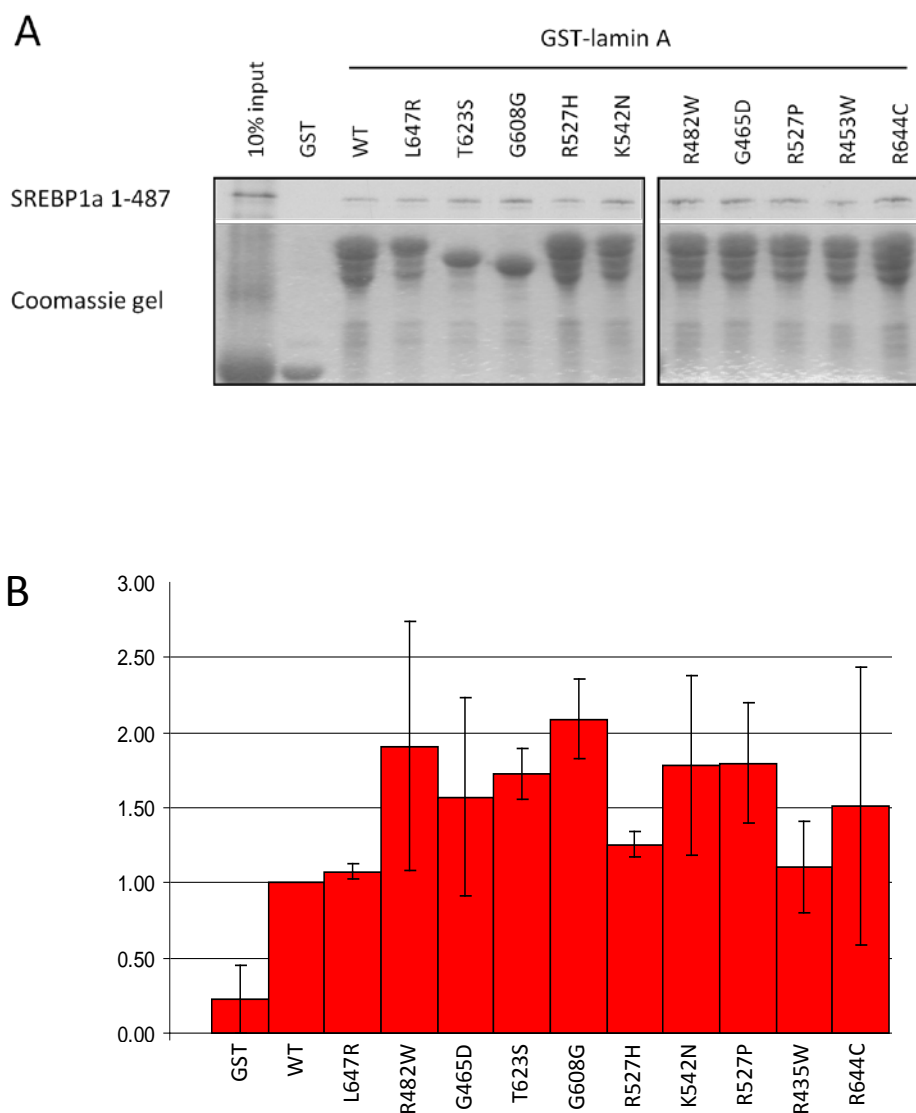


**Figure 5.19** (A) Binding of  $^{35}\text{S}$  labelled *in vitro* translated SREBP1a to GST tagged WT and mutant forms of lamin A. 10% input is 10% of input *in vitro* translated product. (B) Quantification of binding by densitometry, shown as a percentage of WT binding averaged over two experiments  $\pm$  SEM.

for FPLD mutants, (Lloyd *et al* 2002), FPLD mutants bound more strongly to SREBP1 than WT. All lamin A disease mutants in this study bound equally or more strongly to SREBP1 than WT.

## 5.4 Discussion

### 5.4.1 Subcellular localisation of SREBP1 in FPLD and progeria fibroblasts

The transcription factor domain of SREBP1 (amino acids 1-487) is normally expected to be targeted to the nucleus (Sakai *et al* 1996). Previously in the laboratory, detection of transfected SREBP1 transcription factor domain revealed cytoplasmic SREBP1 in 34% of FPLD cells compared to 3.3% of WT. In agreement with this finding, cytoplasmic localisation of transfected SREBP1 transcription factor was found in 26% of FPLD cells compared to 2% in WT. In addition, cytoplasmic SREBP1 was detected in 97% of classical progeria cells and just 2% of late onset progeria fibroblasts.

It was predicted that abnormal localisation of SREBP1 would be observed in FPLD and in progeria cell lines, since lipodystrophy is a feature of all three disorders. In late onset and classical progeria, truncated aberrantly farnesylated lamin A is produced by the use of cryptic splice sites, but in late onset progeria the cryptic splice site is less active resulting in lower levels of mutant lamin A protein. Perhaps in the passage 8-10 cells used in this experiment, abnormal lamin A may not have accumulated in late onset progeria, or the downstream affects may be less severe, allowing SREBP1 localisation to appear as WT. Localisation of SREBP1 may also be linked to individual patient phenotype. If lipodystrophy is mild in the late onset progeria patient compared to FPLD and classical progeria patients, abnormalities in SREBP1 may be undetectable. Likewise, very severe lipodystrophy in classical progeria may be linked to the

mislocalisation of SREBP1 in almost all cells. The findings of this study do not coincide with the findings of Capanni *et al* (2005) who report the accumulation of endogenous SREBP1 at the nuclear rim of FPLD and progeroid fibroblasts due to a build up of prelamin A in these cells. Accumulation of endogenous SREBP1 at the nuclear rim and loss of SREBP1 staining have also been reported in preadipocytes treated with HIV protease inhibitors which cause the accumulation of prelamin A (Caron *et al* 2003). In addition, endogenous SREBP1 staining at the nuclear rim has been detected in FPLD and progeroid fibroblasts as part of this study, Section 4.4.2.

It may be possible that abnormal SREBP1 localisation is due to damage by the nucleofection transfection technique. Nucleofection resulted in cell death in all fibroblast cell lines, and classical progeria cells in particular. Damage to the nuclear envelope by electroporation, for example, may have allowed nuclear proteins to enter the cytoplasm. It has been reported that HeLa cells expressing the HGPS mutant lamin A, progerin, show impaired nuclear import (Busch *et al* 2009). This could explain cytoplasmic SREBP1 in classical HGPS cells.

The localisation of SREBP1 in lipodystrophy could be further investigated by the acquisition of a reliable antibody or by the use of a transfection technique which does not damage target cells. These approaches were both applied.

#### ***5.4.2 Detection of endogenous SREBP1***

Two commercial and two custom made antibodies were tested for their ability to bind SREBP1. The ATCC antibody was found to detect only transfected protein by immunofluorescence microscopy and western blotting. The H160 antibody was found to detect only transfected protein by immunofluorescence microscopy, but detected

endogenous protein by western blotting. Confusingly, when nuclear and cytoplasmic cell fractions were separated, SREBP1 transcription factor domain was detected in the cytoplasmic fraction and SREBP1 cytoplasmic precursor was not detected at all. The antibody could be at fault or the separation technique may have failed. The SREBP1 precursor resides in the ER and could be lost from cytoplasm if the ER was incompletely solubilised and subsequently lost from the nuclear fraction during washing if it did not pellet tightly with nuclei. Equally, the SREBP1 transcription factor domain may have been lost from the nuclear fraction if nuclei burst during swelling or homogenisation, whilst larger insoluble lamins may have been retained. This possibility could be investigated further by probing nuclear and cytoplasmic fractions for the presence of another transcription factor such as Retinoblastoma protein. Further investigation could reveal that this antibody is useful for western blotting.

Custom made antibodies 4056 and 4057 detected only transfected protein by immunofluorescence microscopy. By western blotting, antibody 4056 strongly detected endogenous SREBP1 transcription factor domain in HeLa cells, but did not detect SREBP1 in hFF or FPLD fibroblasts.

The performance of antibodies may have been improved by altering conditions such as blocking agents or incubation temperature or by probing more concentrated cell extracts which were not available at the time of this study. Given that transfected protein was readily detected, altering conditions seems unlikely to improve results.

#### ***5.4.3 The use of Lentiviral GFP SREBP1***

Reliable detection of endogenous SREBP1 by immunofluorescence microscopy and western blotting of dermal fibroblasts would have brought useful information to this

study. Alongside the testing of antibodies discussed above, the use of Lentiviral transduction was explored. Transduction would be advantageous because cells are not harmed by the technique and a good transduction rate can be achieved in slow growing cells such as progeria cells. The transient transfection techniques used in this study rely upon cell division for plasmid expression which probably contributed to poor transfection rates. Studies of GFP-tagged SREBP1 1-487 subcellular localisation and mobility with protein expressed at a low, close to endogenous, levels as Lentivirus can be titrated to do, would have been extremely useful in providing information about the role of SREBP1 in lipodystrophy.

Unfortunately, although virus production was successful on one occasion, the virus did not remain active when stored at  $-80^{\circ}\text{C}$  and virus production could not be repeated. In the future storage problems may be overcome by centrifugation of harvested media and storage of the concentrated virus at  $-80^{\circ}\text{C}$ .

#### ***5.4.4 Localisation of SREBP1 in $Lmna^{-/-}$ MEFs***

The localisation of transfected SREBP1 transcription factor domain was examined in  $Lmna^{-/-}$  MEFs to investigate whether the presence of lamin A/C was necessary for the retention of SREBP1 in the nucleus. Although results were similar for  $Lmna^{-/-}$  and WT MEFs, where 58% of  $Lmna^{-/-}$  and 64% of WT cells contained exclusively nuclear SREBP1, results show that SREBP1 is generally able to remain in the nucleus in the absence of A-type lamins. This finding suggests that an alternative mechanism anchors SREBP1 in the nucleus, different, for example, from the lamin A-dependent anchorage of the retinoblastoma protein transcription factor. Also, it is possible that mutant forms of lamin A may have a dominant effect on SREBP1 localisation in FPLD and progeria fibroblasts. Another explanation is that other factors are present in mouse cells that aid

retention of SREBP1 in the absence of lamin A/C, this possibility fits with the fact that all mouse models of laminopathies are recessive, whilst human diseases are dominant.

#### ***5.4.5 Mobility of SREBP1 in FPLD, progeria and old age***

FRAP studies revealed that the mobility of SREBP1 transcription factor domain is similar to the WT control in FPLD, atypical and classical progeria and in a cell line from an aged individual (aged 88 years). The small increase in mobility of SREBP1 transcription factor domain in FPLD fibroblasts is close to WT mobility and may be a variation of normal. Although similar to control cells, the mobility of SREBP1 transcription factor domain shows a trend towards reduced mobility in late onset, classical progeria and the control aged 88 years which correlates with the increased expression of prelamin A in these cell lines detected by western blotting. This trend is supported by the findings of Capanni *et al* (2005) who suggest that SREBP1 binding to prelamin A sequesters SREBP1 to the nuclear rim, away from its site of normal transcriptional activity. Retention of SREBP1 by prelamin A at the nuclear rim may result in the reduced SREBP1 mobility detected in fibroblasts from late onset and classical progeria patients and the aged control in this study. However, this does not correlate with the localisation study finding that transfected SREBP1 transcription factor domain localised to the cytoplasm in classical progeria cells (Section 5.3.1).

The mobility of SREBP1 in FPLD cells expressing cytoplasmic SREBP1 was identical to those expressing exclusively nuclear SREBP1, suggesting that since SREBP1 mobility is unaltered in cells expressing cytoplasmic SREBP1, loss of SREBP1 from the nucleus due to impaired binding to lamin A appears unlikely to be the mechanism underlying the lipodystrophy phenotype.

#### ***5.4.6 Quantification of SREBP1 binding to lamin A disease mutants by GST pull-down***

In this study, lamin A progeroid mutants T623S, G608G, and K542N show stronger binding to SREBP1 than WT lamin A. The R527H mutant binding is closer to WT. This is linked to disease severity where binding of the R527H mandibuloacral dysplasia mutant is most similar to WT. Stronger binding of progeroid mutants T623S and G608G is supported by the trend that SREBP1 mobility is reduced in late onset and classical progeria fibroblasts.

SREBP1 binding detected in FPLD and most Emery-Dreifuss muscular dystrophy (EDMD) lamin A mutants was found to be stronger than wild type. This is the opposite to previous results in the laboratory where decreased binding to SREBP1 was detected in FPLD and EDMD mutants.

A possible reason for these conflicting results may be that the forms of lamin A incubated with SREBP1 were different. In the previous Lloyd *et al* (2002) study, WT and mutant lamin A constructs were in vitro translated in rabbit reticulocytes where farnesylation occurs but further processing does not (Vorburger *et al* 1989), resulting in detection of farnesylated prelamin A binding to SREBP1. In this study, WT and mutant lamin A constructs were expressed in bacteria as GST-tagged proteins where post translational processing would not be expected to occur, resulting in detection of unprocessed and non farnesylated prelamin A binding to SREBP1. It has been reported that SREBP1 binds both farnesylated and unfarnesylated forms of prelamin A (Maraldi *et al* 2008), but not mature lamin A (Capanni *et al* 2005).

Another modification of the previous study was the use of GST-tagged lamin A and *in vitro* translated SREBP1 whereas Lloyd *et al* (2002) used GST-tagged SREBP1. The Lloyd *et al* method was attempted before swapping GST tags but binding was found to be too weak.

Binding assays would need to be repeated and consistent results obtained before and further insight is gained into SREBP1 binding to lamin A mutants.

### **5.5 Summary of findings**

Overall, mobility and binding studies suggest that SREBP1 is more tightly tethered and less mobile in the nuclei of FPLD and progeria cells than in controls. Additionally, results of indirect immunofluorescence microscopy performed on FPLD, late onset, classical and severe progeria cells all showed nuclear rim staining of endogenous SREBP1 (Figure 4.4). These results support the hypothesis that sequestering of SREBP1 to the nuclear rim away from its site of transcriptional activity contributes to the lipodystrophy phenotype. Unfortunately the SREBP1 antibody stopped working after this one use (Section 4.4.3).

Localisation studies of transfected SREBP1 transcription factor domain show cytoplasmic SREBP1 in classical HGPS cells and in a proportion of FPLD cells. This finding supports the hypothesis that impaired retention of SREBP1 in the nucleus contributes to the lipodystrophy phenotype because SREBP1 is lost from its site of transcriptional activity.

## CHAPTER 6

**Investigating the effect of the familial partial lipodystrophy  
mutation R482W on adipogenic potential.**

## 6.1 Introduction

Adipogenesis is controlled by a network of transcription factors, the main regulators in the pathway are CCAAT-enhancer binding proteins (C/EBPs) and peroxisome proliferator-activated receptor  $\gamma$  (PPAR $\gamma$ ) (Figure 6.1). The principal adipogenic pathway involves the induction of C/EBP $\beta$  and C/EBP $\delta$  which then induce expression of PPAR $\gamma$ . PPAR $\gamma$  and C/EBP $\beta$  and  $\delta$  go on to activate C/EBP $\alpha$ , which in turn further activates PPAR $\gamma$  (reviewed Rosen and MacDougald 2006) (Section 1.8). The synthetic PPAR $\gamma$  activator Troglitazone is commonly used to stimulate the differentiation of mesenchymal stem cells (MSCs) *in vitro* (Lehmann *et al* 1995).

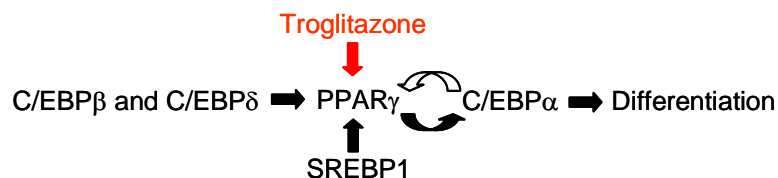


**Figure 6.1** The principal regulators in the adipogenic pathway (black). Troglitazone (red) is a synthetic PPAR $\gamma$  activator

Of interest to this study, PPAR $\gamma$  is also activated by the lamin A-binding transcription factor, sterol response element binding protein 1 (SREBP1) (Kim and Spiegelman 1996, Kim *et al* 1998). Adipogenic studies in the preadipocyte cell line 3T3L1, which was derived from the mouse NIH3T3 cell line by Green and Kehinde in 1974, has been used to show that a dominant negative (non-DNA binding) form of SREBP1 prevents differentiation (Kim and Spiegelman 1996), suggesting that active SREBP1 is necessary for adipogenesis. The requirement for SREBP1 in adipogenesis is of interest because the possible disruption of lamin A binding to SREBP1 or SREBP1 subcellular mis-localisation in FPLD may result in defective adipogenesis, leading to loss of subcutaneous fat.

It was not possible to obtain fat biopsies from FPLD patients for study due to the loss of subcutaneous fat associated with this disorder; therefore bone marrow-derived mesenchymal stem cells (MSCs) were used in this investigation. MSCs are adipocyte precursors and can be induced to form adipocytes in culture (Pittenger *et al* 1999). The standard differentiation protocol for the conversion of pre adipocytes such as 3T3L1 cells to mature adipocytes is to add a cocktail of Dexamethasone (DEX), methylisobutyl xanthine (IBMX) and insulin. These reagents are non-specific activators of adipogenesis. DEX and IBMX repress inhibitors of adipogenesis, whilst insulin stimulates lipid uptake. In standard protocols for *in vitro* activation of adipogenesis in MSCs, PPAR $\gamma$  is a common target for synthetic ligands such as Troglitazone (Figure 6.1).

## 6.2 Aim of the study

The aim of this study was to investigate the effect of the most common FPLD *LMNA* mutation, R482W, on adipogenic differentiation. In FPLD, it is not known whether fat loss is due to disruption of the differentiation pathway or if mature adipocytes are produced but are unable to survive. During adipogenesis, PPAR $\gamma$  has been shown to be activated by SREBP1, thus to avoid masking any changes in SREBP1 activity in FPLD, direct activation of PPAR $\gamma$ , by ligands such as Troglitazone, was avoided and a differentiation protocol developed using only non-specific enhancers of adipogenesis. This protocol was used to test the adipogenic potential of MSCs extracted from FPLD patient and control bone marrow aspirates and of mouse embryonic fibroblasts from a *Lmna* R482W knock in mouse model of lipodystrophy developed in the laboratory.

## 6.3 Testing adipogenic differentiation of 3T3L1 preadipocytes

Test differentiations were performed on the established preadipocyte mouse cell line 3T3L1 (Green and Kehinde 1975) to ensure that the reagents and technique were functional. A standard adipogenic protocol for 3 T3L1 cells was used (Kim *et al* 1998). Cells were seeded at a density of  $2 \times 10^5$  cells onto 3 cm (diameter) plates and grown to confluence. The adipogenic reagents DEX (1  $\mu$ M), IBMX (0.5 mM) and insulin (1  $\mu$ M) were added 48 hours post confluence (day 0). Cells were incubated in adipogenic reagents for 48 hours, then in insulin alone until fixation. Cells were formalin fixed on days 0, 3, 6 and 10 and incubated in oil-red-o to stain lipid droplets. Lipid droplets stained with oil-red-o accumulated over time (Figure 6.2).

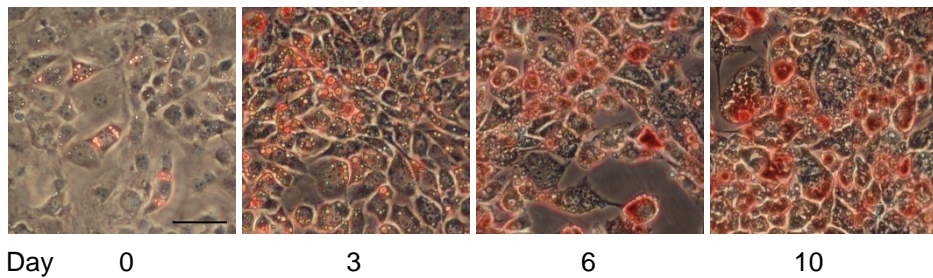


**Figure 6.2** Adipogenic differentiation of 3T3L1 preadipocytes. Efficient detection of differentiation confirms reagents and technique are functional. Cells were seeded and allowed to reach confluence, day 0 is 48 hours post confluence. Samples were fixed and stained on days 0, 3, 6, 10. Lipid droplets are stained red with oil-red-o dye. Bar 70  $\mu\text{m}$

## 6.4 Mesenchymal stem cell (MSC) adipogenesis studies

### 6.4.1 MSCs cultured for this study

MSCs cells were extracted from 6 control bone marrow aspirates, and 3 aspirates obtained from 3 FPLD patients carrying the R482W mutation (Table 6.1). Following the patients' written consent, control bone marrow aspirates were obtained from patients undergoing biopsy due to suspected lymphoma in the clinic of Professor Martin Dyer, Haematology Department, Leicester Royal Infirmary. FPLD donors were recruited to the study through their clinician and participants gave written, informed consent for the donation of bone marrow aspirates. The inclusion criteria for FPLD patients were that they had a confirmed *LMNA* mutation and no other current disease.

MSCs were isolated from bone marrow aspirates with the aid of RosetteSep Mesenchymal Stem Cell Enrichment Cocktail (Stem Cell Technologies) and centrifugation over a density medium (Ficoll-Paque). The MSC enriched fraction was then collected and cultured as described in Section 2.7 . MSCs were cultured in standard Dulbecco's modified Eagle's medium (DMEM), 10% foetal calf serum (FCS), plus 3 ng/ml basic fibroblast growth factor (bFGF).

Cell line	Mutation	Age of donor (years)
MSC control 1	Normal control	34
MSC control 2	Normal control	65
MSC control 3	Normal control	40
MSC control 4	Normal control	62
MSC control 5	Normal control	44
MSC control 6	Normal control	67
MSC FPLD 1	LMNA R482W	33
MSC FPLD 2	LMNA R482W	36
MSC FPLD 3	LMNA R482W	36

**Table 6.1** MSC cell lines cultured

#### **6.4.2 Growth of FPLD MSC cultures**

The 3 FPLD MSC cultures were isolated alongside control cell line 3 and are compared in Figure 6.3. MSCs are fibroblastic in appearance. FPLD patient MSC cultures FPLD 1 and FPLD 2 appeared as control 7 days after isolation, containing a small number of adherent cells of MSC appearance (Figure 6.3A (a-c)). Culture FPLD 3 contained adherent cells of MSC and non-MSC appearance at day 7, this was not observed in any other MSC culture (Figure 6.3A (d)). The non-MSC cells were less adherent and were successfully removed by several rounds of trypsinisation and re-plating. By day 20, control and FPLD 1 and 3 cultures appeared to contain exclusively cells of fibroblastic MSC appearance (Figure 6.3A (e,f,h)). However, culture FPLD 2 stopped growing and could not be cultured further (Figure 6.3A (g)). Both FPLD cultures 1 and 3 grew slowly compared to controls, although due to small cell numbers, cells were conserved for adipogenesis experiments and proliferation rates could not be quantified.

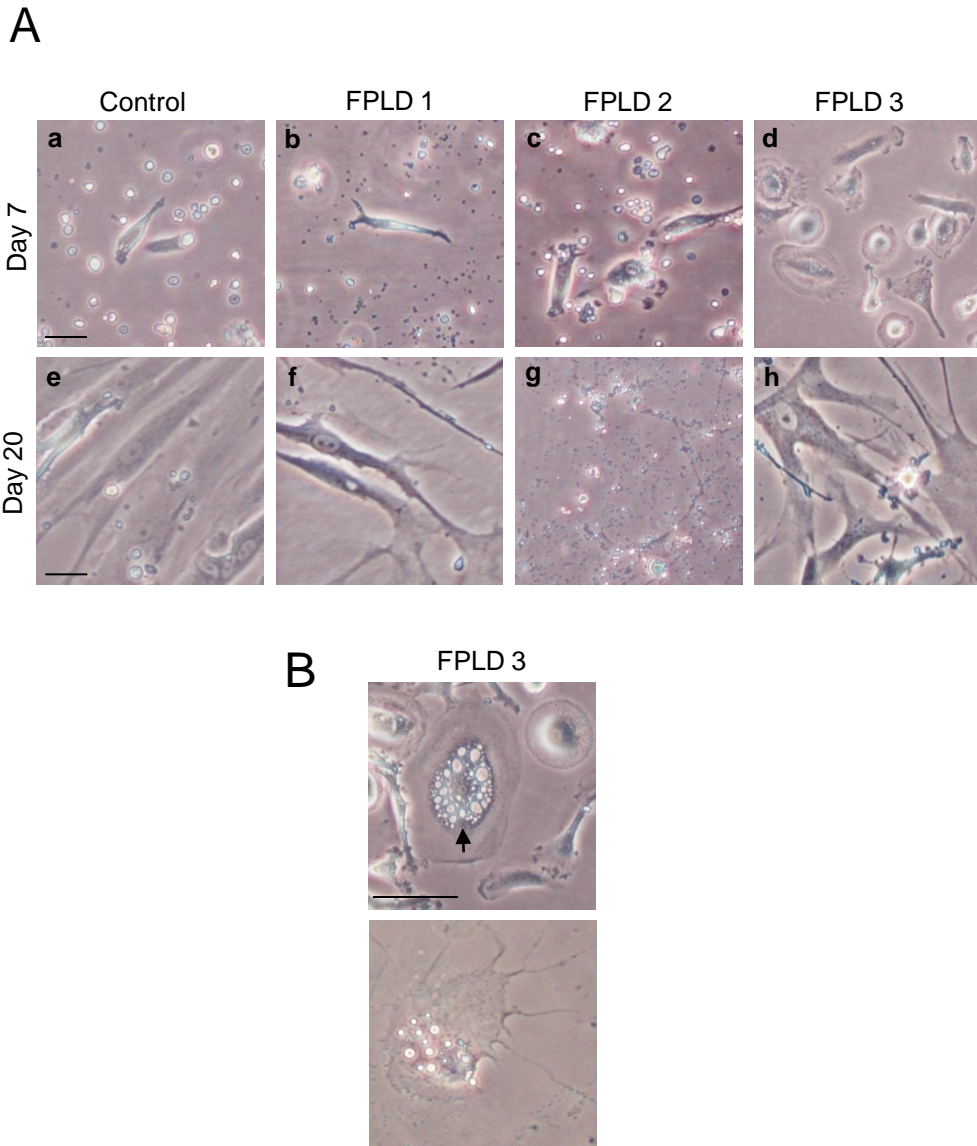


**Figure 6.3** Growth of FPLD patient MSCs 7 days (top panel) and 20 days (bottom panel) after isolation from bone marrow. Bar 50  $\mu\text{m}$  (A) Cultures FPLD 1 and FPLD 2 appeared as control 7 days after isolation, showing adherent cells of MSC appearance (b and c). Culture FPLD 3 contained adherent cells of a non-MSC appearance (d). By day 20, cultures FPLD 1 and 3 appeared to contain exclusively MSCs (e and h), however, culture FPLD 2 stopped growing and could not be cultured further (g). (B) The non-MSC adherent cells in culture FPLD 3 included cells of lipid-containing appearance (arrow, top panel). However, following fixation and incubation in oil-red-o, these cells did not stain positively for lipid (bottom panel).

The non-MSc adherent cells in culture FPLD 3 included cells of lipid-containing appearance (Figure 6.3B (top panel)). However, following fixation and incubation in oil-red-o, these cells did not stain positively for lipid (bottom panel) suggesting that the cells may contain vacuoles.

#### ***6.4.3 FPLD patient cell lines 1 and 3 stained positively for MSC markers***

To give an indication as to whether the cells isolated were indeed MSCs, cells were grown on coverslips, fixed and stained with antibodies against MSC markers CD29, CD105 and lamin A/C and observed by immunofluorescence microscopy. Staining of MSC markers CD29 and CD105 was observed at the plasma membrane (Figure 6.4A, indicated by white arrows), cells also stained positive for lamin A/C (Figure 6.4B). Whilst dermal fibroblasts would also be expected to stain positive for these markers and there is no definitive MSC marker, homogenous expression of these proteins suggests that the MSC cultures were not contaminated with other haematopoietic cell types (Schieker *et al* 2007).

#### ***6.4.4 FPLD patient MSC nuclear morphology***

Lamin A/C staining revealed abnormal nuclear morphology in FPLD patient cell lines 1 and 3 compared to control cell line 1 (Figure 6.4B). Counts of 100 nuclei stained at passage 3 revealed that 73% of FPLD cell line 1 and 30% of FPLD cell line 3 nuclei were abnormal compared to control cell line 4 in which only 6% of nuclei were abnormal. A description of nuclei classified as abnormal is given in Section 4.3. Almost every abnormal FPLD nucleus showed the same unusual dysmorphology consisting of multiple buds in the nuclear envelope. The 6% of control nuclei

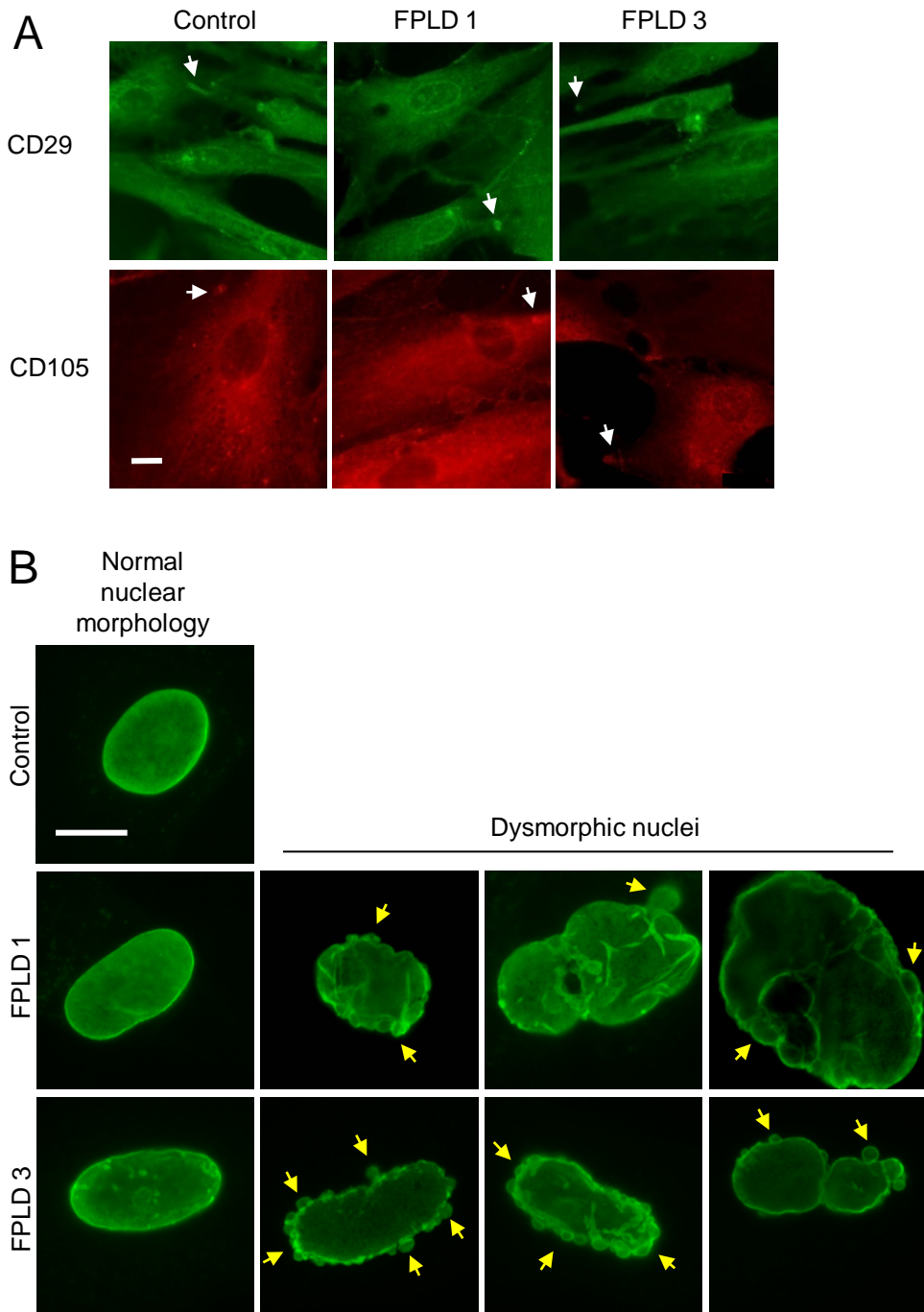


**Figure 6.4** Isolated MSCs stained positive for markers (A) CD29 (green) and CD105 (red) (B) lamin A/C, white arrows indicate staining at the plasma membrane. Lamin A/C staining (B) shows unusual nuclear dysmorphism with numerous buds from the lamina indicated by yellow arrows. Bars 10  $\mu$ m.

classified as abnormal all contained areas of thickened lamina or twisting, buds were never observed in the control.

#### ***6.4.5 Development of a protocol allowing adipogenic conversion of control MSC using only non-specific enhancers of adipogenesis DEX, IBMX and insulin***

Differentiation of cultured MSCs using the 3T3L1 adipogenic protocol described in Section 6.3 resulted in poor differentiation in comparison with the addition of the synthetic PPAR $\gamma$  ligand Troglitazone (Figure 6.5). There are a great many variations in published adipogenic differentiation protocols for MSCs, however, protocols almost always involve a single stimulation in DEX, IBMX and insulin plus the addition of a PPAR $\gamma$  ligand throughout adipogenesis, based upon Pittenger *et al* (1999). In this study we wished to investigate changes in SREBP1 activity in FPLD. Since PPAR $\gamma$  is activated by SREBP1 (Kim *et al* 1998), it was important to avoid masking the effect of any changes in SREBP1 activity by directly stimulating PPAR $\gamma$  with Troglitazone or similar ligands.

##### ***6.4.5.1 Optimal differentiation conditions***

To enhance adipogenesis a protocol involving re-stimulation of cells with adipogenic reagents every 3 days was developed (adapted from Janderova *et al* 2003). Control MSC cell lines 1 and 4 were grown to confluence in triplicate. Two days post-confluence, cells were incubated with adipogenic factors: DEX (1  $\mu$ M), IBMX (0.5 mM) insulin (1.7  $\mu$ M), in the presence or absence of 5  $\mu$ M Troglitazone for 3 days, then switched to insulin alone for 3 days. This 6 day regimen was repeated for 18 days then cells were incubated in insulin alone to allow lipid uptake for a further 12 days.

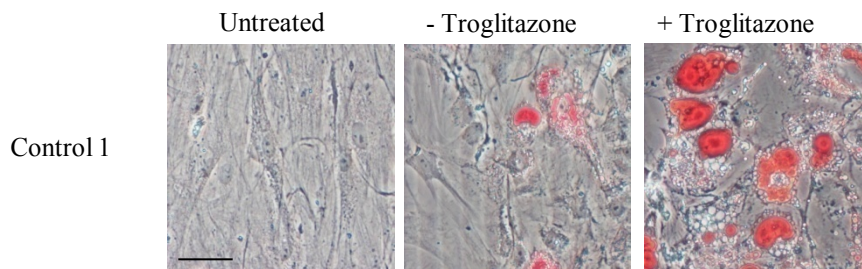


**Figure 6.5** Adipogenic differentiation of MSCs with DEX (1  $\mu$ M), IBMX (0.5 mM), insulin (1  $\mu$ M) following conventional published protocols in the presence and absence of Troglitazone (5  $\mu$ M). Samples of control cell line 1 at passage 2 were fixed and stained on day 21. Bar 70  $\mu$ m

Images of the cells stained with oil-red-o at 30 days post differentiation are shown for cell line 4 and are representative of the overall result (Figure 6.6A). The highest levels of differentiation were observed with the addition of the PPAR $\gamma$  activator Troglitazone (Figure 6.6 f). However, by re-stimulating cells with DEX, IBMX and insulin, significant differentiation could be achieved in the absence of Troglitazone (Figure 6.6 e). No differentiation occurred in the untreated control (Figure 6.6 d). For semi-quantitative analysis of lipid accumulation, bound oil-red-o was eluted from cells in 100% isopropanol and the absorbance of the resulting solution measured at 520 nm. Figure 6.6 shows scans of plates and images of oil-red-o stained (6.6A) and post-elution cells (6.6B), scans a-c and images d-f show staining with oil-red-o, scans g-i and images j-l show that stain was completely eluted. Plotting absorbance shows that, whilst the highest level of lipid accumulation is achieved with the use of Troglitazone, by restimulating cells, quantifiable levels of lipid accumulation could be achieved with DEX, IBMX and insulin alone (Figure 6.6C).

#### *6.4.5.2 Efficacy of basic fibroblast growth factor (bFGF)*

The addition of 3 ng/ml bFGF to adipogenic media has been reported to enhance MSC differentiation in PPAR $\gamma$  ligand-induced adipogenesis (Neubauer *et al* 2004). To determine whether the addition of bFGF was playing a significant role in the stimulation of adipogenesis in this study, the 30 day differentiation was repeated for MSC control cell line 1 in the presence and absence of 3 ng/ml bFGF. The absorbance of oil-red-o was measured and the average of 2 experiments is shown in Figure 6.7. Results indicated that the addition of bFGF causes no increase in lipid accumulation, therefore bFGF was not used in subsequent adipogenic conversions.

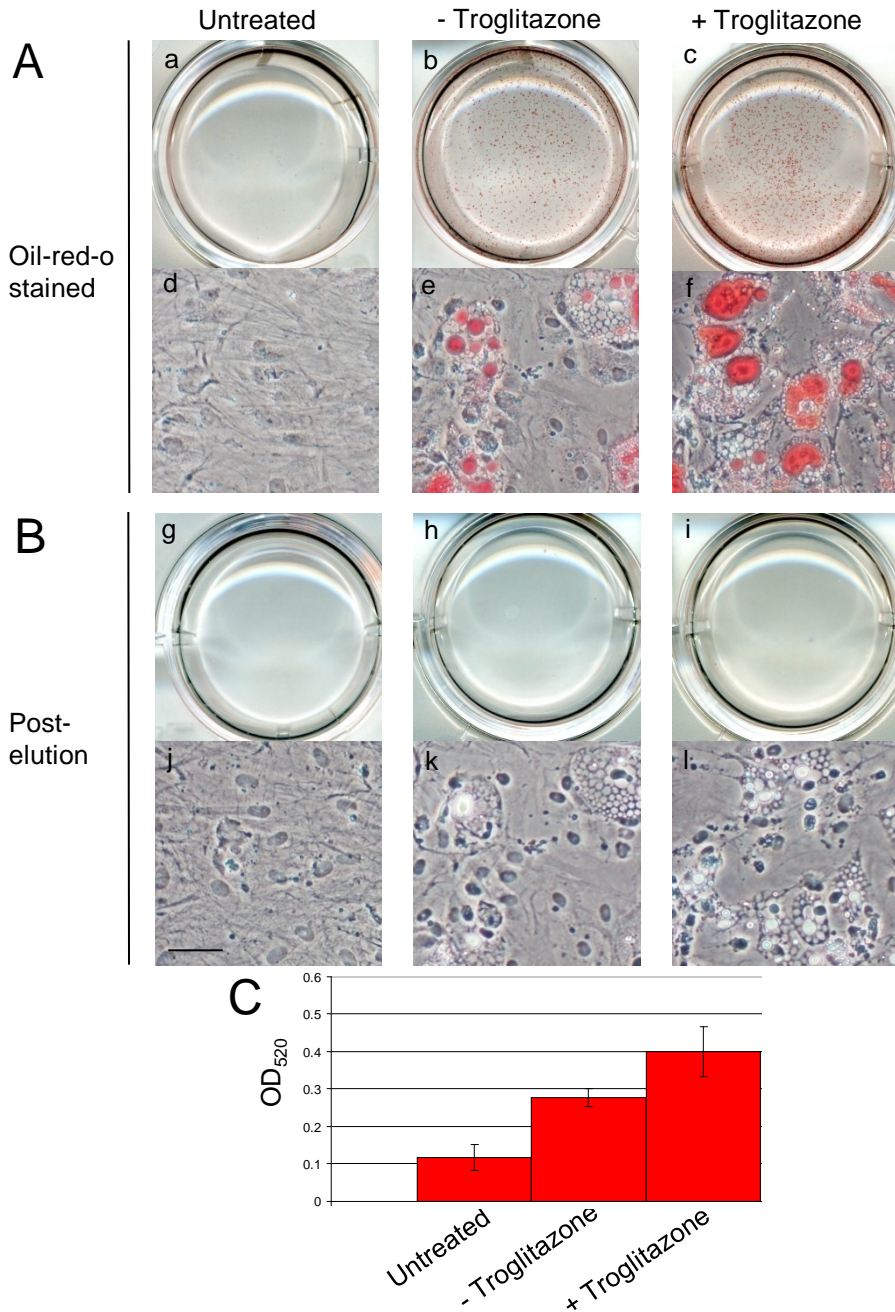


**Figure 6.6** (A) Representative images of control cell line 4 untreated and differentiated with or without 5  $\mu$ m Troglitazone as indicated. Cells were differentiated using DEX (1  $\mu$ m), IBMX (0.5 mM), insulin (1.7  $\mu$ m) then fixed in formalin and oil-red-o stained. Plates were imaged before (A) and after (B) elution of oil-red-o with 100% isopropanol. Upper panels show view of the whole plate, lower panels show a representative view of cells at 10x magnification. Cells were fixed and stained on day 30. (C) Graph of OD<sub>520</sub> of eluted oil-red-o, combined for cell lines 1 and 4, average of 3 experiments +/- SEM. Bar 70  $\mu$ m

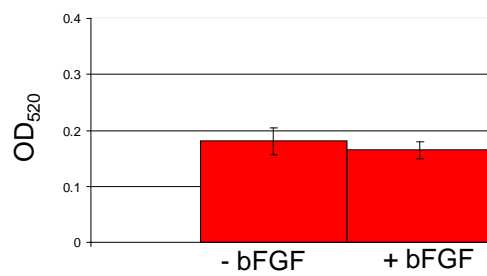


**Figure 6.7** Lipid accumulation in control cell line 1 was slightly reduced in the samples to which basic fibroblast growth factor (bFGF) was added. Samples were differentiated in 0.5 mM IBMX, 1  $\mu$ M DEX, 1.7  $\mu$ M insulin plus or minus 3 ng/ml bFGF. Lipids were stained with oil-red-o, stain was then eluted and graph shows OD measured at 520 nm, n=2 +/-SEM.

#### *6.4.5.3 MSCs acquired a senescent phenotype at approximately passage 6*

MSC cultures have been reported to cease growth at around 40-50 population doublings (Stenderup *et al* 2003). In this study, cells were counted in passages where one passage equalled a 1:4 split when cells were 80-90% confluent. Undifferentiated MSC cultures appeared senescent at around passage 6 (Figure 6.8A) which equates to approximately 12 population doublings.

To determine the efficiency of differentiation at different passage numbers, MSC control cell lines 1 and 4 were differentiated at passages 4 and 6 using the adipogenic protocol described in Section 6.4.5.1 in the absence of Troglitazone. Higher passage MSC differentiated poorly compared to those at a lower passage. Differentiation of cell line 1 at passages 4 and 6 is illustrated (Figure 6.8B). Due to the poor differentiation of higher passage cells in this study, cells lines used in subsequent experiments were of low passage.

#### *6.4.5.4 Adipogenic conversion protocol using only the non-specific enhancers of adipogenesis DEX, IBMX and insulin*

Cells were seeded in 12 well plates,  $6 \times 10^4$  cells per well and grown to confluence. Two days post-confluence, bFGF was removed and cells were incubated with adipogenic factors: DEX (1  $\mu$ M), IBMX (0.5 mM) and insulin (1.7  $\mu$ M) for 3 days, then switched to insulin alone for 3 days. This 6 day regimen was repeated for 18 days then cells were incubated in insulin alone for a further 12 days.

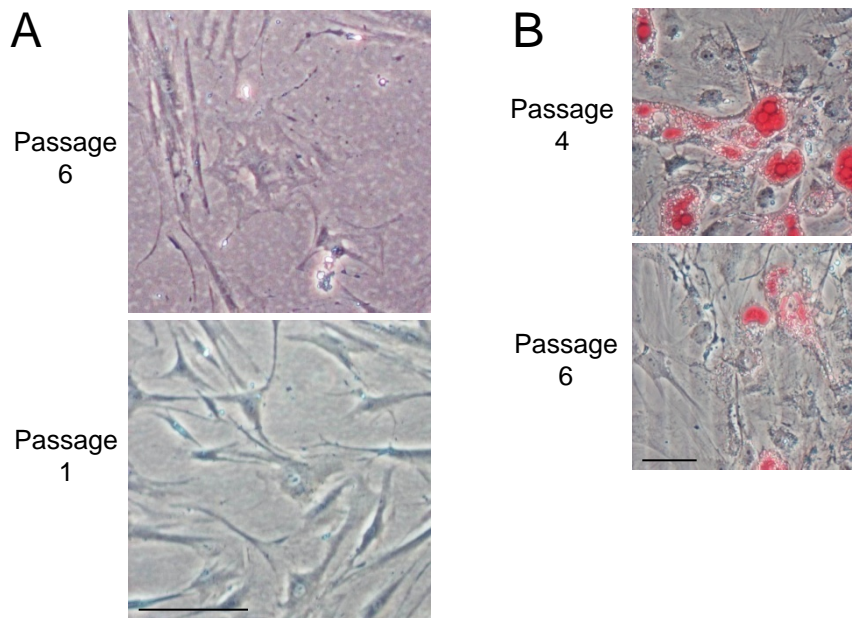


**Figure 6.8** (A) Undifferentiated cultured MSC cell line 2 acquired a senescent phenotype at around passage 6 (top panel), passage 1 (bottom panel) is shown for comparison. Bar 200  $\mu\text{m}$  (B) Representative oil-red-o stained images of MSC cell line 1, differentiated in the absence of Troglitazone, shows high passage cells differentiated poorly (bottom panel) compared to those at a low passage (top panel)  $n=2$ . Bar 70  $\mu\text{m}$

#### **6.4.5.5 Adipogenic differentiation of FPLD MSC cell line 3**

FPLD cell line 3 was differentiated alongside control cell lines 1, 4, 5 and 6 in triplicate (Figure 6.9) following the protocol described in Section 6.4.5.4. All cell lines were at passage 2. FPLD cell line 1 proliferated too poorly to obtain sufficient cells for this experiment. Adipogenic differentiation was carried out both in the absence and presence of Troglitazone (Figure 6.9A). Semi-quantitative analysis of lipid accumulation revealed that in FPLD cell line 3, in the absence of Troglitazone, a very small amount of lipid was accumulated compared to untreated cells (Figure 6.9B). However, it is possible that this is due to variation in lipid accumulation between individuals since the pattern of lipid accumulation is almost identical to control cell line 1. Lipid accumulation was highly variable in the controls; control cell line 4, for example, differentiated well, whereas differentiation of control cell line 5 was extremely poor. Overall, comparison of FPLD cell line 3 with the control cell lines using the Student's T-Test revealed no significant difference in differentiation potential, P values are shown in Figure 6.9B.

#### **6.5. *Lmna* R482W mouse embryonic fibroblast (MEF) studies**

To support the data gained from human MSCs, adipogenesis potential and nuclear morphology were examined in *Lmna* R482W MEFs. A knock-in FPLD mouse model has been generated in the laboratory in which *Lmna* gene has been replaced with a copy carrying the R482W mutation. Heterozygotes were crossed by Dr Carolyn Dent and MEF cell lines 13.1, 13.2, 13.3, 13.4, 13.5, 13.6 were isolated from these crosses by Dr Dent. Further heterozygote crosses were set up by Dr Sue Shackleton and cell lines 6.6, 6.7, 6.8 and 7.3, 7.4, 7.5, 7.6, 7.7, 7.8 were isolated by Dr Shackleton then cultured and genotyped as part of this study. MEF littermates are indicated by the first

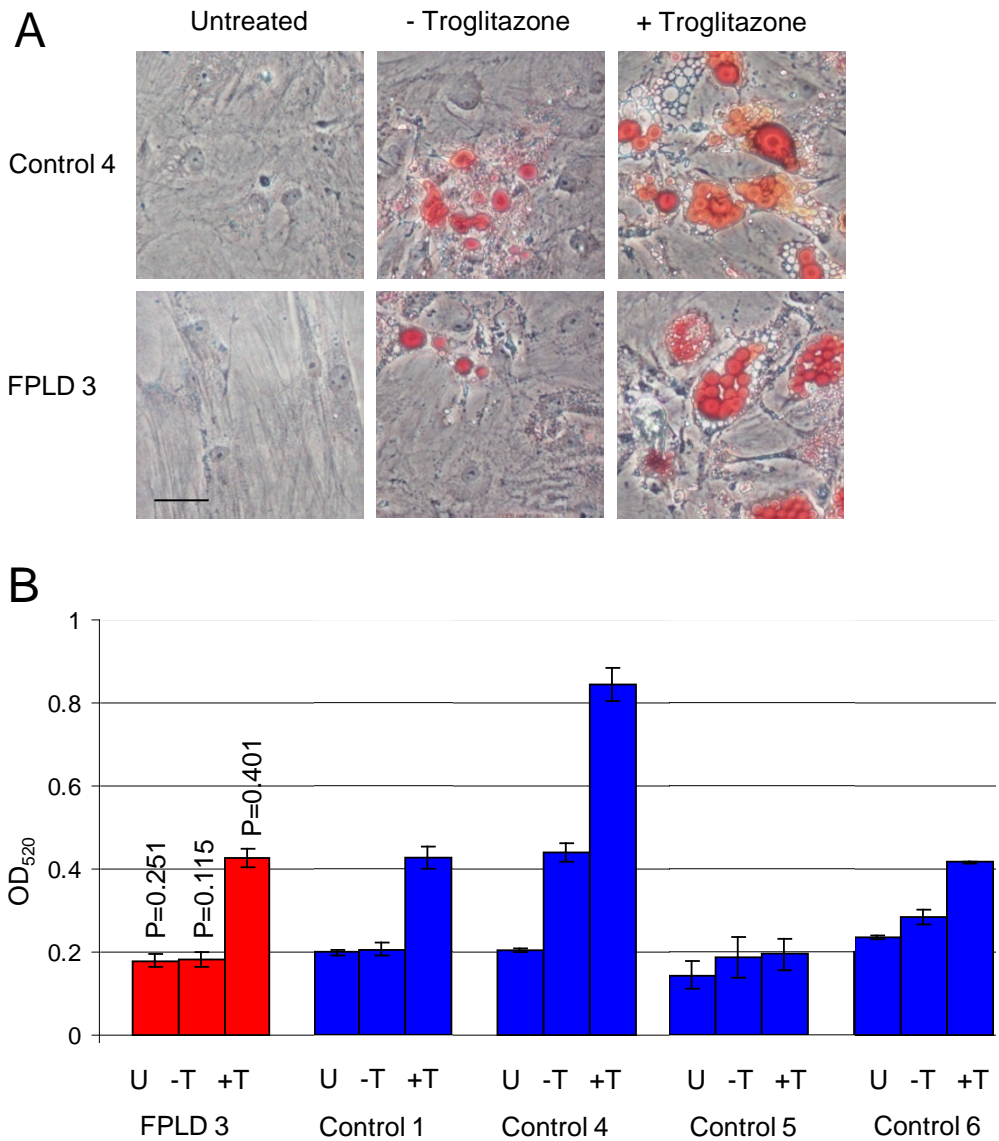


**Figure 6.9** (A) Adipogenic differentiation of FPLD MSC and control cell line 4. Bar 70  $\mu\text{m}$  (B) Graphs show  $\text{OD}_{520}$  of eluted oil-red-o stain in FPLD (red) and 4 control MSC cell lines (blue). U=untreated samples, -T = adipogenic reagents minus Troglitazone, +T= adipogenic reagents plus Troglitazone, n=3 +/- SEM. P indicates P value

number of the cell line, for example cell lines 13.1-13.6 were produced from littermates.

### **6.5.1 *Lmna* R482W MEF nuclear morphology**

Nuclear morphology was examined by lamin A/C staining of *Lmna* R482W homozygote, heterozygote and wild type (WT) cell lines. Four MEF cell lines were examined for each genotype and representative images from cell lines 13.1 (WT), 13.2 (heterozygote) and 13.3 (homozygote) are shown in Figure 6.10. Dymorphologies included budding, holes and buds containing a honeycomb pattern of lamin A staining. Budding of the lamina observed in FPLD MSCs (Figure 6.4) was also a feature of R482W homozygote MEFs and was observed to a lesser degree in heterozygotes. Budding and honeycomb patterns of lamin A staining have been reported in FPLD patient fibroblasts (Vigouroux *et al* 2001), were observed in FPLD fibroblasts in this study (Section 4.1). However, multiple buds throughout the nuclear envelope have not been reported in FPLD fibroblast cell lines.

Abnormal nuclear morphology was examined in WT, heterozygous and homozygous cell lines. Each cell line was at passage 2 and at least 300 cells per cell line were counted. The percentage of abnormal nuclei in each cell line is shown in Table 6.2 and Figure 6.11, illustrating that abnormalities in WT nuclei are low but increase in heterozygous and homozygous nuclei, presumably as the amount of mutant lamin A present in the cell increases. The Student's T-Test was used to compare the percentage of abnormal nuclei in heterozygous and homozygous cell lines to WT. The percentage of abnormalities were found to be statistically significant in heterozygote ( $P=0.026$ ) and homozygote ( $P=0.003$ ) nuclei (Figure 6.11). Counts in Table 6.2 also illustrate the variation between different cell lines of the same genotype. In

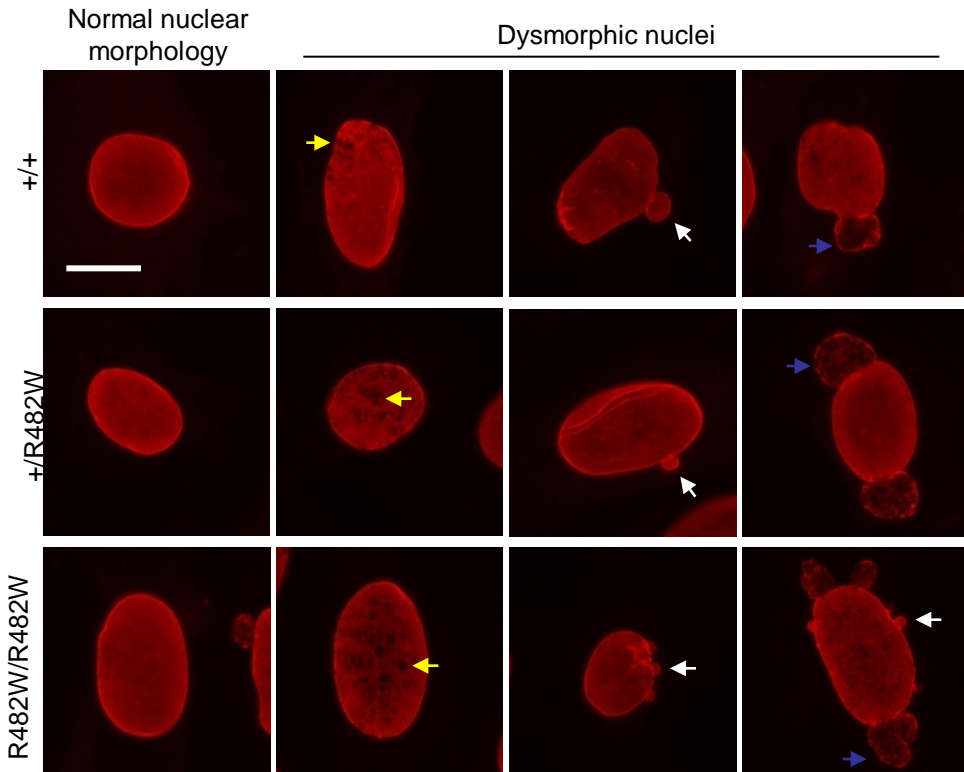


**Figure 6.10** Lamin A/C staining of *Imna* R482W knock in mouse embryonic fibroblasts and WT littermate control. Nuclear morphology abnormalities were present in homozygote, heterozygote and WT cell lines. Arrows indicate abnormalities observed; white: buds, yellow: holes, blue: honeycomb lamina. Bar 10  $\mu$ m.

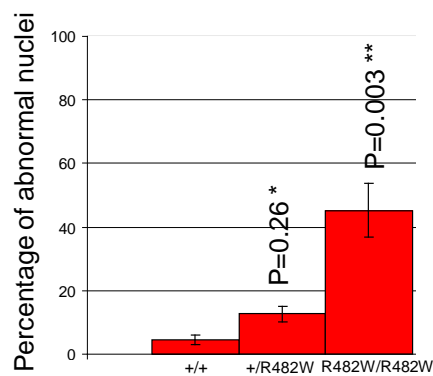


**Figure 6.11** Percentage of MEFs with abnormal nuclear morphology, n=300, +/- SEM. P indicates P value

Cell line	<i>Lmna</i> R482W genotype	Percentage of cells with abnormal nuclei
7.3	+/+ (WT control)	2
7.4	+/+ (WT control)	2
13.1	+/+ (WT control)	7
13.5	+/+ (WT control)	7
7.7	+/R482W (heterozygous)	10
7.8	+/R482W (heterozygous)	8
13.2	+/R482W (heterozygous)	19
13.4	+/R482W (heterozygous)	14
7.5	R482W/R482W (homozygous)	28
7.6	R482W/R482W (homozygous)	36
13.3	R482W/R482W (homozygous)	66
13.6	R482W/R482W (homozygous)	51

**Table 6.2** Percentage of abnormal nuclei in MEF cell lines. n=300 nuclei at passage 2.

homozygote cell line 7.5, for example, 28% of nuclei are abnormal, but in cell line 13.3 abnormalities were observed in 66% of nuclei. MEFs from litter 13 appear to show higher rates of abnormality than litter 7, suggesting that although the mice are inbred, genetic background may play a part in the effect of the R482W mutation.

### **6.5.2 *Lmna* R482W MEF adipogenic differentiation**

MEFs have been successfully differentiated into adipocytes (Boguslavsky *et al* 2006). To support the adipogenesis data from FPLD MSC differentiation, a MEF differentiation study was undertaken. Cell lines used in the study are listed in Table 6.3. Results of two separate experiments were pooled.

Cell line	Mutation
Mouse embryonic fibroblast (MEF) wild type littermate control cell lines 6.6, 7.3, 7.4, 13.5	WT control (+/+)
Mouse embryonic fibroblast (MEF) heterozygote cell lines 6.8, 7.7, 7.8, 13.4	Heterozygous (+/R482W)
Mouse embryonic fibroblast (MEF) homozygote cell lines 6.7, 7.5, 7.6, 13.6	Homozygous (R482W/R482W)

**Table 6.3** MEF cell lines used in the adipogenic conversion study.

Adipogenic differentiation was achieved in both the absence and presence of Troglitazone for all cell lines (Figure 6.12A). Semi-quantitative analysis of lipid accumulation revealed that, in the absence of Troglitazone, a very small amount of lipid is accumulated, at an intermediate level between untreated and Troglitazone treated samples. Homozygous MEFs differentiated at a lower level than WT MEFs and reached a similar level of lipid accumulation as heterozygotes (Figure 6.12B). Therefore, there appears to be a reduction in the adipogenic potential of both heterozygous and homozygous MEFs, however this was not found to be statistically significant (Figure 6.12).

## 6.6 Discussion

There have been conflicting findings concerning the localisation of the adipogenic transcription factor SREBP1 in FPLD. These include mislocalisation of endogenous protein from the nucleoplasm to the nuclear rim (Capanni *et al* 2005, Figure 4.4 of this study), mis-localisation of transfected protein to the cytoplasm, (previous findings in the laboratory and Figure 5.2 of this study), increased strength of SREBP1 binding to the lamin A R482W mutant, (Figure 5.15 of this study) and decreased mobility of

SREBP1 in FPLD fibroblasts, (Figure 5.6 of this study). SREBP1 is necessary for adipogenesis to take place (Kim and Spiegelman 1996) due to its activation of PPAR $\gamma$  (Kim *et al* 1998, Fajas *et al* 1999). Any of the above factors, therefore, could impact upon the transcriptional activation activity of SREBP1, potentially altering its ability to activate PPAR $\gamma$  and stimulate adipogenesis.

An adipogenic protocol was developed to allow evaluation of the adipogenic potential of FPLD patient MSC. This protocol differs from conditions reported in the literature which are based on Pittenger *et al* 1999, because it does not involve direct stimulation of PPAR $\gamma$  by synthetic ligand. By the protocol developed in this study, any defect in differentiation caused by defective transcriptional activity of SREBP1 is not masked by downstream activation of PPAR $\gamma$ .

The result of the preliminary differentiation study shows that FPLD MSCs carrying the R482W mutation are almost completely unable to differentiate into adipocytes in the absence of the PPAR $\gamma$  activator Troglitazone, however that was also the case for one of the control cell lines. Higher levels of FPLD MSC and differentiation were obtained in the presence of Troglitazone. In the both the presence and absence of Troglitazone, FPLD MSC accumulated lipid to levels similar to that of control MSC. The differentiation study would need to be repeated with more MSCs from other FPLD patients before conclusions about adipogenic potential in FPLD can be drawn. A great deal of variation was found in the ability of different control cell lines to accumulate lipid. Due to this apparent innate variability in differentiation from one control sample to another, a significant number of FPLD patient samples would be needed for conclusive results.

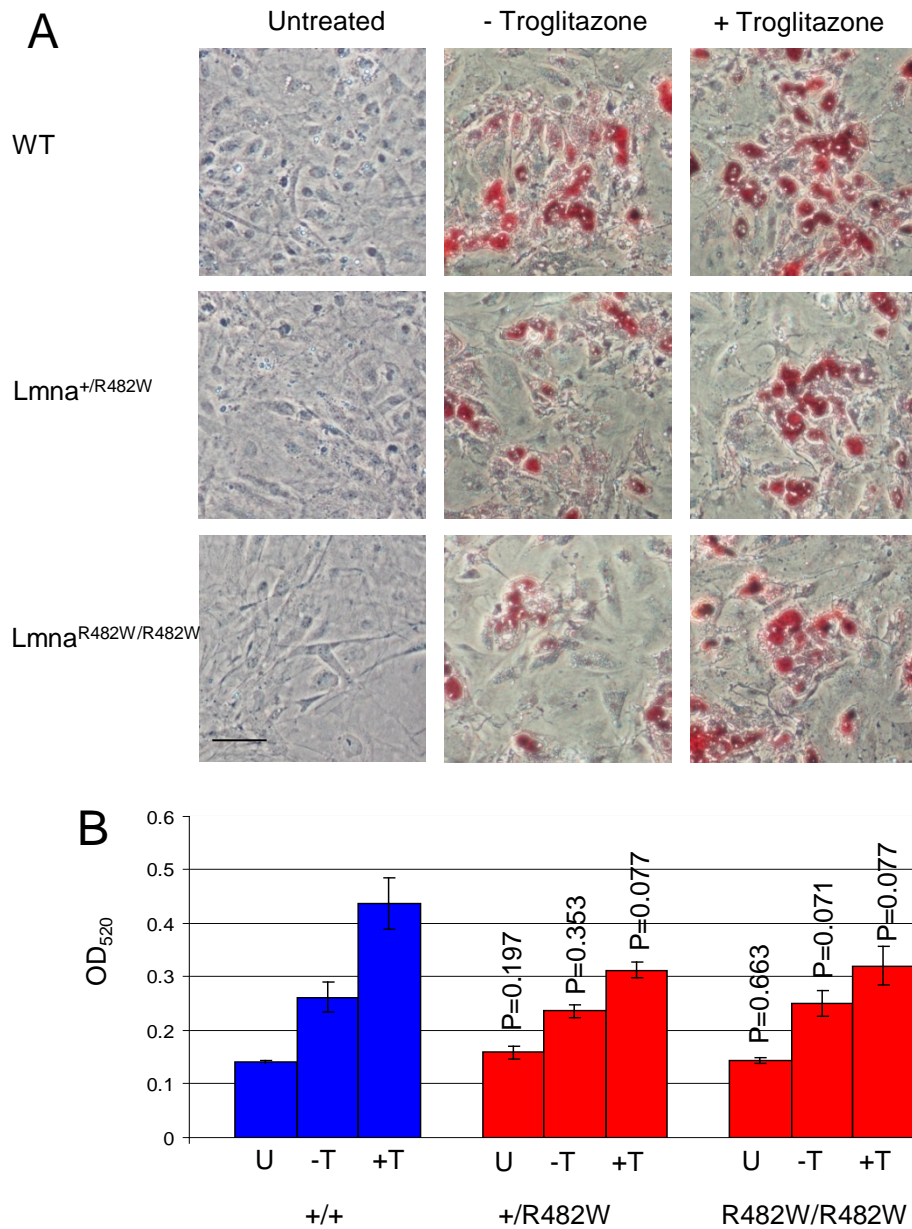


**Figure 6.12** Adipogenic differentiation of *Lmna* R482W knock in mouse embryonic fibroblasts and WT littermate control. **(A)** Representative images of WT (+/+), heterozygote (+/R482W) and homozygote (R482W/R482W) cell lines untreated or differentiated with or without 5  $\mu$ M Troglitazone as indicated, then fixed and oil-red-o stained. Bar 70  $\mu$ m **(B)** Graphs show OD of eluted oil-red-o stain in heterozygotes and homozygotes (red) and WT control (blue), U=untreated samples, -T = adipogenic reagents minus Troglitazone, +T= adipogenic reagents plus Troglitazone, average of 4 different cell lines per genotype in 2 separate experiments, +/- SEM. P indicates P value

*Lmna* R482W homozygous and heterozygous MEFs were able to form adipocytes both in the presence and absence of Troglitazone at approximately half the efficiency of WT MEFs. Adipogenic conversion was enhanced by the addition of Troglitazone to homozygous and heterozygous and WT MEFs. This is in contrast to FPLD MSCs, which appeared unable to produce detectable levels of adipogenesis in the absence of Troglitazone and could represent differences between mouse and human FPLD cells.

If the hypothesis that SREBP1 function is defective in FPLD is correct, we would expect that lipid accumulation would be detected in control cell lines in the absence of the PPAR $\gamma$  activator, but that there would be no adipogenic differentiation in cells carrying the R482W mutation with this treatment due to defective activation of PPAR $\gamma$  by SREBP1. Furthermore we would expect that addition of the PPAR $\gamma$  activator Troglitazone would act downstream of SREBP1 to rescue adipogenesis. Adipogenic conversion of the FPLD MSC cell line (Figure 6.9) supports this hypothesis, however one of the control cell lines was also unable to differentiate in the absence of Troglitazone and a second control cell line failed to differentiate at all, even in the presence of Troglitazone.

There is significant variation in the phenotype of Dunnigan-type FPLD patients and even between patients carrying the same mutation (Cao and Hegele 2000). Taken together with the significant variation in the ability of control MSC to accumulate lipid, it cannot be suggested that lipid accumulation in FPLD MSC culture 3 is representative of the adipogenic potential in FPLD. It should be noted that due to the cessation of proliferation of FPLD MSC culture 2, the slow proliferation rate of FPLD MSC culture 1 and time constraints on this study, these cell lines could not be included in the adipogenesis study to provide further information.

FPLD patient and control MSC were isolated by exactly the same method and appeared identical in culture, with the exception of early observations in FPLD MSC culture 3. FPLD culture 3 contained adherent cells of a non-MSC morphology not found in any other MSC cultures. These unusual cells were removed by rounds of trypsinisation and re-plating. A number of the non-MSC cells appeared morphologically similar to adipocytes. The possibility was considered that abnormal adipogenic differentiation may have led to stem cell depletion and subsequent loss of subcutaneous fat around the time of puberty. Stem cell exhaustion is proposed to occur in Hutchinson-Gilford progeria syndrome (Halaschek-Wiener and Brooks-Wilson 2007). However, staining with oil-red-o revealed that cells did not contain lipid. These unusual, non-MSC cells remain unidentified.

A large number of molecular markers of human MSC such as CD29 (beta 1 integrin) and CD105 (endoglin) and lamin A are used to detect MSC. These markers are not exclusively expressed by MSC, but the expression of a combination of markers increases the likelihood that cells being cultured are MSCs (Boheler 2004). An MSC culture is likely to contain fibroblasts and MSC in different progenitor states of osteoblastic, chondrocytic and adipocytic lineages (Aubin 2001) which are phenotypically indistinguishable. For the purpose of this study, all MSC were isolated identically, consequently the cultures although likely to be heterogeneous, are comparable.

The nuclear morphology of FPLD MSC cultures 1 and 3 were examined by indirect immunofluorescence microscopy and lamin A/C staining revealed that a significant percentage had abnormal nuclear morphology. Multiple buds were observed in the nuclear envelope of almost all dysmorphic nuclei. The same pattern of nuclear

envelope budding was found in *Lmna* R482W MEFs. This specific abnormality appears to be a feature of FPLD nuclei and has been reported in FPLD fibroblasts by Vigouroux *et al* 2001 and in Section 4.3.1 of this study; however there are much lower levels of abnormal nuclei in fibroblasts. The reason for the high level of dysmorphology observed in human FPLD MSCs compared to human fibroblasts is not clear; perhaps there is a lack of expression of other nuclear proteins in FPLD MSCs so they are more severely affected. This could be examined in further studies.

## CHAPTER 7

### Conclusions and future work

#### 7.1 Detection of mutations in *LMNA* and *ZMPSTE24* genes

The aim of this study was to screen genomic DNA samples from patients with a lipodystrophic phenotype for mutation of the *LMNA* gene, and patients with a progeroid phenotype for mutation of both *LMNA* and *ZMPSTE24* genes.

Patients with an atypical progeria phenotype can be difficult to diagnose clinically, disorders are extremely rare and there are overlapping phenotypic features between the premature aging disorders. Genetic analysis is very useful for accurate diagnoses, treatment and for genetic counselling for families. For example, the atypical progeria patient ET, screened in this study, was first diagnosed with a connective tissue disorder, but later re-diagnosed with progeria and screening was requested. The patient was found to have a *LMNA* mutation reported only twice in the literature (Fukuchi *et al* 2004, Shalev *et al* 2007). Accurate diagnosis meant patient 004 had the opportunity to take part in clinical trials using FTIs to treat progeria. The use of FTIs to ameliorate the disease process in HGPS is discussed in Section 1.6.7.

Unlike atypical progeria, the classical progeria phenotype is consistent between patients (Mazereeuw- Hautier *et al* 2007, Hennekam *et al* 2006). Since there is little variation in the development of features of classical progeria, this disorder is usually diagnosed clinically and confirmed by mutation screening. In this study, causative mutations were identified in two patients with a classical HGPS phenotype who were found to be carrying identical *LMNA* G608G mutations.

Compound heterozygous *ZMPSTE24* mutations were identified by collaborators in a patient with a severe progeroid phenotype. Screening showed that the patient inherited one mutated *ZMPSTE24* allele from each of her healthy unrelated parents. This diagnosis was useful in terms of genetic counselling because the parents had a 1:4 chance of having another child with progeria.

There were a further 11 patients with a progeroid phenotype in whom *LMNA* and *ZMPSTE24* genes were sequenced but no mutation was found. These patients may be suffering from progeroid disorders with a related phenotype (Table 3.6).

No mutations were identified in lipodystrophy patients screened in this study. FPLD caused by mutation of the *LMNA* gene involves a particular pattern of fat distribution and metabolic disturbance (Garg *et al* 2001), however, the phenotype is variable (Vigouroux *et al* 2001). Patients without the typical FPLD pattern of fat loss were screened in case they showed a variation of the phenotype. These patients may be suffering from lipodystrophy disorders with a related phenotype (Table 3.5).

In conclusion, atypical progeria and lipodystrophy are phenotypically heterogeneous disorders for which genetic screening is a valuable tool in accurate diagnosis.

Future work could involve further investigation of the patients who did not carry *LMNA* or *ZMPSTE24* mutations. Detailed descriptions of the patient phenotypes could be obtained to search for additional candidate genes to sequence.

## **7.2 Analysis of the expression, localisation and mobility of lamin A and associated nuclear proteins in progeria and FPLD**

This is the first comparative study of protein expression in different types of progeria.

Mobility studies and Western blot analysis confirmed that permanently farnesylated forms of lamin A persist in late onset and severe progeria in addition to classical progeria in which this has been previously reported (Goldman *et al* 2004, Capell *et al* 2005). Levels of farnesylated lamin A correlated with patient phenotype such that the highest levels were found in the patient with the most severe phenotype. Identical cellular defects were found in fibroblasts from all 3 patients, however, severity of defects increased with increased levels of farnesylated lamin A.

The presence of farnesylated lamin A in severe, late onset and classical progeria was associated with depletion of nucleoplasmic lamin A as visualised by indirect immunofluorescence microscopy. Depletion of nucleoplasmic lamin A may disrupt the Lamin A-LAP2 $\alpha$ -Rb complex and lead to down regulation of LAP2 $\alpha$  and Rb. Reduced proliferation has been associated with LAP2 $\alpha$  down regulation (Pekovic *et al* 2007) and the reduction in proliferation in all progeria fibroblasts in this study, supports the association with LAP2 $\alpha$  and suggests that disruption of the complex of lamin A, LAP2 $\alpha$  and Rb disrupts proliferation.

Prelamin A accumulation is thought to lead to SREBP1 mislocalisation to the nuclear rim and disruption of a dipogenesis (Capanni *et al* 2005). Nuclear rim staining of SREBP1 was observed in progeria fibroblasts and in FPLD, supporting this theory. Further studies of SREBP1 localisation were not possible due to the lack of a good antibody to detect endogenous protein. Published SREBP1 expression studies mainly

involve mRNA expression (Shimano *et al* 1997, Horton *et al* 2003) and there are few studies of the SREBP1 protein, perhaps because of the lack of a reliable antibody. Prelamin A accumulation was also found to be associated with SUN1 recruitment to the nuclear membrane in progeria, possibly further thickening the lamina and contributing to increased nuclear rigidity. SUN1 was only observed in classical HGPS cells, this could be extended to include late onset and severe progeria and FPLD cell lines in future studies.

FRAP mobility studies revealed the farnesylation status of a range of lamin A mutants. This was confirmed by Western blotting of cell extracts, where, in the absence of a splicing mutation, the presence of a band of higher molecular weight than lamin A indicated aberrant farnesylation. Mobility of lamin A was decreased in late onset, classical and severe progeria where defective prelamin A processing occurs (described in sections 1.6.1, 3.6.2 and 3.6.3 respectively). WT mobility levels were expected for progeria point mutations which were not expected to interfere with prelamin A processing. However, unexpected results were obtained from S143F and E578V point mutants. S143F mobility was equal to that of farnesylated mutants and E578V mobility was twice that of wild type. Since Western blotting indicated that neither mutant was farnesylated the most likely explanation is that the interactions of S143F at the nuclear envelope are abnormally strong whilst E578V interactions are weak. At the end of this project, new atypical progeria cell lines from patients carrying S143F and E578V point mutations in lamin A arrived in the laboratory. Future studies to detect the expression of lamin A binding proteins in S143F and E578V cell lines may highlight interesting differences or similarities with progeria mutations in which farnesyl lamin A accumulates.

Cellular defects in the FPLD cell line in this study appeared less pronounced than in other reports (Vigouroux *et al* 2000). This may be due to phenotypic heterogeneity. It would be interesting for a future study to compare cellular defects with age and phenotype in a range of FPLD patients. It would also be interesting to investigate disease progression by looking for an association between increasing age, severity of phenotype and an increase in cellular defects.

### **7.3 An investigation into the interaction between lamin A and SREBP1**

FPLD mutations in lamin A/C are thought to alter its interaction with SREBP1, and impair SREBP1 function contributing to the lipodystrophy phenotype.

Previous evidence in the laboratory suggested that disruption of the SREBP1-lamin A interaction could result in lost tethering of SREBP1 in the nucleus so that SREBP1 is lost from its site of transcriptional activity. The SREBP1 transcription factor domain was found to bind less strongly to lamin A FPLD mutants than to WT lamin A (Lloyd *et al* 2002). In addition, immunofluorescence microscopy showed the transfected SREBP1 transcription factor domain localised to the nucleus in control cells, but localised to the cytoplasm in 34% of FPLD cells (Dr Sue Shackleton unpublished data). In this study, indirect immunofluorescence microscopy also revealed transfected SREBP1 transcription factor domain in the cytoplasm in a subpopulation of FPLD cells and in almost all classical HGPS cells. Interestingly, it has been reported that nuclear pore import is reduced in progeria (Busch *et al* 2009), perhaps suggesting another mechanism by which SREBP1 localises to the cytoplasm in FPLD and progeria. Weaker binding of SREBP1 to lamin A FPLD mutants had been reported (Lloyd *et al* 2002) but was not confirmed in this study, in fact, a trend towards tighter binding and decreased mobility was found in both FPLD and progeria mutants.

An alternative mechanism for mislocalisation of SREBP1 has been described by Capanni *et al* 2005. SREBP1 may be sequestered to the nuclear rim by prelamin A, removing SREBP1 from its site of transcriptional activity. In this study, the trend towards tighter binding to SREBP1 and decreased mobility in FPLD and progeria mutants supports the sequestration hypothesis.

SREBP1 antibodies tested in this study did not give reliable results on endogenous protein. If a reliable antibody against SREBP1 could be found, detection of localisation by indirect immunofluorescence microscopy and Western blotting of nuclear and cytoplasmic cell extracts could be performed on FPLD and progeria cell lines in future studies. An alternative approach would be the use of Lentiviral expression of GFP SREBP1 to investigate subcellular localisation and mobility. The production and use of the Lentiviral construct could not be achieved within the time constraints of this study.

#### **7.4 The effect of the FPLD mutation R482W on adipogenic potential**

In FPLD, fat loss may be due to disruption of the differentiation pathway; perhaps via disruption of the interaction between SREBP1 and R482W lamin A. Alternatively, mature adipocytes may be produced but cannot survive. In this study the adipogenic potential of FPLD patient MSCs carrying the R482W mutation and *Lmna* R482W MEFs were investigated.

PPAR $\gamma$  activators are standard additions to the adipogenic cocktail used to stimulate differentiation in MSCs. An adipogenic protocol was developed in this study to avoid direct activation of PPAR $\gamma$ . PPAR $\gamma$  is activated by SREBP1, and other factors, therefore its direct activation would mask the affect of any defective SREBP1 signalling. The

developed differentiation protocol was used for adipogenic conversion of FPLD patient MSCs and *Lmna* R482W MEFs.

Three MSC cell lines were cultured from bone marrow samples donated by FPLD patients. Two of these cell lines did not grow sufficiently to be tested for differentiation. A preliminary differentiation study with one FPLD MSC cell line was carried out. FPLD MSCs were almost completely unable to differentiate into adipocytes in the absence of the PPAR $\gamma$  activator Troglitazone, differentiation was rescued by the addition of Troglitazone suggesting that the R482W FPLD mutation inhibits differentiation of MSCs. However, the small sample size (one FPLD cell line) and huge variation among control cell lines meant that no conclusions about differentiation in FPLD cells could be made. To overcome variation between individuals a large number of control and FPLD samples would be needed, the rarity of this disorder coupled with the procedure required for bone marrow donation would hamper a future human study of this kind.

The adipogenic potential of *Lmna* R482W MEFs was investigated. *Lmna* R482W homozygous and heterozygous MEFs were investigated alongside WT MEF controls. Four cell lines were differentiated for each genotype. Homozygous and heterozygous MEFs were able to form adipocytes in the presence and absence of Troglitazone but at slightly lower efficiency than WT MEFs. Thus, SREBP1 dysfunction may reduce, but does not prevent adipogenesis in R482W MEFs. If time constraints had allowed, interesting information may have been gained by performing qPCR on RNA extracted from MEFs at different stages of adipogenesis to compare expression of SREBP1 and other genes in WT, heterozygous and homozygous cells.

## Bibliography

Aaronson, R.P., Blobel, G. (1975). Isolation of nuclear pore complexes in association with a lamina. *Proc Natl Acad Sci U S A*, **72**, (3), 1007-1011.

Aebi, U., Cohn.J., Buhle L, Gerace L. (1986) The nuclear lamina is a meshwork of intermediate-type filaments. *Nature.*, **323**, 560-564.

Agarwal, A.K., Fryns, J.P., Auchus, R.J. & Garg, A. (2003) Zinc metalloproteinase, ZMPSTE24, is mutated in mandibuloacral dysplasia. *Hum Mol Genet*, **12**, 1995-2001.

Agarwal, A.K., Garg, A. (2006) Genetic disorders of adipose tissue development, differentiation, and death. *Annu Rev Genomics Hum Genet.*, **7**, 175-199

Agarwal, A.K., Zhou, X.J., Hall, R.K., Nicholls, K., Bankier, A., Van Esch, H., Fryns, J.P. & Garg, A. (2006) Focal segmental glomerulosclerosis in patients with mandibuloacral dysplasia owing to ZMPSTE24 deficiency. *J Investig Med*, **54**, 208-213.

Allsopp, R.C., Vaziri, H., Patterson, C., Goldstein, S., Younglai, E.V., Futcher, A.B., Greider, C.W. & Harley, C.B. (1992) Telomere length predicts replicative capacity of human fibroblasts. *Proc Natl Acad Sci U S A*, **89**, 10114-10118.

Araújo-Vilar D, Lado-Abeal J, Palos-Paz F, Lattanzi G, Bandín MA, Bellido D, Domínguez-Gerpe L, Calvo C, Pérez O, Ramazanov A, Martínez-Sánchez N, Victoria B, Costa-Freitas AT. (2008) A novel phenotypic expression associated with a new mutation in LMNA gene, characterized by partial lipodystrophy, insulin resistance, aortic stenosis and hypertrophic cardiomyopathy. *Clin Endocrinol* **69**, 61-68, Epub.

Aubin, J.E. (2001) Regulation of osteoblast formation and function. *Rev Endocr Metab Disord*, **2**, 81-94.

Avram MM, Avram AS, James WD. (2007) Subcutaneous fat in normal and diseased states 3. Adipogenesis: from stem cell to fat cell. *J Am Acad Dermatol.*, **56**, (3), 472-492.

Baksh, D., Song, L., Tuan, R.S. (2004) Adult mesenchymal stem cells: characterization, differentiation, and application in cell and gene therapy. *J Cell Mol Med.*, **8**, (3), 301-316.

Banerjee, S..S, Feinberg, M.W., Watanabe, M., Gray, S., Haspel, R.L., Denking, D.J., Kawahara, R., Hauner, H., Jain, M.K. (2003) The Krüppel-like factor KLF2 inhibits peroxisome proliferator-activated receptor-gamma expression and adipogenesis. *J Biol Chem.*, **278**, (4), 2581-2584.

- Batchvarova, N., Wang, X.Z., Ron, D. (1995) Inhibition of adipogenesis by the stress-induced protein CHOP (Gadd153). *EMBO J.* **14**, 4654-4661.
- Beck, L.A., Hosick, T.J. & Sinensky, M. (1990) Isoprenylation is required for the processing of the lamin A precursor. *J Cell Biol*, **110**, 1489-1499.
- Bengochea-Alonso, M.T. & Ericsson, J. (2007) SREBP in signal transduction: cholesterol metabolism and beyond. *Curr Opin Cell Biol*, **19**, 215-222.
- Bengtsson, L. & Wilson, K.L. (2004) Multiple and surprising new functions for emerin, a nuclear membrane protein. *Curr Opin Cell Biol*, **16**, 73-79.
- Bennett, C.N., Ross, S.E., Longo, K.A., Bajnok, L., Hemati, N., Johnson, K.W., Harrison, S.D., MacDougald, O.A. (2002) Regulation of Wnt signaling during adipogenesis. *J Biol Chem.*, **277**, (34), 30998-31004.
- Bennett, C.N., Longo, K.A., Wright, W.S., Suva, L.J., Lane, T.F., Hankenson, K.D., MacDougald, O.A. (2005) Regulation of osteoblastogenesis and bone mass by Wnt10b. *Proc Natl Acad Sci U S A.*, **102**, (9), 3324-3329.
- Bergo, M.O., Gavino, B., Ross, J., Schmidt, W.K., Hong, C., Kendall, L.V., Mohr, A., Meta, M., Genant, H., Jiang, Y., Wisner, E.R., Van Bruggen, N., Carano, R.A., Michaelis, S., Griffey, S.M., Young, S.G. (2002) Zmpste24 deficiency in mice causes spontaneous bone fractures, muscle weakness, and a prelamin A processing defect. *Proc Natl Acad Sci U S A.*, **99**, (20), 13049-13054.
- Bione, S., Maestrini, E., Rivella, S., Mancini, M., Regis, S., Romeo, G., Toniolo, D. (1994). Identification of a novel X-linked gene responsible for Emery-Dreifuss muscular dystrophy. *Nat Genet.* **8**, 323-327.
- Boguslavsky, R.L., Stewart, C.L. & Worman, H.J. (2006) Nuclear lamin A inhibits adipocyte differentiation: implications for Dunnigan-type familial partial lipodystrophy. *Hum Mol Genet*, **15**, 653-663.
- Boheler, K.R. (2004) Functional markers and the "homogeneity" of human mesenchymal stem cells. *J Physiol*, **554**, 592.
- Bridger, J.M., Kill, I.R., O'Farrell, M., Hutchison, C.J. (1993). Internal lamin structures within G1 nuclei of human dermal fibroblasts. *J Cell Sci.* **104 (Pt 2)**, 297-306.
- Bridger, J.M. & Kill, I.R. (2004) Aging of Hutchinson-Gilford progeria syndrome fibroblasts is characterised by hyperproliferation and increased apoptosis. *Exp Gerontol*, **39**, 717-724.
- Brown, M.S. & Goldstein, J.L. (1997) The SREBP pathway: regulation of cholesterol metabolism by proteolysis of a membrane-bound transcription factor. *Cell*, **89**, 331-340.

Busch, A., Kiel, T., Heupel, W.M., Wehnert, M. & Hubner, S. (2009) Nuclear protein import is reduced in cells expressing nuclear envelopathy-causing lamin A mutants. *Exp Cell Res*, **315**, 2373-2385.

Cao, H. & Hegele, R.A. (2000) Nuclear lamin A/C R482Q mutation in canadian kindreds with Dunnigan-type familial partial lipodystrophy. *Hum Mol Genet*, **9**, 109-112.

Cao, H. & Hegele, R.A. (2003) LMNA is mutated in Hutchinson-Gilford progeria (MIM 176670) but not in Wiedemann-Rautenstrauch progeroid syndrome (MIM 264090). *J Hum Genet*, **48**, 271-274.

Cao, K., Capell, B.C., Erdos, M.R., Djabali, K. & Collins, F.S. (2007) A lamin A protein isoform overexpressed in Hutchinson-Gilford progeria syndrome interferes with mitosis in progeria and normal cells. *Proc Natl Acad Sci U S A*, **104**, 4949-4954.

Cao, Z., Umek, R.M., McKnight, S.L. (1991) Regulated expression of three C/EBP isoforms during adipose conversion of 3T3-L1 cells. *Genes Dev.*, **5**, (9), 1538-1552.

Capanni, C., Cenni, V., Mattioli, E., Sabatelli, P., Ognibene, A., Columbaro, M., Parnaik, V.K., Wehnert, M., Maraldi, N.M., Squarzoni, S., Lattanzi, G. (2003). Failure of lamin A/C to functionally assemble in R482L mutated familial partial lipodystrophy fibroblasts: altered intermolecular interaction with emerin and implications for gene transcription. *Exp Cell Res*. **291**, 122-134.

Capanni C, M.E., Columbaro M, Lucarelli E, Parnaik VK, Novelli G, Wehnert M, Cenni V, Maraldi NM, Squarzoni S, Lattanzi G. (2005) Altered pre-lamin A processing is a common mechanism leading to lipodystrophy. *Hum Mol Genet.*, **14**, 1489-1502.

Capanni, C., Del Coco, R., Mattioli, E., Camozzi, D., Columbaro, M., Schena, E., Merlini, L., Squarzoni, S., Maraldi, N.M. & Lattanzi, G. (2009) Emerin-prelamin A interplay in human fibroblasts. *Biol Cell*, **101**, 541-554.

Capell, B.C., Erdos, M., Madigan JP, Fiordalisi JJ, Varga R, Conneely KN, Gordon LB, Der CJ, Cox AD, Collins FS. (2005) Inhibiting farnesylation of progerin prevents the characteristic nuclear blebbing of Hutchinson-Gilford progeria syndrome. *Proc Natl Acad Sci U S A.*, **102**, 12879-12884.

Capell, B.C., Collins, F.S. (2006). Human laminopathies: nuclei gone genetically awry. *Nat Rev Genet*. **7**, 940-952.

Caplan, A.I. (1991) Mesenchymal stem cells. *J Orthop Res.*, **9**, (5), 641-650.

Caron, M., Auclair, M., Sterlingot, H., Kornprobst, M. & Capeau, J. (2003) Some HIV protease inhibitors alter lamin A/C maturation and stability, SREBP-1 nuclear localization and adipocyte differentiation. *Aids*, **17**, 2437-2444.

Chellappan, S.P., Hiebert, S., Mudryj, M., Horowitz, J.M., Nevins, J.R. (1991) The E2F transcription factor is a cellular target for the RB protein. *Cell.*, **65**, (6), 1053-1061.

Chen, P.L., Riley, D.J., Chen, Y. & Lee, W.H. (1996) Retinoblastoma protein positively regulates terminal adipocyte differentiation through direct interaction with C/EBPs. *Genes Dev*, **10**, 2794-2804.

Chen, Z., Torrens, J.I., Anand, A., Spiegelman, B.M., Friedman, J.M. (2005) Krox20 stimulates adipogenesis via C/EBP $\beta$ -dependent and -independent mechanisms. *Cell Metab.*, **1**, (2), 93-106.

Chi, Y.H., Chen, Z.J. & Jeang, K.T. (2009) The nuclear envelopathies and human diseases. *J Biomed Sci*, **16**, 96.

Christy, R.J., Kaestner, K., Geiman, D.E., Lane, M.D. (1991) CC AAT/enhancer binding protein gene promoter: binding of nuclear factors during differentiation of 3T3-L1 preadipocytes. *Proc Natl Acad Sci U S A.*, **88**, (6), 2593-2597.

Columbaro, M., Mattioli, E., Schena, E., Capanni, C., Cenni, V., Levy, N., Navarro, C.L., Del Coco, R., Squarzone, S., Camozzi, D., Hutchison, C.J., Wehnert, M., Lattanzi, G. (2010) Prelamin A processing and functional effects in restrictive dermopathy. *Cell Cycle*, **9**, (23), 4766-4768.

Crisp, M., Liu, Q., Roux, K., Rattner, J.B., Shanahan, C., Burke, B., Stahl, P.D. & Hodzic, D. (2006) Coupling of the nucleus and cytoplasm: role of the LINC complex. *J Cell Biol*, **172**, 41-53.

Croft, J.A., Bridger, J.M., Boyle S., Perry, P., Teague, P., Bickmore, W.A. (1999). Differences in the localization and morphology of chromosomes in the human nucleus. *J Cell Biol*. **145**, 1119-1131.

Csaki C, Matis U, Mobasheri A, Ye H, Shakibaei M. (2007) Chondrogenesis, osteogenesis and adipogenesis of canine mesenchymal stem cells: a biochemical, morphological and ultrastructural study. *Histochem Cell Biol.*, **128**, (6), 507-520.

Csoka, A.B., Cao, H., Sammak, P.J., Constantinescu, D., Schatten, G.P. & Hegele, R.A. (2004) Novel lamin A/C gene (LMNA) mutations in atypical progeroid syndromes. *J Med Genet*, **41**, 304-308.

Csoka, A.B., English, S.B., Simkevich, C.P., Ginzinger, D.G., Butte, A.J., Schatten, G.P., Rothman, F.G. & Sedivy, J.M. (2004) Genome-scale expression profiling of Hutchinson-Gilford progeria syndrome reveals widespread transcriptional misregulation leading to mesodermal/mesenchymal defects and accelerated atherosclerosis. *Aging Cell*, **3**, 235-243.

- Dahl, K.N., Scaffidi, P., Islam, M.F., Yodh, A.G., Wilson, K.L. & Misteli, T. (2006) Distinct structural and mechanical properties of the nuclear lamina in Hutchinson-Gilford progeria syndrome. *Proc Natl Acad Sci U S A*, **103**, 10271-10276.
- Davies, B.S., Fong, L.G., Yang, S.H., Coffinier, C. & Young, S.G. (2009) The posttranslational processing of pre lamin A and disease. *Annu Rev Genomics Hum Genet*, **10**, 153-174.
- De Sandre-Giovannoli, A., Bernard, R., Cau P, Navarro C, Amiel J, Boccaccio I, Lyonnet S, Stewart CL, Munnich A, Le Merrer M, Lévy N. (2003) Lamin a truncation in Hutchinson-Gilford progeria. *Science*, **300**, 2055.
- Dechat, T., Vlcek, S. & Foisner, R. (2000) Review: lamina-associated polypeptide 2 isoforms and related proteins in cell cycle-dependent nuclear structure dynamics. *J Struct Biol*, **129**, 335-345.
- Dechat, T., Shimi, T., Adam, S.A., Rusinol, A.E., Andres, D.A., Spielmann, H.P., Sinensky, M.S. & Goldman, R.D. (2007) A iterations in mitosis and cell cycle progression caused by a mutant lamin A known to accelerate human aging. *Proc Natl Acad Sci U S A*, **104**, 4955-4960.
- Dechat, T., Pflieger, K., Sengupta, K., Shimi, T., Shumaker, D.K., Solimando, L. & Goldman, R.D. (2008) Nuclear lamins: major factors in the structural organization and function of the nucleus and chromatin. *Genes Dev*, **22**, 832-853.
- Delbarre, E., Tramier, M., Coppey-Moisan, M., Gaillard, C., Courv alin, J.C. & Buendia, B. (2006) The truncated prelamin A in Hutchinson-Gilford progeria syndrome alters segregation of A-type and B-type lamin homopolymers. *Hum Mol Genet*, **15**, 1113-1122.
- Denecke, J., Brune, T., Feldhaus, T., Robenek, H., Kranz, C., Auchus, R.J., Agarwal, A.K. & Marquardt, T. (2006) A homozygous ZMPSTE24 null mutation in combination with a heterozygous mutation in the LMNA gene causes Hutchinson-Gilford progeria syndrome (HGPS): insights into the pathophysiology of HGPS. *Hum Mutat*, **27**, 524-531.
- Dhe-Paganon, S., Werner, E.D., Chi, Y.I. & Shoelson, S.E. (2002) Structure of the globular tail of nuclear lamin. *J Biol Chem*, **277**, 17381-17384.
- Dominici, M., Le Blanc, K., Mueller, I., Slaper-Cortenbach, I., Marini, F., Krause, D., Deans, R., Keating, A., Prockop, D. J., Horwitz, E. (2006) Minimal criteria for defining multipotent mesenchymal stromal cells. The International Society for Cellular Therapy position statement. *Cytotherapy*, **8**, (4), 315-317.
- Dorner, D., Vlcek, S., Foeger, N., Gajewski, A., Makolm, C., Gotzmann, J., Hutchison, C.J. & Foisner, R. (2006) Lamina-associated polypeptide 2alpha regulates cell cycle

progression and differentiation via the retinoblastoma-E2F pathway. *J Cell Biol*, **173**, 83-93.

Dreuillet, C., Tillit, J., Kress, M., Ernoult-Lange, M. (2002). In vivo and in vitro interaction between human transcription factor MOK2 and nuclear lamin A/C. *Nucleic Acids Res.* **30**, 4634.

Dyson, N. (1998) The regulation of E2F by pRB-family proteins. *Genes Dev*, **12**, 2245-2262.

Eberle, D., Hegarty, B., Bossard, P., Ferre, P. & Foufelle, F. (2004) SREBP transcription factors: master regulators of lipid homeostasis. *Biochimie*, **86**, 839-848.

Ellis, J.A., Craxton, M., Yates, J.R. & Kendrick-Jones, J. (1998) Aberrant intracellular targeting and cell cycle-dependent phosphorylation of emerin contribute to the Emery-Dreifuss muscular dystrophy phenotype. *J Cell Sci*, **111** ( Pt 6), 781-792.

Eriksson, M., Brown, W., Gordon LB, Glynn MW, Singer J, Scott L, Erdos MR, Robbins CM, Moses TY, Berglund P, Dutra A, Pak E, Durkin S, Csoka AB, Boehnke M, Glover TW, Collins FS. (2003) Recurrent de novo point mutations in lamin A cause Hutchinson-Gilford progeria syndrome. *Nature.*, **432**, 293-298.

Fajas, L., Auboeuf, D., Raspé, E., Schoonjans, K., Lefebvre, A.M., Saladin, R., Najib, J., Laville, M., Fruchart, J.C., Deeb, S., Vidal-Puig, A., Flier, J., Briggs, M.R., Staels, B., Vidal, I.H., Auwerx, J. (1997) The organization, promoter analysis, and expression of the human PPARgamma gene. *J Biol Chem.*, **272**, (30), 18779-18789.

Fajas, L., Schoonjans, K., Gelman, L., Kim, J.B., Najib, J., Martin, G., Fruchart, J.C., Briggs, M., Spiegelman, B.M. & Auwerx, J. (1999) Regulation of peroxisome proliferator-activated receptor gamma expression by adipocyte differentiation and determination factor 1/sterol regulatory element binding protein 1: implications for adipocyte differentiation and metabolism. *Mol Cell Biol*, **19**, 5495-5503.

Fajas, L., Landsberg, R.L., Huss-Garcia, Y., Sardet, C., Lees, J.A., Auwerx, J. (2002) E2Fs regulate adipocyte differentiation. *Dev Cell.*, **3**, (1), 39-49.

Fanti, L. & Pimpinelli, S. (2008) HP1: a functionally multifaceted protein. *Curr Opin Genet Dev*, **18**, 169-174.

Farmer, S.R. (2006) Transcriptional control of adipocyte formation. *Cell Metab.*, **4**, (4), 263-273.

Farnsworth, C.C., Wolda, S.L., Gelb, M.H., Glomset, J.A. (1989) Human lamin B contains a farnesylated cysteine residue. *J Biol Chem*, **264**, (34), 20422-20429.

- Ferris, W.F., Crowther, N.J. (2011) Once fat was fat and that was that: our changing perspectives on adipose tissue. *Cardiovasc J Afr.* **22**, (3), 147-154.
- Fidzianska, A., Hausmanowa-Petrusewicz, I. (2003) Architectural abnormalities in muscle nuclei. Ultrastructural differences between X-linked and autosomal dominant forms of EDMD. *J Neurol Sci*, **210**, 47-51.
- Fisher, D.Z., Chaudhary, N. & Blobel, G. (1986) cDNA sequencing of nuclear lamins A and C reveals primary and secondary structural homology to intermediate filament proteins. *Proc Natl Acad Sci U S A*, **83**, 6450-6454.
- Foisner, R., Gerace, L. (1993). Integral membrane proteins of the nuclear envelope interact with lamins and chromosomes, and binding is modulated by mitotic phosphorylation. *Cell*. **73**, 1267-1279.
- Fong, L.G., Frost, D., Meta, M, Qiao, X., Yang, S.H., Coffinier, C., Young, S.G. (2006) A protein farnesyltransferase inhibitor ameliorates disease in a mouse model of progeria. *Science*, **311**, (5767), 1621-1623.
- Fong, L.G., Ng, J.K., Lammerding, J., Vickers, T.A., Meta, M., Cote, N., Gavino, B., Qiao, X., Chang, S.Y., Young, S.R., Yang, S.H., Stewart, C.L., Lee, R.T., Bennett, C.F., Bergo, M.O. & Young, S.G. (2006) Prelamin A and lamin A appear to be dispensable in the nuclear lamina. *J Clin Invest*, **116**, 743-752.
- Forman, B.M., Tontonoz, P., Chen, J., Brun, R.P., Spiegelman, B.M., Evans, R.M. (1995) 15-Deoxy-delta 12, 14-prostaglandin J2 is a ligand for the adipocyte determination factor PPAR gamma. *Cell*. **83**, (5), 803-812.
- Fraser. P., Bickmore, W.A. (2007). Nuclear organization of the genome and the potential for gene regulation. *Nature*. **447**, 413-417.
- Freytag, S.O., Paielli, D.L., Gilbert, J.D. (1994) Ectopic expression of the CCAAT/enhancer-binding protein alpha promotes the adipogenic program in a variety of mouse fibroblastic cells. *Genes Dev.*, **8**, (14), 1654-1663.
- Friend, S.H., Bernards, R., Rogelj, S., Weinberg, R.A., Rapaport, J.M., Albert, D.M., Dryja, T.P. (1986) A human DNA segment with properties of the gene that predisposes to retinoblastoma and osteosarcoma. *Nature*, **323**, (6089), 643-646.
- Fukuchi, K., Katsuya, T., Sugimoto, K., Kuremura, M., Kim, H.D., Li, L. & Ogihara, T. (2004) LMNA mutation in a 45 year old Japanese subject with Hutchinson-Gilford progeria syndrome. *J Med Genet*, **41**, e67.
- Furukawa, K., Hotta, Y. (1993). cDNA cloning of a germ cell specific lamin B3 from mouse spermatocytes and analysis of its function by ectopic expression in somatic cells. *EMBO J*. **12**, 97-106.

Furukawa, K., Inagaki, H., Hotta, Y. (1994). Identification and cloning of an mRNA coding for a germ cell-specific A-type lamin in mice. *Exp Cell Res.* **212**, (2), 426-430.

Furukawa, K. (1999) LAP2 binding protein 1 (L2BP1/BAF) is a candidate mediator of LAP2-chromatin interaction. *J Cell Sci.*, **112**, ( Pt 15):2485-92

Garavelli, L., D'Apice, M.R., Rivieri, F., Bertoli, M., Wischmeijer, A., Gelmini, C., De Nigris, V., Albertini, E., Rosato, S., Viridis, R., Bacchini, E., Dal Zotto, R., Banchini, G., Iughetti, L., Bernasconi, S., Superti-Furga, A., Novelli, G. (2009) Mandibuloacral dysplasia type A in childhood. *Am J Med Genet*, **149A**, 2258-2264.

Garg, A. (2000) Lipodystrophies. *Am J Med.* **108**, 143-152.

Garg, A., Vinaitheerthan, M., Weatherall PT, Bowcock AM. (2001) Phenotypic heterogeneity in patients with familial partial lipodystrophy (dunnigan variety) related to the site of missense mutations in lamin a/c gene. *J Clin Endocrinol Metab*, **86**, 59-65

Garg, A., Speckman, R.A., Bowcock, A.M. (2002) Multisystem dystrophy syndrome due to novel missense mutations in the amino-terminal head and alpha-helical rod domains of the lamin A/C gene. *Am J Med.* **112**, 549-55.

Garg, A., Cogulu, O., Ozkinay, F., Onay, H., Agarwal, A.K. (2005). A novel homozygous Ala529Val LMNA mutation in Turkish patients with mandibuloacral dysplasia. *J Clin Endocrinol Metab.* **90**, 5259-5264.

Garg, A., Agarwal, A. (2006) Lipodystrophies: disorders of a dipose tissue biology. *Biochim Biophys Acta*, **1791**, 507-513.

Gerace, L., Blum, A., Blobel, G. (1978) Immunocytochemical localization of the major polypeptides of the pore complex-lamina fraction. Interphase and mitotic distribution. *J. Cell Biol.* **79**, (2), 546-566.

Gilchrist, S., Gilbert, N., Perry, P., Ostlund, C., Worman, H.J. & Bickmore, W.A. (2004) Altered protein dynamics of disease-associated lamin A mutants. *BMC Cell Biol*, **5**, 46.

Glynn, M.W. & Glover, T.W. (2005) Incomplete processing of mutant lamin A in Hutchinson-Gilford progeria leads to nuclear abnormalities, which are reversed by farnesyltransferase inhibition. *Hum Mol Genet*, **14**, 2959-2969.

Goldberg MW, H. I., Hutchison CJ, Stick R. (2008). Filaments made from A- and B-type lamins differ in structure and organization. *J Cell Sci.* **121** (pt 2), 215-225.

Goldman, R.D., Shumaker, D., Erdos MR, Eriksson M, Goldman AE, Gordon LB, Gruenbaum Y, Khuon S, Mendez M, Varga R, Collins FS. (2004) Accumulation of mutant lamin A causes progressive changes in nuclear architecture in Hutchinson-Gilford progeria syndrome. *Proc Natl Acad Sci U S A.*, **101**, 8963-8968.

Goodrich, D.W., Wang, N.P., Qian, Y.W., Lee, E.Y., Lee, W.H. (1991) The retinoblastoma gene product regulates progression through the G1 phase of the cell cycle. *Cell.*, **67**, (2), 293-302.

Goodsell, D.S. (2003) The molecular perspective: protein farnesyltransferase. *Oncologist*, **8**, (6), 597-598.

Gordon, L.B., Harling-Berg, C.J., Rothman, F.G. (2008) Highlights of the 2007 Progeria Research Foundation Scientific Workshop: Progress in translational science. *J Gerontol A Biol Sci Med Sci*, **63**, 777-87.

Gorlin, R.J., Cervenka, J., Moller, K., Horrobin, M., Witkop, J. (1975) Rieger anomaly and growth retardation (The S-H-O-R-T Syndrome). *Birth Defects* **1**, 46-48.

Goto, T., Nagai, H., Egawa, K., Kim, Y.I., Kato, S., Taimatsu, A., Sakamoto, T., Ebisu, S., Hohsaka, T., Miyagawa, H., Murakami, S., Takahashi, N., Kawada, T. (2011) Farnesyl pyrophosphate regulates adipocyte functions as an endogenous PPAR $\gamma$  agonist. *Biochem J.*, **438**, (1), 111-119.

Gray, S., Feinberg, M.W., Hull, S., Kuo, C.T., Watanabe, M., Sen-Banerjee, S., DePina, A., Haspel, R., Jain, M.K. (2002) The Krüppel-like factor KLF15 regulates the insulin-sensitive glucose transporter GLUT4. *J Biol Chem.* **277**, (37), 34322-34328.

Green, H., Kehinde, O. (1975) An established preadipose cell line and its differentiation in culture. II. Factors affecting the adipose conversion. *Cell*, **5**, 19-27.

Green, H., Kehinde, O. (1976) Spontaneous heritable changes leading to increased adipose conversion in 3T3 cells. *Cell*, **7**, 105-113.

Halaschek-Wiener, J. & Brooks-Wilson, A. (2007) Progeria of stem cells: stem cell exhaustion in Hutchinson-Gilford progeria syndrome. *J Gerontol A Biol Sci Med Sci*, **62**, 3-8.

Haque, F., Lloyd, D., Smallwood DT, Dent CL, Shanahan CM, Fry AM, Trembath RC, Shackleton S. (2006) SUN1 interacts with nuclear lamin A and cytoplasmic nesprins to provide a physical connection between the nuclear lamina and the cytoskeleton. *Mol Cell Biol.*, **26**, 3738-3751.

Haque, F., Mazzeo, D., Patel JT, Smallwood DT, Ellis JA, Shanahan CM, Shackleton S. (2010) Mammalian SUN protein interaction networks at the inner nuclear membrane and their role in laminopathy disease processes. *J Biol Chem.*, **285**, 3487-3498.

- Hegele, R.A., Cao, H., Harris SB, Zinman B, Hanley AJ, Anderson CM. (2000) Genetic variation in LMNA modulates plasma leptin and indices of obesity in aboriginal Canadians. *Physiol Genomics*, **3**, 39-44.
- Heitlinger, E., Peter, M., Lustig, A., Villiger, W., Nigg, E.A., Aebi, U. (1992). The role of the head and tail domain in lamin structure and assembly: analysis of bacterially expressed chicken lamin A and truncated B2 lamins. *J Struct Biol.* **108**, (1), 74-89.
- Hellemans, J., Preobrazhenska, O., Willaert, A., Debeer, P., Verdonk, P.C., Costa, T., Janssens, K., Menten, B., Van Roy, N., Vermeulen, S.J., Savarirayan, R., Van Hul, W., Vanhoenacker, F., Huylebroeck, D., De Paepe, A., Naeyaert, J.M., Vandesompele, J., Speleman, F., Verschueren, K., Coucke, P.J., Mortier, G.R. (2004). Loss-of-function mutations in LEMD3 result in osteopoikilosis, Buschke-Ollendorff syndrome and melorheostosis. *Nat Genet.* **36**, 1213-1218.
- Hennekam, R.C. (2006) Hutchinson-Gilford progeria syndrome: review of the phenotype. *Am J Med Genet A*, **140**, 2603-2624.
- Hetzer, M.W. (2010). The nuclear envelope. *Cold Spring Harb Perspect Biol.* **2**, (3), a000539.
- Hoger, T.H., Krohne, G. & Franke, W.W. (1988) Amino acid sequence and molecular characterization of murine lamin B as deduced from cDNA clones. *Eur J Cell Biol*, **47**, 283-290.
- Hoger, T.H., Zatloukal, K., Waizenegger, I. & Krohne, G. (1990) Characterization of a second highly conserved B-type lamin present in cells previously thought to contain only a single B-type lamin. *Chromosoma*, **100**, 67-69.
- Holaska, J.M. & Wilson, K.L. (2007) An emerin "proteome": purification of distinct emerin-containing complexes from HeLa cells suggests molecular basis for diverse roles including gene regulation, mRNA splicing, signaling, mechanosensing, and nuclear architecture. *Biochemistry*, **46**, 8897-8908.
- Horton, J.D., Shimomura, I., Brown, M. S., Hammer, R.E., Goldstein, J. L., Shimano, H. (1998) Activation of cholesterol synthesis in preference to fatty acid synthesis in liver and adipose tissue of transgenic mice overproducing sterol regulatory element-binding protein-2. *J. Clin. Investig.* **101**, 2331-2339
- Horton, J.D., Shimomura, I., Ikemoto, S., Bashmakov, Y., Hammer, R.E. (2003) Overexpression of sterol regulatory element-binding protein-1a in mouse adipose tissue produces adipocyte hypertrophy, increased fatty acid secretion, and fatty liver. *J Biol Chem.* **278**, (38), 36652-36660.
- Hua, H., Wu, J., Goldstein, J.L., Brown, M.S., Hobbs, H. (1994) Structure of the human gene encoding sterol regulatory element binding protein-1 (SREBF1) and localisation of SREBF1 and SREBF2 to chromosomes 17p11.2 and 22q13. *Genomics* **25**, 667-673.

Huang, H.J., Yee, J.K., Shew, J.Y., Chen, P.L., Bookstein, R., Friedmann, T., Lee, E.Y., Lee, W.H. (1988). Suppression of the neoplastic phenotype by replacement of the RB gene in human cancer cells. *Science*. **242**, 1563-1566.

Huang, S., Risques, R.A., Martin, G.M., Rabinovitch, P.S. & Oshima, J. (2008) Accelerated telomere shortening and replicative senescence in human fibroblasts overexpressing mutant and wild-type lamin A. *Exp Cell Res*, **314**, 82-91.

Hübner, S., Eam, J., Hübner A, Jans DA. (2006) Laminopathy-inducing lamin A mutants can induce redistribution of lamin binding proteins into nuclear aggregates. *Exp Cell Res.*, **312**, 171-183.

Hübner, S., Eam, J., Wagstaff KM, Jans DA. (2006) Quantitative analysis of localization and nuclear aggregate formation induced by GFP-lamin A mutant proteins in living HeLa cells. *J Cell Biochem.*, **98**, 810-826.

Huh, M.S., Parker, M.H., Scimè, A., Parks, R., Rudnicki, M.A. (2004). Rb is required for progression through myogenic differentiation but not maintenance of terminal differentiation. *J Cell Biol.* **166**, 865-876.

Hutchison, C.J., Alvarez-Reyes, M., Vaughan, O.A. (2001). Lamins in disease: why do ubiquitously expressed nuclear envelope proteins give rise to tissue-specific disease phenotypes? *J Cell Sci.* **114 (Pt1)**, 9-19.

Ijpenberg, A., Jeannin, E., Wahli, W., Desvergne, B. (1997) Polarity and specific sequence requirements of peroxisome proliferator-activated receptor (PPAR)/retinoid X receptor heterodimer binding to DNA. A functional analysis of the malic enzyme gene PPAR response element. *J Biol Chem.*, **272**, (32), 20108-20117.

Inoue, H., Nojima, H., Okayama, H. (1990) High efficiency transformation of *Escherichia coli* with plasmids. *Gene*, **96**, (1), 23-28.

Jagadeesh, S., Bhat, L., Suresh, I., Muralidhar, S.L. (2009) Prenatal diagnosis of restrictive dermopathy. *Indian Pediatr.*, **46**, (4), 349-351.

Janderová, L., McNeil, M., Murrell, A.N., Mynatt, R.L., Smith, S.R. (2003) Human mesenchymal stem cells as an in vitro model for human adipogenesis. *Obes Res.* **11**, 65-74.

Johnson, B.R., Nitta, R.T., Frock, R.L., Mounkes, L., Barbie, D.A., Stewart, C.L., Harlow, E. & Kennedy, B.K. (2004) A-type lamins regulate retinoblastoma protein function by promoting subnuclear localization and preventing proteasomal degradation. *Proc Natl Acad Sci U S A*, **101**, 9677-9682.

Kang, S., Bennett, C.N., Gerin, I., Rapp, L.A., Hankenson, K.D., Macdougald, O.A. (2007) Wnt signaling stimulates osteoblastogenesis of mesenchymal precursors by suppressing CCAAT/enhancer-binding protein alpha and peroxisome proliferator-activated receptor gamma. *J Biol Chem.*, **282**, (19), 14515-14524.

Kawamura, Y., Tanaka, Y., Kawamori, R., Maeda, S. (2005) Overexpression of Kruppel-like factor 7 regulates adipocytokine gene expressions in human adipocytes and inhibits glucose-induced insulin secretion in pancreatic beta-cell line. *Mol Endocrinol.* **20**, (4), 844-856.

Kemp, K.C., Hows, J. & Donaldson, C. (2005) Bone marrow-derived mesenchymal stem cells. *Leuk Lymphoma*, **46**, 1531-1544.

Kennell, J.A. & MacDougald, O.A. (2005) Wnt signaling inhibits adipogenesis through beta-catenin-dependent and -independent mechanisms. *J Biol Chem*, **280**, 24004-24010.

Kieran, M.W., Gordon, L. & Kleinman, M. (2007) New approaches to progeria. *Pediatrics*, **120**, 834-841.

Kim, J.B. & Spiegelman, B.M. (1996) ADD1/SREBP1 promotes adipocyte differentiation and gene expression linked to fatty acid metabolism. *Genes Dev*, **10**, 1096-1107.

Kim, J.B., Wright, H.M., Wright, M. & Spiegelman, B.M. (1998) ADD1/SREBP1 activates PPARgamma through the production of endogenous ligand. *Proc Natl Acad Sci U S A*, **95**, 4333-4337.

Kirschner, J., Brune, T., Wehnert, M., Denecke, J., Wasner, C., Feuer, A., Marquardt, T., Ketelsen, U.P., Wieacker, P., Bonnemann, C.G. & Korinthenberg, R. (2005) p.S143F mutation in lamin A/C: a new phenotype combining myopathy and progeria. *Ann Neurol*, **57**, 148-151.

Kiseleva, E., Goldberg, M., Cronshaw J, Allen TD (2000) The nuclear pore complex: structure, function, and dynamics. *Critical reviews in eukaryotic gene expression*, **10**, 101-112.

Knudson, A.G. Jr. (1971) Mutation and cancer: statistical study of retinoblastoma. *Proc Natl Acad Sci U S A.*, **68**, (4), 820-823.

Komiya, Y., Habas, R. (2008) Wnt signal transduction pathways. *Organogenesis*, **4**, (2), 68-75.

Konstantinopolous, P.A., Papavassiliou, A.G (2007) Multilevel modulation of the mevalonate and protein-prenylation circuitries as a novel strategy for anticancer therapy. *Trends Pharmacol Sci*, **28**, 6-13

Koutnikova, H., Cock, T.A., Watanabe, M., Houten, S.M., Champy, M.F., Dierich, A., Auwerx, J. (2003) Compensation by the muscle limits the metabolic consequences of lipodystrophy in PPAR gamma hypomorphic mice. *Proc Natl Acad Sci U S A.*, **100**, (24), 14457-14462.

Krimm, I., Ostlund, C., Gilquin, B., Couprie, J., Hossenlopp, P., Mornon, J.P., Bonne, G. (2002). The Ig-like structure of the C-terminal domain of lamin A/C, mutated in muscular dystrophies, cardiomyopathy, and partial lipodystrophy. *Structure* **10**, 811-823.

Lammerding, J., Schulze, P.C., Takahashi, T., Kozlov, S., Sullivan, T., Kamm, R.D., Stewart, C.L., Lee, R.T. (2004). Lamin A/C deficiency causes defective nuclear mechanics and mechanotransduction. *J Clin Invest.* **113**, 370-378.

Lange, A., Mills, R.E., Lange, C.J., Stewart, M., Devine, S.E., Corbett, A.H. (2007). Classical nuclear localization signals: definition, function, and interaction with importin alpha. *J Biol Chem.* **282**, (8), 5101-5105.

Lanktree, M., Cao, H., Rabkin, S.W., Hanna, A., Hegele, R.A. (2007) Novel LMNA mutations seen in patients with familial partial lipodystrophy subtype 2 (FPLD2; MIM 151660). *Clin Genet.* **71**, 183-186.

Lattanzi, G., Columbaro, M., Mattioli, E., Cenni, V., Camozzi, D., Wehnert, M., Santi, S., Riccio, M., Del Coco, R., Maraldi, N.M., Squarzoni, S., Foisner, R. & Capanni, C. (2007) Pre-Lamin A processing is linked to heterochromatin organization. *J Cell Biochem.* **102**, 1149-1159.

Lehmann, J.M., Moore, L.B., Smith-Oliver, T.A., Wilkison, W.O., Willson, T.M., Kliewer, S.A. (1995) An antidiabetic thiazolidinedione is a high affinity ligand for peroxisome proliferator-activated receptor gamma (PPAR gamma). *J Biol Chem.*, **270**, (22), 12953-12956.

Leiden Open (source) Variation Database (LOVD)  
[http://www.dmd.nl/nmdb/home.php?select\\_db=LMNA](http://www.dmd.nl/nmdb/home.php?select_db=LMNA)

Leung, G.K., Schmidt, W.K., Bergo, M.O., Gavino, B., Wong, D.H., Tam, A., Ashby, M.N., Michaelis, S., Young, S.G. (2001) Biochemical studies of Zmpste24-deficient mice. *J Biol Chem.*, **276**, (31), 29051-29058.

Li, D., Yea, S., Li, S., Chen, Z., Narla, G., Banck, M., Laborda, J., Tan, S., Friedman, J.M., Friedman, S.L., Walsh, M.J. (2005) Krüppel-like factor-6 promotes preadipocyte differentiation through histone deacetylase 3-dependent repression of D LK1. *J Biol Chem.*, **280**, (29), 26941-26952.

Liang, L., Zhang, H. & Gu, X. (2009) Homozygous LMNA mutation R527C in atypical Hutchinson-Gilford progeria syndrome: evidence for autosomal recessive inheritance. *Acta Paediatr.* **98**, 1365-1368.

- Lin, F., Blake, D.L., Callebaut, I., Skerjanc, I.S., Holmer, L., McBurney, M.W., Paulin-Levasseur, M., Worman, H.J. (2000). MAN1, an inner nuclear membrane protein that shares the LEM domain with lamina-associated polypeptide 2 and emerin. *J Biol Chem.* **275**, 4840-4847.
- Lin, H.K., Bergmann, S., Pandolfi, P.P. (2004). Cytoplasmic PML function in TGF-beta signalling. *Nature.* **431**, 205-211.
- Liu, J., Lee, K.K., Segura-Totten, M., Neufeld, E., Wilson, K.L., Gruenbaum, Y. (2003). MAN1 and emerin have overlapping function(s) essential for c chromosome segregation and cell division in *Caenorhabditis elegans*. *Proc Natl Acad Sci U S A.* **100**, 4598-4603.
- Liu, B., Wang, J., Chan, K.M., Tjia, W.M., Deng, W., Guan, X., Huang, J.D., Li, K.M., Chau, P.Y., Chen, D.J., Pei, D., Pendas, A.M., Cadinanos, J., Lopez-Otin, C., Tse, H.F., Hutchison, C., Chen, J., Cao, Y., Cheah, K.S., Tryggvason, K. & Zhou, Z. (2005) Genomic instability in laminopathy-based premature aging. *Nat Med*, **11**, 780-785.
- Liu, Y., Rusinol, A., Sinensky, M., Wang, Y. & Zou, Y. (2006) DNA damage responses in progeroid syndromes arise from defective maturation of prelamin A. *J Cell Sci*, **119**, 4644-4649.
- Lloyd, D.J., Trembath, R.C. & Shackleton, S. (2002) A novel interaction between lamin A and SREBP1: implications for partial lipodystrophy and other laminopathies. *Hum Mol Genet*, **11**, 769-777.
- Lowe, C.E., O'Rahilly, S., Rochford, J.J. (2011) Adipogenesis at a glance. *J Cell Sci.* **124**, (16), 2681-2686.
- Lutz, R.J., Trujillo, M.A., Denham, K.S., Wenger, L. & Sinensky, M. (1992) Nucleoplasmic localization of prelamin A: implications for prenylation-dependent lamin A assembly into the nuclear lamina. *Proc Natl Acad Sci U S A*, **89**, 3000-3004.
- MacDougald, O.A., Lane, M. (1995) Adipocyte differentiation. When precursors are also regulators. *Curr Biol.* **5**, 618-621.
- Machiels, B.M., Zorenc, A.H., Ender, J.M., Kuijpers, H.J., van Eys, G.J., Ramaekers, F.C., Broers, J.L. (1996). An alternative splicing product of the lamin A/C gene lacks exon 10. *J Biol Chem.* **271**, (16), 9249-9253.
- Mansharamani, M., Wilson, K.L. (2005). Direct binding of nuclear membrane protein MAN1 to emerin in vitro and two modes of binding to barrier-to-autointegration factor. *J Biol Chem.* **280**, 13863-13870.

Maraldi, N.M., Capanni, C., Lattanzi, G., Camozzi, D., Facchini, A., Manzoli, F.A. (2008) SREBP1 interaction with prelamin A forms: a pathogenic mechanism for lipodystrophic laminopathies. *Adv Enzyme Regul.* **48**, 209-223.

Markiewicz, E., Dechat, T., Foisner, R., Quinlan, R.A. & Hutchison, C.J. (2002) Lamin A/C binding protein LAP2alpha is required for nuclear anchorage of retinoblastoma protein. *Mol Biol Cell*, **13**, 4401-4413.

Markiewicz, E., Tilgner, K., Barker, N., van de Wetering, M., Clevers, H., Dorobek, M., Hausmanowa-Petrusewicz, I., Ramaekers, F.C., Broers, J.L., Blankesteyn, W.M., Salpingidou, G., Wilson, R.G., Ellis, J.A. & Hutchison, C.J. (2006) The inner nuclear membrane protein emerin regulates beta-catenin activity by restricting its accumulation in the nucleus. *Embo J*, **25**, 3275-3285.

Martins, S., Eikvar, S., Furukawa, K., Collas, P. (2003). HA95 and LAP2 beta mediate a novel chromatin-nuclear envelope interaction implicated in initiation of DNA replication. *J Cell Biol.* **160**, 177-188.

Mattout-Drubezki, A., Gruenbaum, Y. (2003). Dynamic interactions of nuclear lamina proteins with chromatin and transcriptional machinery. *Cell Mol Life Sci.* **60**, 2053-2063.

Mazereeuw-Hautier, J., Wilson, L., Mohammed S, Smallwood D, Shackleton S, Atherton DJ, Harper JI. (2007) Hutchinson-Gilford progeria syndrome: clinical findings in three patients carrying the G608G mutation in LMNA and review of the literature. *Br J Dermatol.*, **156**, 1308-1314.

McGregor RA, Choi MS. (2011) microRNAs in the regulation of adipogenesis and obesity. *Curr Mol Med.* **11**, 304-316.

McKeon, F.D., Kirschner, M.W. & Caput, D. (1986) Homologies in both primary and secondary structure between nuclear envelope and intermediate filament proteins. *Nature*, **319**, 463-468.

Meaburn, K.J., Cabuy, E., Bonne, G., Levy, N., Morris, G.E., Novelli, G., Kill, I.R., Bridger, J.M. (2007) Primary laminopathy fibroblasts display altered genome organization and apoptosis. *Aging Cell*, **6**, (2), 139-153.

Merideth, M.A., Gordon, L.B., Clauss, S., Sachdev, V., Smith, A.C., Perry, M.B., Brewer, C.C., Zalewski, C., Kim, H.J., Solomon, B., Brooks, B.P., Gerber, L.H., Turner, M.L., Domingo, D.L., Hart, T.C., Graf, J., Reynolds, J.C., Gropman, A., Yanovski, J.A., Gerhard-Herman, M., Collins, F.S., Nabel, E.G., Cannon, R.O., 3rd, Gahl, W.A. & Intronc, W.J. (2008) Phenotype and course of Hutchinson-Gilford progeria syndrome. *N Engl J Med*, **358**, 592-604.

- Mesa, J.L., Loos, R., Franks, P.W., Ong, K.K., Luan, J., O'Rahilly, S., Wareham, N.J., Barroso, I. (2007) Lamin A/C polymorphisms, type 2 diabetes, and the metabolic syndrome: case-control and quantitative trait studies. *Diabetes*, **56**, 884-889.
- Misteli, T., Scaffidi, P. (2005) Genome instability in progeria: when repair gets old. *Nat Med*, **11**, 718-719.
- Mofrad, M.R.K. (2009) Rheology of the cytoskeleton. *Annu. Rev. Fluid Mech.*, **41**, 433-453.
- Moir, R.D., Montag-Lowy, M., Goldman, R.D. (1994). Dynamic properties of nuclear lamins: lamin B is associated with sites of DNA replication. *J Cell Biol.* **125**, (6), 1201-1212.
- Moir, R.D., Spann, T.P., Herrmann, H., Goldman, R.D. (2000). Disruption of nuclear lamin organization blocks the elongation phase of DNA replication. *J Cell Biol.* **149**, 1179-1192.
- Moldes, M., Boizard, M., Liepvre, X.L., Fève, B., Dugail, I., Pairault, J. (1999) Functional antagonism between inhibitor of DNA binding (Id) and adipocyte determination and differentiation factor 1/sterol regulatory element-binding protein-1c (ADD1/SREBP-1c) trans-factors for the regulation of fatty acid synthase promoter in adipocytes. *Biochem J.* **344**, (Pt 3), 873-880.
- Morel, C.F., Thomas, M.A., Cao, H., O'Neil, C.H., Pickering, J.G., Foulkes, W.D., Hegele, R.A. A (2006) LMNA splicing mutation in two sisters with severe Dunnigan-type familial partial lipodystrophy type 2. *J Clin Endocrinol Metab.* **91**, 2689-2695.
- Moulson, C.L., Go, G., Gardner, J.M., van der Wal, A.C., Smitt, J.H., van Hagen, J.M. & Miner, J.H. (2005) Homozygous and compound heterozygous mutations in ZMPSTE24 cause the laminopathy restrictive dermopathy. *J Invest Dermatol*, **125**, 913-919.
- Moulson, C.L., Fong, L., Gardner JM, Farber EA, Go G, Passariello A, Grange DK, Young SG, Miner JH. (2007) Increased progerin expression associated with unusual LMNA mutations causes severe progeroid syndromes. *Hum Mutat*, **28**, 882-889.
- Mueller, E., Drori, S., Aiyer, A., Yie, J., Sarraf, P., Chen, H., Hauser, S., Rosen, E.D., Ge, K., Roeder, R.G., Spiegelman, B.M. (2002) Genetic analysis of a dipogenesis through peroxisome proliferator-activated receptor gamma isoforms. *J Biol Chem.*, **277**, (4) 41925-41930.
- Muschke, P., Kölsch, U., Jakubiczka, S., Wieland, I., Brune, T., Wieacker, P. (2007) The heterozygous LMNA mutation p.R471G causes a variable phenotype with features of two types of familial partial lipodystrophy. *Am J Med Genet A.* **143A**, (23), 2810-2814.

Muralikrishna, B., Dhawan, J., Rangaraj, N., Parnaik, V.K. (2001) Distinct changes in intranuclear lamin A/C organization during myoblast differentiation. *J Cell Sci.* **114**, (Pt 22), 4001-11.

Murase, Y., Yagi, K., Katsuda, Y., Asano, A., Koizumi, J. & Mabuchi, H. (2002) An LMNA variant is associated with dyslipidemia and insulin resistance in the Japanese. *Metabolism*, **51**, 1017-1021.

Naetar, N., Korbei, B., Kozlov, S., Kerényi, M.A., Dorner, D., Kral, R., Gotic, I., Fuchs, P., Cohen, T.V., Bittner, R., Stewart, C.L. & Foisner, R. (2008) Loss of nucleoplasmic LAP2alpha-lamin A complexes causes erythroid and epidermal progenitor hyperproliferation. *Nat Cell Biol*, **10**, 1341-1348.

Navarro, C.L., De Sandre-Giovannoli, A., Bernard R, Boccaccio I, Boyer A, Geneviève D, Hadj-Rabia S, Gaudy-Marqueste C, Smitt HS, Vabres P, Faivre L, Verloes A, Van Essen T, Flori E, Hennekam R, Beemer FA, Laurent N, Le Merrer M, Cau P, Lévy N. (2004) Lamin A and ZMPSTE24 (FACE-1) defects cause nuclear disorganization and identify restrictive dermopathy as a lethal neonatal laminopathy. *Hum Mol Genet.*, **13**, 2493-2503.

Navarro, C.L., Cadiñanos, J., De Sandre-Giovannoli A, Bernard R, Courrier S, Boccaccio I, Boyer A, Kleijer WJ, Wagner A, Giuliano F, Beemer FA, Freije JM, Cau P, Hennekam RC, López-Otín C, Badens C, Lévy N. (2005) Loss of ZMPSTE24 (FACE-1) causes autosomal recessive restrictive dermopathy and accumulation of Lamin A precursors. *Hum Mol Genet.*, **14**, 1503-1513.

Nelson, W.J. & Nusse, R. (2004) Convergence of Wnt, beta-catenin, and cadherin pathways. *Science*, **303**, 1483-1487.

Neubauer, M., Fischbach, C., Bauer-Kreisel, P., Lieb, E., Hacker, M., Tessmar, J., Schulz, M.B., Goepferich, A., Blunk, T. (2004) Basic fibroblast growth factor enhances PPARgamma ligand-induced adipogenesis of mesenchymal stem cells. *FEBS Lett.* **577**, (1-2), 277-283.

Nili, E., Cojocaru, G.S., Kalma, Y., Ginsberg, D., Copeland, N.G., Gilbert, D.J., Jenkins, N.A., Berger, R., Shaklai, S., Amariglio, N., Brok-Simoni, F., Simon, A.J., Rechavi, G. (2001). Nuclear membrane protein LAP2beta mediates transcriptional repression alone and together with its binding partner GCL (germ-cell-less). *J Cell Sci.* **114** (Pt 18), 3297-3307.

Novelli, G., Muchir, A., Sangiuolo, F., Helbling-Leclerc, A., D'Apice, M.R., Massart, C., Capon, F., Sbraccia, P., Federici, M., Lauro, R., Tudisco, C., Pallotta, R., Scarano, G., Dallapiccola, B., Merlini, L. & Bonne, G. (2002) Mandibuloacral dysplasia is caused by a mutation in LMNA-encoding lamin A/C. *Am J Hum Genet*, **71**, 426-431.

Ogihara, T., Tabuchi, Y., Fukuchi, K.C., Mikami, H., Masugi, F., Rakugi, H., Fukuda, M., Tanaka, A. & Kumahara, Y. (1986) An autopsied case of a 45-year-old man with Hutchinson-Gilford progeria syndrome. *Nippon Naika Gakkai Zasshi*, **75**, 746-752.

Ogino, S., Gulley, M. L., Dunnen, J.T., Wilson, R.B. and the Association for Molecular Pathology Training and Education Committee. (2007) Standard Mutation Nomenclature in Molecular Diagnostics Practical and Educational Challenges. *J Mol Diagn.*, **9**, (1), 1–6.

Oishi, Y., Manabe, I., Tobe, K., Tsushima, K., Shindo, T., Fujiu, K., Nishimura, G., Maemura, K., Yamauchi, T., Kubota, N., Suzuki, R., Kitamura, T., Akira, S., Kadowaki, T., Nagai, R. (2005) Krüppel-like transcription factor KLF5 is a key regulator of adipocyte differentiation. *Cell Metab.*, **1**, (1), 27-39.

Olins, A.L., Rhodes, G., Welch, D.B., Zwerger, M., Olins, D.E. (2010). Lamin B receptor: multi-tasking at the nuclear envelope. *Nucleus*. **1**, 53-70.

Owen, K.R., Groves, C.J., Hanson, R.L., Knowler, W.C., Shuldiner, A.R., Elbein, S.C., Mitchell, B.D., Froguel, P., Ng, M.C., Chan, J.C., Jia, W., Deloukas, P., Hitman, G.A., Walker, M., Frayling, T.M., Hattersley, A.T., Zeggini, E. & McCarthy, M.I. (2007) Common variation in the LMNA gene (encoding lamin A/C) and type 2 diabetes: association analyses in 9,518 subjects. *Diabetes*, **56**, 879-883.

Ozaki, T., Saijo, M., Murakami, K., Enomoto, H., Taya, Y. & Sakiyama, S. (1994) Complex formation between lamin A and the retinoblastoma gene product: identification of the domain on lamin A required for its interaction. *Oncogene*, **9**, 2649-2653.

Pai, J. T., Guryev, O., Brown, M.S., Goldstein, J.L. (1998) Differential stimulation of cholesterol and unsaturated fatty acid biosynthesis in cells expressing individual nuclear sterol regulatory element-binding proteins. *J. Biol. Chem.* **273**, 26138-26148.

Pekovic, V., Harborth, J., Broers, J.L., Ramaekers, F.C., van Engelen, B., Lammens, M., von Zglinicki, T., Foisner, R., Hutchison, C. & Markiewicz, E. (2007) Nucleoplasmic LAP2alpha-lamin A complexes are required to maintain a proliferative state in human fibroblasts. *J Cell Biol*, **176**, 163-172.

Petruschke, T., Hauner, H. (1993) Tumor necrosis factor-alpha prevents the differentiation of human adipocyte precursor cells and causes delipidation of newly developed fat cells. *J Clin Endocrinol Metab.* **76**, 742-747.

Pittenger, M.F., Mackay, A.M., Beck, S.C., Jaiswal, R.K., Douglas, R., Mosca, J.D., Moorman, M.A., Simonetti, D.W., Craig, S. & Marshak, D.R. (1999) Multilineage potential of adult human mesenchymal stem cells. *Science*, **284**, 143-147.

Pivnick, E.K., Angle, B., Kaufman, R.A., Hall, B.D., Pitukcheewanont, P., Hersh, J.H., Fowlkes, J.L., Sanders, L.P., O'Brien, J.M., Carroll, G.S., Gunther, W.M., Morrow, H.G., Burghen, G.A. & Ward, J.C. (2000) Neonatal progeroid (Wiedemann-Rautenstrauch) syndrome: report of five new cases and review. *Am J Med Genet*, **90**, 131-140.

Plasilova, M., Chattopadhyay, C., Pal P, Schaub NA, Buechner SA, Mueller H, Miny P, Ghosh A, Heinimann K. (2004) Homozygous missense mutation in the lamin A/C gene causes autosomal recessive Hutchinson-Gilford progeria syndrome. *J Med Genet.*, **41**, 609-614.

Pollard, K.M., Chan, E.K., Grant, B.J., Sullivan, K.F., Tan, E.M. & Glass, C.A. (1990) In vitro posttranslational modification of lamin B cloned from a human T-cell line. *Mol Cell Biol*, **10**, 2164-2175.

Prokocimer, M., Davidovich, M., Nissim-Rafinia, M., Wiesel-Motiuk, N., Bar, D.Z., Barkan, R., Meshorer, E. & Gruenbaum, Y. (2009) Nuclear lamins: key regulators of nuclear structure and activities. *J Cell Mol Med*, **13**, 1059-1085.

Razafsky, D. & Hodzic, D. (2009) Bringing KASH under the SUN: the many faces of nucleo-cytoskeletal connections. *J Cell Biol*, **186**, 461-472.

Reddy, K.L., Zullo, J.M., Bertolino, E., Singh, H. (2008). Transcriptional repression mediated by repositioning of genes to the nuclear lamina. *Nature*. **452**, (7184), 243-247.

Reya, T., Duncan, A.W., Ailles, L., Domen, J., Scherer, D.C., Willert, K., Hintz, L., Nusse, R., Weissman, I.L. (2003) A role for Wnt signalling in self-renewal of haematopoietic stem cells. *Nature.*, **423**, (6938), 409-414.

Reya, T., Clevers, H. (2005) Wnt signalling in stem cells and cancer. *Nature*, **434**, (7035), 843-850.

Richon, V.M., Lyle, R.E., McGehee, R.E. Jr. (1997) Regulation and expression of retinoblastoma proteins p107 and p130 during 3T3-L1 adipocyte differentiation. *J Biol Chem.*, **272**, (15), 10117-10124.

Rober, R.A., Weber, K. & Osborn, M. (1989) Differential timing of nuclear lamin A/C expression in the various organs of the mouse embryo and the young animal: a developmental study. *Development*, **105**, 365-378.

Ron, D., Habener, J.F. (1992) CHOP, a novel developmentally regulated nuclear protein that dimerizes with transcription factors C/EBP and LAP and functions as a dominant-negative inhibitor of gene transcription. *Genes Dev*. **6**, 439-453.

Rosen, E.D., Spiegelman, B.M. Molecular regulation of adipogenesis. (2000) *Annu Rev Cell Dev Biol.*, **16**, 145-171.

- Rosen, E.D., (2005) The transcriptional basis of adipocyte development. *Prostaglandins Leukot Essent Fatty Acids.*, **73**, (1), 31-34.
- Rosen, E.D. & MacDougald, O.A. (2006) Adipocyte differentiation from the inside out. *Nat Rev Mol Cell Biol*, **7**, 885-896.
- Rosenow, A., Arrey, T.N., Bouwman, F.G., Noben, J.P., Wabitsch, M., Mariman, E.C., Karas, M., Renes, J. (2010) Identification of novel human adipocyte secreted proteins by using SGBS cells. *J Proteome Res.*, **9**, (10), 5389-5401.
- Ross, S.E., Hemati, N., Longo, K.A., Bennett, C.N., Lucas, P.C., Erickson, R.L. & MacDougald, O.A. (2000) Inhibition of adipogenesis by Wnt signaling. *Science*, **289**, 950-953.
- Sagelius, H., Rosengardten, Y., Schmidt, E., Sonnabend, C., Rozell, B. & Eriksson, M. (2008) Reversible phenotype in a mouse model of Hutchinson-Gilford progeria syndrome. *J Med Genet*, **45**, 794-801.
- Sakai, J., Duncan, E.A., Rawson, R.B., Hua, X., Brown, M.S. & Goldstein, J.L. (1996) Sterol-regulated release of SREBP-2 from cell membranes requires two sequential cleavages, one within a transmembrane segment. *Cell*, **85**, 1037-1046.
- Savage, D.B., O'Rahilly, S. (2002) Leptin: a novel therapeutic role in lipodystrophy. *J Clin Invest.*, **109**, 1285-1286.
- Savage, D.B., Soos, M.A., Powlson, A., O'Rahilly, S., McFarlane, I., Halsall, D.J., Barroso, I., Thomas, E.L., Bell, J.D., Scobie, I., Belchetz, P.E., Kelly, W.F., Schafer, A.J. (2004) Familial partial lipodystrophy associated with compound heterozygosity for novel mutations in the LMNA gene. *Diabetologia*, **47**, (4), 753-756.
- Scaffidi, P., Gordon, L., Misteli T. (2005) The cell nucleus and aging: tantalizing clues and hopeful promises. *PLoS Biol.*, **3**, e395.
- Scaffidi, P. & Misteli, T. (2005) Reversal of the cellular phenotype in the premature aging disease Hutchinson-Gilford progeria syndrome. *Nat Med.*, **11**, 440-445.
- Scaffidi, P., Misteli, T. (2006). Lamin A-dependent nuclear defects in human aging. *Science*. **312**, 1059-1063.
- Scaffidi, P. & Misteli, T. (2008) Lamin A-dependent misregulation of adult stem cells associated with accelerated ageing. *Nat Cell Biol*, **10**, 452-459.
- Schieker, M., Pautke, C., Haasters, F., Schieker, J., Docheva, D., Bocker, W., Guelkan, H., Neth, P., Jochum, M. & Mutschler, W. (2007) Human mesenchymal stem cells at the single-cell level: simultaneous seven-colour immunofluorescence. *J Anat*, **210**, 592-599.
- Schirmer, E.C., Florens, L., Guan, T., Yates, J.R. 3rd, Gerace, L. (2003). Nuclear membrane proteins with potential disease links found by subtractive proteomics. *Science* **301**, (5638), 1380-1382.

Schirmer, E.C., Florens, L., Guan, T., Yates, J.R. 3rd, Gerace, L. (2005). Identification of novel integral membrane proteins of the nuclear envelope with potential disease links using subtractive proteomics. *Novartis Found Symp.* **264**, 63-76.

Schirmer, E.C., Foisner, R. (2007). P roteins that associate with lamins: many faces, many functions. *Exp Cell Res.* **313**, 2167-2179.

Schmidmaier, R., Simsek, M., Baumann, P., Emmerich, B., Meinhardt G. (2006) Synergistic antimyeloma effects of zoledronate and simvastatin. *Anticancer drugs*, **17**, 621-629

Schmidt, H.H.J., Genschel, J., Baier, P., Schmidt, M., Ockenga, J., Tietge, U.J.F., Propsting, M., Buttner, C., Manns, M.P., Lochs, H., Brabant, G. (2001) Dyslipemia in familial partial lipodystrophy caused by an R482W mutation in the LMNA gene. *J Clin Endocrinol Metab*, **86**, (5), 2289-2295

Schwingshandl, J., Mache, C.J., Rath, K., Borkenstein, M.H. (1993) SHORT syndrome and insulin resistance. *Am J Med Genet.* **1**, 47, 907-909.

Shackleton, S., Lloyd, D., Jackson SN, Evans R, Niermeijer MF, Singh BM, Schmidt H, Brabant G, Kumar S, Durrington PN, Gregory S, O'Rahilly S, Trembath RC. (2000) LMNA, encoding lamin A/C, is mutated in partial lipodystrophy. *Nat Genet.*, **24**, 153-156.

Shackleton, S., Smallwood, D., Clayton P, Wilson LC, Agarwal AK, Garg A, Trembath RC. (2005) Compound heterozygous ZMPSTE24 mutations reduce prelamin A processing and result in a severe progeroid phenotype. *J Med Genet.*, **42**, e36.

Shalev, S.A., De Sandre-Giovannoli, A., Shani, A.A. & Levy, N. (2007) An association of Hutchinson-Gilford progeria and malignancy. *Am J Med Genet A*, **143A**, 1821-1826.

Shao, D. & Lazar, M.A. (1997) Peroxisome proliferator activated receptor gamma, CCAAT/enhancer-binding protein alpha, and cell cycle status regulate the commitment to adipocyte differentiation. *J Biol Chem*, **272**, 21473-21478.

Shen, J.J., Brown, C.A., Lupski, J.R., Potocki, L. (2003) Mandibuloacral dysplasia caused by homozygosity for the R527H mutation in lamin A/C. *J Med Genet*, **40**, 854-857.

Shimano, H., Horton, J.D., Shimomura, I., Hammer, R.E., Brown, M.S., Goldstein, J.L. (1997) Isoform 1c of sterol regulatory element binding protein is less active than isoform 1a in livers of transgenic mice and in cultured cells. *J Clin Invest*, **99**, (5), 846-854.

Shimi, T., Pflieger, K., Kojima, S., Pack, C.G., Solovei, I., Goldman, A.E., Adam, S.A., Shumaker, D.K., Kinjo, M., Cremer, T. & Goldman, R.D. (2008) The A- and B-

type nuclear lamin networks: microdomains involved in chromatin organization and transcription. *Genes Dev*, **22**, 3409-3421.

Shimomura, I., Bashmakov, Y., Shimano, H., Horton, J.D., Goldstein, J.L. & Brown, M.S. (1997) Chol esterol feeding reduces nuclear forms of sterol regulatory element binding proteins in hamster liver. *Proc Natl Acad Sci U S A*, **94**, 12354-12359.

Shimomura, I., Shimano, H., Horton, J.D., Goldstein, J.L. & Brown, M.S. (1997) Differential expression of exons 1a and 1c in mRNAs for sterol regulatory element binding protein-1 in human and mouse organs and cultured cells. *J Clin Invest*, **99**, (5), 838-845.

Shumaker, D.K., Kuczmarski, E.R., Goldman, R.D. (2003) The nucleoskeleton: lamins and actin are major players in essential nuclear functions. *Curr Opin Cell Biol.*, **15**, 358-366.

Shumaker, D.K., Dechat, T., Kohlmaier, A., Adam, S.A., Bozovsky, M.R., Erdos, M.R., Eriksson, M., Goldman, A.E., Khuon, S., Collins, F.S., Jenuwein, T. & Goldman, R.D. (2006) Mutant nuclear lamin A leads to progressive alterations of epigenetic control in premature aging. *Proc Natl Acad Sci U S A*, **103**, 8703-8708.

Simha, V., Agarwal, A.K., Oral, E.A., Fryns, J.P., Garg, A. (2003) Genetic and phenotypic heterogeneity in patients with mandibuloacral dysplasia-associated lipodystrophy. *J Clin Endocrinol Metab*, **88**, (6), 2821-2824.

Sinensky, M., Fantle, K., Trujillo, M., McLain, T., Kupfer, A. & Dalton, M. (1994) The processing pathway of prelamin A. *J Cell Sci*, **107** ( Pt 1), 61-67.

Smallwood, D.T., Shackleton, S. (2010) Lamin A-linked progerias: is farnesylation the be all and end all? *Biochem Soc Trans.*, **Feb**, 281-286.

Spann, T.P., Moir, R.D., Goldman, A.E., Stick, R., Goldman, R.D. (1997). Disruption of nuclear lamin organization alters the distribution of replication factors and inhibits DNA synthesis. *J Cell Biol.* **136**, 1201-1212.

Spann, T.P., Goldman, A.E., Wang, C., Huang, S., Goldman, R.D. (2002). Alteration of nuclear lamin organization inhibits RNA polymerase II-dependent transcription. *J Cell Biol.* **156**, 603-608.

Speckman, R.A., Garg, A., Du F, Bennett L, Veile R, Arioglu E, Taylor SI, Lovett M, Bowcock AM. (2000) Mutational and haplotype analyses of families with familial partial lipodystrophy (Dunnigan variety) reveal recurrent missense mutations in the globular C-terminal domain of lamin A/C. *Am J Hum Genet*, **66**, 1192-1198.

Steinle, N.I., Kazlauskaitė, R., Imumorin IG, Hsueh WC, Pollin TI, O'Connell JR, Mitchell BD, Shuldiner AR. (2004) Variation in the lamin A/C gene: associations with metabolic syndrome. *Arterioscler Thromb Vasc Biol.*, **24**, 1708-1713.

- Stenderup, K., Justesen, J., Clausen, C. & Kassem, M. (2003) Aging is associated with decreased maximal life span and accelerated senescence of bone marrow stromal cells. *Bone*, **33**, 919-926.
- Stuurman, N., Heins, S. & Aebi, U. (1998) Nuclear lamins: their structure, assembly, and interactions. *J Struct Biol*, **122**, 42-66.
- Subramanyam, L., Simha, V., Garg, A. (2010) Overlapping syndrome with familial partial lipodystrophy, Dunnigan variety and cardiomyopathy due to amino-terminal heterozygous missense lamin A/C mutations. *Clin Genet*. **78**, (1), 66-73. Epub.
- Sullivan, T., Escalante-Alcalde, D.D., Bhatt, H., Anver, M., Bhat, N., Nagashima, K., Stewart, C.L., Burke, B. (1999). Loss of A-type lamin expression compromises nuclear envelope integrity leading to muscular dystrophy. *J Cell Biol*. **147**, 913-920.
- Till, J.E., McCulloch, E.A. (1980) Hemopoietic stem cell differentiation. *Biochim Biophys Acta.*, **605**, (4), 431-459.
- Tong, Q., Tsai, J., Tan, G., Dalgin, G., Hotamisligil, G.S. (2005) Interaction between GATA and the C/EBP family of transcription factors is critical in GATA-mediated suppression of adipocyte differentiation. *Mol Cell Biol*. **25**, 706-715.
- Toth, J.I., Yang, S., Qiao X, Beigneux AP, Gelb MH, Moulson CL, Miner JH, Young SG, Fong LG. (2005) Blocking protein farnesyltransferase improves nuclear shape in fibroblasts from humans with progeroid syndromes. *Proc Natl Acad Sci U S A.*, **102**, 12873-12878.
- Tontonoz, P., Hu, E., Spiegelman, B.M. (1994) Stimulation of adipogenesis in fibroblasts by PPAR gamma 2, a lipid-activated transcription factor. *Cell.*, **79**, (7), 1147-1156.
- Toriello, H.V., Wakefield, S., Komar, K., Higgins, J.V. & Waterman, D.F. (1985) Report of a case and further delineation of the SHORT syndrome. *Am J Med Genet*, **22**, 311-314.
- Vaughan, A., Alvarez-Reyes, M., Bridger, J.M., Broers, J.L., Ramaekers, F.C., Wehnert, M., Morris, G.E., Whitfield, W.G.F. & Hutchison, C.J. (2001) Both emerin and lamin C depend on lamin A for localization at the nuclear envelope. *J Cell Sci*, **114**, 2577-2590.
- Varela, I., Pereira, S., Ugalde, A.P., Navarro, C.L., Suárez, M.F., Cau, P., Cadiñanos, J., Osorio, F.G., Foray, N., Cobo, J., de Carlos, F., Lévy, N., Freije, J.M., López-Otín, C. (2008). Combined treatment with statins and aminobisphosphonates extends longevity in a mouse model of human premature aging. *Nat Med*. **14**, 767-772.

Verstraeten, V.L., Broers, J.L., van Steensel, M.A., Zinn-Justin, S., Ramaekers, F.C., Steijlen, P.M., Kamps, M., Kuijpers, H.J., Merckx, D., Smeets, H.J., Hennekam, R.C., Marcelis, C.L. & van den Wijngaard, A. (2006) Compound heterozygosity for mutations in LMNA causes a progeria syndrome without prelamin A accumulation. *Hum Mol Genet*, **15**, 2509-2522.

Verstraeten, V.L., Ji, J.Y., Cummings, K.S., Lee, R.T. & Lammerding, J. (2008) Increased mechanosensitivity and nuclear stiffness in Hutchinson-Gilford progeria cells: effects of farnesyltransferase inhibitors. *Aging Cell*, **7**, 383-393.

Vigouroux, C., Magré, J., Vantyghem MC, Bourut C, Lascols O, Shackleton S, Lloyd DJ, Guerci B, Padova G, Valensi P, Grimaldi A, Piquemal R, Touraine P, Trembath RC, Capeau J. (2000) Lamin A/C gene: sex-determined expression of mutations in Dunnigan-type familial partial lipodystrophy and absence of coding mutations in congenital and acquired generalized lipodystrophy. *Diabetes*, **49**, 1958-1962.

Vigouroux, C., Auclair, M., Dubosclard E, Pouchelet M, Capeau J, Courvalin JC, Buendia B. (2001) Nuclear envelope disorganization in fibroblasts from lipodystrophic patients with heterozygous R482Q/W mutations in the lamin A/C gene. *J Cell Sci.*, **114**, 4459-4468.

Vorburger, K., Kitten, G.T. & Nigg, E.A. (1989) Modification of nuclear lamin proteins by a mevalonic acid derivative occurs in reticulocyte lysates and requires the cysteine residue of the C-terminal CXXM motif. *Embo J*, **8**, 4007-4013.

Wagner, N., Krohne, G. (2007). LEM-Domain proteins: new insights into lamin-interacting proteins. *Int Rev Cytol.* 261, 1-46.

Wang, H., Liu, F., Millette, C., Kilpatrick, D.L. Expression of a Novel, Sterol-Insensitive Form of Sterol Regulatory Element Binding Protein 2 (SREBP2) in Male Germ Cells Suggests Important Cell- and Stage-Specific Functions for SREBP Targets during Spermatogenesis (2002) *Mol. Cell. Biol.* **22**, (24), 8478-8490.

Wang, N.D., Finegold, M.J., Bradley, A., Ou, C.N., Abdelsayed, S.V., Wilde, M.D., Taylor, L.R., Wilson, D.R., Darlington, G.J. (1995) Impaired energy homeostasis in C/EBP alpha knockout mice. *Science.*, **269**, (5227), 1108-1112.

Wang, X., Sato R., Brown, M.S., Hua, X., Goldstein, J.L. (1994) SREBP-1, a membrane-bound transcription factor released by sterol-regulated proteolysis. *Cell*, **77**, 53-62.

Wang, Y., Sul, H.S. (2009) Pref-1 regulates mesenchymal cell commitment and differentiation through Sox9. *Cell Metab.* **9**, 287-302.

Weber, K., Plessmann, U. & Traub, P. (1989) Maturation of nuclear lamin A involves a specific carboxy-terminal trimming, which removes the polyisoprenylation site from the precursor; implications for the structure of the nuclear lamina. *FEBS Lett*, **257**, 411-414.

Wegner, L., Andersen, G., Sparso, T., Grarup, N., Glumer, C., Borch-Johnsen, K., Jorgensen, T., Hansen, T. & Pedersen, O. (2007) Common variation in LMNA increases susceptibility to type 2 diabetes and associates with elevated fasting glycemia and estimates of body fat and height in the general population: studies of 7,495 Danish whites. *Diabetes*, **56**, 694-698.

Wilson, K.L., Berk, J.M. (2010). The nuclear envelope at a glance. *J Cell Sci.* **123**, (pt 12), 1973-1978.

Wilson, K.L., Holaska, J., Montes de Oca, R., Tiffit, K., Zastrow, M., Segura-Totten, M., Mansharamani, M., Bengtsson, L. (2005). Nuclear membrane protein emerin: roles in gene regulation, actin dynamics and human disease. *Novartis Found Symp.* **264**, 51-58.

Wolford, J.K., Hanson, R.L., Bogardus, C. & Prochazka, M. (2001) Analysis of the lamin A/C gene as a candidate for type II diabetes susceptibility in Pima Indians. *Diabetologia*, **44**, 779-782.

Worman, H.J., Yuan, J., Blobel, G., Georgatos, S.D. (1988). A lamin B receptor in the nuclear envelope. *Proc Natl Acad Sci U S A.* **85**, 8531-8534.

Worman, H.J., Evans, C.D., Blobel, G. (1990). The lamin B receptor of the nuclear envelope inner membrane: a polytopic protein with eight potential transmembrane domains. *J Cell Biol.* **111**, 1532-1542.

Worman, H.J., Courvalin, J.C. (2004). How do mutations in lamins A and C cause disease? *J Clin Invest.* **113**, 349-351.

Worman, H.J., Bonne, G. (2007) "Laminopathies": a wide spectrum of human diseases. *Exp Cell Res.*, **313**, 2121-2133.

Worman, HJ, Fong, L.G., Muchir, A, Young, SG. (2009). Laminopathies and the long strange trip from basic cell biology to therapy. *J Clin Invest.* **119**, (7), 1825-1836.

Xu, H.E., Lambert, M.H., Montana, V.G., Parks, D.J., Blanchard, S.G., Brown, P.J., Sternbach, D.D., Lehmann, J.M., Wisely, G.B., Willson, T.M., Kliewer, S.A., Milburn, M.V. (1999) Molecular recognition of fatty acids by peroxisome proliferator-activated receptors. *Mol Cell*, **3**(3), 397-403.

Yang, S.H., Bergo, M., Toth JI, Qiao X, Hu Y, Sandoval S, Meta M, Bendale P, Gelb MH, Young SG, Fong LG. (2005) B locking protein farnesyltransferase improves

nuclear blebbing in mouse fibroblasts with a targeted Hutchinson-Gilford progeria syndrome mutation. *Proc Natl Acad Sci U S A.*, **102**, 10291-10296.

Yang, S.H., Meta, M., Qiao, X., Frost, D., Bauch, J., Coffinier, C., Majumdar, S., Bergo, M.O., Young, S.G. & Fong, L.G. (2006) A farnesyltransferase inhibitor improves disease phenotypes in mice with a Hutchinson-Gilford progeria syndrome mutation. *J Clin Invest*, **116**, 2115-2121.

Yang, S.H., Qiao, X., Fong, L.G. & Young, S.G. (2008) Treatment with a farnesyltransferase inhibitor improves survival in mice with a Hutchinson-Gilford progeria syndrome mutation. *Biochim Biophys Acta*, **1781**, 36-39.

Zacksenhaus, E., Jiang, Z., Chung, D., Marth, J.D., Phillips, R.A., Gallie, B.L. (1996). pRb controls proliferation, differentiation, and death of skeletal muscle cells and other lineages during embryogenesis. *Genes Dev.* **10**, 3051-3064.

Zhang, J. Fu, M., Cui, T., Xiong, C., Xu, K., Zhong, W., Xiao, Y., Floyd, D., Liang, J., Li, E., Song, Q., Chen, Y.E. (2004) Selective disruption of PPARgamma 2 impairs the development of adipose tissue and insulin sensitivity. *Proc Natl Acad Sci U S A.*, **101**, (29), 10703-10798.

Zhu, L. (2005) Tumour suppressor retinoblastoma protein Rb: a transcriptional regulator. *Eur J Cancer.*, **41**, (16), 2415-2427.

Zirn, B., Kress, W., Grimm, T., Berthold, L.D., Neubauer, B., Kuchelmeister, K., Muller, U. & Hahn, A. (2008) Association of homozygous LMNA mutation R471C with new phenotype: mandibuloacral dysplasia, progeria, and rigid spine muscular dystrophy. *Am J Med Genet A*, **146A**, 1049-1054.

Zuk, P.A., Zhu, M., Mizuno, H., Huang, J., Futrell, J.W., Katz, A.J., Benhaim, P., Lorenz, H.P., Hedrick, M.H. (2001) Multilineage cells from human adipose tissue: implications for cell-based therapies. *Tissue Eng.*, **7**, (2), 211-228.

Zuo, Y., Qiang, L., Farmer, S.R. (2006) Activation of C/EBP alpha expression by C/EBP beta during adipogenesis requires a peroxisome proliferator-activated receptor-gamma-associated repression of HDAC1 at the C/ebp alpha gene promoter. *J Biol Chem.*, **281**, (12), 7960-7967.

## **Published articles removed:**

Due to third party copyright restrictions the published articles have been removed from the appendix of the electronic version of this thesis. The unabridged version can be consulted, on request, at the University of Leicester's David Wilson Library.